Dimensional Sandstones: Weathering Phenomena, Technical Properties and Numerical Modeling of Water Migration

Dissertation

zur Erlangung des mathematisch-naturwissenschaftlichen Doktorgrades

„Doctor rerum naturalium“

der Georg-August-Universität Göttingen

im Promotionsprogramm Geowissenschaften

der Georg-August University School of Science (GAUSS)

vorgelegt von

Heidrun Louise Stück

aus Bad Homburg

Göttingen 2013

Betreuungsausschuss:

Prof. Dr. Siegfried Siegesmund
Abt. Strukturgeologie & Geodynamik
Geowissenschaftliches Zentrum der Georg-August Universität Göttingen

Prof. Dr. Roman Koch
Abt. Angewandte Sedimentologie & Bausteinforschung
GeoZentrum Nordbayern
Univsität Erlangen-Nürnberg

Mitglieder der Prüfungskommission:

Prof. Dr. Siegfried Siegesmund
Abt. Strukturgeologie & Geodynamik
Geowissenschaftliches Zentrum der Georg-August Universität Göttingen

Prof. Dr. Roman Koch
Abt. Angewandte Sedimentologie & Bausteinforschung
GeoZentrum Nordbayern
Univsität Erlangen-Nürnberg

Weitere Mitglieder der Prüfungskommission:

Prof. Dr. Bent T. Hansen
Abt. Isotopengeologie
Geowissenschaftliches Zentrum der Georg-August Universität Göttingen

Prof. Dr. Jonas Kley
Abt. Strukturgeologie & Geodynamik
Geowissenschaftliches Zentrum der Georg-August Universität Göttingen

Prof. Dr. Sharon Webb
Abt. Experimentelle und Angewandte Mineralogie
Geowissenschaftliches Zentrum der Georg-August Universität Göttingen

Prof. Dr. Michael Hoppert
Institut für Mikrobiologie und Genetik
Fakultät für Biologie der Georg-August Universität Göttingen

Tag der mündlichen Prüfung: 08.03.2013

Abstract

This here presented thesis is focused on the systematically evaluation of the durability of natural sandstones by the detailed characterization of their petrographical, petrophysical, deterioration and weathering properties. The thesis presents a new combined approach for the detailed analyses at sandstones by onsite studies (deterioration phenomena and weathering behavior), in laboratory (measurement and determination of petrophysical and petrographical properties), by statistical considerations (i.e. establish correlations between petrography, petrophysical and weathering properties) and by numerical modeling (evaluation of water transport and water storage in dependence to pore space). Additionally, special emphasis is set on the influence and relationships of fabric, diagenetic path and pore space properties on the material and weathering behavior of sandstones.

Statistical methods were applied to a large dataset of more than ~300 sandstones and comprise among others wisker data distributions plots, linear regression with confidence regions for the petrophysical and weathering properties of the sandstones. Based on the results of on-site studies, laboratory experiments and statistical analyses, i.e. principal component- and cluster analyses was possible to identify similarities in the material properties and weathering behavior of individual sandstones. This was used to define groups of specific sandstones types by establishing relationships between the composition, depositional environment, stratigraphic association and diagenetic pathway. This allows us to compile a sandstone quality catalogue.

In order to evaluate the moisture distribution and moisture transport as well as to evaluate their effect on the weathering and deterioration behavior, numerical modeling for each of the defined pore radii type was performed based on detailed, sandstone specific material functions. Modeling results confirm our observations from on-site studies and statistical analyses and prove the established relationships between compositional, depositional, stratigraphical and diagenetic aspects and the material properties. For example, it can be proved that the pore radii distribution is one of the main variables governing both material and weathering properties of sandstones by its large impact on e.g. water absorption, salt loading and hygric dilatation behavior.

Table of Contents

1 General Introduction

1.1 Motivation

Since they are the most ubiquitous rocks on earth, sandstones have always been a popular and commonly used material for monuments as well as secular and sacred buildings. Historically, the utilization of natural stones depended mainly on their regional availability because the transport of heavy rocks over long distances required immense effort. Therefore, the origin of building materials for historical objects (e.g. castles) has often been the castle hill itself. Evidence of previous extraction of natural stones is often evidenced by small open pits in close vicinity to villages, where the stones have been used mainly for secular buildings. Therefore, the regional geology is often well-reflected within the buildings of villages and cities. With increasing improvement of infrastructure, more remotely-located deposits have been able to be used, and finally have led to a worldwide exchange of natural stones. Today, only a few quarries are still operational in Germany.

Concerning sandstones, it was also known early on that some are more suitable for special purposes, e.g. sculpture works, than others. This can be attributed to different material properties, which are not only important when evaluating their applicability, but also are important for their resistance to decay. Once exposed to the environmental climate, the material properties govern the weathering behavior and, thus, significantly dictate their durability as dimension stones. In the natural environment, the process of weathering is one aspect of the rock cycle and contributes to the genesis of new rocks and landscapes. In contrast, the weathering processes in natural stones lead to the undesirable deterioration of cultural heritage and, thus, need to be prevented.

Accordingly, many studies within different disciplines deal with the processes of the weathering mechanisms of sandstones. The resulting accumulation of knowledge should help to develop conservation strategies for retarding the natural process of the weathering of historical buildings in order to find suitable replacement stones for irreversibly damaged dimension stones, as well as to help evaluate new dimensional stone deposits in terms of their construction suitability. This is commonly accomplished via standardized measurements of DIN material properties, such as porosity, density, water uptake and strength.

However, those studies are generally based on smaller data sets and predominantly do not include detailed data concerning the lithology, fabric, depositional milieu or diagenetic paths. Hence, the more exact evaluation of these parameters based on a larger data set in combination with petrophysical properties could reveal more detailed relationships between those parameters and should allow for better evaluation of weathering behavior and, thus, sandstone durability. However, at the same time, the evaluation of such a data set barely shed light on the effects or impact of a

temporally fluctuating climate on moisture accumulation, important with regards to weathering. To evaluate such a relationship, complex numerical modeling of sandstones, concerning all available water-transport- and storage-relevant data, would be necessary.

1.2 Aims of the Thesis

According to the above stated limitations in the previous consideration of the weathering behavior and construction suitability of sandstones, the here present study shall contribute to a better understanding of the material and weathering behavior of sandstones used as natural stones.

The main objectives are to evaluate the relationship between the petrography of sandstones and their material behavior with respect to sedimentary aspects, such as their depositional environments, stratigraphic association and diagenetic paths. In addition, special attention should be paid to the evaluation of the influence of pore-space properties on the weathering behavior of sandstones. In this context, special emphasis will be placed on the evaluation of moisture migration behavior with dependence on lithology and pore-space properties. The consideration of the relationships between those parameters shall be used to improve the evaluation process of sandstone´s durability.

More specific objectives are:

1. *An on-site study of dimension stones and their deterioration behavior*

   The on-site study will focus on the deterioration behavior of sandstones with different lithologies which are exposed to the same climatic conditions. Observations should be correlated with other parameters, such as lithological aspects and exposition. Additionally, in order to evaluate the general construction suitability of the investigated sandstones, on-site findings should be correlated with petrographical, petrophysical and weathering properties which should be determined by accompanying laboratory analyses.

2. *Statistical analyses of* petrographical, petrophysical and weathering properties

   Most of the recent studies on the petrophysical, petrographical and weathering properties of sandstones are based on a small data set of samples and parameters. Therefore, general statements covering concerning relationships between those parameters cannot be made for a wide stratigraphic range and different sandstone types of varying depositional environments and/or diagenetic developments. A statistical analysis of parameters such as grain size, compositional and textural maturity and cementation and fabric, which essentially control the material properties of sandstones, is lacking.

Therefore, based on our own analyses as well as data from the literature, a comprehensive data set of the petrographical, petrophysical and weathering properties of a broad variety of sandstones used as dimension stones should be compiled. On the basis of this data set, methods of statistical analysis should be used in order to establish criteria and systems which aid in predicting the weathering behavior of various sandstone types, as well as to evaluate the influence of compositional differences, depositional environment and diagenetic paths on the material and weathering behavior of sandstones. Additionally, based in the statistical analyses, the grouping of the analyzed sandstones into different types, characterized by distinct material or weathering behavior, should be attempted.

Over the course of statistical analyses, previously assumed relationships between basic parameters of petrophysical properties (e.g. porosity, pore-radii distribution, strength or water absorption), which are almost entirely established based on the consideration of a statistically negligible amount of data, should be evaluated to prove their consistence on the basis of statistically significant observations.

3. *Influence of porosity and pore-radii distribution on the water balance and water migration of sandstones*

Usually, the suitability of a sandstone for use as a building stone is evaluated with standard values (DIN) by measuring its petrophysical properties. These single values are mostly used in the natural stone industry without consideration of lithology or pore-radii distribution. Coevally, these single values do not reveal the locations of possible moisture accumulations which typically correspond with many kinds of deterioration phenomena. To what extent heterogeneities, such as clay layers, have influence on moisture accumulation and distribution likewise cannot be evaluated in detail from those values.

Therefore, based on the results of the statistical analyses, characteristic types of pore-radii distribution should be defined. These types should be related to water transport and storage parameters, which govern the water balance and water migration behavior. Additionally, the migration of moisture in those sandstones, dependent on different climatic conditions, should be evaluated with numerical modeling. The models should also be used to evaluate the effect of heterogeneities (e.g. clay layers) on the aforementioned parameters, as well as to reveal locations of moisture accumulation in order to identify possible zones of excessive deterioration.

In order to evaluate the effects of hydrophobic treatment as a commonly used method in the restoration and conservation of natural stones concerning the water migration and water balance in sandstones, all models should be run for ‘natural’ and ‘hydrophobized’ sandstones.

Finally, results from numerical modeling should be compared and evaluated with findings from the on-site study (see above) as well as the established assumptions concerning water transport and hydrophobic treatment.

4. *Impact of clay minerals and their pore-building network on water migration*

Findings from the aforementioned methods should be used to characterize the impact of pore-space properties and pore-building materials on water migration behavior. Special attention should be paid to the influence of spatial arrangement of clay minerals, as well as on the defined sandstone lithotypes (see above).

1.3 Structure of the Thesis

Chapter 2 gives an introduction to the methodological aspects of this thesis.

Chapters 3, 4, and 5 are built from three manuscripts, two of which have already been published (see list below).

Chapter 3 presents a regional on-site study and analyses of sandstones used as building materials for the Gleichen Castle (Thuringia, Germany). The region, situated in the Thuringian Basin, was chosen because various sandstone deposits representing different stratigraphic age and depositional environments are concentrated in a small-scale area. On one hand, this allows analyses of the deterioration of various natural stones under identical climatic conditions. This has been documented by the on-site mapping of lithology and associated deterioration phenomena. On the other hand, petrographical and petrophysical properties as well as the associated fabric are analyzed and interpreted with respect to the depositional environment of the sandstone. The results are also used to evaluate the general suitability of the analyzed sandstones for construction. This chapter was written in collaboration with several co-authors. The contribution of the co-authors includes a critical review of the manuscript in the pre-review state as well as suggestions concerning the structure of the manuscript.

Chapter 4 represents an approach to predicting the material behavior and construction suitability of sandstones through statistical analyses based on their petrographical and petrophysical properties. Thereby, the previously discussed relationships between petrography, stratigraphy and material behavior in Chapter 3 are extended into a trans-regional context via an enlargement of the sandstone data set to more than 300 samples, based on our own detailed analyses as well as available data from literature. The sandstones considered are widely distributed across Germany and represent various stratigraphic origins, as well as cover a wide range of petrographical and petrophysical variability. The data are statistically analyzed in order to characterize different lithotypes which can be used to predict their material behavior. In particular, the pore-space

properties will be considered in the context of lithology, depositional environment and diagenesis, with respect to strength properties. Special attention is paid to the fabric parameters, such as cementation, grain size, sorting and the position of clay minerals. Finally, all of this information is condensed within a sandstone catalogue of construction suitability. This chapter was written in collaboration with several co-authors. The contribution of the co-authors includes a re-structuring and review of the manuscript.

Chapter 5 focuses on the numerical modeling of moisture accumulation in sandstones. Therefore, characteristic sandstone types (see above), differing in composition and material properties, have been analyzed. Each type represents a different diagenetic development and depositional environment. Based on this data, which was integrated with detailed, material-specific water transport and storage functions, a numerical modeling of coupled heat and moisture transport under real climatic conditions within the modeled sandstone monoliths has been accomplished. Aside from the differences caused by lithology and pore space, the influence of clay layers (heterogeneities) and hydrophobic treatment is also investigated. The impact of lithology and pore-radii distribution is modeled with consideration for i) the single sandstone monolith, ii) the sandstone monolith with clay layers and iii) the sandstone monolith with clay layers and hydrophobic treatment. The modeling results provide a far better understanding of the moisture transport and storage behavior of the sandstones and grant critical clues for the evaluation of weathering behavior dependent on the material properties of sandstones. This chapter was written in collaboration with several co-authors. The measurement and implementation of petrophysical parameters in the modeling software was done by the scientific staff of the Department of Building Physics, TU Dresden. The contribution of the co-authors includes a critical review of the manuscript.

Chapter 6 presents a summarizing discussion of the most important results from chapters 3 through 5. Especially the most sensitive parameter important to the material- and weathering behavior will be compiled in an integrated manner in order to evaluate the construction suitability and durability of sandstones.

Chapter 7 thoroughly summarizes the main conclusions which can be drawn from the results presented in the Chapters 3 through 6.

This thesis incorporates the following publications:

Chapter 3: Stück, H., Ruedrich, J., Siegesmund, S. (2011): Weathering Behavior and Construction Suitability of Dimension Stones from the Drei Gleichen Area (Thuringia, Germany). Environmental Earth Sciences 63:1763–1786; DOI: 10.1007/s12665-011-1043-7.

Chapter 4: Stück, H., Koch R. & Siegesmund, S. (2012): Petrographical and Petrophysical Properties of Sandstones: Statistical Analysis as an Approach to Predicting Material Behavior and Construction Suitability. Environmental Earth Sciences 69/4: 1299 – 1332; DOI: 10.1007/s12665-012-2008-1.

Chapter 5: Stück, H., Plagge, R. & Siegesmund, S. (2013): Numerical Modeling of Moisture Transport in Sandstone: The Influence of Pore Space, Fabric and Clay Content. Environmental Earth Sciences 69/4: 1161 – 1187; DOI: 10.1007/s12665-013-2405-0.

2 Methodology

The methods used in the present study include field analyse for on-site study, laboratory analyses of petrography, petrophysical and weathering properties (Fig. 2.1), statistical analyses as well as numerical modelling. In the following chapter a short review on techniques is presented which were used to perform afore mentioned topics.

2.1 Mapping of Lithology and Deterioration

The field analyses include a mapping of rocks and type of deterioration under natural environment. Therefore in a first step all occurring sandstones were characterized after their lithology and documented in a map with assigned signature. For mapping of deterioration all occurring surface decay was documented, classified and finally represented in a map for deterioration.

2.2 Petrography

In order to determine the petrography of the samples, different methods were used (Fig.2.1).

Non-clay minerals were identified by conventional thin section microscopy (classification after McBride 1963, point counting after Van der Plas and Tobi 1965; fabric, cementation, alteration), supported by scanning electron microscopy (SEM) coupled with cathodoluminescence (SEM-CL) as well as X-ray fluorescence (XRF). In order to further constrain the mineralogy of clays in the samples, clay-mineral fine-fractions were produced by differential settling in distilled water (Atterberg method following Stoke's Law) accelerated by ultra-centrifugation.

Clay mineral analyses were done by XRD analysis on oriented (textured) compounds using a diffractometer in a step scan mode in the range of 2 – 35 °2θ. Preparation, sample treatment and mineral identification followed standard techniques described elsewhere (e.g. Moore and Reynolds 1997). In order to support the identification, especially of clay minerals, samples were further analysed by scanning electron microscopy (SEM), X-ray fluorescence (XRF), cation exchange capacity (CEC), differential thermal analyses (DTA) as well as infrared spectroscopy (IR spectroscopy). An overview on the sample preparation, analytical procedure and interpretation techniques can be found in Hiltmann & Stribrny (1998).

The SEM, SEM-CL and EDS analyses were performed at the GZG whereas the XRD, XRF, CEC, DTA and IR measurements were accomplished by the department of technical mineralogy of Federal Institute for Geosciences and Natural Resources Hannover (BGR).

2.3 Petrophysical Properties

The petrophysical properties were measured at the GZG as well as at the laboratory of Institute of Building physics (TU Dresden). The measurements at the GZG are used in the first and second publication (Chapters 3 and 4). As basis for the numerical modelling of moisture transport-and storage (Chapter 5, third publication), the measurements from the TU Dresden were used, because the numerical algorithms of the software were calibrated to the laboratory techniques used at the TU Dresden.

The petrophysical properties of sandstones can be divided into pore space-, mechanical/elastical-, water transport- and storage properties. The following sections give a brief summary on the analytical techniques used in order to determine these parameters.

2.3.1 Pore Space Properties (Density, Porosity, Mercury Injection Porosimetry)

The effective porosity, matrix density and bulk density were determined with the weight buoyancy method, based on the measurement of dry-, wet-and buoyancy weight following DIN 52102. The dry weight was measured at sample cubes with an edge length of 65 mm after they were conditioned two days in a drying cabinet at a temperature of 60°C. To measure the weight of water-saturated samples, cubes were brought into vacuum stage in a dessicator. After vacuum was reached, samples were saturated with demineralised water for 24 h. The buoyancy weight was measured by submerging the sample cubes in in a water bath with simultaneous weight-measurement by an under-floor balance.

By the three determined parameters masses of a sample in dry (m_d), wet (m_w) and under water (buoyancy, m_b) conditions the parameters bulk density (ρ bulk), matrix density (ρ_r) and effective porosity (Φ) can be determined in accordance to Archimedes Principle by the following equations:

Effective porosity: $\phi = \frac{m_w - m_d}{m_w - m_b} \cdot 100$ [vol.-%]

Bulk density: $\rho_{bulk} = \frac{m_d}{m_w - m_b}$ [kg/cm^3]

Matrix density: $\rho_{mat} = \frac{m_d}{m_d - m_b}$ [kg/cm^3]

m_w= weight of wet sample, m_d= weight of dry sample, m_b=weight of buoyancy

The pore radii distribution was determined by mercury porosity with a Porosimeter 2000 unit of Carlo Erba. As samples for the determination of the pore size distribution cylinders of 10 mm diameter and 40 mm length were used. Sample cylinders were placed in a vacuum cell and evacuated. Afterwards the cell was filled with mercury, which is then forced into the pore space of the sample cylinders by progressively applying high pressure to the cell. The pressure used to force mercury into the the pore

space of the samples is inversely proportional to the pore size, wherefore the pore space dimensions can be calculated based on a combination of Poiseuille´s Law of viscous flow and the Young-Laplace for capillarity by the Washburn equation:

Washburn equation: $$r_p = \frac{-2\gamma\cos\theta}{P}$$

Rp = pore throat radius of capillary pore, γ= surface tension at fluid interface, Θ = liquid-solid contact angle, P= pressure

Thereby every capillary pore radius is characterized by a particular, associated pressure, necessary to push the fluid into the pore (Doveton 1987). This law only is valid at non-wetting fluids with a contact angle of >90° like mercury (141°). The determined pore radii with this method do not correspond to the real pore radii, but to idealized, cylindrical pores and to the radius of entrance. Accordingly, a large pore with a very small pore throat will become filled with mercury at a very high pressure, corresponding to small pores. However, the volume which fills the large pore will finally count to the small pore. For more details see Brakel et al. (1981).

2.3.2 Mechanical and Elastic Properties

The mechanical properties of a sandstone decide whether and when a stress applied lead to a failure of the rock. In the present study tensile and compressive strength were determined.

Compressive Strength

The measurement of (the uniaxial) compressive strength followed procedures suggested in DIN EN 1926. Cylindrical sample with a diameter and height of 50 mm (co-planar end-surfaces) were loaded into a servo-hydraulic testing machine (Universal Testing Machine 1 by the Walter & Bai AG) between two pressure plates and loaded with a strain rate of 10^{-5} s^{-1} until failure. In order to recognize any anisotropy, the compressive strength was determined perpendicular and parallel to the bedding. Based on the measured force until failure (F_{max}) of the sample and the known sample dimensions (A), the uniaxial compressive strength can be determined by the equation

Compressive strength $$\beta_{comp} = \frac{F_{max}}{A_0}$$ [MPa]

F_{max}= maximal force, A_0= initial cross-sectional area [mm^2]

The Tensile Strength

The tensile strength was measured following the Brazilian test (or indirect tensile strength test) according to DIN EN 22024. The experiment was accomplished with a 50 KN load cell with type PCS-200 of Walter & Bai AG. Thereby a cylindrical sample (20 mm height, 40 mm diameter) is subjected to a progressive compressional load in a uniaxial test set-up within two opposite surface lines. Within the specimen a tensile strength is created perpendicular to direction of applied pressure which is

increased by $30Ns^{-1}$. Based on the measured force at failure (F) and the samples diameter (d) and lwngth (l), the tensile strength (σ T) can be calculated by the following equation:

tensile strength: $$\sigma T = \frac{2F}{dl\pi}$$

F = maximum force at failure, d = sample diameter, l = sample length

Young´s modulus

The Young´s modulus (E) is determined from the uniaxial compressive strength (ucs) test and is a measurement of the materials resistance against deformation by an uniaxial force applied to it. Therefore it relates the applied strength (σ) applied and the strain (ε) of this material, by the equation:

Young's modulus $$E = \frac{d\sigma \cdot ucs}{d\epsilon}$$

2.4 Water Transport and Water Storage Mechanisms

The ability of moisture or water absorption is in particular of high importance at sandstones due to their pronounced pore space in general. The transport and storage mechanism can be divided each in liquid and vapour stage.

2.4.1 Coefficient of Water Absorption (w-value, Capillary Water Absorption/Uptake)

When liquid water is present (e.g. rain of groundwater) for a porous medium, capillarity lead to absorption within the pore space. This process is related to the capillary absorption force and is attributed to pore sizes between 1 µm and 1 mm. The process depends on the surface tension of the liquid, and the adsorption forces of the pore wall resulting in the so called capillary suction. The capillary water absorption can be expressed by the water absorption coefficient so called w-value. Therefore a cubic sample with an edge-length of 65 mm was fixed at an under-floor balance upon above a basin filled with water, and the weight every 10 seconds measured with connected software. The w-value is determined by the relationship of capillary water absorption versus time

w-value $$w = \frac{m_w}{\sqrt{t}} \qquad [kg/m^2h^{0.5}]$$

m_w= water absorption [kg/m^2], t = time [h]

The capillary water absorption was measured according to DIN 52103 with an under-floor balance, parallel and perpendicular to the bedding. The measurements were performed on sample cubes (65 x 65 x 65 mm), which were dipped to 5 mm in water. The weight increase was digitally measured every 20 s. The capillary water absorption can be expressed by the water absorption coefficient (w value), which represents the absorbed water amount dependent on area and time ($kg/(m^2*\sqrt{h})$).

2.4.2 Moisture Adsorption (sorption)

Next to liquid water porous materials are also able to absorb water by moisture from atmosphere at their pore surface. The sorption was determined in a climate chamber (Feutron KPK 400) at cylindrical samples of 100 mm height and 20 mm in diameter. First the samples were dried two days in a drying cabinet at 60°C, and afterwards the dry weight determined. In a climatic chamber the samples were exposed a stepwise increased rel. humidity from 15-95% (10%/step) at a constant temperature of 30°C. After each calibration at the particular humidity, the weight was documented and the percentage change calculated.

2.4.3 Water Vapour Diffusion

The permeability of vapour water is an important parameter for the drying behaviour of a sandstone. When a completely wet or soaked sandstone starts to dry, capillarity is the ruling parameter. During further drying, the water vapour diffusion is the main controlling parameter.

Water vapour diffusion was measured with the wet-cup method (DIN 52615) on samples 40 mm in diameter and 10 mm in length. Samples were exposed at 30 °C and a relative humidity of 50 %. The weight was measured four times every 24 h. The water vapour diffusion can be expressed by the dimensionless number of vapour diffusion resistance and is expressed by:

$$\mu = \frac{1}{S} \cdot (\delta_L \cdot A \cdot \left(\frac{p_1 - p_2}{L}\right) - S_L)$$

2.4.4 Saturation degree (S-value)

The S-values comprise describes the proportion of water saturation filled by capillary water uptake. The value was determined according to DIN 52103 and was calculated from the water uptake under atmospheric and vacuum conditions.

s –value = $\frac{w_{atm}}{w_{vac}}$

w_{atm} = water absorption under atmospheric conditions, w_{vac} = water absorption under vaccum

2.5 Weathering Properties

The hygric dilatation was determined in dependence of water saturation and was performed at cylindrical sample of 15 mm in diameter and 10 cm length. A preconditioning of the specimen was achieved by drying in a climatic chamber at 20°C and 15% rel. humidity. The resolution of the displacement transducer amounts 0.5 µm with an accuracy of 1.0 µm.

Salt splitting test were accomplished in order to determine the salt resistance. Salt splitting test were accomplished following DIN 52111 with a 10 % solution of sodium sulphate. The sample cubes (65 mm edge length) were soaked for 6 h in solution and afterwards dried for 12 h in a drying chamber at

60°C. Afterwards, they were weighed and photographically documented. The experiment was ended after reaching 100 cycles or after loss of 40% the original material.

During changes in temperature, all rocks show a change in volume, which results from the increasing movement of the atoms of minerals during heat input. Thermal dilatation tests were made according to the EN 14581 by means of an individual 6 channel inductive dilatometer on cylindrical specimens (Ø 12.5 mm; length 50 mm) along the x and z axes (for details, see Strohmeyer 2003). The specimens were heated uniformly with a temperature change of 0.75°C/min from 20°C to 90/99°C and slowly cooled down to room temperature.

$$\alpha = \frac{\Delta l}{l \cdot \Delta T}$$

α =expansion coeffient [K^{-1}], Δl = length change [mm], ΔT = change of temperature [K^{-1}], l = sample length

2.6 Statistical Analyses

The statistical analyses were accomplished within the large data set investigated in Chapter 4 and is used to identify characteristically sandstone types, for which a specific material- and weathering behaviour can be expected and estimated.

The analyses include i) univariate analyses with normal distribution, ii) bivariate analyses of regression analyes with confidence regions and iii) multivariate analyses with principle component- and cluster analyses. The statistical treatment of the data was performed with the open software “R GUI”.

The distribution of standard parameter of e.g. porosity, density, strength, capillary water absorption and saturation degree was analysed and illustrated with so called whisker-box-plots. This “five-point-summary” consists of the median, two quartiles, extreme values and outliers. The box represents where 50% of the data are distributed and is limited by the upper (75% quartile) and the lower median (25% quartile).The inter quartile range is expressed by the length of the box and also characterizes the degree of scattering. Moreover, the location of median within the box allows an evaluation concerning the skewness of the data distribution. The definition of the eponymous whisker is not consistent in statistics. According to Tukey (1977), the length of the whiskers is limited by 1.5 times the interquartile range. Values, which are located outside of the box, are characterized as outliers.

The relationship between two properties was performed with the bivariate method of linear regression. Thereby, the data were presented in correlation point diagrams. The correlation coefficient of Bravais-Pearson coefficient expresses the relationship of two features and can vary between +1 and -1. A positive value describes a linear relationship with a positive increase, whereas a negative value describes a relationship with a negative increase. Cloud arrangements of points are

characteristic for a no-linear relationship. Additionally, within regression analyses confidence regions with 80% probability range (see also Chapter 4, Fig. 4.1c; ellipsoid) are determined under the assumption that basic properties like e.g. porosity, density or strength show are normal distributed.

The multivariate methods of principle component and cluster analyses were accomplished to analyse the relationship of all measured parameter to each other. Principle component analyses try to reduce a multidimensional problem as it is the case for the material and weathering behaviour of sandstones. In the present study the principal component analyses is illustrated with biplots, which include information on variables (rock properties) and samples in one diagram (see also Chapter 4, Fig. 4.1d) (e.g. Dohrmann and Kühn). The position of variables to each other is expressed by the loadings, which are calculated by the variances of the variables. They are illustrated as arrows, and the position to each other expresses the particular relationship. Arrows pointing in the same direction have a positive relationshipto each other. In contrast, arrows pointing in opposite directions exhibit a negative relationship to each other. If there is no relationship between two properties, arrows stand perpendicular to each other. Samples are depicted as points and the coordinates within the diagram in this multidimensional system are calculated via *scores*, which are based on the *loadings* of the components.

The method of cluster analyses were used for identifying groups of similar sandstones, based on all known properties. The groups defined will not have any similarity to each other. The principle of cluster analysis follows two steps: (1) determination of similarities between the objects and their properties, and (2) determination of the cluster number. The similarity is determined via proximity degree and is calculated with *the Euclidian distance matrix*. For illustration, a so-called dendrogram was used.

2.7 Numerical Modelling of Moisture

The numerical modelling of moisture within the pore space of sandstones is applied to identify the location of moisture accumulations with respect to various climatic conditions, which is essential for characterization and validation zones of subjects for weathering. The software DELPHIN 5 used within the present study is developed at TU Dresden of Institute of Building Physics and is used to model the coupled heat and moisture transfer within porous media.

The modelling is based on complex material functions in which each parameter, which is relevant for water transport or storage, is considered. In order to obtain a most realistic result, for each sandstone modelled a specific material data base was determined.

The calculation of material functions is based on these DIN-values measured on the laboratory of TU Dresden and includes next to porosity, bulk- and matrix density, moisture retention following DIN EN

ISO 12571, water vapour diffusion with wet-cup and dry cup method following EN ISO 12572, sorption following DIN EN ISO 12571 and liquid conductivity measured by flow measurement at saturated samples. Additionally, drying behaviour, heat conductivity and capacity are determined. The pore volume distribution was recalculated by the water retention experiment. For more details the reader is referred to Chapter 5 of the present study and in particular to Scheffler & Plagge (2009) as well as Nicolai et al (2008).

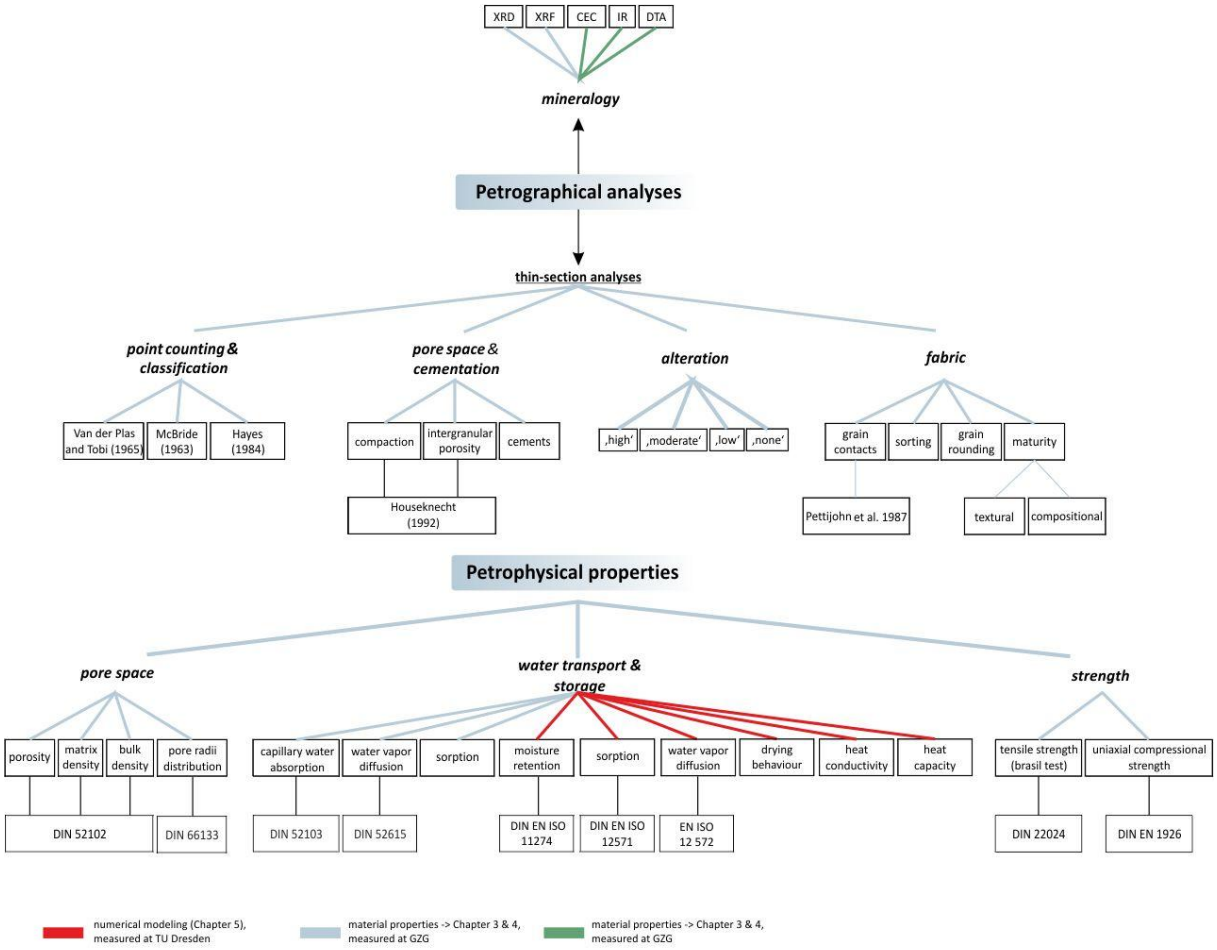

Fig. 2.1: Methods used for the analyses of petrographical and petrophysical properties.

Chapter 3

On-Site Studies on the Weathering Phenomena of Dimension Sandstones

This chapter is largely identical to the manuscript entitled "Weathering Behavior and Construction Suitability of Dimension Stones from the Drei Gleichen Area (Thuringia, Germany)" that is published in Environmental Earth Sciences 63:1763–1786. DOI:10.1007/s12665-011-1043-7.

Authored by: Heidrun Stück • Siegfried Siegesmund •Jörg Ruedrich

3 On-Site Studies on the Weathering Phenomena of Dimension Sandstones

3.1 Abstract

The construction suitability of a dimension stone depends on its weathering properties along with the petrology and the petrophysical properties. The aim of this study was to evaluate the suitability of the dimension stones from the ‘‘Drei Gleichen’’ area for construction and replacement purposes. In total, six sandstones (Ingersleben, Wachsenburg, Hindfelden, Seeberg, Röhnberg, Gleichenberg; Upper Triassic) as well as two carbonates (Wachsenburg sinter; Quaternary, Wandersleben dolomite; Middle Triassic) were analysed. The results from our laboratory and on-site studies of the dimension stones show that rocks from the same stratigraphic layer, like the sandstones from the upper Triassic, can show major differences in their petrophysical and weathering properties. These differences are attributed to their different diagenesis, resulting, e.g. in varying pore space, water balance and strength properties. The pore size distribution can be divided into four different groups based on their occurring maxima and micropore content. The determined water balance properties as well as moisture expansion and salt attack depend on these groups. Next to this, the mineralogical composition significantly influences the weathering resistance. Sandstones with a high content of altered lithoclasts show a high amount of moisture expansion, low strength and, in consequence, a low weathering resistance against salt attack. Based on the results of the present study, an evaluation of construction suitability could be accomplished. From the analysed sandstones, only the Seebergen sandstone is suitable for construction purposes due to its good availability, good strength properties (high compressive and tensile strength, low softening degree) as well as a low porosity. Furthermore, the Wachsenburg sandstone also shows good petrophysical and petrological properties, but exploitable deposits are too sparse to be of commercial interest. From the carbonates, the Wachsenburg sinter shows very suitable rock parameters, but only sparse outcrops occur, which are not appropriate for mining.

3.2 Introduction

The construction of castles in the Middle Ages only used regionally occurring stones and those easily accessible. One example investigated in this study occurs in the Drei Gleichen area of Thuringia. Three castles named after their respective mountaintops were built on sedimentary rocks (Keuper in age) in the Thuringian Basin (Figs. 3.1, 3.2). Due to their geological situation and environment, the late Triassic sediments show a wide range of stones with different petrological and petrophysical properties.

During the Middle Ages, natural building stones were mined because of their availability and easy handling, less so according to certain structural and engineering specifications. Stones were extracted, for example, because of their hardness for use as foundation stones or for their workability, especially when stones were used for complex decorative design purposes. Weathering resistance played a rather unimportant role. Today, however, to preserve historical cultural assets, the exact weathering behaviour of a natural building stone has to be defined in terms of structural and engineering qualifications before being used as a replacement stone (Siegesmund and Snethlage 2011).

Besides the weathering due to thermal expansion, the moisture expansion as well as salt weathering is especially important for the deterioration of sandstones, which often appear in the Drei Gleichen area. Thermal dilation can occur on every rock and is characterised by a volume change during changing temperature. The intensity of thermal dilation depends on the expansion coefficient of the occurring minerals and also on the arrangement of the single minerals.

In most cases, many damage phenomena can be attributed to the volume increase during moisturisation, which is also known as moisture expansion. The deterioration can be observed as a multiple decay phenomena. Backweathering, related to fabric discontinuities, such as bedding and scaling parallel to the surface, is often observed and induced by hygric swelling. Individual decay phenomena mostly superimpose on each other, where the hygric swelling and salt weathering are caused by the infiltration of deleterious salts from the surrounding mortar. This results in the multiple flaking and efflorescence of salts.

The requirements for a replacement stone depend on the compatibility to the other rocks in the structure and on the part of the castle ensemble Drei Gleichen. On a selected part of the castle, the type of stones used as well as their particular deterioration was mapped and documented. Furthermore, thin sections were analysed in detail, and pore size distributions of the surface deterioration were determined. To evaluate the structural and engineering specifications of the stones used, the petrological and petrophysical properties as well as selected weathering mechanisms were investigated and simulated in the laboratory. The material properties of pore

space, water balance and storage, as well as the strength, were determined. For investigating the weathering behaviour, the thermal dilation, moisture expansion and salt loading tests were carried out.mining situation in the area, if the original state of the building is to be reconstructed. The present day mining situation in the Drei Gleichen area for the original stone is concentrated only on the mining of the Seebergen sandstone. The remaining original dimension stones were mined from historical and closed quarries or borrow pits. Therefore, during the restoration work the travertine from Bad Langensalza was also used as a possible restoration stone.

In the present study, the weathering form and deterioration of eight regionally mined stones (Keuper in age) from the Thuringia Basin were investigated at the Castle Gleichen (Gotha, Germany), which is part of the castle ensemble Drei Gleichen. On a selected part of the castle, the type of stones used as well as their particular deterioration was mapped and documented. Furthermore, thin sections were analysed in detail, and pore size distributions of the surface deterioration were determined. To evaluate the structural and engineering specifications of the stones used, the petrological and petrophysical properties as well as selected weathering mechanisms were investigated and simulated in the laboratory. The material properties of pore space, water balance and storage, as well as the strength, were determined. For investigating the weathering behaviour, the thermal dilation, moisture expansion and salt loading tests were carried out.

Fig. 3.1: Overview of the Drei Gleichen area and the buttes consisting of the Rät sandstone. Location of each castle is indicated.

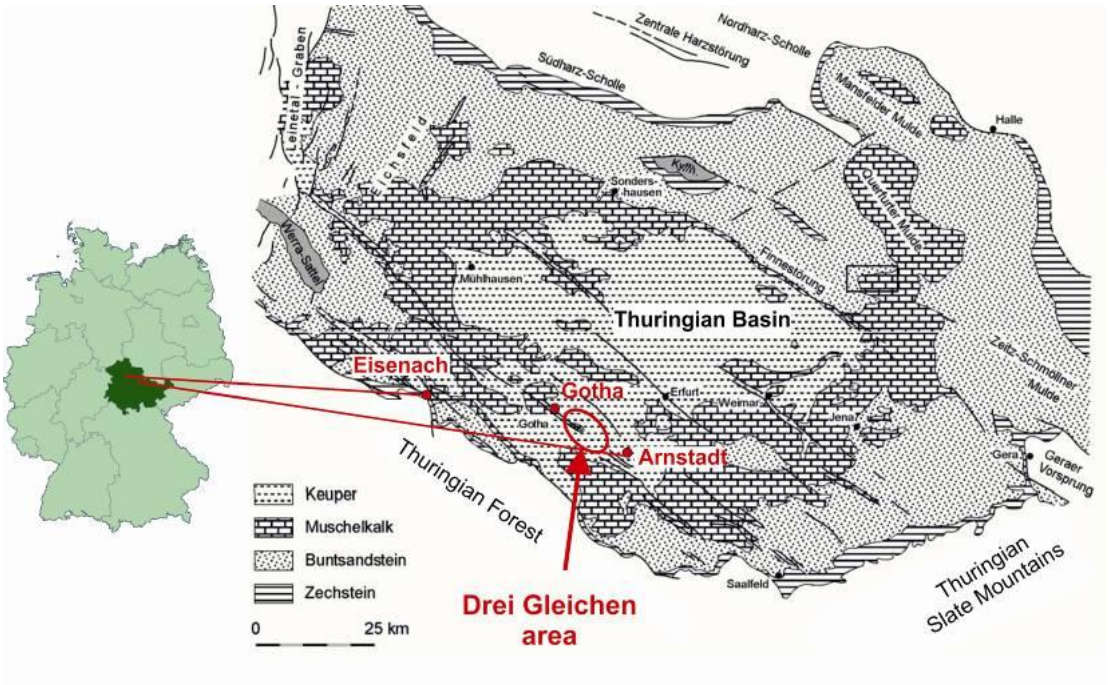

Fig. 3.2: Geological map of the Thuringia Basin and the location of the study area (modified after Puff 1994).

3.3 Geological Context and Building Stones of the Drei Gleichen Area

The Drei Gleichen area is situated in the Thuringian Basin (see discussion in Beutler et al. 2010 and Schubert et al. 2010). It extends 10 km between Arnstadt and Mühlberg in a northwest direction and 3 km in a southwest to northeast direction (Fig. 3.2). The outcrops, ranging in age from Lower Muschelkalk up to the Jurassic (Figs. 3.3, 3.4), mainly consist of Triassic and are also called ‘‘Triassic Land’’. The redcoloured Middle Keuper is the typical rock type in the area, which forms ‘‘together with Upper Keuper’’ the tops of the castle mountains (Wachsenburg, Mühlburg and Gleichen), along with minor outcrops of the Jurassic (Beutler 1980; Siegesmund et al. 2010).

3.3.1 Deposits and Depositional Environments of the Drei Gleichen Area

The sediments of the German Triassic (Figs. 3.3a, b, 3.5) were deposited in the intracontinental German Basin and are divided into lithostratigraphic subgroups of Buntsandstein (red beds), Muschelkalk (chalk) and Keuper (shales). The basin extends from Great Britain to White Russia in a west–east direction and from the Baltic Sea to Bavaria in a north–south direction (e.g. Beutler et al. 2010). This middle European classification is not transferrable to the international classification or the alpine Triassic, which is classified into lower, middle and upper Triassic, based on the occurrence of ammonites. Especially in the Thuringian Basin, the Keuper is classified into regional and locally limited facies.

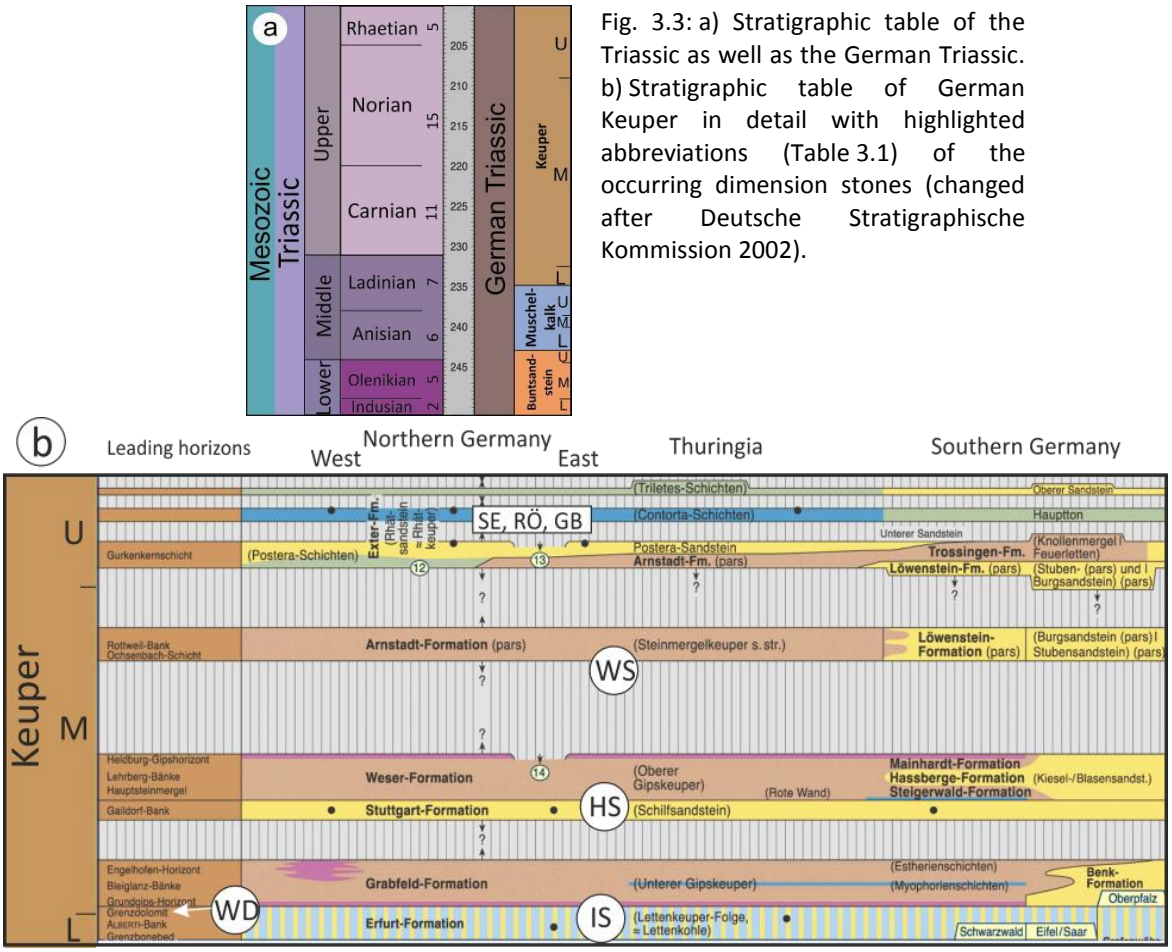

Fig. 3.3: a) Stratigraphic table of the Triassic as well as the German Triassic. b) Stratigraphic table of German Keuper in detail with highlighted abbreviations (Table 3.1) of the occurring dimension stones (changed after Deutsche Stratigraphische Kommission 2002).

In Fig. 3.3 a and b, the geologic timescale of the German Basin of the Triassic is shown in comparison to the international timescale. The basin, lying between the 25° and 35° northern latitude, is situated in a semiarid area. It is surrounded in the north by the Fenno-Scandinavian Shield and in the south by the Bohemian-Vindelizian Shield where different sediments were deposited (Beutler 1980; Beutler et al. 2010, Paul et al. 2008; Wurster1964). During the Buntsandstein, the German Basin was surrounded by the Variscan Orogen, which rapidly eroded due to the arid climate. At the beginning of the Keuper (Lower Keuper), when the former Muschelkalk Sea was regressed, numerous rivers flowed into the basin and deposited large alluvial fans. The transported sediment was deposited at the border of the numerous deltas. The still existing sea with the extension of the Muschelkalk period, eventually flattened out and diminished in size due to the continued deposition, until the basin totally closed. During this time, an extended lagoonal landscape developed with diverse vegetation. In the transitional period between the river system and the lagoonal landscape, local moors arose, which are documented by the brackishmarine delta sediments of the Lettenkohlenkeuper (Lower Keuper/Upper Ladinian). Eponymous for this facies is the locally occurring coal layers (Beutler and Schubert 1987; Paul et al. 2008; Wurster1964). One sandstone from this unit was mined near Ingersleben and was used as a common natural building stone in the region (Table 3.1; Fig. 3.5b).

Continued deposition caused further subsidence, so that a further transgression took place, thus changing the depositional environment from terrigenous to marine. Carbonates with a low thickness and low fossil content developed. One of these horizons is represented by the ‘‘boundary dolomite’’ (Lower Keuper/Lower Ladinian), which not only includes the bivalves such as Costatoria goldfussi but also cephalopods (e.g. Beutler et al. 2010). This stone was also used as a natural building material in the region and was mined near the town of Wandersleben (Table 3.1; Fig. 3.5b).

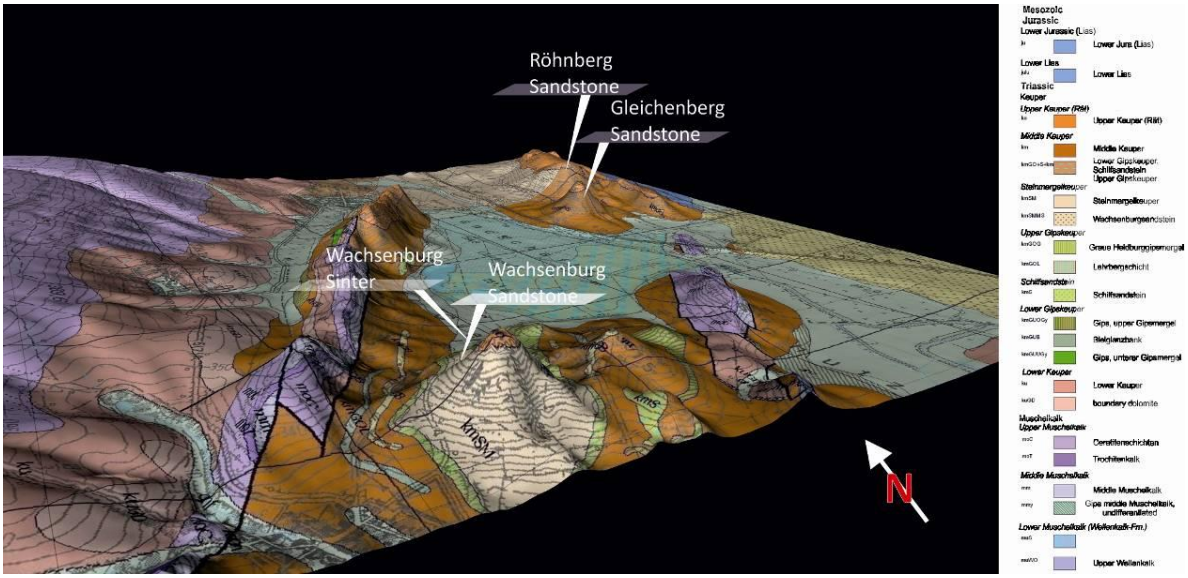

Fig. 3.4: 3-D geologic model of the Drei Gleichen area with the investigated quarries, based on digital contour lines (Landesamt für Vermessung und Geoinformation Thüringen).

At the beginning of the Middle Keuper (Upper Ladinian–Lower Carnian), a predominant saline depositional environment developed, which is called the interior sabkha. The Middle Keuper begins with the gypsum Keuper, which is overlain by the delta facies of the Schilfsandstein (Carnian ~225 Ma). Over the flat shelf that was covered by a marine silt layer (Wurster 1964), the delta arms meandered leaving up to 50 m of fine sand in their channels. The Schilfsandstein was mined as a natural building stone at Hindfelden (near Meiningen, Fig. 3.5c). A further exception in the mainly dominant saline environment is the thin bedded formation of the Semionotus sandstone at the Wachsenburg (Fig. 3.4), which is defined by the presence of fresh- and brackish water fish fossils. This sandstone of low thickness was also used as a natural building stone, mainly for the construction of the three castles (Wachsenburg sandstone, Table 3.1).

Table 3.1: International and German Triassic stratigraphic classification of the investigated sandstones with their mining status (a.m. = active mining, c.q. = closed quarry).

name	abbr.	Stratigraphic Designation of Thuringian Basin	International Stratigraphy	quarry or outcrop
Wandersleben Dolomite	WD	Grenzdolomite (ku)	233-235 Ma Ladinian	glory holes around Wandersleben
Ingersleben Sandstone	IS	Lettenkohlenkeuper (ku) ~ Erfurt Formation		quarry Ingersleben, near Erfurt; c.q.
Wachsenburg Sandstone	WS	„Semionotus-sandstone“/ Wachsenburg (km1)	Norian	strict limited outcrop near Wachsenburg (1 m thickness/120 m long)
Hindfelden Sandstone	HS	Schilfsandstein (km2)	224,5-226 Ma Carnian	Hindfelden near Meiningen; c.q.
Seebergen Sandstone	SE	Rätsandstein (ko)	209-200 Ma Upper Norian-Rhaetian	multiple quarries Seebergen/Gotha; a.m.
Gleichenberg Sandstone	GB			outcrop at Gleichenberg
Röhnberg Sandstone	RÖ			quarry at Röhnberg near the castle Gleichen; c.q.
Wachsenburg Sinter	WT	Holocene (q), calcareous sinter		multiple borrow pits around Wachsenburg

The youngest facies of the Middle Keuper is the Steinmergel Keuper (Norium), which is overlain by the Rät sandstones (Upper Keuper/Rhaetian). Locally the facies is also called the Seeberg Formation. These show evidence of changing depositional environments from low marine to lacustrine-terrestrial. The sediments represent alternating beds of fine sands and mudstones (Seidel 2003). The investigated Rhaetian sandstones form the top of the mountains, where the castles are located and were used for their construction. The localities where the Rät sandstones originate are from (Table 3.1) the Kammerberg at Seebergen (type locality, Fig. 3.5e), and the mountain of Gleichen (Fig. 3.5f) and Röhnberg (Fig. 3.5g). The Seebergen sandstone is still mined today, whereas the quarry at Röhnberg is closed and unapproachable, but still visible at a distance. At Gleichen Mountain, the present mining of the sandstones is not observable.

The Upper Keuper was closed over a period of six million years, ending with a regressive phase and a deposition of limnic mudstones. These were then displaced by the marine sediments of the Lower Lias (Lower Jurassic). At Kallenberg and Röhnberg, a complete stratigraphic sequence from Lias to Dogger (Middle Jurassic) crops out (Ernst 1970). With the beginning of the Lower Dogger, the sedimentation in the Thuringian Basin ended and was interrupted by a new transgression in the Upper Cretaceous. During the Tertiary and Quaternary, the area was completely eroded. The youngest and also the most recently developed sediments are calcareous sinter (Fig. 3.5h) and travertines Holocene in age. They were deposited in the lowest part of the Drei Gleichen valley, in a lixiviation depression. The calcareous sinter deposit at Wachsenburg was also used for construction of the castles.

3.4 The Castles of Drei Gleichen - Construction History

In the present investigation, on-site studies at Castle Gleichen were accomplished. This castle is part of the ensemble ‘‘Drei Gleichen’’, consisting of the castles Mühlburg, Wachsenburg and Gleichen. This ensemble is architecturally very significant, because the structures span the architectural periods from Romanticism to the Renaissance and ending in Historicism. The earliest written reference to a castle in the State of Thuringia is the Castle Mühlburg, which was first mentioned in the year 704. Castle Gleichen attained fame through the legend of the Earl of Gleichen, who was allowed to have two wives. In 1900, a historically correct construction expanded the size of Castle Wachsenburg (Hobohm 2010; Hopf 2010).

Castle Gleichen only has one tower, where the stonework has been reconstructed within the framework of specific safety margins. All the other castle buildings are in ruins. Only a few areas or parts of the castle walls have been restored over the last several years to ensure their structural integrity. For reconstructing the walls and castle buildings, dimension stones from the immediate surroundings were utilised. These consist of travertine, different formations of Rät sandstone, Semionotus sandstone, Grenzdolomite and limestones. Of special interest are the types of mortars applied in connection with the natural building stones used. Gypsum mortars were applied, which were probably produced from the Heldburg gypsum and Grenzdolomite (Keuper in age) located in the immediate area. Other mortars have also been used in the most recent restoration work and these have led to the development of strong salt efflorescences in the stones.

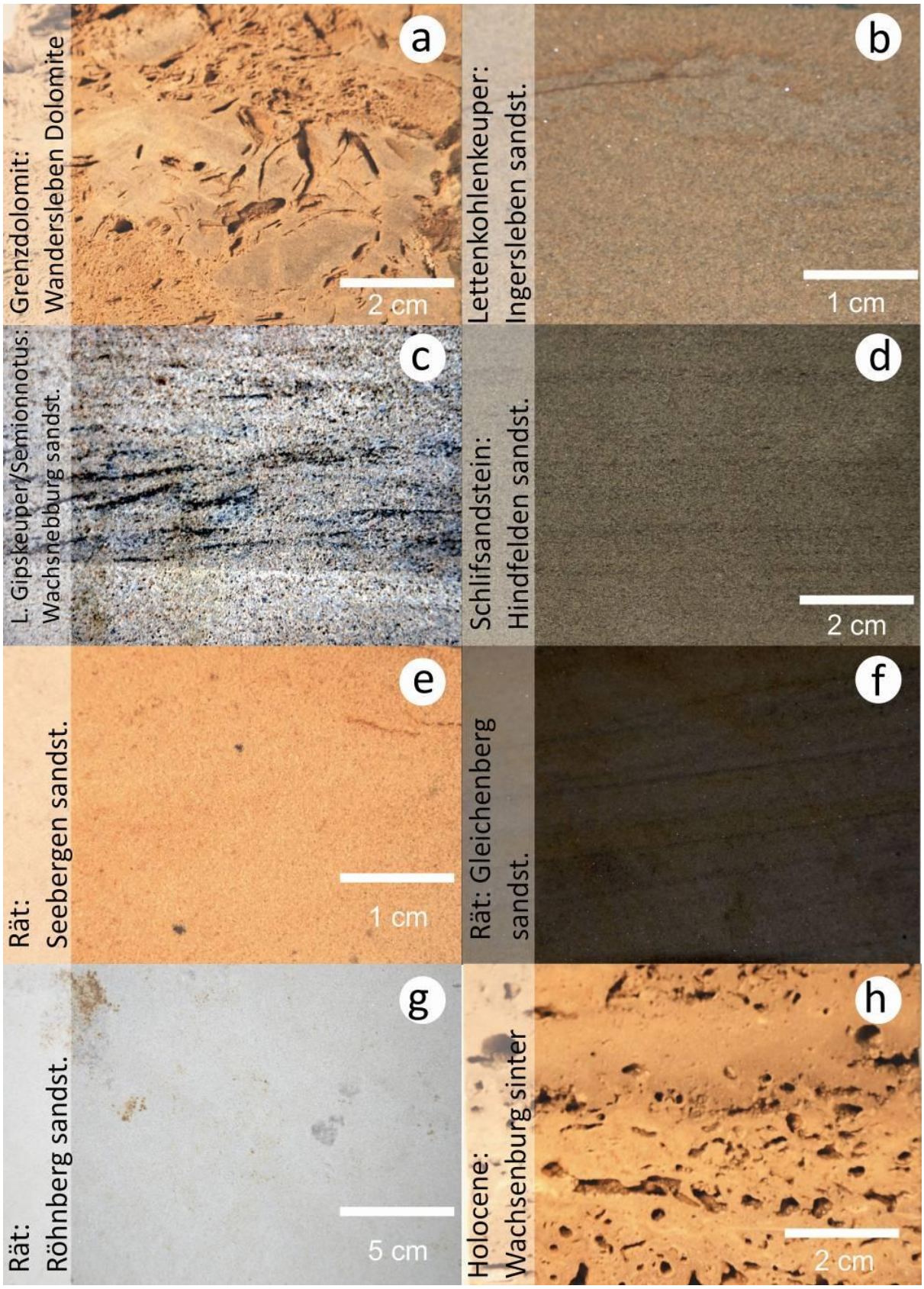

Fig. 3.5: Macroscopic images of the dimension stones occurring at the Drei Gleichen area. Besides the local name, the stratigraphic designation is also given.

3.5 On-Site Studies on Dimension Stones at Castle Gleichen: Mapping of Lithology and Decay Phenomena

The diverse geology of the Drei Gleichen area is suitable for the mining of different dimension stones (Fig. 3.5). During earlier times, borrow pits as well as quarries were created for the construction of the Drei Gleichen castles on the top of the Rät mountains. Based on their petrophysical properties and their petrogenesis, they also show a very different weathering behaviour as rocks used for dimension stones. To determine whether a possible link among the lithology, petrophysical properties and the weathering behaviour of natural building stones exists from the Drei Gleichen area, the rocks were investigated at one of the castles in the Drei Gleichen area. Since nearly all of the occurring dimension stones of the area are still observable at the Gleichen Castle, the investigation of the different weathering shapes was found to be most suitable at this location. The wall mapped in this study is located in the inner part of the Romanesque residential building and is exposed in a west–east direction (Fig. 3.6). After mapping the lithology, all the occurring decay phenomena were classified and divided into categories. With the help of this decay scheme, a mapping of the deterioration was undertaken (see Siedel and Sterflinger 2011).

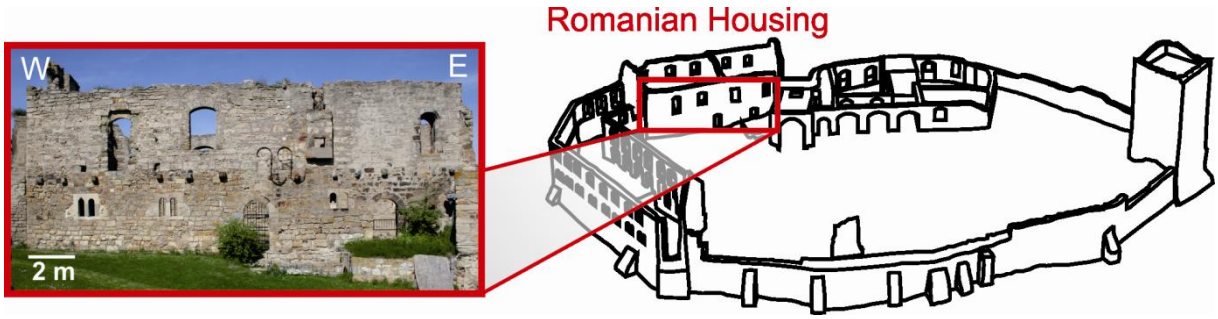

Fig. 3.6: Schematic drawing of the Gleichen Castle with the mapped wall at the Romanesque residential building.

3.5.1 Categories of Decay

The appearing decay phenomena were classified into the categories of displacement, loss of particles and crustal formation. The occurring phenomena were documented in a map according to their intensity as primary, secondary and inferior shapes (Fig. 3.9).

In contrast to the displacement of particles, the whole surface was affected by the loss of material. Here, the stone loss was represented by shapes generated from backweathering and relief. The decay phenomenon is a homogenous loss of material parallel to the surface. Relief is defined for all decay phenomena, which cause a heterogeneous loss of material parallel to the surface (Fig. 3.7a, b). This includes the decay of more resistant areas of the surrounding material. In addition to the rounding of edges and angles, alveolar weathering was also documented as creating relief on the surface (Fig. 3.7a). The latter is characterised by ellipsoid erosion in the stone.

Detachment includes every change on a rock surface, which is characterised by the peeling of the rock or when the material is still in partial contact with the original surface. This also includes sanding, flaking and scaling.

Sanding of the surface means the displacement of millimetre-sized particles or smaller. Flaking is the displacement of loose, small centimetre-sized particles, which peel parallel to the surface (Fig. 3.7c). Sometimes the displacement occurs in a blister-like manner or as a bulging. Scaling includes large-scale displacement parallel to the surface (Fig. 3.7c). Locally, scales up to 4 cm in thickness are observable. Furthermore, the flaking and scaling occur in multiple layers over each other, which is mainly observable at the edges of the natural building stones (Fig. 3.7d). The surface of the scales in general is more lightly coloured than the original intact rock surface.

All decay phenomena, which show a surface accretion of material, belong to the category of crustal deformation. Material accretion is related to visually recognisable changes of the rock surface, including biological settling, crusting and efflorescence. The observed crusts reach a thickness of up to 5 mm.

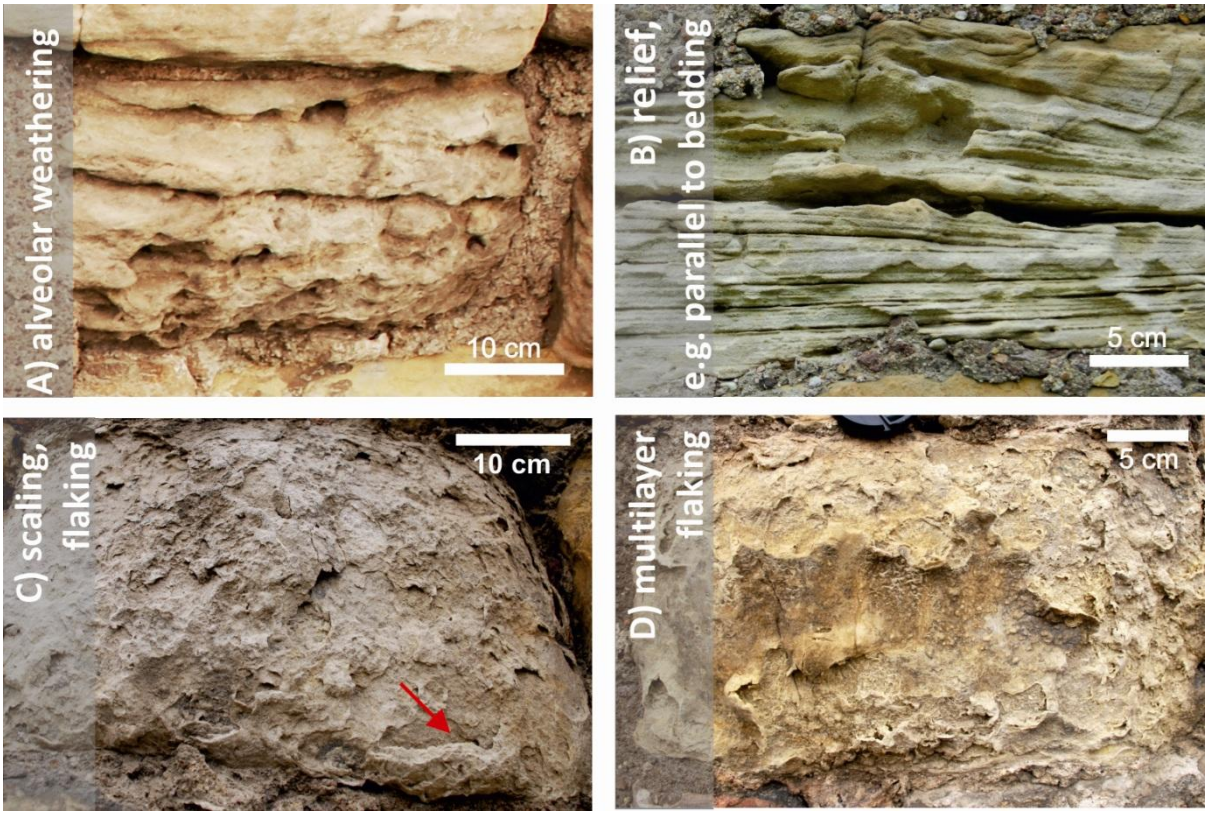

Fig. 3.7: Selected decay phenomena occurring on dimension stones at the Gleichen Castle. a Alveolar weathering of the Gleichenberg sandstone, b relief and back-weathering due to the bedding of the Hindfelden sandstone, c scaling and flaking at the Röhnberg sandstone and d multilayer flaking of the Gleichenberg sandstone.

3.5.2 Mapping of Lithology

From the eight occurring natural building stones in the region, only seven could be observed in the Romanesque residential building (Fig. 3.8). Two different construction phases were also observable by the particular types of building stones used. In the lower part, almost every occurring rock type was applied in the construction, whereas in the upper part only Wachsenburg sinter was used. Decorating elements were made of the soft and easy to sculpt sandstone from Hindfelden. Rät sandstones were used in the lower part of the wall, which originated from Seebergen, Gleichenberg and partially from Röhnberg. Wachsenburg sandstone and the Wandersleben dolomite (Grenzdolomite) were also used. The former was applied continuously in a thin line 1 m up from the bottom, whereas the dolomite was only arbitrarily used (Fig. 3.8). The Wachsenburg sinters were cut into rectangular forms, whereas the lower part of the wall was constructed from Rät sandstones that were uncut.

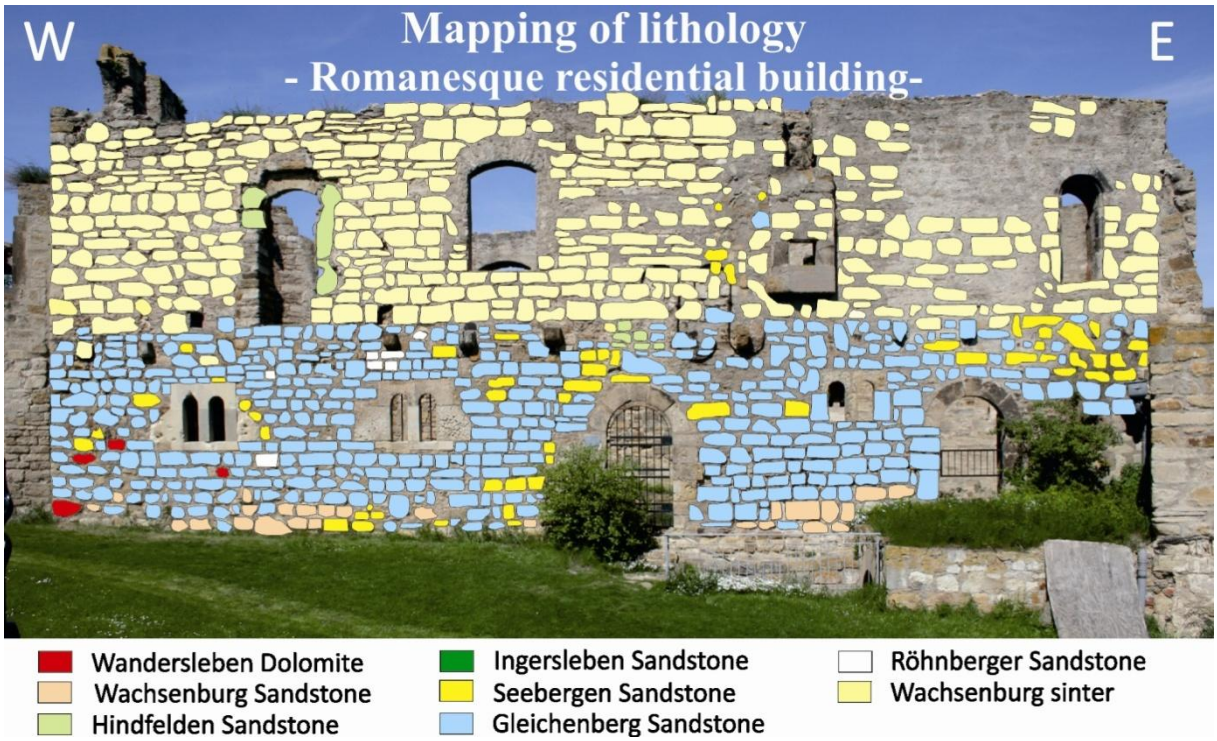

Fig. 3.8: Lithological map of the Romanesque residential building wall.

3.5.3 Mapping of Decay Phenomena

The appearance of decay phenomena (Fig. 3.9) depends on the lithology and the position of the stone within the wall. For example, the travertine shows just a shallow settling of microbes, which is characterised by a darkened surface. The decay is concentrated in the lower part of the wall, where the various lithologies exhibit the different types of decay structures. The Hindfelden sandstone, which is exclusively used for the decorative elements, mainly exhibits a relief controlled by the bedding. In particular, the iron-rich zones are untouched by the weathering. Close to the bottom of the wall (~1 m above the ground), most of the rocks show crusts, efflorescences and reliefs. The

cumulative crusts and efflorescences observable here were probably due to permanent moisture penetration by capillary water entering from the bottom. The salts and crust material most likely originated from the surrounding mortar. Scaling occurred in the lower part, mainly on the Seebergen and Wandersleben sandstone. Directly above the windows, nearly no decay could be observed. However, at the right and left of the windows, highly decayed Rät sandstones with alveolar structures were observable. The Seebergen sandstones often show a previously developed millimetre-thick iron crust on the surface, which are called liesegang rings. Liesegang rings result from a specific weathering process, caused by the diffusion of iron-rich solutions and the precipitation into deeper parts of the rock. They form concentric rings parallel to the surface and are often linked to joints and cracks. The isolated and seldom used Wandersleben dolomite is characterised by the back-weathering of the rock's compact and micritic fabric and shows flaking at the rims. Röhnberg sandstones characteristically exhibit sanding and flaking.

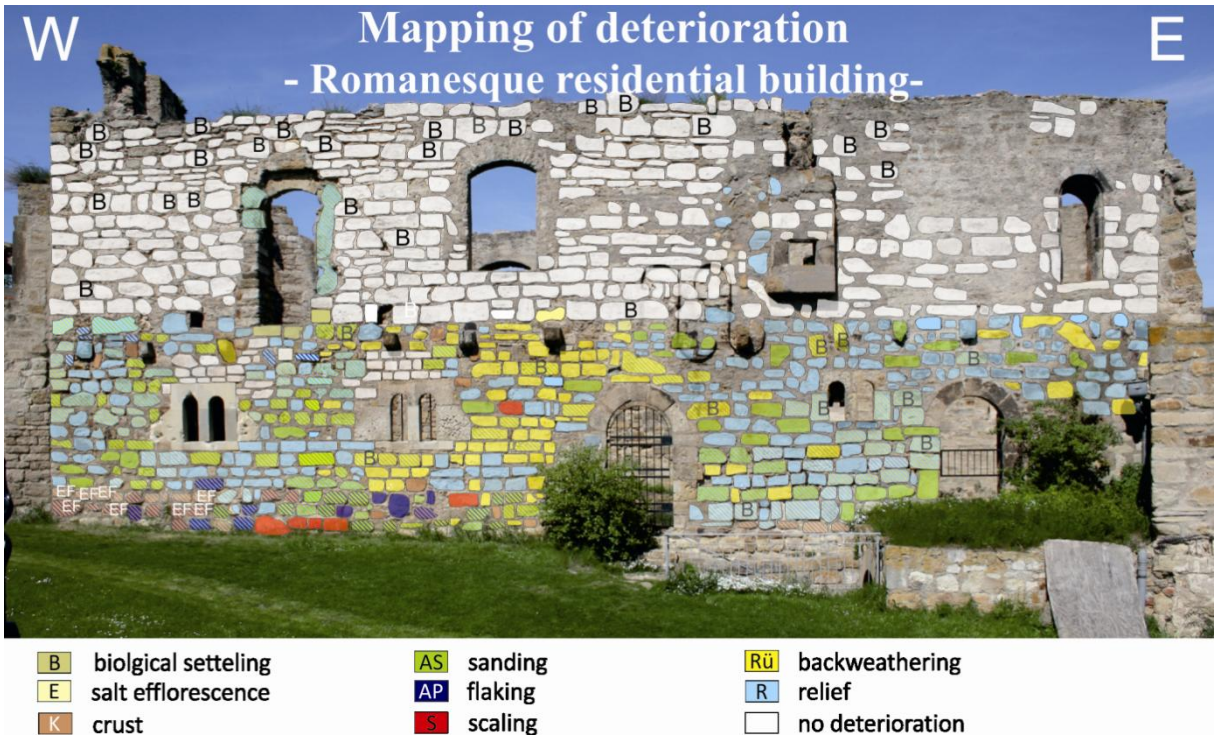

Fig. 3.9: Mapping of deterioration at the Romanesque residential building wall. The dominant deterioration shapes are completely filled, the secondary ones are striped and the subordinate shapes are indicated with a letter.

3.6 Dimension Stones: Petrology and Fabrics

Understanding the geological setting of sandstones is necessary, when considering their use as a natural building stone. The geological setting affects the mineralogical composition, petrophysical properties and to a certain degree the weathering behaviour of natural building stones. The investigation of the mineralogical composition and fabric was done by polarisation microscopy, scanning electron microscope and cathodoluminescence. Observations with the scanning electron microscope can reveal information about the pore space properties as well as the crystallisation of

new minerals in the pore space, which can influence the petrophysical and weathering properties. Cathodoluminescence can uncover information about diagenetic processes and the types of cement phases present (e.g. authigenic quartz), which is critical since it can influence the strength properties of a stone. Using this method, different provenance areas of detrital quartz grains can be determined. In the following section, each of the sandstones will be described in their stratigraphic order (Tables 3.1, 3.2).

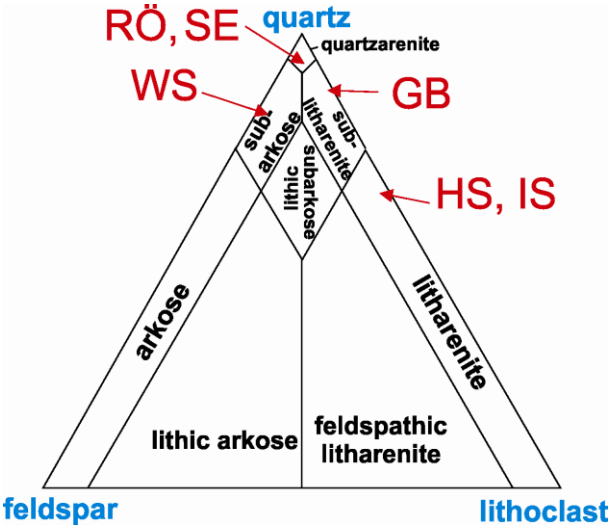

Fig. 3.10: Classification of the investigated sandstones after McBride (1963); for abbreviations see Table 3.1.

3.6.1 Lower Keuper

The Wandersleben dolomite represents the youngest cycle in the hanging wall of the Lower Keuper. This horizon crops out in the northeast and southeast of the Wachsenburg Castle (Wandersleben) and shows an approximate thickness of 2 m. The yellowish-brown, highly porous dolomite is characterised by its high content of fossils of up to 8 mm in size. Microscopic analyses show a sparitic recrystallisation at the fossil rims. The macroscopically visible pores, traced by the hollow space of fossils, only show a weak alignment. Besides the fossil-rich areas, which mainly show a sparitic fabric, a very compact micritic part also occurs (Figs. 3.10, 3.11a).

The fine-grained, yellowish-grey sandstone from Ingersleben is characterised by its well-developed bedding (mm in thickness) and its accumulation of coaled plant particles on bedding planes. The stone consists of 60% quartz, 30% lithoclasts and 10% feldspars. Subordinated mica also occurs. The pseudomatrix comprises about 20%, with isolated grains occurring in the matrix. The grain contact is sometimes elongated, but point contacts are more prevalent. Quartz grains are subangular and the rock is well graded (Figs. 3.10, 3.11c).

3.6.2 Middle Keuper

The white-rose, fine-grained and cross-bedded Wachsenburg sandstone is partially interstratified with thin coal layers (Fig. 3.6c). At the bedding surface, mudcracks can be found. The sandstone

consists of about 75% quartz, 20% feldspar and 5% lithoclasts. The grain contact is concave– convex to sutured and the grading is moderate. The quartz grains are, if not surrounded by quartz cement, subangular to angular. In some areas, the cement is totally composed of silica and in other parts composed of calcite, which induces a very low porosity. Furthermore, the feldspars are mostly altered to clay minerals (Figs. 3.10, 3.11e).

Table 3.2: Overview of sandstones investigated: compositional data, grain size, roundness, grain contact, sorting as well as classification after McBride (1963).

Sample	Qtz/Fsp/Lith ocl.	Grain size max [mm]	Roundness	Grain contact	Sorting	Classification & Comments
Semionotus Sandstone	75% / 20% / 5%	0,45	subangular-angular	concave - convex up to sutured	well-moderate	arkose, strongly altered feldspars, partially calcitic cement, accretional silica
Hindfelden Sandstone	60% / 10% / 30%	0,25	subangular	point	moderate	arkositic litharenite, strongly altered feldspars and micas; micas trace the bedding, chloritisized clasts (volcanic)
Ingersleben Sandstone	60% / 10% / 30%	0,35	subangular	point-elongated	well	lithic arkose, chlorite: primary & secondary, clay fragments, strong altered feldspar: sericite, epidote, calcite; locally hematite, mafic clasts altered to chlorite (blue)
Seebergen Sandstone	95% / 5% / -	0,25	lightly rounded-subangular	convex-concave up to sutured	well	quartzarenite, lightly goethite overlays of quartz grains
Gleichenberg Sandstone	85% / 10% / 5%	0,4	subangular	elongated-point	moderate	sublitharenite, bedding represented by grain size and material changes
Röhnberg Sandstone	90% / 5% / 5%	0,2	rounded-subangular	point-elongated	very well - well	quartzarenite, tangential illite and hematite

3.6.3 Schilf sandstone

The fine-grained, yellowish-brown silty sandstone of Hindfelden is macroscopically characterised by thin iron oxide layers and thin layers of coaled organic material on the bedding plane. The stone is composed of 60% quartz grains, 25% lithoclasts, 10% feldspar and 5% mica chlorite. Furthermore, a pseudomatrix comprises 20% of the rock, which is composed of pelitic lithoclasts. Many clasts are altered to chlorite and are volcanic in origin. The feldspars are strongly altered, and the micas are oriented parallel to the bedding where they developed as kink bands. The quartz grains are subangular, the grains have point contacts and the grading is moderate to well (Figs. 3.10, 3.12a).

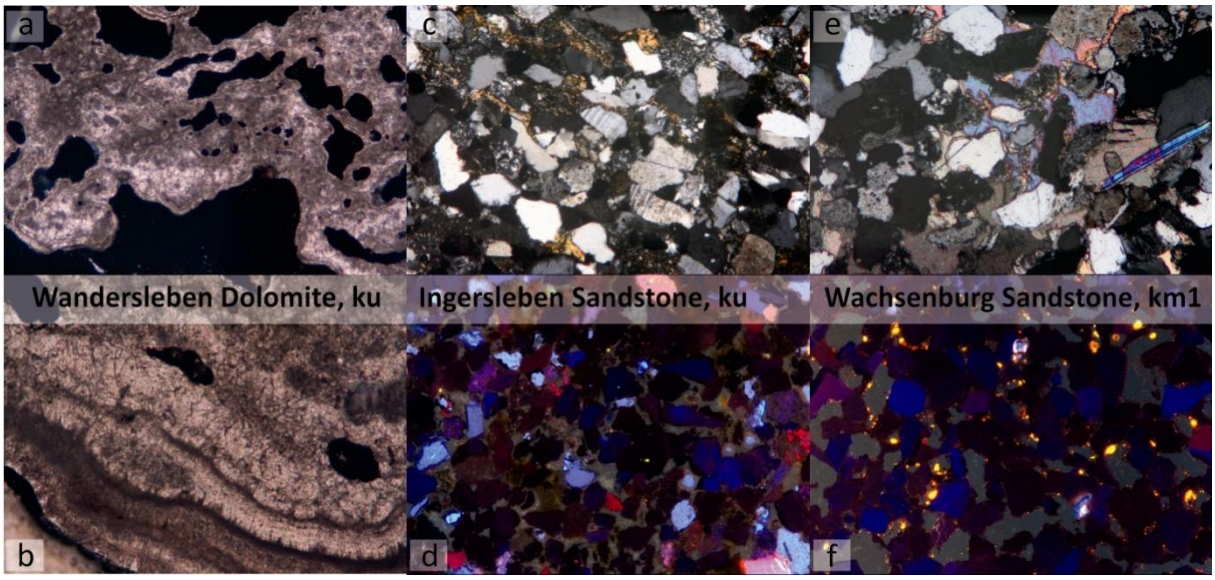

Fig. 3.11: Thin sections and cathodoluminescence (CL) images of (a, b) Wanderleben dolomite in thin section, (c, d) thin section and CL-picture of the Ingersleben sandstone and (e, f) thin section and CL-picture of the Wachsenburg sandstone.

3.6.4 Upper Keuper—Rät Sandstones

The Rät sandstones represent a group of mature sandstones, enriched in quartz grains, and depleted in feldspars and lithoclasts. The yellowish, fine-grained sandstone of Seebergen (Fig. 3.12c) is characterised by local iron oxide precipitations also known as liesegang rings. The stone is composed of 95% quartz and 5% feldspar. After the process of quartz cementation, the quartz grains were coated by iron oxides. The grains are somewhat rounded to subangular, the grain contact is concave–convex and the rock is well graded. The almost white, fine grained Rät sandstone from Röhnberg (Fig. 3.12e) is similar to the adjacent Seebergen sandstone, which contains no visible bedding. Spots of dark brown iron precipitations are recognisable. The stone consists of 90% quartz, 5% lithoclasts and 5% feldspar. The subangular grains are surrounded by tangential illite coatings. The grain contact is pointed to elongated, the grading is very well developed and the quartz grains are, with exception at the grain contacts, coated by illites. The light yellow–grey sandstone from the Gleichenberg (Fig. 3.12g) is characterised by thin bedding. The sandstone is composed of 85% quartz, 10% feldspar and 5% lithoclasts. The grain contacts are almost concave–convex, but sometimes pointed. The bedding is represented by grain size and material changes. Some areas are fine grained and rich in micas and clay, while some other areas are coarser grained, with lower mica and clay contents.

3.6.5 Quaternary (Holocene)

The yellowish-white Wachsenburg sinter is characterised by large-scale pores, which reach a size of up to 5 cm in length. Furthermore, bedding is observable, which is partially formed by completely calcitised plant stripes. In thin section, the plants and fossils show a sparitic fabric, whereas the

surrounding matrix exhibits a micritic fabric (Fig. 3.13a, b). After Dunham (1962), the sinter can be classified as a wackestone.

3.6.6 Microfabrics of the Dimensional Stones

Under cathodoluminescence microscope, the Rät sandstones show more than one provenance of quartz and authigenic quartz in different intensity. Seebergen sandstones contain quartz grains originating from different volcanic, metamorphic and magmatic provenances (Fig. 3.12d). The authigenic quartz coatings are very common. Röhnberg sandstone consists of two types of quartz, magmatic and volcanic. The authigenic quartz content is very low (Fig. 3.12f). The quartzes of the Gleichenberg sandstone originate from volcanic and metamorphic areas. The authigenic quartz is common, but mostly dissolute (Fig. 3.12h). The investigation with the scanning electron microscope shows that the pore space of the Rät sandstones developed differently. Pores, lined with illite coatings (small needles), are observable around the well-sorted quartz grains in the Röhnberg (Fig. 3.14e) and Seebergen, which has little effect on the porosity but reduces the permeability by blocking the pore throats. Furthermore, a loose packing or grain contact in the Röhnberg (Fig. 3.14f) and Gleichenberg sandstones is observable, which mainly show point contacts and cubic packing of grains. Sandstones from Ingersleben and Hindfelden show authigenic quartz cement, where the occurrence is very rare in Ingersleben and very prevalent in the Hindfelden sandstone (Figs. 3.11d, 3.12b). Quartz margins are clearly dissolved. The origin of the quartzes and feldspars is different, and the pink colour of feldspars represents a high alteration. Under the scanning electron microscope, the altered lithoclasts or pseudomatrix of the Hindfelden and Ingersleben sandstones show typical fibrous clay minerals (Fig. 3.14b). Furthermore, hexagonal platelets of kaolinite, which build a network, are observable in the pore spaces of the Hindfelden sandstone (Fig. 3.14c).

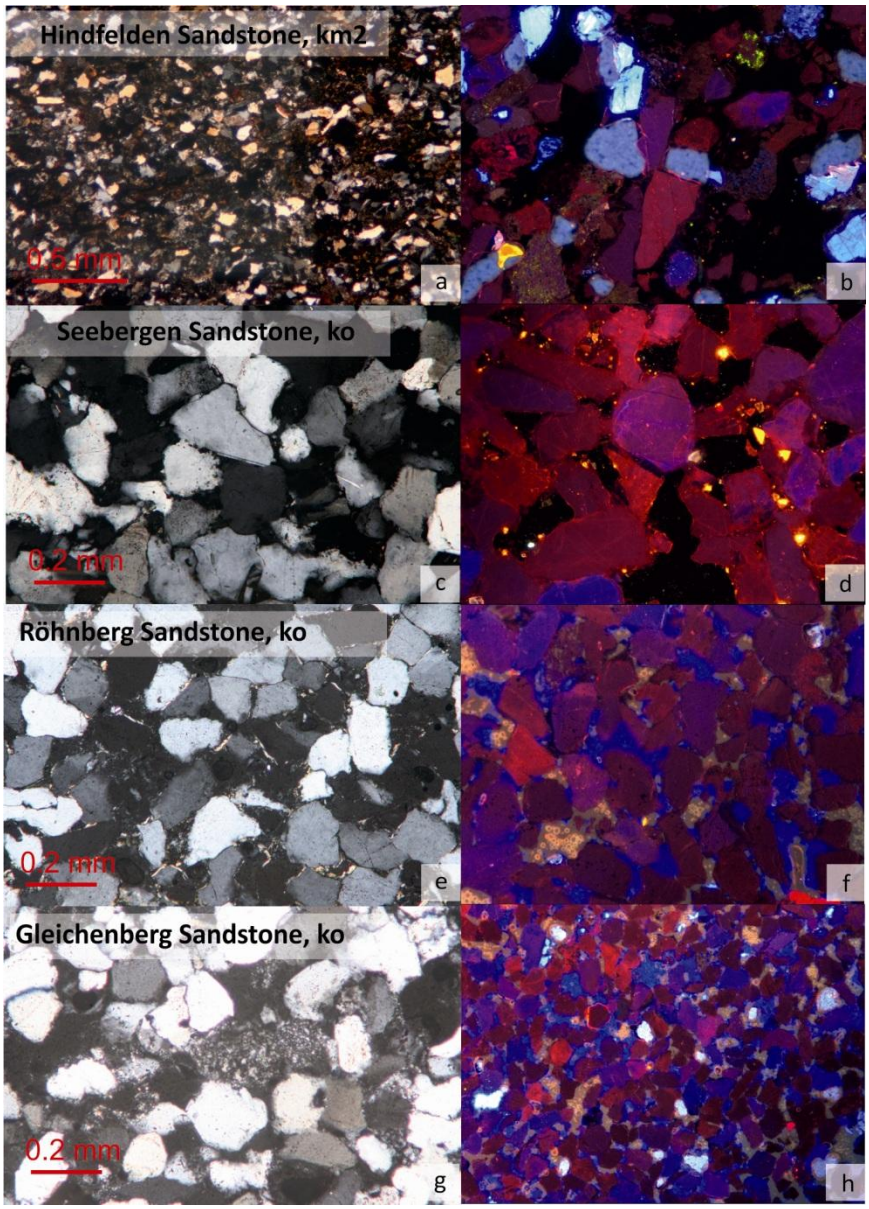

Fig. 3.12: Thin sections and cathode-luminescence images of (a, b) Hindfelden sandstone, (c, d) Seebergen sandstone, (e, f) Röhnberg sandstone and (g, h) the Gleichenberg sandstone.

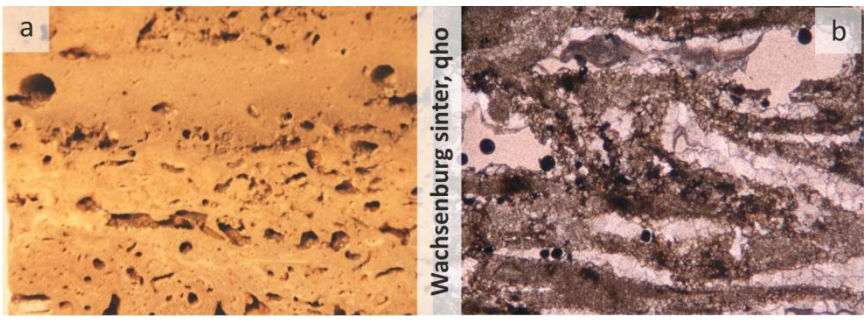

Fig. 3.13: Macroscopic and microscopic images showing the fabric and microstructures of the Wachsenburg sinter.

3.7 Dimension Stones: Petrophysical Properties

Next to the petrology and the fabric properties, the size, distribution and the interconnection of the pore space mainly affect the weathering resistance of natural building stones. These properties make them highly relevant for the water balance in rocks (Fitzner 1988; Fitzner and Snethlage 1982; Putnis et al. 1995; Putnis and Mauthe 2000; Siegesmund and Dürrast 2011). Thus, to characterise the structural and engineering qualifications of natural building stones, it is necessary to analyse the pore

space properties and its influence on the water transport and retention properties. A further important parameter of a building stone represents its strength. This parameter is also strongly controlled by the pore space properties (Ruedrich et al. 2010a, b).

To determine the directional dependence of the petrophysical properties, investigations were carried out on specimens from two mutually perpendicular directions parallel (X-direction) and perpendicular (Z-direction) to the bedding. If the specimens did not show any macroscopically visible fabric elements, an arbitrary coordinate system was defined.

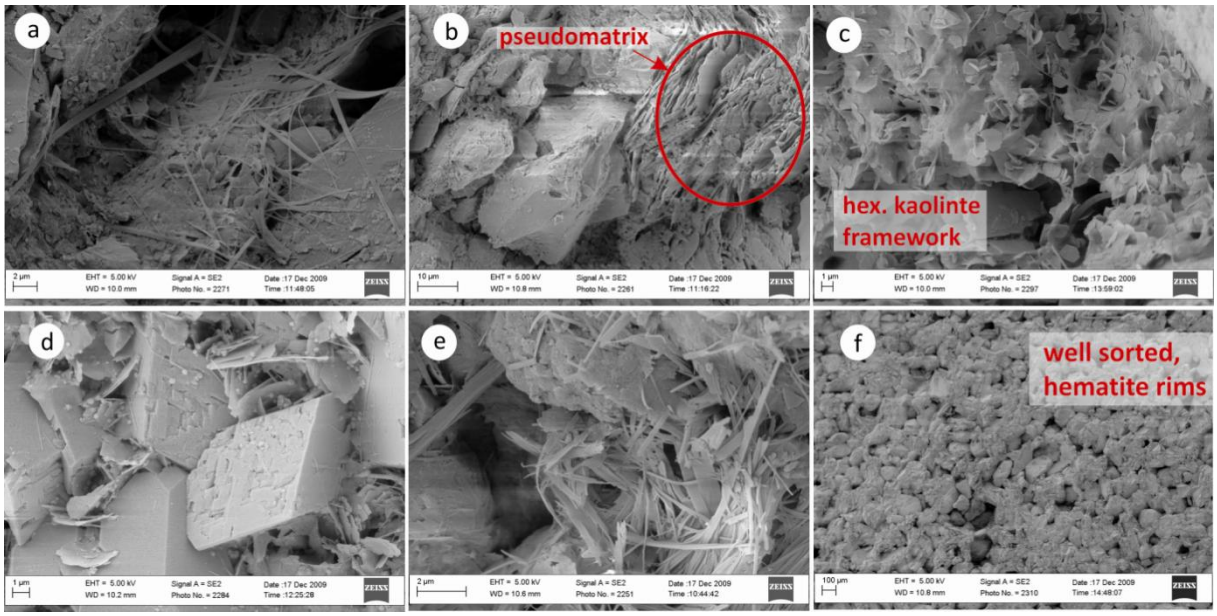

Fig. 3.14: Scanning electron microscope images of the investigated samples. a) Layers of illite over quartz grains in the Ingersleben sandstone. b) The highlighted area marks an altered lithoclast in the Ingersleben sandstone. c) Network of kaolinite platelets in the Hindfelden sandstone. d) Idiomorphic calcite as well as hexagonal kaolinite platelets in the Semionotus sandstone. e) Illite needles above a quartz grain in the Röhnberg sandstone. f) Overview of the wellsorted Röhnberg sandstone with its loose packing.

3.7.1 Porosity, Density and Pore-Size Distribution

The porosity and density were determined according to the DIN 52102 (1988). The investigations were carried out on cubic samples with 65 mm edge lengths. For that purpose, the dry, hydrostatic and water-saturated mass was measured. The dry mass was determined after 2 days of preconditioning the samples at 20°C and 15% relative humidity. The hydrostatic and the saturated mass were detected after water saturation under vacuum.

The porosities of the investigated rocks vary between 8.7 vol.% and 27.7 vol.% (Tables 3.3, 3.4). This range can be divided into three different porosity classes, low (<10 vol.%), medium (10–20 vol.%) and high (>30 vol.%). The Wachsenburg sandstone shows the lowest porosity with 8.7 vol.%. Medium porosities are exhibited by the samples from Seebergen (15.80 vol.%) and the Wachsenburg sinter (16.45 vol.%). All other samples are characterised by a high porosity ranging from 20.08 to 26.75 vol.%.

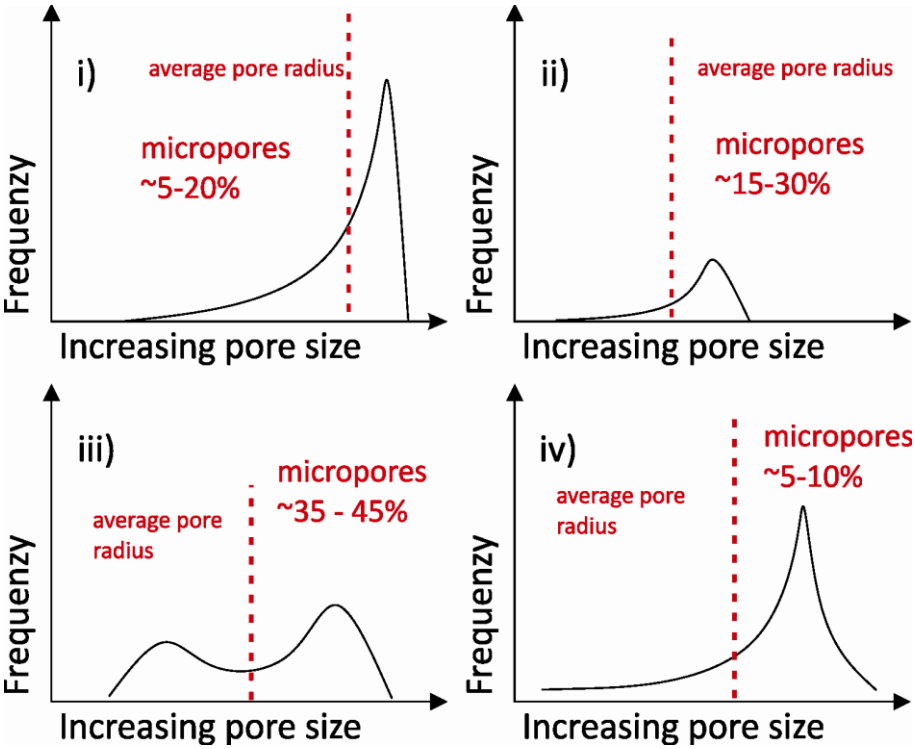

Fig. 3.15: Diagrams depicting the pore size distributions in four distinct groups. The average pore radius is marked by the dashed red line. The amount of micropores is also given for each group.

From the sample masses used for the porosity, the matrix and bulk densities were also calculated (cf. Ruedrich 2010b). The matrix densities were controlled by the rock forming minerals. The sandstones generally show a low matrix density between 2.65 and 2.67 g/cm^3. This correlates with the mineral densities of quartz and feldspar. The Wandersleben dolomites are characterised by a value of 2.88 g/cm^3. The density of the dolomite single crystal is 2.87 g/cm^3 (Tröger 1967), and thus the sample from Wandersleben represents a more or less pure dolomitic rock. In contrast, the Wachsenburg sinter has a matrix density of 2.64 g/cm^3, which is markedly lower than the density of the calcite single crystal (2.72 g/cm^3). This can be traced back to inclusions of material with a lower matrix density. The bulk densities of the investigated rocks show a variation between 1.92 g/cm^3 for the Ingersleben and 2.42 g/cm^3 for the Wachsenburg sandstone. The bulk density was mainly controlled by two parameters: (1) the density of the involved minerals and (2) the porosity of the rock (Table 3.3).

To determine the pore size distribution of the samples, mercury porosimetry was applied (van Brakel et al. 1981). The investigations were carried out with pressures up to 2 kbar, which allows the evaluation of pore radii of about 0.005 µm. Cylindrical specimens (diameter 12.5 x 20.0 mm) were analysed. The pore size distribution shows a large variation. These different patterns can be divided into four types (Figs. 3.15, 3.16): (1) unimodal with one maximum in the range of macropores and a micropore content of <20% (Wandersleben dolomite, Ingersleben, Gleichenberg sandstone), (2) unequal unimodal with one maximum in the range of capillary pores and micropore content between 15 and 30% (Wachsenburg sandstone), (3) unequal bimodal with a high micropore content of 35–

45% (Hindfelden sandstone) and (4) unequal unimodal with one maximum in the range of macropores and a micropore content between 5 and 10% (Seebergen, Röhnberg sandstone). The calcareous sinter covers a wide range of pore sizes with no significant maximum. The average pore radius of the investigated rocks can be subdivided into: small (0–1 µm), medium (1–2 µm) and high (2–5 µm). The medium pore radius varies from 0.24 µm for the Hindfelden sandstone up to 6.87 µm for the Wandersleben dolomite (Table 3.3).

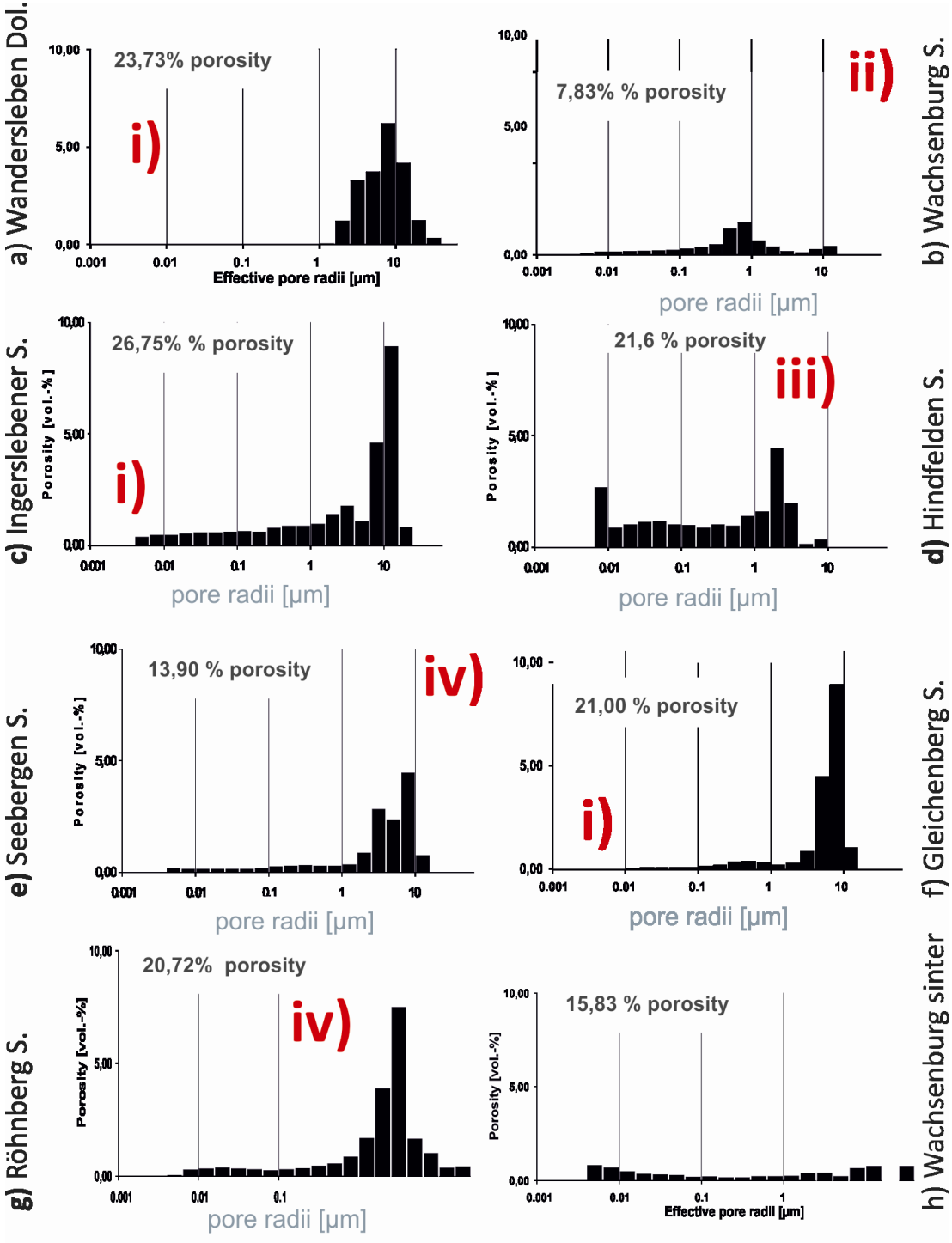

Fig. 3.16: Pore size distributions in the investigated sandstones. The red letters represent the previously explained groups of pore size distribution.

Table 3.3: Pore size distributions and medium pore radius. The most occupied pore size is highlighted.

sample	Pore Class [µm]					
	Micropores		0.1-1	1--10	10--100	Medium Pore Radius[µm]
	0.001-0.01	0.01-0.1				
Wandersleben Dolomite	0.00	0.00	0.00	**71.60**	28.40	6.87
Ingersleben Sandstone	5.83	11.34	13.27	**34.96**	34.60	1.78
Wachsenburg Sandstone	2.80	12.58	**56.48**	22.47	5.67	0.52
Hindfelden Sandstone	13.01	24.75	23.59	**38.64**	0.00	0.24
Seebergen Sandstone	2.05	4.94	9.86	**77.82**	5.33	2.64
Gleichenberg Sandstone	0.00	2.72	8.45	**82.88**	5.95	4.42
Röhnberg Sandstone	1.43	7.39	11.83	**75.65**	3.70	1.58
Wachsenburg Sinter	20.10	21.44	12.50	**25.43**	20.52	0.37

3.8 Water Transport and Retention Properties

The water transport and retention properties of a porous natural building stone considerably affect the weathering behaviour. The water balance of rocks were normally described by the parameters of capillary water uptake, sorption and desorption, degree of saturation and water vapour diffusion. The capillary water uptake was measured according to DIN 52103 (1988) with an underfloor balance, parallel and perpendicular to the bedding. The measurements were performed on sample cubes (65 x 65 x 65 mm), which were dipped 5 mm in water. The weight increase was digitally measured every 20 s. The capillary water uptake can be expressed by the water absorption coefficient (w value, Table 3.4), which represents the absorbed water amount in dependence to area and time (kg/(m^2 √h)). The investigated samples show a wide range of w values from 0.75 kg/(m^2 √h) for the Wachsenburg sandstone up to 20.05 kg/(m^2 √h) for the Ingersleben sandstone. The highest w values are exhibited by the sandstones from Hindfelden, Ingersleben and the Wandersleben dolomite, followed by the three Rhaetian sandstones, Röhnberg, Seebergen and Gleichenberg. Low to very low w values were detected for the Wachsenburg sandstone and the Wachsenburg sinter. In the case of the sandstones, the w values show a pronounced directional dependence. Generally, the highest w values occur parallel to bedding. The reason for this anisotropy is in most cases a grainshape preferred orientation, which is typical for sandstones (Ruedrich et al. 2010a). In the case of the two carbonates (Wachsenburg sinter and Wandersleben dolomite), the anisotropy is only marginally developed. However, in the Wandersleben dolomite, this can be explained by the small interstitial fossils, which are not aligned parallel to the bedding. The sorption/desorption was measured in a climate chamber during a stepwise increase of moisturisation between 15 and 95% relative humidity. Following the relative humidity, a stepwise decrease was performed until the air humidity reached the initial state of 15%. Every humidity stage was held for 24 h. After equilibration the mass of the samples were weighed. Sorption characterises the hygroscopic water uptake and is a degree for the

adsorption of water at the internal surfaces of a rock. The stepwise (10%) increase and decrease of relative air humidity shows the same progress in all the samples, but the intensity is different (Fig. 3.17). Between 15 and 80% relative humidity, the sandstones show a more or less linear weight increase. Above 80% relative humidity, a surge in weight of the samples occurs. The largest increase is exhibited by the sandstones from Hindfelden and Ingersleben. All the other samples show with one percent maximal weight increase (at 95%) a very low hygroscopic water uptake (Table 3.4). The degree of saturation depends on the pore sizes and the interconnection of the pores. The presence of cements can clearly affect the permeability of sandstones. The degree of saturation covers a range from 0.43 for the Rät sandstone of Seebergen to 0.8 for the silty sandstone of Hindfelden (Table 3.4).

The water vapour diffusion coefficient was determined with the ‘‘wet-cup’’ method according to DIN 52615 (1987) and was carried out on disc-shaped samples (40 x 10 mm). The rim of the specimens were sealed up with an adhesive strip and closed over a Teflon fryer. The measurement was accomplished at 20°C and 50% relative humidity in a climate chamber. The change in weight of the water filled Teflon cup was measured in 24-h intervals. The water vapour diffusion (µ value) is a measure of the vapour diffusion through the rock and is mainly controlled by the pore size distribution (Ruedrich et al. 2010a). The non-dimensional l values vary from 9 to 49 (Table 3.4), which indicates only slight differences between the rocks.

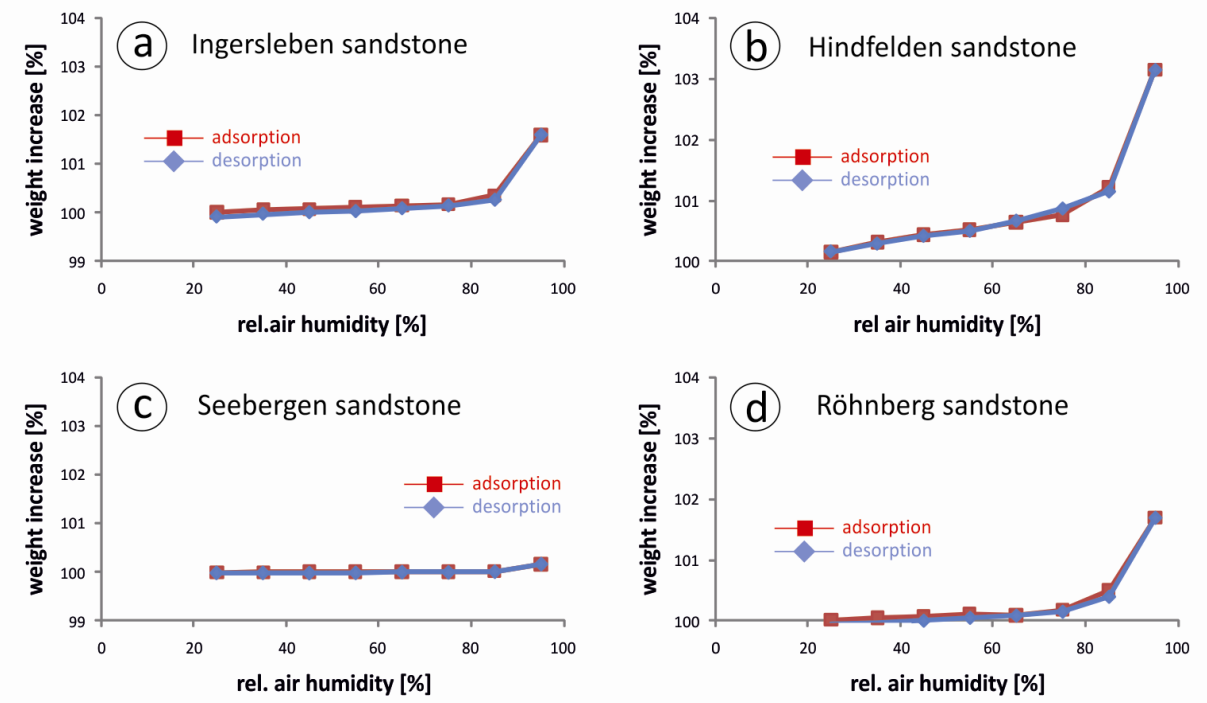

Fig. 3.17: Sorption/desorption in dependence to relative air humidity of a Ingersleben sandstone, b Hindfelden sandstone, c Seebergen sandstone and d Röhnberg sandstone. Red line adsorption, blue line desorption.

Table 3.4: Water transport properties (capillary and hygroscopic water uptake, maximum degree of saturation, water vapour diffusion coefficient) as well as tensile and compressive strength of the specimens.

	Direct.	Wanders-leben Dolomite	Ingers-leben Sandstone	Wachsen-burg Sandstone	Hind-felden Sandstone	Seebergen Sandstone	Gleichen-berg Sandstone	Röhnberg Sandstone	Wachsen-burg Sinter
Porosity [Vol.-%]	-	23.73	27.71	8.71	22.07	15.80	21.87	22.40	16.45
Matrix density [g/cm^3]	-	2.88	2.66	2.65	2.66	2.67	2.66	2.65	2.64
Bulk Density [g/cm^3]	-	2.20	1.92	2.42	2.07	2.25	2.08	2.05	2.21
w-value	X	18.94	24.21	0.98	9.98	4.90	11.85	8.01	0.81
[kg/ m^2 *h$^{1/2}$]	Z	18.56	20.05	0.75	8.50	4.17	10.03	7.50	-
µ-value	-	10.08	5.20	39.90	10.88	22.72	5.80	6.70	18.25
Sorption [%]	-	0.18	1.43	0.40	3.00	0.16	0.50	1.50	0.23
S-value	-	0.57	0.76	0.55	0.80	0.43	0.62	0.54	0.58
Tensile strength [N/mm^2]	X	2.37	1.03	6.04	1.12	5.5	2.99	1.54	2.94
	Z	2.76	1.43	6.57	1.89	6.01	3.91	1.58	3.01
Compressive strength / dry [N/mm^2]	X	40.07	15.21	102.14	21.55	100.82	41.54	34.03	55.34
	Z	42.63	19.59	124.41	25.68	113.07	46.07	31.64	57.08
Compressive strength / wet [N/mm^2]	X	34.89	7.98	93.75	9.81	87.67	30.48	25.46	47.56
	Z	35.12	11.57	114.69	13.45	101.57	34.50	28.54	41.14

3.8.1 Tensile and Compressive Strength

Strength properties such as tensile strength and compressive strength are important rock parameters, which also influence the weathering behaviour of dimension stones. The cause for this is that stresses induced by mechanical weathering processes have to exceed the strength of a material before a failure occurs. Thus, the strength properties are a measure for the grain fabric cohesion. Important fabric parameters for the tensile strength are the grain size, the shape of the grain contacts and a preferred grain boundary orientation. However, of most significance is the type and intensity of cementation. To obtain the values of tensile strength, measurements were made using the Brazil test according to DIN 22024 (1989). The investigations were performed on disc-shaped specimens (40 x 20 mm). By loading the discs in parallel lying surface lines, a tensile strength is induced in the sample perpendicular to the applied pressure. The tensile strength of the sandstones ranges from 1.23 MPa to 6.64 N/mm^2 (Table 3.4). The Wachsenburg and the Seebergen sandstones show high values of 6.24 and 6.63 N/ mm^2, whereas Hindfelden, Ingersleben and Röhnberg only exhibit low tensile strength values up to 2 MPa. The remaining samples show a medium strength. The anisotropy of all the rocks is not very well pronounced.

The uniaxial compressive strength was measured on cylindrical samples (50 x 50 mm) with coplanar end faces (accuracy of 0.1%) in the dry and water-saturated state. The load was applied to the end

faces of the specimen with a strain rate of 1,000 N/s until failure. The compressive strength varied between 16.97 and 113.27 N/mm^2 (Table 3.3). The highest compressive strength in the dry sample state was exhibited by the Wachsenburg sandstone, followed by the Rhaetian sandstones. The compressive strength in the water-saturated state ranged from 7.98 N/mm^2 for sandstone Ingersleben and 93.75 N/mm^2 for Wachsenburg sandstone (parallel to bedding/Table 3.4).

3.9 Laboratory Weathering Tests

The dimension stones show in a natural environment a manifold deterioration (see Chapter 3.4). Several weathering mechanisms are assumed to be responsible for the actual state of the rocks. In general, the weathering can be divided into chemical, physical and biological processes, whereby the single mechanisms overlap each other and lead to multifarious deterioration. To determine and evaluate the weathering behaviour of the dimension stones from the Drei Gleichen area, thermal dilatation, moisture expansion and salt weathering were simulated and accomplished in the laboratory.

3.9.1 Thermal Dilation

During changes in temperature, all rocks show a change in volume, which results from the increasing movement of the atoms of minerals during heat input. Natural building stones are exposed to continuous temperature fluctuations during the cycles of day and night. Thermal dilation was measured by heating the samples from 20 to 90°C followed by a cooling down to 20°C. The length change was detected by an incremental displacement transducer with an accuracy of 1 µm.

All the samples are characterised by an expansion with increasing temperature and during cooling a contraction (Fig. 3.18). The path of the curves proceeds differently: Some samples, such as Seebergen and Semionotus, show a more or less linear progression, whereas other samples show a distinct departure from this linear path. During heating at temperatures ranging between 55 and 85°C, some of the curves clearly show a flattening. This is especially the case for the Hindfelden sandstone, which does not show a linear progression. When reaching a temperature of 55°C, the path runs parallel to the abscissa. Furthermore, at reaching the initial temperature of 20°C, some samples show shrinkage, but different intensities occur based on rock types.

The intensity of thermal dilation mainly depends on the types of minerals present and can be expressed by the thermal expansion coefficient (Table 3.5). The coefficients of the investigated sandstones are very similar, with the exception of the sandstones from Ingersleben and Hindfelden. The mineralogical composition affects the thermal dilation, especially swellable clay minerals, and at least altered lithoclasts and pseudomatrix, enriched in swellable clay minerals. All the four sandstones mentioned above have a high content of altered lithoclasts or pseudomatrix, which also

show a departure from the linear progression. All the samples investigated exhibit an anisotropy, which is very well pronounced in the case of the altered lithoclasts in the stones of Hindfelden and Ingersleben sandstone. The contraction during heating, resulting from clay mineral shrinkage, strongly depends on the kind of clay mineral present. The shrinkage intensity is well pronounced in the case of the Ingersleben and Hindfelden sandstones. These all contain a high amount of altered clay-rich lithoclasts.

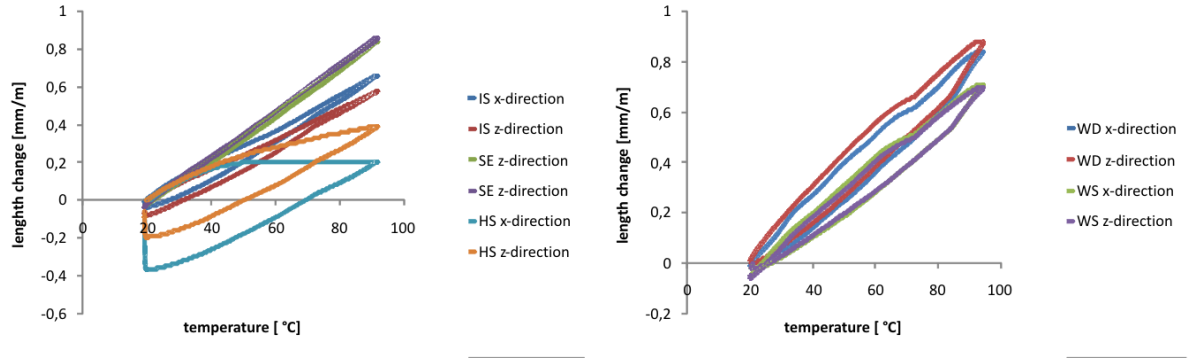

Fig. 3.18: Length change (mm/m) of samples investigated dependent on the temperature.

Table 3.5: Thermal expansion coefficients and shrinkage [mm/m] after measuring.

Sample	x-direction	z-direction	Shrinkage [mm/m]
Wandersleben Dolomite	8.04865E-06	8.013462-06	-
Ingersleben Sandstone	9.0391E-06	7.9079E-06	0.08
Wachsenburg Sandstone	9.9448E-06	1.00715E-05	0.02
Hindfelden Sandstone	2.7675E-06	5.418E-06	0.35
Seebergen Sandstone	1.1658E-05	1.183E-05	0.01
Röhnberg Sandstone	1.1481E-05	1.1935E-05	0.02
Gleichenberg Sandstone	1.15379E-05	1.19331E-05	0.02
Wachsenburg Sinter	8.46775E-06	8.127656-06	-

3.9.2 Moisture Expansion

In many cases, moisture expansion is held responsible for the damages visible in rocks. The swelling and shrinking during changing moisturisation can induce stresses within the rock fabric. In the course of time, this leads to a breaking up of the grain cohesion. Moisture expansion can occur for almost every type of rock (Weiss et al. 2004, Ruedrich et al. 2010a, Siegesmund and Dürrast 2011). However, porous rocks with certain clay mineral content like sandstones show pronounced moisture expansion wetting. Pore spaces with a high content of micropores, in combination with clay minerals (partly swellable) at least in the lithoclasts, is probably responsible for the intensity of this weathering process (Ruedrich et al. 2010a).

In the present study, moisture expansion was measured under water-saturated conditions (hydric wetting). The investigations were carried out on cylindrical samples (100 x 15 mm). A preconditioning of the specimens was achieved by drying in a climatic chamber at 20°C and 15% relative humidity. The final resolution of the displacement transducers was better than 0.5 µm.

The measured swelling during water absorption of the rocks varies from 0.015 mm/m for the Wachsenburg sinter to 5.2 mm/m for the Hindfelden sandstone (both measured parallel to the Z-direction, Table 3.6). In general, quartz-rich rocks like the Rät sandstones show only slight moisture expansion, whereas rocks with a high content of altered lithoclasts like the Hindfelden and Ingersleben sandstones are characterised by large values of moisture expansion.

All investigated rocks show a directional dependence of moisture expansion. The expansion perpendicular to the bedding is in general more pronounced than parallel to the bedding. Sandstones with a distinct bedding show a wellpronounced anisotropy, such as the rocks from Gleichenberg, Ingersleben, Hindfelden and also Wachsenburg.

Table 3.6: Moisture expansion at water saturation [mm/m].

Sample	**moisture expansion [mm/m]**		
	x-direction	**y-direction**	**z-direction**
Wandersleben Dolomite	0.175	0.180	0.190
Ingersleben Sandstone	0.500	0.290	1.800
Wachsenburg Sandstone	0.120	0.050	0.130
Hindfelden Sandstone	2.400	1.800	5.200
Seebergen Sandstone	0.010	-	0.020
Gleichenberg Sandstone	0.110	0.080	0.470
Röhnberg Sandstone	0.130	0.090	0.190
Wachsenburg Sinter	0.016	0.015	0.015

3.9.3 Salt Attack Test

In order to determine the weathering resistance of the investigated samples against crystallisation of salt within the pore space, salt attack tests were performed according to the German VDI 3797. Cubic samples (65 mm edge length) were saturated with a solution of 10% NaSO4 at different cycles. After 6 h of saturation the samples were dried at 60°C for 16 h. Afterwards, the samples were weighed and the macroscopic damages were photographically documented. The experiment was completed after a maximum of 15 cycles. The sample weights as well as the surface consistency of all the rocks were changed by the salt attack test. All samples show after the first test cycle a slight weight increase. This can be traced back to crystallisation of salt within the pore spaces of the rocks without damaging effect. For the following cycles a rock specific weight decrease is observable. This is strong for the Ingersleben sandstone and very slight for the Wachsenburg sinter (Fig. 3.19).

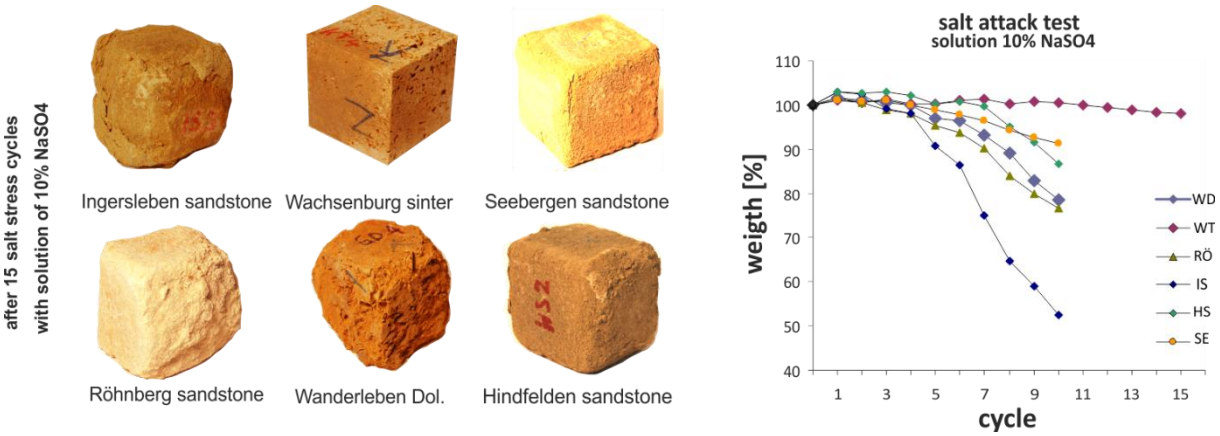

Fig. 3.19: Salt weathering test: damage phenomena of the samples on the left and diagram of the weight change with each cycle.

The decay phenomena observed are different in shape and intensity, and are also specific for each rock. For the Röhnberg and Ingersleben sandstone a first loss of material is observable after the third test cycle. The visible decay phenomena are sanding at the edges, which lead to a rounding of the samples. Furthermore, a crack formation is detectable for the rocks from Röhnberg. In contrast, the Ingersleben sandstone shows a higher variation in the type of decay, besides sanding and rounding, scaling, flaking as well as back-weathering of iron-rich areas occur. The Hindfelden sandstone as well as the Wandersleben dolomite reached a 10% loss of material after five to six cycles. Therefore, the Hindfelden sandstone exhibits a similar decay pattern as the Ingersleben rock. For the Wandersleben dolomite, a back-weathering of the fine-grained, micritic and fossil-rich areas are observable. After ten cycles, the Hindfelden and Ingersleben sandstones as well as the Wandersleben dolomite show a highly rounded and globular shape. In contrast, the Seebergen sandstone exhibits a better salt attack resistance. The rock only shows slight sanding and rounding. The Wachsenburg sinter shows the best weathering resistance within the test. After reaching the 15th cycle, the sample exhibits more or less no loss of material. Also, no decay phenomena are observable.

3.10 Discussion and Summary

The geology of the Drei Gleichen area is dominated by sediments of the Late Triassic age. This sedimentary sequence is characterised by a high diversity of different rock types, where some of the rocks are also suitable for use as dimension stones. Of lesser importance are the younger rocks (Quaternary in age), which mainly occur as exposed outcrops in the floodplain. Regionally quarried rocks were used for the construction of the three castles in the Drei Gleichen area. Eight different building stones were mined, six sandstones (Late Triassic) as well as two carbonates (Late Triassic and Quaternary).

The field observations as well as the laboratory experiments indicate that there are strong differences between the various rock types in respect to their suitability for construction. This is the

result of their respective depositional environment and geological history, which lead to strong variations in the fabric and their petrophysical properties. The investigations have shown that the deterioration of the rocks was mainly controlled by physical weathering processes such as salt crystallisation and moisture expansion. In these processes water transport and retention properties of the rocks play an important role, which are also controlled by the rock fabric and the pore space properties.

3.10.1 Relationship between Petrology and Pore-Space Properties

In general, the porosity of sandstone depends on its diagenesis, where the controlling factors are compaction, cementation or dissolution. However, the (primary) pore size distribution is controlled by the sorting of the sandstone (Füchtbauer 1988; Tucker 2001). The porosity evolution of the six sandstones investigated in this study and their pore size distribution can be classified into mature and immature rocks. The maturity can be divided into compositional and textural sediments. Textural immature sediments are those with poor sorting and angular grains; mature sediments are those with moderate to good sorting and subrounded to rounded grains. The compositional maturity is characterised by the content of stable grains such as quartz in proportion to labile grains consisting of lithoclasts and feldspars (Pettijohn 1975; Folk 1974; Tucker 2001).

The Seebergen, Gleichenberg and Wachsenburg sandstones represent quartz-arenites to subarkoses (Fig. 3.11; Table 3.2) and are characterised by a pronounced textural and compositional maturity. However, the compaction and cementation leads to differences in the porosities. Whereas the Seebergen sandstone exhibits a clearly reduced primary porosity by compaction and quartz cementation, the Röhnberg sandstone shows a low compaction with accompanying point contacts between the grains. Moreover, the well sorting causes a narrow spaced maximum of capillary pores in the pore size distribution of the Seebergen and Gleichenberg sandstones (Fig. 3.16f; Table 3.2). The pore size distribution of the Röhnberg sandstone differs from the other two sandstones. In this case the presence of quartz enclosed by illite coatings also generates smaller pores. The Wachsenburg sandstone exhibits a higher content of feldspar and is poorly sorted. The low porosity was generated by compaction, which is evidenced by numerous pressure solution phenomena and syntaxial quartz growth fringes. Another diagenetic phase of calcite cementation further reduced the porosity. Although all three sandstones form the top of the Rhaetian Hills in the Drei Gleichen area, they show a very different porosity evolution with an accompanying different material behaviour (see explanation below).

The sandstones from Hindfelden and Ingersleben are litharenite in composition (Fig. 3.11) and originated in a fluvial environment. They are compositionally immature (Table 3.2); however, they are moderately to well sorted. In both sandstones, all quartz grains show overgrowths (Figs. 3.11d,

3.12b). Furthermore, alteration and partial replacement of feldspar and lithic clasts are accompanied by the formation of new clay minerals. The replacement increases the volume making up the interstitial matrix, which affects the homogeneity appreciably and gives rise to a greywacke-type of fabric (Tucker 2001). The clay does not retain its shape, but becomes squeezed between more rigid grains. Simultaneously, the porosity increases by the dissolution or replacement of unstable grains. Generally, the alteration from original stable grains or lithoclasts goes along with an increase of smaller pores between the newly generated networks of clay minerals. In the case of the Hindfelden sandstone, the volume of micropores is higher than in the sandstone of Ingersleben (Fig. 3.16c, d).

The porosity development in the two carbonates is due to their different origin in contrast to the sandstones, since delivery coincides with deposit area. Carbonates that develop in shallow water form metastable calcite during deposition and undergo phase transition to stable calcite or dolomite during diagenesis. During the process of diagenesis, grain size can either increase (sparitic growth) or decrease (micritization), as well as the pore space can increase (solution) and decrease (cementation, compaction).

The porosity in the Wandersleben dolomite depends on its genesis and the fossil content, which influences the development of a primary or secondary porosity. The dolomite is generally altered by a secondary process from calcite to dolomite. Since dolomite has a higher density than calcite, vugs or cavities are common for dolomites and creates an increase in the porosity. In contrast, the porosity decreases when calcite is recrystallised and forms a sparitic calcite cement around the fossils. Moreover, when abundant fossils are present large-scale pore spaces are generated, whereas the micritic fabric does not allow the development of micropores. Therefore, the dolomite shows a unimodal pore size distribution with a large average pore size (Fig. 3.16a).

The porosity development of the Holocene non-compacted Wachsenburg sinter mainly depends on the calcified plant particles incorporated into the rock during its formation. Since the plant particles show a size of up to several centimetres in length, the stones are characterised by a well-developed pore space network (Fig. 3.13b). The remaining material consists of micritic calcite, which does not allow for the development of many micropores.

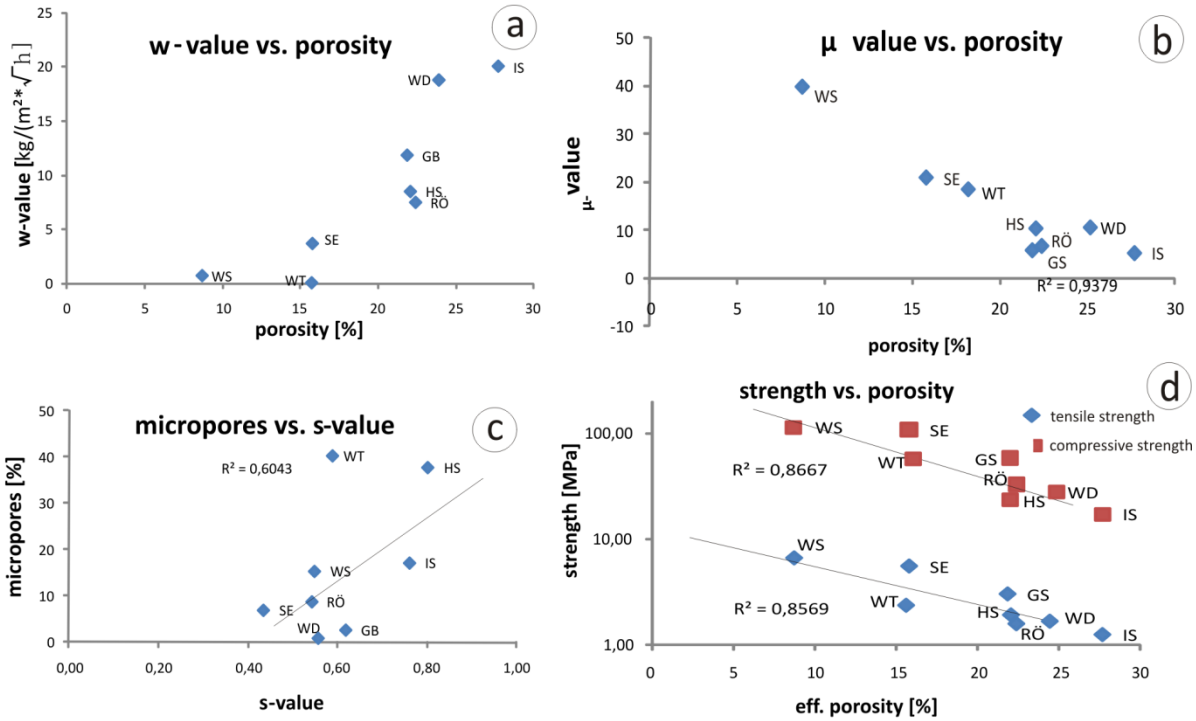

Fig. 3.20: Correlations of petrophysical properties. a w value dependent on porosity, b µ value dependent on porosity, c content of micropores dependent on s value and d tensile and compressive strength dependent on porosity.

3.10.2 Relationship between Pore Space, Water Balance and Strength

The pore space and its properties significantly affects the weathering resistance of a natural building stone, since the pore space coevally rules the water balance (Fitzner 1988; Fitzner and Snethlage 1982; Putnis et al. 1995; Putnis and Mauthe 2000; Ruedrich et al. 2010a). Therefore, properties such as capillary water uptake, water vapour diffusion and saturation degree correlate in the present study with the porosities of the rocks. However, the pore size distribution and the network of single pore sizes among each other defines the intensity of the water uptake (Ruedrich and Siegesmund 2006; Siegesmund and Dürrast 2011) and at least the weathering resistance of sandstones (Fitzner and Snethlage 1982).

The ability of the rocks for capillary water uptake strongly depends on the porosity as well as on (the group of) pore size distributions. In general, the higher the water uptake, the higher is the porosity (Fig. 3.20a). The Wachsenburg sinter does not fit this trend. The large pores of the Wachsenburg sinter cannot connect, and thereby create a network between the few occurring capillary pores.

The Wachsenburg sandstone with a pore size distribution, belonging to group ii (Fig. 3.15) and showing a unimodal distribution with a maximum in capillary pores, exhibits a very low w value. A medium water uptake can be seen in the sample from groups iii (weak bimodal distribution; Hindfelden sandstone) and iv (weak unimodal distribution; Seebergen and Röhnberg sandstone) (Figs. 3.15, 3.16). The samples with the highest w values belong to group i: Wandersleben dolomite,

Ingersleben sandstone and Gleichenberg sandstone (Figs. 3.15, 3.16). This suggests that not only the abundance of capillary pores is important for the intensity of capillary water uptake, but also the connection of capillary pores, which can be confirmed by the saturation degree (s value). The correlation between saturation degree and micropores as well as the sorption (max. weight increase) is nearly linear (Fig. 3.20c). The porosity correlates positively to the capillary water uptake (Fig. 3.20a). If the values deviate from this path, the samples not only show a high amount of macropores, but also a high content of micropores (Fig. 3.16). The observed interconnection between the w value and the (fabric) texture is different. The sandstones with a well-pronounced bedding also show a distinct anisotropy of the w value. The reason for this anisotropy may be the grain shape as well as the orientation of the grains. Parallel to the bedding, the pore space or the network of pores is well developed. Water can easily pass through the rock, and thus the pores build an interconnected network. The anisotropy of the two carbonates is not that well pronounced. In the case of the Wandersleben dolomite this can be explained by the small interstitial fossils, which are not aligned parallel to the bedding. The w value of the Wachsenburg sinter is very small, so that any conclusion concerning the anisotropy is difficult to make.

The water transport via water vapour diffusion also depends on the porosity, but here the higher the l value, the lower is the porosity (Fig. 3.20b). This means that sandstones with a large medium pore radii show a high w value and a low l value. The hygroscopic water uptake depends significantly on the amount of micropores, because the hygroscopic water absorption takes place in smaller pores (Peschel 1983; Klopfer 1985; Siegesmund and Dürrast 2011). Therefore, samples with a high micropore content also show a very high increase in weight at higher humidities. However, some samples do not follow this trend. For example, although the sandstone Seebergen exhibits more or less the same amount of micropores, the hygroscopic water uptake is clearly lower than the Röhnberg sandstone. Most likely the micropores of the Seebergen sandstone are not very well interconnected. In general, the weight increase does not depend on the porosity. Highly porous sandstones, such as the Ingersleben and Gleichenberg sandstone and the low porous Wachsenburg and Seebergen sandstones, can show medium weight increases.

Along with the water balance, the strength in stones is important for the resistance against weathering, because when the strength of a rock is exceeded the fabric begins to disintegrate. The measured tensile and compressive strength in the sandstones depend on these three factors: the porosity (medium pore radii), the grain contact and cementation. Sandstones with low porosity show mainly quartz cementation, concave–convex to sutured grain contacts and they exhibit a high tensile and compressive strength. This type of rock is represented by the sandstones of Seebergen and the Wachsenburg. They show sutured grain contacts as well as quartz cementation and partially calcite cement, which stabilizes the framework and results in a high strength. In contrast, the sandstones

from Hindfelden and Ingersleben are characterised by a highly ductile clayey matrix or lithoclasts that do not allow the formation of stable grains to be built for generating a strong granular grain structure. Moreover, the Rät sandstones from Röhnberg and Gleichenberg show a low strength, caused by is high porosity and the predominant point contact. The observed decrease of strength at the water-saturated state was already mentioned by Hirschwald (1908) and is called ‘‘softening’’. According to Morales et al. 2007 or Siedel (2010), this effect can reach a decrease of 50% in sandstones. In the present study, the Hindfelden and Ingersleben sandstone nearly reach a decrease of this amount. Seebergen and Semionotus sandstones only show a slight decrease through water saturation.

The strength of the two carbonates is, besides the amount of porosity and micritic/sparitic areas, controlled by the heterogeneous distribution of large pores, which is also confirmed by the high standard deviation. Measured samples with an inappropriate distribution of large, elongated pores cannot develop a stable network of calcite, which is why they exhibit a very low strength. In contrast, some areas consisting of smaller pores and a micritic fabric show very high strength properties.

3.10.3 Weathering Properties

The investigation of weathering behaviour on-site and in the laboratory show that many occurring decay phenomena can be traced back to moisture expansion as well as salt crystallisation in the pore space. Moreover, the intensity and shape of deterioration depends on different rock parameters.

Sandstones with a high porosity, high content of micropores and altered lithoclasts ([20%), like the litharenites from Hindfelden and Ingersleben, show very high values for moisture expansion, which is confirmed by the studies of Ruedrich et al. (2010a). The Hindfelden sandstone reaches the maximum length change for sandstones during moisturisation with a value of ~5 mm/m (Schuh 1987; Snethlage and Wendler 1996). In contrast, the quartz arenites and subarkoses with high quartz contents show low porosities and low contents of micropores as well as low moisture expansion values. Furthermore, sandstones with distinctly pronounced bedding, such as Hindfelden, Ingersleben and Gleichenberg sandstones, show a clear anisotropy.

The results of the salt attack tests agree with other studies on German sandstones (Snethlage and Wendler 1996, Fitzner and Snethlage 1982, Rossi-Manaresi and Tucci 1991, Ruedrich et al. 2005, Ruedrich and Siegesmund 2006), where samples with a high amount of smaller capillary pores and micropores are highly sensitive to salt attack. According to Snethlage and Wendler (1996), the pore space properties, such as porosity and pore size distribution, control the solution transportation and restore behaviour, and in consequence also the salt distribution and enrichment in the rock. Thus, a link between the salt attack resistance and the groups of pore size distributions is observable. Rocks

belonging to group i and iii (Figs. 3.16, 3.17) have high amount of micropores and exhibit low resistance during salt attack.

According to Ruedrich and Siegesmund (2007), the different deterioration phenomena during salt attack tests can be traced back to the pore space properties. Sandstones, showing a slow drying rate, exhibit scaling as the main phenomenon. In contrast, sandstones with a high drying velocity show sanding as the prevalent deterioration phenomenon. Moreover, the strength of the rocks seems to influence the sensitivity to salt attack. Rocks, showing a low strength, such as Hindfelden and Ingersleben, are less resistant than rocks with a high strength, like the Wachsenburg sandstone or Wachsenburg sinter. This was also observed by Ruedrich et al. 2005.

3.11 Conclusions - Construction Suitability

The investigation of the material behaviour and the deterioration at the residential building ruins allows an evaluation to be made concerning construction suitability and possible material replacement. Without considering the present day mining situation in the Drei Gleichen area, any possible replacement of deteriorated stones at the building may not be done, if no suitable material can be found in the region. At present, the mining of natural building stones depends on the availability of the material, but less so on the means of transporting the stones. However, luctrative mining is limited by the material behaviour of the rocks.

- In the natural environment, only the Wachsenburg sinter shows a marginal deterioration, which was also verified by the laboratory tests. Besides a low thermal coefficient, the rock shows a minor moisture expansion and a high resistance against salt loading. This behaviour can probably be traced back to its pore space properties, which allows just minor water uptake or water storage in the pore spaces. The other carbonate behaves differently. The Wandersleben dolomite deterioration is characterised by different shapes and intensities. In laboratory tests, the rock exhibits a distinct moisture expansion similar to the sandstones, which also results in decay-like flaking, scaling and salt efflorescence. Here the pore size distribution promotes the capillary water uptake, whereas hygroscopic water uptake is marginal. Simultaneously, the minor strength also allows a slight deterioration through salt loading.

- Even though the sandstones from Seebergen, Röhnberg and Gleichenberg are exposed relatively close and show the same stratigraphical age, they all exhibit a totally different material behaviour. The Seebergen sandstone mainly shows a weak deterioration in the natural environment and in laboratory tests. This is due to its mineralogical composition that results in a high strength. Furthermore, the pore space properties promote a low water uptake. In contrast, under outdoor conditions, the Röhnberg sandstone shows intensive

deterioration in the shape of flaking and sanding. This is due to the grain boundary configuration, e.g. the rock exhibits grain point contacts. The crystallisation of salt in the pore space of this weakly cemented sandstone can easily exceed the strength of the rock. The Gleichenberg sandstone mainly shows deterioration in the form of relief, which is due to its well-developed bedding. In this sandstone, the pore space distribution shows a high water uptake, whereas the grain contact that results in a high porosity causes the rock to have a low strength. All Rät sandstones show a low hygric swelling and also small thermal expansions coefficients, which are the results of the rock's mineralogical composition. Only salt loading causes a difference. Whereas the Gleichenberg and Röhnberg sandstones show a distinct deterioration due to salt (also in the field), the sandstone from Seebergen only exhibits a slight disintegration. Therefore, the Seebergen sandstone can be considered a suitable dimension or replacement stone.

- Next to the Seebergen sandstone, one of the most weathering resistant stones of the Drei Gleichen area is the Wachsenburg sandstone that only occurs as minor exposures. In the field as well as in the laboratory, this stone shows just a weak deterioration, which can be explained by its porosity evolution and the low water uptake and high strength. The water uptake and the strength properties prove that this sandstone meets the structural and engineering specifications for use as a dimension stone. However, the deposit is only locally exposed in a small area below the Wachsenburg, and thus replacing the deteriorated stones with fresh ones is near to impossible.
- The most susceptible stones with regard to weathering in the area are the altered lithoclast-rich sandstones from Hindfelden and Ingersleben. Because of their low strength the stones are easily workable, but also show a low resistance to weathering. The presence of altered lithoclasts as well as an inappropriate pore size distribution results in low strength properties and a high water uptake. Sandstones showing a better water balance but similar strength properties (e.g. lower content of altered lithoclasts) would probably be more suitable as a replacement stone.

Acknowledgments

We would like to thank the Deutsche Bundesstiftung Umwelt for supporting the Drei Gleichen project and the long-term PhD fellowship for H. Stück (AZ 20008/997). Furthermore, gratitude also goes to A. Török for his very helpful comments on an earlier version of this paper and to Chr. Gross for editing the English.

References

Beutler G (1980) Beitrag zur Stratigraphie des Unteren und Mittleren Keupers. Z Geol Wiss 8(8):1001–1018

Beutler G, Schubert J (1987) Fazielle Entwicklung des Mittleren Lettenkeupers im Thüringer Becken. Z Geol Wiss 15:475–484

Beutler G, Schubert J, Siegesmund S (2010) Geologie und Landschaftsentwicklung des Drei-Gleichen-Gebietes. In: Siegesmund S, Hoppert M (eds) Die Drei Gleichen–Naturdenkmäler und Naturraum. Edition, Leipzig, pp 48–62

Deutsche Stratigraphische Kommision, Menning M, Hendrich A (eds) (2002) Stratigraphische Tabelle von Deutschland 2002. ISBN 3-00-010197-7

DIN 52102 (1988) Bestimmung von Dichte, Trockenrohdichte, Dichtigkeitsgrad und Gesamtporosität. Berlin: Beuth

DIN 52103 (1988) Bestimmung von Wasseraufnahme und Sättigungswert. 3 S., Berlin: Beuth

DIN 22024 (1989) Bestimmung der Spaltzugfestigkeit von Festgesteinen. Berlin: Beuth

DIN 52615(1987) Bestimmung der Wasserdampfdurchlässigkeit von Bau- und Dämmstoffen. 5 S., Berlin: Beuth

Dunham RJ (1962) Classification of carbonate rocks according to depositional texture. In: Ham WE (ed) classification of carbonate rocks–a symposium; AAPG Memoirs 1, 108–121, Tulsa

Ernst W (1970) Der Lias am NE-Abhang des Röhnbergrückens (südöstlich von Gotha). Geologie 19.

Fitzner B (1988) Untersuchung der Zusammenhänge zwischen dem Hohlraumgefüge von Natursteinen und physikalischen Verwitterungsvorgängen. Mitt. Ing.-u.Hydrogeologie, 29, Aachen

Fitzner B, Snethlage R (1982) Einfluß der Porenradienverteilung auf das Verwitterungsverhalten ausgewählter Sandsteine. Bautenschutz und Bausanierung. Nr 3:97–103

Folk RL (1974) Petrology of sedimentary rocks. Hemphill Publishing, Austin

Füchtbauer H (1988) Sedimente und Sedimentgesteine.- 4. Auflage. Stuttgart, Schweizerbart, p 1141

Hirschwald J (1908) Die Prüfung der natürlichen Bausteine auf ihre Wetterbeständigkeit. Z. prakt. Geologie 16:257–264

Hobohm C (2010) Sagen und Märchen aus dem Drei Gleichen Gebiet–Eine literarische Wanderung. In: Siegesmund S, Hoppert M (eds) Die Drei Gleichen–Naturdenkmäler und Naturraum. Edition, Leipzig, pp 10–45

Hopf U (2010) Geschichte und Baugeschichte der Drei Burgen. In: Siegesmund S, Hoppert M (eds) Die Drei Gleichen–Naturdenkmäler und Naturraum. Edition, Leipzig, pp 76–101

Klopfer H (1985) Feuchte. In: LUTZ et al (eds) Lehrbuch der Bauphysik. Teubner Verlag, Stuttgart, pp 265–434

McBride EF (1963) A classification of common sandstones. J Sed Petrol 33(3):664–669

Morales M, Jahns E, Ruedrich J, Oyhantc¸abal P, Siegesmund S (2007) The impact of partial water saturation in rock strength: an experimental study on sandstones. Z. dt. Ges Geowiss 158(4): 869–882

Paul J, Wemmer K, Ahrend H (2008) Provenance of Triassic siliciclastic sediments in Central Europe. Z. dt. geol. Ges. 159: 641–650

Peschel A (1983) Natursteine.-2. Auflage, 448 S.; VEB Deutscher Verlag für Grundstoffindustrie, S. 447, Leipzig

Pettijohn FJ (1975) Sedimentary rocks. Harpers u. Brothers, New York

Puff P (1994) Thüringen–Geologische Übersicht 1:400,000. Gotha, Perthes

Putnis A, Mauthe G (2000) The effect of pore size on cementation in porous rocks. Geofluids 1:37–41

Putnis A, Prieto M, Fernandez-Diaz L (1995) Supersaturation and crystallisation in porous media. Geol Mag 132:1–13

Rossi-Manaresi R, Tucci A (1991) Pore structure and the disruptive or cementing effect of salt crystallization in various types of stone. Stud Conserv 36:53–58

Ruedrich J, Siegesmund S (2006) Salt and ice crystallisation in porous sandstones. Environ Geol 52(2):225–249

Ruedrich J, Siegesmund S (2007) Salt induced weathering: an experimental approach. Environ Geol 52:225–249

Ruedrich J, Kirchner D, Seidel M, Siegesmund S (2005) Deterioration of natural building stones induced by salt and ice crystallisation in the pore space as well as hygric expansion processes. In: Siegesmund S, Auras M, Ruedrich J, Snethlage R (eds) Geowissenschaften und Denkmalpfleg. Zeitschrift Deutsche Geologische Gesellschaft, 156/1, 59–73

Ruedrich J, Bartelsen T, Dohrmann R, Siegesmund S (2010a) Building sandstone integrity affected by the process of hygric expansion. Environ Earth Sci. doi:10.1007/s12665-010-0767-0

Ruedrich J, Kirchner D, Siegesmund S (2010b) Physical weathering of building stones induced by freeze–thaw action: a laboratory long-term study. Environ Earth Sci, Special Issue

Schubert J, Klug W, Hopf U, Siegesmund S (2010) Geologische, botanische und burgengeschichtliche Exkursionen. In: Siegesmund S, Hoppert M (eds) Die Drei Gleichen. Naturdenkmäler und Naturraum, Edition Leipzig, pp 312–351

Schuh H (1987) Physikalische Eigenschaften von Sandsteinen und ihren verwitterten Oberflächen. Münchner Geowiss. Abh., 6: S. 66; Enke Verlag, Stuttgart

Seidel G (2003) Geologie von Thüringen, Schweizerbart'sche Verlagsbuchhandlung, Stuttgart, 2. Aufl

Siedel H (2010) Historic building stones and flooding: changes of physical properties due to water saturation. J Perform Constr Facil 24(5). doi:10.1061/(ASCE)CF.1943-5509.0000066

Siedel H, Siegesmund S, Sterflinger K (2011). Characterisation of stone deterioration on buildings, 2011. In: Siegesmund S,Snethlage R (eds) Stone in architecture. pp 347–410. doi: 10.1007/ß78-3-642-14475-2_6 Springer-Verlag, Berlin

Siegesmund S, Dürrast H (2011). Mechanical and physical properties of rocks, 2011. In: Siegesmund S, Snethlage R (eds) Stone in architecture. pp 97–225. doi: 10.1007/ß78-3-642-14475-2_3 Springer-Verlag, Berlin

Siegesmund S, Snethlage R (2011). Stone in architecture. Springer, 4th ed. doi:10.1007/978-3-642-14475-2, Sprinter-Verlag, Berlin, 1–552 pp

Siegesmund S, Grimm WD, Dürrast H, Ruedrich J (2010). Limestones in architecture: the German view. In: Smith B, Gomez-Heras M, Viles H, Cassar J (eds) Limestone in the built environment: present day challenges to preserve the past. Geol Soc Spec Pub London 331:37–59

Snethlage R, Wendler E (1996) Moisture cycles and sandstone degradation. In: Baer NS, Snethlage R (eds) Saving our architectural heritage, the conservation of historic stone structures. Elsevier, Chichester, pp 7–24

Tröger WE (1967) Optische Bestimmung der gesteinsbildenden Minerale, Teil 2: textband. Schweizerbart'sche Verlagsbuchhandlung, Stuttgart, x. Auflage

Tucker M (2001) Sedimentary petrology. Blackwell Science Inc, Oxford, p Revised 272

van Brakel J, Modry S, Svata M (1981) Mercury porosimetry: state of the art. Powder Technol 29: S. 1–12

Weiss T, Siegesmund S, Kirchner D, Sippel J (2004) Insolation weathering and hygric dilatation: two competitive factors in stone degradation. Environ Geol, Special Issue: Stone Decay Hazards, 46/3-4, S. 402–413

Wurster P (1964) Geologie des Schilfsandsteins, Heft 33, S. 140. Mitteilungen des GeologischenStaatsinstitutes, Hamburg

Chapter 4

Statistical Analyses of Petrographical and Petrophysical Properties

This chapter is largely identical to the manuscript entitled "Petrographical and Petrophysical Properties of Sandstones: Statistical Analysis as an Approach to Predicting Material Behavior and Construction Suitability" that is published in Environmental Earth Sciences DOI: 10.1007/s12665-012-2008-1.
Authored by: Heidrun Stück • Roman Koch •Siegfried Siegesmund

4 Statistical Analyses of Petrographical and Petrophysical Properties

4.1 Abstract

Most studies dealing with material properties of sandstones are based on a small data set. The present study utilizes petrographical and petrophysical data from 22 selected sandstones and ~300 sandstones from the literature to estimate/predict the material and weathering behaviour of characteristic sandstones. Composition and fabric properties were determined from detailed thin section analyses. Statistical methods applied consist of data distributions with whisker plots and linear regression with confidence regions for the petrophysical and weathering properties. To identify similarities between individual sandstones and to define groups of specific sandstone types, principal component and cluster analyses were applied. The results confirm an interaction between the composition, depositional environment, stratigraphic association and diagenesis, which leads to a particular material behaviour of sandstones. Three different types of pore radii distributions are observed, whereby each is derived from different pore space modifications during diagenesis and is associated with specific sandstone types: (1) bimodal with a maximum in capillary and micropores, (2) unimodal unequal with a maximum in smaller capillary pores and (3) unimodal equable with a maximum in larger capillary pores. Each distribution shows specific dependencies to water absorption, salt loading and hygric dilatation. The strength porosity relationship shows dependence on the content of unstable lithic fragments, grain contact and type of pore radii distribution, cementation and degree of alteration. Sandstones showing a maximum of capillary pores and micropores (bimodal) exhibit a distinct hygric dilatation and low salt resistance. These sandstones are highly immature sublitharenites–litharenites, characterized by altered unstable rock fragments, which show pointedelongated grain contacts, and some pseudomatrix. Quartz arenites and sublitharenites–litharenites which are stronglycompacted and cemented, show unimodal unequal pore radii distributions, low porosity, high strength and a high salt resistance. The presence of swellable clay minerals in sublitharenites–litharenites leads to a medium to high hygric dilatation, whereas quartz arenites show little hygric dilatation. Sandstones with unimodal equal pore radii distribution mostly belong to weakly compacted and cemented mature quartz arenites. These are characterized by high water absorption and high porosity, low to medium strength and a low salt resistance. The data compiled in this study are used to create a sandstone quality catalogue. Since material properties are dependent on many different parameters of influence, the transition between differentlithotypes is fluent.

4.2 Introduction

Due to their great availability, sandstones are commonly used as a natural stone for buildings, monuments and sculptures. The wide variety of different applications increases the need to understand their characteristic material properties. Complex sedimentary processes are involved in the origin of sandstones. These include the source material, transport processes, the depositional environment and diagenesis. Characterizing and predicting the material properties of sandstone requires detailed investigations of sedimentological, petrographical and petrophysical parameters (Koch and Sobott 2008; Morales Demarco et al. 2007; Ruedrich et al. 2010). Thereby, the characteristics of the pore space such as porosity, permeability and pore geometry are most important for the weathering behaviour of porous sandstones (cf. Fitzner 1988; Fitzner and Snethlage 1982; Putnis et al. 1995; Putnis and Mauthe 2000; Ruedrich et al. 2010). In this context, a linear correlation between porosity and compressive strength and flexural strength as well as water balance and storage properties has been reported by Ruedrich et al. (2010).

However, most of these studies are based on a small data set of samples and parameters. Therefore, general statements covering a wide stratigraphic range and different sandstone types of varying depositional environments and diagenetic development cannot be made. A statistical analysis of the parameters such as grain size, compositional and textural maturity, cementation and fabric, which essentially control the material properties of sandstones, is lacking.

Therefore, the aim of the present study is to establish criteria and systems, which aid in predicting the weathering behaviour of various sandstone types. This is based on a statistical analysis of a large data set that includes most of the parameters generally used when analysing the quality of a sandstone. The study is based on a large amount of petrographical and petrophysical data collected from 300 sandstones described in the literature. Twenty-two of the total samples analysed represent important sandstones used in Germany. These sandstones were investigated in detail by petrographic analysis, determining the fabric characteristics, measuring the petrophysical properties and combining all these data using statistical analyses.

When using data from the literature, it has to be taken into account that the data might not be complete in regard to petrographical analyses and petrophysical measurements. Commonly, just single samples are taken when analysing a quarry, and thus the samples collected may not represent the wide variety of facies types present. For sandstones frequently used, this might be less problematic because only certain qualities are generally regarded. Further possible sources of error may be caused by different approaches during sampling, preparation of samples, different methods and the apparatus used for analysis (Rac and Chernyshev 1970). Data found on the Internet or from company brochures need to be used with caution, since the information may only reflect the

optimum quality but not the natural variations of quality in a quarry. Therefore, the data utilized in the present study originates from scientific non-commercial sources, which deal with material testing and/or research.

4.3 Sedimentary Processes as a Key to Understanding Material Behaviour of Sandstone

The path from unconsolidated sediment to lithified sandstone suitable for construction is controlled by complex sedimentary and diagenetic processes (Tucker 2001). The mineralogical composition of sandstone (compositional maturity) and the textural maturity are dependent on sedimentological parameters (e.g. transport, depositional environment), which contribute to the petrophysical properties, and to a certain degree the weathering behaviour. Diagenesis begins immediately after/with deposition and includes processes of compaction, pressure solution, recrystallization, dissolution, replacement/alteration, clay mineral and feldspar authigenesis as well as cementation by varying mineral phases (Burley et al. 1985; Morad et al. 2000; Tucker 2001; Koch and Sobott 2008). Diagenetic realms include eo-, meso- and telogenetic processes (Choquette and Pray 1970) acting from shallow to deep burial conditions depending on the chemistry of pore water present. The development of pore space geometry through time together with the alteration of grain contacts are parameters of special importance. Cements and compaction lead to the reduction of the primary intergranular pore space. Eogenetic cements also shelter the rock against later compaction during deeper burial (Worden and Morad 2000). Some cement is dissolved by processes forming a late-stage secondary porosity.

Clay material as a primary matrix, pseudomatrix and/or later infiltration into open pore spaces is a significant problem of sandstones with regard to their weathering stability, since they considerably influence porosity and permeability (Houseknecht and Pittman 1992). Neoformation, transformation and alteration of different clay minerals under varying conditions (temperature, pressure and water access) define clay minerals as a special parameter in sandstones that requires careful analysis when characterizing the material behaviour of a sandstone.

4.4 Methods

To support this investigation, a large data set was taken from the literature (Fig. 4.2; Table 4.1) dealing with the petrographical and petrophysical analysis of sandstones (Bartelsen 2008; Seidel 2004; Chitsazian 1985; David 2006; Fitzner 1970; Grimm 1990; Holzwarth 1996; Kirsten 2009; Mosch and Siegesmund 2007). Basic parameters such as porosity, density, water uptake and strength are included for the sandstones from all over the world, partially originating from the natural stone industry and from the data collected in detailed studies dealing with German sandstones.

Petrographical and petrophysical properties of 22 selected sandstones representative for sandstone types from various geological periods were analysed. Standard parameters were measured according to the DIN standards (German Industry Norm) for material testing.

Material parameters measured according to international standards (e.g. DIN) were used without any further adaptation. In contrast, the petrographic data had to be adapted in some cases for the development of a uniform classification. Data quality for grain size and sorting is different depending upon whether detailed analyses are made or just estimations are given. Furthermore, not for every rock each petrophysical property could be found in literature. Therefore, the number of samples shown in the diagrams (see Chapter 4. 3.2) can vary.

4.5 Petrographical Analysis

Thin section analysis was carried out on the 22 representative samples. Classification was done by point counting (Van der Plas and Tobi 1965) and using the classification system of McBride (1963), which allows integrating the weathering sensibility of sandstones (Hayes 1984). Füchtbauer (1988) counts chert and quartzite fragments as a group of rock fragments, whereas in the classification of McBride both are interpreted as stable grains and thus belong to the quartz group. Therefore, in the classification system of McBride, two weathering-sensitive end members and a weathering-resistant one are differentiated.

In the classifications of Gilbert (1954) and Pettijohn (1975), the matrix is generally considered, which is useful for rocks with a matrix content >15 %. Thus, (grey-) wackes are seldom used for construction because of their unsuitable weathering properties and are therefore not considered in the present study. According to this, data from the classification of sandstones investigated by David (2006), Grimm (1990) and Fitzner (1970) were transferred to McBride's classification. Fabric parameters determined by thin section analysis are grain contacts, sorting (Pettijohn et al. 1987), roundness as well as textural and compositional maturity. Grain size analyses determined by thin section do not completely correspond to grain sizes measured by sieving as discussed by Müller (1964). The visible intergranular porosity and amount of cements were estimated to acquire information about the compaction history. The data were plotted in the ''Houseknecht diagram'' (Houseknecht 1992). Besides the classification of maturity by McBride (1963), the varying degrees of alteration, reflecting increasing alteration of unstable components such as feldspar and lithoclasts, were subdivided into the classes (1) high, (2) moderate, (3) little and (4) no degree of alteration.

X-ray diffractometry (XRD) and X-ray fluorescence were applied to determine the bulk and clay mineral composition of selected sandstone samples. The cation exchange capacity for crushed whole rock samples was analysed using Cu(II)-triethylene tetramine. X-ray diffraction was done for grain size fractions of <2 µm. Grain size fractions <2 µm were collected from fractions <63 µm by

differential settling in distilled water, i.e. by using the Atterberg method following Stoke's law. The collected sample is prepared by placing them onto ceramic plates, air dried and coated with ethylene glycol. The samples were measured at 2Θ = 2°–35° with 0.02° and 3 s per step.

4.6 Petrophysical Analyses

Petrophysical parameters including data on the pore space, strength as well as water transport and storage were determined according to the DIN standards. Porosity, matrix density and bulk density were measured in accordance with DIN 52102. The dry mass was determined on samples after 2 days of preconditioning at 20 °C and 15 % relative humidity. The hydrostatic and the saturated mass were detected after water saturation under vacuum. Pore radii distribution was accomplished on cylindrical samples (10 mm in diameter, ca. 20 mm in length) using mercury porosimetry (van Brakel et al. 1981; porosimeter 2000 Carlo Erba). The pressures used up to 2 kbar allow the evaluation of pore radii of about 0.005 µm. The capillary water absorption was measured according to DIN 52103 with an under-floor balance, parallel and perpendicular to the bedding. The measurements were performed on sample cubes (65 x 65 x 65 mm), which were dipped to 5 mm in water. The weight increase was digitally measured every 20 s. The capillary water absorption can be expressed by the water absorption coefficient (w value), which represents the absorbed water amount dependent on area and time (kg/(m^2*√h)). The saturation degree was calculated from the water uptake under atmospheric and vacuum conditions on the same samples. Water vapour diffusion was measured with the wet-cup method (DIN 52615) on samples 40 mm in diameter and 10 mm in length. Samples were exposed at 30 °C and a relative humidity of 50 %. The weight was measured four times every 24 h. The sorption/desorption was measured in a climate chamber during a stepwise increase of moisture between 15 and 95 % relative humidity. A stepwise decrease was performed until the humidity reached the initial level of 15 %. Every humidity level was held for 24 h. After equilibration, the mass of the samples was weighed.

The tensile strength was measured using the Brazil test according to DIN 22024. The uniaxial compressive strength was measured on cylindrical samples (50 mm x 50 mm in size) with coplanar end faces (accuracy of 0.1 %) in the dry and water-saturated state. The load was applied to the end faces of the specimen with a strain rate of 1,000 N/s until failure.

4.7 Analysis of Weathering Properties

The hygric dilatation was determined in dependence of the water saturation. In general, the expansion is determined with an incremental displacement transducer (resolution about 5 µm) on samples of 10 cm in length and 15 mm in diameter. A preconditioning of the specimens was achieved by drying in a climatic chamber at 20 °C and 15 % relative humidity. Salt splitting tests were

accomplished following DIN 52111 with a 10 % solution of sodium sulphate. The sample cubes (65 mm edge) were soaked for 6 h in solution and afterwards dried for 12 h in a drying chamber at 60 °C. After this, they were weighed and photographically documented. The experiment was ended after reaching 100 cycles or after a loss of 40 % of the original material. The salt weathering resistance of sandstones analysed as well as data from David (2006) were grouped as follows:

Group A = no material loss until the 100th cycle

Group B = 50 % material loss until 30–40 cycles

Group C = lose 50 % of their weight after the 15th cycle.

4.8 Statistical Methods (univariate, bivariate and multivariate)

Statistical analyses can be divided into univariate, bivariate and multivariate methods and each method considers a different dimensional problem. The statistical treatment of the data set was performed with the open software ‘‘R GUI’’. To analyse the distribution of one rock property (univariate), box-whisker plots were used as shown in Fig. 4.1a). The data are illustrated in a ‘‘five-point-summary’’, which includes the median, two quartiles, extreme values and outliers. The box represents the area where 50 % of the data are included and which is limited by the upper (75 % quartile) and lower median (25 % quartile). The length of the box expresses the so-called interquartile ranges (IQR) and is also a degree of scattering. The median divides the total diagram into two parts, and its position allows an evaluation concerning the skewness of the data distribution. According to Tukey (1977), the length of the whiskers is limited by 1.5 times the interquartile range. All values outside of the whiskers are characterized as outliers. In the present study, this method was used for all data of individual properties as well as for recognizing interrelationships between the composition and age of the sandstones. To investigate the relationship between two properties, essentially a two-dimensional problem, a linear regression was performed (bivariate method). The values of two properties are represented in correlation point diagrams. The correlation coefficient expresses the relationship of two features (Bravais–Pearson coefficient). The coefficient can vary between +1 and -1; thereby, a positive value describes a linear relationship with a positive increase (Fig. 4.1b i) and a negative value a relationship with a negative increase (Fig. 4.1b ii). Correlations with no linear relationships, e.g. a cloud arrangement of points, are shown in Fig. 4.1b iii. Furthermore, within regression analyses confidence regions with 80 % probability range are determined under the assumption that basic properties like porosity, density or strength show normal distribution. Exemplarily, the relationship between water absorption and porosity (Fig. 4.1c) is illustrated, where 80 % probability range is presented by a small, elongated ellipse. To combine the relationships of all the measured parameters, which are important for characterizing the material behaviour of sandstone, multivariate methods of principal component

and cluster analyses were performed. Principal component analyses try to reduce a multidimensional problem. The hypothetical variables are constructed, which minimize the entire sum of squared deviations of a best-fit straight line. The calculated components try to describe the wide difference/variance between the properties and the samples. Since the data of sandstones are based on different physical units, they differ in dimension and the influence of properties with high variance can overlay the variance of other properties, which would lead to an incorrect calculation of components. Therefore, principal component analyses were accomplished after previous standardization. The pre-treatment includes a calculation of the q–q-norm and a correlation matrix (Dohrmann and Kühn 2009). Where necessary, data were logarithmized. Principal component analyses are illustrated with biplots, which include information on variables (rock properties) and samples in one diagram (Fig. 4.1d). The position of variables to each other is expressed by the loadings, which are calculated by the variances of the variables. They are illustrated as arrows, and the position to each other expresses the particular relationship (Fig. 4.1d). Arrows pointing in the same direction have a positive relationshipto each other. In contrast, arrows pointing in opposite directions exhibit a negative relationship to each other. If there is no relationship between two properties, arrows stand perpendicular to each other. Samples are depicted as points and the coordinates within the diagram in this multidimensional system are calculated via *scores*, which are based on the *loadings* of the components.

Cluster analyses were done for identifying groups of similar sandstones, based on all known properties. The principle of cluster analysis follows two steps: (1) determination of similarities between the objects and their properties, and (2) determination of the cluster number. The similarity is determined via proximity degree and is calculated with *the Euclidian distance matrix*. For illustration, a so-called dendrogram was used.

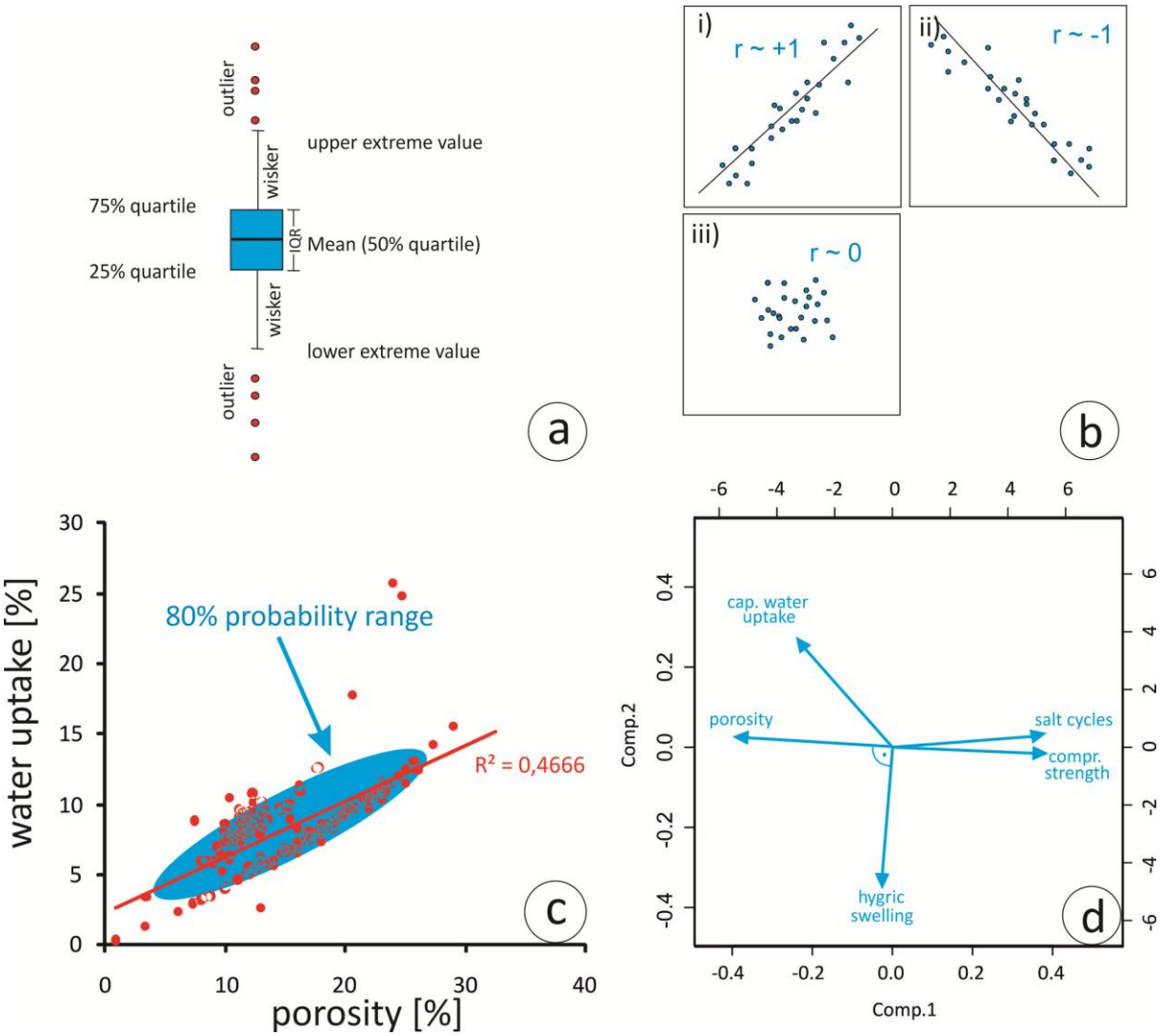

Fig. 4.1: a Whisker plot showing mean, lower and upper extreme data as well as outliers of univariate data, b possible distribution of data inside a regression analysis with regression coefficient, and c example for regression analyses between water uptake and porosity with confidence region of 80 % probability range, illustrated by the blue ellipsoid. d Diagram of the multivariate method showing the principal component analyses: rock properties present the variables and are illustrated by blue axes. Arrows pointing in the same direction are dependent on each other; arrows pointing in the opposite direction show negative correlation, whereas arrows that perpendicular to each other are independent of each other. For further explanation, see text.

4.9 Results

The petrographic analysis includes all the data from this study as well as from the literature. Both reveal a great variety of sandstone properties based on data from different stratigraphic levels.

4.9.1 General remarks on sandstones from different sources and stratigraphic position

Most of the data originate from Middle European sandstones (Fig. 4.2), which were predominantly deposited in a cratonic basin. For a discussion of the petrography and material properties, the stratigraphic position must also be taken into account as documented by Grimm (1990), Chitsazian (1985), David (2006), Fitzner (1970), Holzwarth (1996), Kirsten (2009), Seidel (2004), Bartelsen (2008) and Koch and Sobott (2008). The occurrence of different sandstones in the stratigraphic column is

grouped according to their importance and regional distribution. In Germany, the most important sandstones occur in the Lower and Upper Triassic (Fig. 4.2). Ten sandstone quarries were evaluated and analysed in the present study. Lower Triassic sandstones are quarried at the Weser River, in the Hessische Senke, in Spessart, Odenwald, in the Pfälzerwald Mountains and in the Black Forest. Upper Triassic sandstones are predominantly mined in the Thuringian Basin, at the River Main, and between the Black Forest and the Swabian Alb. Sandstones, Cretaceous in age, are also significant (six quarries evaluated), which are concentrated in the ‘‘Münsterländer Becken’’, the Hildesheim Bay in northeastern Germany and at the Elbe River in eastern Germany. Carboniferous and Permian sandstones are rare due to their low occurrence. They are mined in the north of the Harz Mountains, at the Thuringian– Bavarian border, Hunsrück and in the north of the Rhenish Slate Mountains.

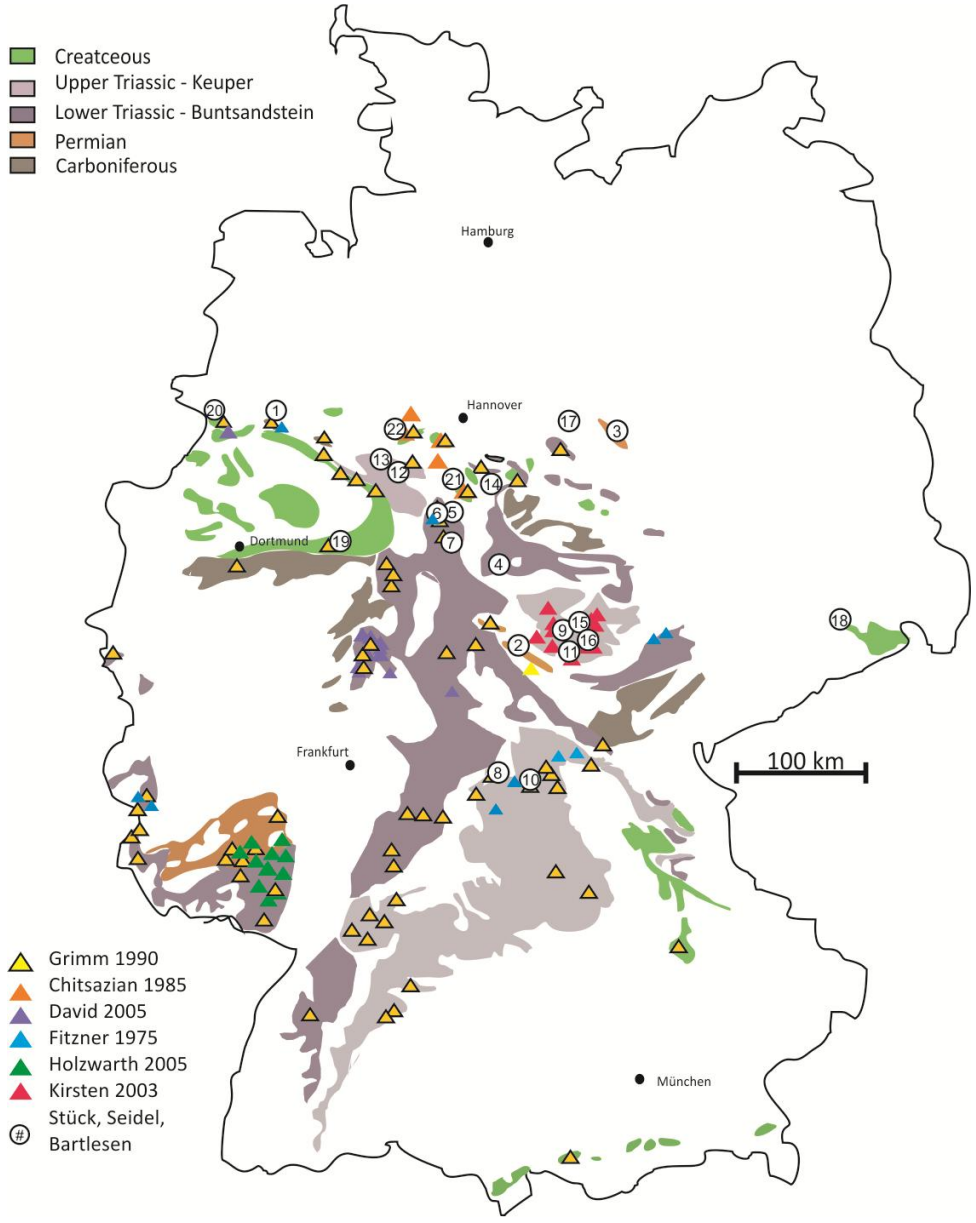

Fig. 4.2 Map of quarries and sandstones investigated. Outcrops of deposits from Carboniferous, Permian, Lower and Upper Triassic as well as Cretaceous are illustrated. Sample locations and literature sources for different sandstones are indicated. Numbers represent the sandstones investigated in this study (Table 4.1).

The sediments of the geologic ages considered are the result of changing depositional environments through time, associated with transgressive and regressive marine influence. The depositional environments of the sandstones range from pure clastic terrigeneous (fluviatile, aeolian) to marine facies, which are also reflected in their characteristic sedimentary structures. Most of the sandstones can be classified as quartzites, lithic subarkoses, sublitharenites as well as minor litharenites and subarkoses. The distribution of sandstone types is characteristic for epicontinental basins such as the German Basin. Therefore, arkoses are represented only in very minor amounts. Short descriptions of different depositional facies are given, which change in each sedimentary basin through time.

Carboniferous are the oldest sandstones analysed in the present study (e.g. the Ibbenbüren sandstone). The sediments were deposited in flood plains and alluvial fans to the north of the Variscan orogeny (Katzung 1975; Plein 1993). They consist of feldspathic litharenites and sublitharenites and partially contain conglomeratic layers and coal particles. The Ibbenbüren sandstone is characterized by strong compaction and cementation and also a clayey matrix.

During the Permian, the German Basin was filled with shallow marine to terrestrial mixed carbonate/siliciclastic sediments (Aigner and Bachmann 1992). The Rotliegend sandstones crop out in southern Germany, Thuringia and at the Flechtinger mountain range, where terrestrial deposits formed lithic subarkoses and sublitharenites. According to Strack and Stapf (1980), they are fluviatile deposits from flood plains and channel facies.

Triassic sandstones of the Buntsandstein are terrigeneous deposits of predominantly sublitharenitic composition. Sandstones of the Middle Buntsandstein commonly show quartz arenitic to sublitharenitic composition. The depositional environment of the Bunter sediments changes markedly through time. In the Lower Bunter playa facies, braided river systems formed at the margins (Paul 1982), which are characterized by fining upward cycles. The sandstones of the Middle Buntsandstein are characterized by prograding fluvial sandstones with a common channel facies (Karlshafen, Arholzen, Uder and Lobach). Sandstones of the Upper Bunter are seldom used as building stones because they mainly consist of clayey and silty deposits.

Sandstones of Upper Triassic (Keuper) age are characterized by marked changes of the depositional environment through time. They also document a great variability in their physical properties. Considerable natural stone deposits belong to the Lettenkohlenkeuper, Schilfsandstein and Rhät Formations (Lower, Middle and Upper Keuper). Sandstones deposited during the Schilfsandstein and Lettenkohlenkeuper are mainly litharenites and sublitharenites, commonly with highly altered unstable rock fragments. Sandstones of the Lettenkohlenkeuper (Ingersleben and Schleerieth sandstones) were deposited in a brackish marine delta environment with local moors. Local coal layers also occur with the same name designation (Beutler and Schubert 1987; Paul et al. 2008).

Sediments of the Schilfsandstein (Sander, Hindfelden, Schötmarer and Barkhausen sandstones) were deposited in a wide delta facies covering a flat shelf. They formed meandering delta arms filled by up to 50 m of fine sand (Wurster 1964). Rhät sandstones are characterized by quartz arenites (the Velpke, Hockeln, Seebergen and Röhnberg sandstones). They were deposited under changing depositional environments from marine to lacustrine-terrestrial. The sediments are predominantly composed of alternating fine sands and mudstones (Seidel 2003). Very coarse channel fills also occur (Koch et al. 2003; Sobott and Koch 2009) in the Franconian Rhät deposits.

Cretaceous sandstones (Cotta, Rüthen, Hilssandstein, Obernkirchen and Bad Bentheim) were deposited in the coastal rim area formed by a transgression from the north. They mainly consist of quartz arenites, in which the marine environment is partially well documented by the occurrence of glauconite (greensands).

4.10 Petrographical Analyses - Composition and Fabric

Compositionally, the sandstones investigated can generally be defined as quartz arenites, sublitharenites, litharenites and lithic subarkoses according to McBride (1963, Fig. 4.3). Arkoses and lithic arkoses are very rare in this data set. The 22 sandstones which were analysed in detail comprise a wide range of different sandstone types and are representative for the entire dataset compiled from the literature (~300 samples) in terms of composition, depositional settings and age.

The Ibbenbüren sandstone (Fig. 4.3; Table 4.1) of Carboniferous age shows a sublitharenitic composition and is less mature due to its clayey matrix, subangular–subrounded grain shape and well to moderate sorting. The grain contact is predominantly sutured but also concave–convex (Fig. 4.5a) and visible pore spaces are only moderately recognizable. Cementation occurs as syntaxial quartz overgrowths, whereby the original grain shape is marked by a thin rim of impurities. The Permian Tambach and Bebertal sandstones are both characterized by a sublitharenitic composition. The Bebertal aeolian sandstone only shows moderate sorting (Figs. 4.4a, 4.6) with a bimodal grain size, whereby the larger grains are rounded and the smaller grains rather subrounded. Grain contacts are mostly elongated– concave–convex. Syntaxial quartz overgrowths (Fig. 4.5a, c) and calcite occur as cement. Locally, the grains are surrounded by early infiltrated clay minerals (illite). Furthermore, X-ray diffraction indicates smectite as the clay mineral found in these sandstones. Cation exchange capacity (CEC) for the whole rock fraction amounts to 1.0 meq/100 mg (Bartelsen 2008). The Tambach sandstone is characterized by well sorting and subrounded–subangular grain shapes, concave–convex grain contacts and very well-pronounced syntaxial quartz overgrowths. Furthermore, calcite occurs as a pore-filling cement and feldspar as a grain overgrowth. In addition, detrital grains are surrounded by finely dispersed iron oxides. Partially altered lithoclasts show

replacement by chlorite, which was also determined by XRD analyses. The cation exchange capacity is with 1.1 meq/100 mg marginally higher than for the Bebertal sandstone (Bartelsen 2008).

The fluviatile Uder, Lobach, Arholzen and Karlshafen sandstones belong to the Lower Triassic of Buntsandstein (Table 4.1). They are sublitharenites in composition with the exception of the Uder sandstone, which is defined as a quartz arenite. While the samples of Lobach, Arholzen and Karlshafen (Weser sandstones) all show distinct alteration of feldspars and lithoclasts, the Uder sandstone shows only little alteration. The three Wesersandstones are characterized by a subangular grain shape, predominantly concave– convex grain contact, syntaxial quartz overgrowth, calcite cement, locally feldspar cement and often a haematite overprinting of the grain surfaces (Fig. 4.4b). However, the amount of cement and also the degree of compaction varies. Most of the (quartz-) cementation occurs in the Karlshafen sandstone, followed by Arholzen and finally Lobach. Furthermore, the Karlshafen sandstone shows the strongest compaction. The grains of the Uder sandstone are subrounded, grain contacts pointed-elongated and little stabilizing cement is present; only a clay matrix is recognizable. This sandstone shows little compaction since the grain contacts are predominantly pointed. The sorting and grain size of the Bunter sandstones exhibits distinct variations, whereas the Lobach, Arholzen and Karlshafen sandstones (Wesersandstones) show a moderate to well sorting. The Uder sandstone (Thuringia) is well sorted (Fig. 4.6). Weser sandstones can be classified as fine sand, whereas the Karlshafen sandstone even shows a fine-silty grain size. The Uder sandstone exhibits a fine–medium grain size. In general, the Uder sandstone is compositionally and texturally more mature than the distinct immature Weser sandstones. The cation exchange capacity for the Karlshafen sandstone equals 2.0, and XRD analyses indicate the presence of chlorite, smectite and kaolinite in the clay fractions <2 µm (Bartelsen 2008).

Both the Schleerieth and Ingersleben sandstones belong to the Lower Keuper (Table 4.1). They are characterized by a litharenitic composition. The Schleerieth sandstone exhibits little syntaxial quartz overgrowths, a clayey matrix, predominantly point-elongated grain contacts and subrounded grains. Feldspar grains are sericitized and the mainly volcanogenic rock fragments are distinctly altered. Chloritization of volcanogenic rock fragments is also observable. The grain size is coarse silty to fine sandy and the sorting well developed (Fig. 4.6). XRD analyses show chlorite and illite within the sandstone and its CEC amounts to 2.1 meq/100 g (Bartelsen 2008). Thus, this rock can be defined as very immature sandstone. The Ingersleben sandstone can also be defined as highly immature and is characterized by little compaction and cementation; however, the rock shows a distinct visible pore space. The volcanogenic rock fragments present are highly altered to chlorite and the feldspars show alteration by sericitization. Often, loose fragments of pseudomatrix between the few stable grains can be observed, and rarely a grain contact between stable components is visible. Locally, relicts of feldspar cement are recognizable, which are also now replaced. The grain contact is mainly pointed

or elongated and the grain shape subangular and locally angular. Furthermore, at grain surfaces, chlorite and porelining illite are observable. XRD analyses indicate the presence of chlorite, kaolinite and illite (Fig. 4.7) and its CEC amounts to 1.4 meq/100 g.

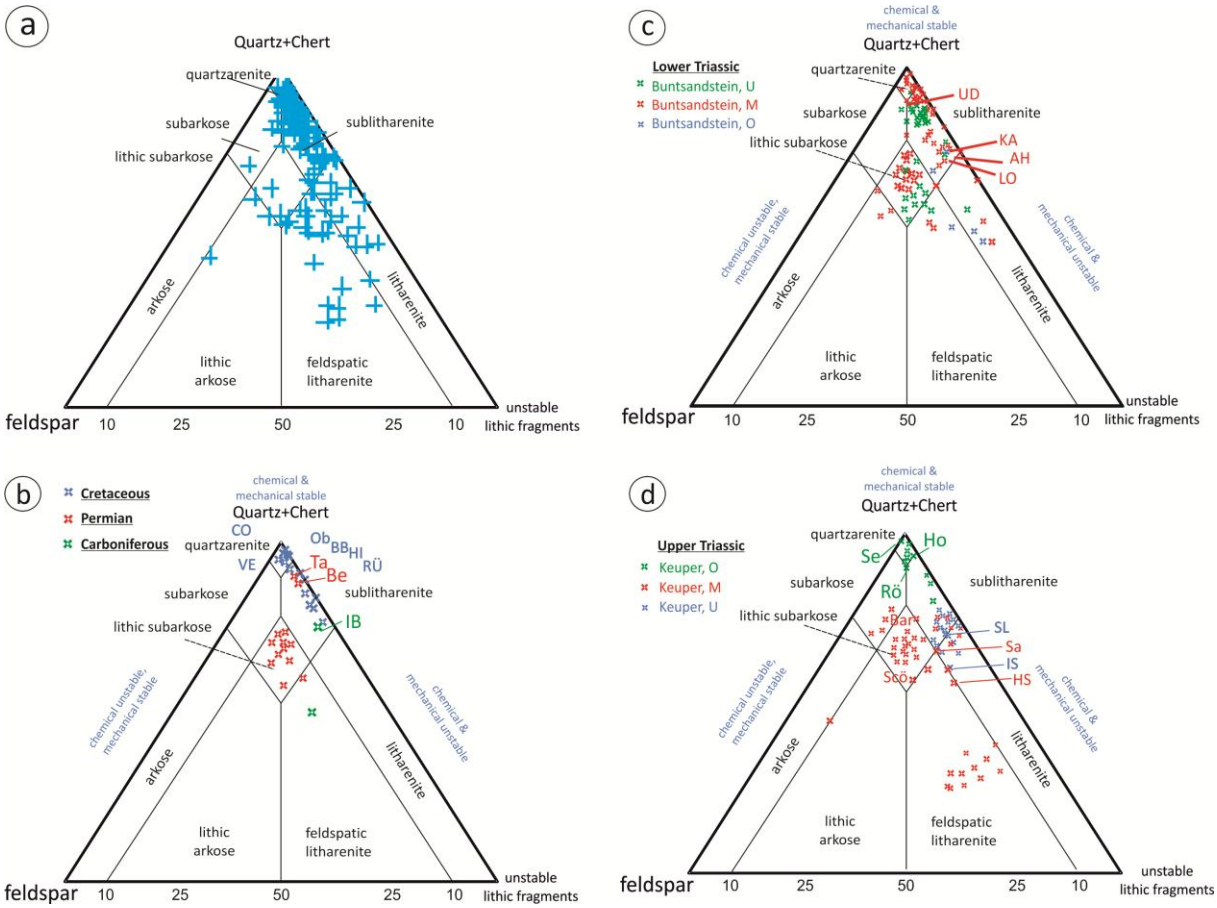

Fig. 4.3: Classification of sandstones investigated after McBride (1963) and Hayes (1984). b IB Ibbenbüren sandstone, Ta Tambach sandstone, Be Bebertal sandstone, Ve Velpke sandstone, CO Cotta sandstone, RÜ Rüthen sandstone, BB Bad Bentheim sandstone, Hi Hilssandstein, Ob Obernkirchen sandstone; c LO Lobach sandstone, AH Arholzen sandstone, KA Karlshafen sandstone, UD Uder sandstone; d SL Schleerieth sandstone, IS Ingersleben sandstone, HS Hindfelden sandstone, SA Sander sandstone, SCÖ Schötmar sandstone, BAR Barkhausen sandstone, RÖ Röhnberg sandstone, SE Seebergen sandstone, HO Hockeln sandstone.

Sandstones of the Middle Keuper (Table 4.1) are predominantly compositionally immature, since the Sander and Hindfelden sandstones are feldspathic litharenites and the Barkhausen and Schötmar sandstones lithic subarkoses. The Barkhausen, Schötmar and Sander sandstones contain quartz cement, locally feldspar cement and a clayey matrix, whereas the Hindfelden sandstone shows very little quartz cement and a distinct pseudomatrix (Figs. 4.4c, 4.5e). The grain surfaces of the Barkhausen, Schötmar and Sander sandstones are overprinted with haematite, while the grain surfaces of the Hindfelden sandstone are overprinted by thick clay–chlorite rims (Fig. 4.5d). Alteration of feldspar and unstable rock fragments are distinctly developed in the latter sample and rarely a grain contact between stable quartz grains can be observed. Instead of this, quartz grains commonly are floating in the pseudomatrix. In contrast to the Barkhausen and Schötmar sandstones that show concave– convex grain contacts, the Sander sandstone exhibits elongated grain contacts.

All Middle Keuper sandstones exhibit a well to moderate sorting and subrounded–subangular grain shape. The grain size of the Barkhausen sandstone is about 100 µm, the Schötmar sandstone ranges 100–200 µm, the Hindfelden standstone shows sizes of 80–100 µm and the sandstone Sander has a size of around 175 µm. XRD analyses show a large chlorite and illite content and a small amount of kaolinite in the Hindfelden sandstone (Fig. 4.7), where its CEC amounts to 4.6 meq/ 100 g. The CEC amounts to Sander sandstone 3.4 meq/100 g and swellable mixed layer minerals and kaolinite are detected by XRD analyses.

Seebergen, Röhnberg, Hockeln and Velpke sandstones of the Upper Keuper (Rhät) are all quartz arenites in composition, well to very well sorted, rounded to subrounded and classified as fine, mature sands. They can be distinguished by their different degrees of compaction, early infiltrated clay minerals and cementation. Seebergen sandstones are moderate–strongly compacted, show concave– convex grain contacts, clean grain surfaces (Figs. 4.4d, 4.5a, c) and distinct syntaxial quartz overgrowths.

In contrast, the Röhnberg sandstone is characterized by little compaction and quartz cementation, but also shows a distinct early infiltrated grain lining with illite and kaolinite pore fillings (Fig. 4.4e). The Hockeln sandstone is mainly characterized by quartz cementation, low clayey matrix contents, little infiltrated early clay minerals and sericitized feldspars. Sandstone Velpke is characterized by distinct amounts of syntaxial quartz overgrowth, iron oxides and pore-filling kaolinite. The feldspars are altered to kaolinite. Grain contact of the Röhnberg sandstone predominantly is punctiform, whereas the Seebergen exhibits concave–convex, the Velpke pointed–elongated and the Hockeln elongated– concave–convex grain contacts.

Table 4.1: Petrography and fabric of all 22 sandstones analysed. (*) = Bartelsen (2008)/Ruedrich et al (2011), (**)= Seidel (2004)/Ruedrich et al (2005). Alt.=alteration, fsp = feldspar, kaol.= kaolinite, mat.= mature, mod.= moderate, polyqtz= polyquartz, sed.= sedimentary, **s**yn. qtz = syntaxial quartz overgrowth (silica cement).

		sample	Classification McBride 1963	Qtz/Fsp /Litho	cement / matrix	roundness/sorting	grain contact	maturity & degree of alteration, clay minerals, rock fragments
Cretaceous		Cotta(CO)	Quartz-arenite	95/5/0	Clayeymatrix	subangular/well	elongated	lower mat.through clay matrix & altered fsp, glaukonite
		Rüthen(RÜ)	Quartz-arenite	90/10/0	fewsynt. Qtz / kaolinite, illite	subrounded/well	elong.con cave-con.	high mat., glauconite
		Obernkirchen (OB)	Quartz-arenite	95/3/2	Highamount synt. Qtz / clay	subangular/well	point-elongated	high mat.,low alt.(fsp,Illite coatings,kaol*), polyqtz
		Hilssandstein(HI)	Quartz-arenite	95/5/0	Mod. Synt. Qtz.	rounded/mod.	concave-convex	high mat., low alt. ;polyquartz, glauconite
		Bentheim(BB)	Quartz-arenite	95/3/2	Few. synt. Qtz / kaol., illite	subrounded/well	concave-convex	high mat., kaolinite, swellable clay minerals, polyqtz.
Triassic	Keuper *Rhät*	Velpke(VE)	Quartz-arenite	95/5/0	Distinct synt. qtz.	subrounded/verywell	point-elongated	high mat., pore filling kaolinite, alt. off fsp.
		Seebergen(SE)	Quartz-arenite	98/2/0	Qtz, few ironoxides	subrounded/verywell	concave-convex	very high mat., very low alt., few kaol.
		Röhnberg(RÖ)	Quartz-arenite	95/3/2	kaolinite, illite	subrounded/verywell	point-elongated	high mat., low alt. (swell.clay, porefill. kaol.)
		Hockeln(HO)	Quartz-arenite	98/2/0	Qtz, clay	subrounded/verywell	elongated	high mat., low. alt.
	Keuper *Schilfsandstein*	Barkhausen(BA)	lith.sub-arkose	75/10/15	Qtz, few carbonate	subang./well	concave-convex	low alt.; chlorite/volcanic clasts
		Schötmar(SCÖ)	lith.sub-arkose	56/20/24	Qtz, few carbonate, hematite	subang./mod.-well	concave-convex	low alt.; chlorite/volcanic clasts
		Hindfelden(HS)	feldsp.-litharenite	60/10/30	Little qtz	subang./well	point	low mat., high alt. fsp &clasts, ill., chl, kaol; mixedlayers
		Sander(SA)	feldsp.-litharenite	65/10/25	synt. qtz, fsp, clay	subang./mod.-well	point-elongated	low mat., high alt. Fsp., claymatrix, mixedlayer*,chlorite
		Ingersleben(IS)	litharenite	60/10/30	Clayleymatrix, few synt. qtz	subang./mod.-well	point	Illite, chlorite, kaolinite
		Schleerieth(SL)	litharenite	65/5/30	Few synt. Qtz / pseudo-matrix	subang./mod.-well	elongated-point	low mat., high alt. fsp, claymatrix, mica, chlorite
	Buntsand-stein *Solling*	Karlshafen(KA)	Sub-litharenite	52/17/27	synt. qtz, clay & ferritic, Ca	angular/mod.-well	elongated-conc.	mod. mat., mod. alt., smectite*, kaolinite*
		Arholzen(AH)	Sub-litharenite	80/10/10	synt. Qtz , clay & ferritic, Ca	angular/mod.-well	elongated	mod. mat., mod. alt; sed.clasts
		Lobach(LO)	Sub-litharenite	80/10/10	synt. qtz, clay	angular/mod.-well	elongated	mod. mat., mod. alt.; sed.clasts
		Uder(UD)	Quartz-arenite	90/5/5	Qtz, clayferritic	angular/mod.-well	point(elongated)	mod. mat., low alt., sed.clasts
Permian	Rotliegend	Bebertal(BE)	Sub-litharenite	78/8/14	Clay ferritic, few synt qtz & Ca	subrounded/mod.	point-elongated	mod-well mat., low. alt., smectite*
		Tambach(TA)	Sub-litharenite	90/2/8	synt. qtz, calc., ferritic	subrounded/mod.	point-elongated	mod-well mat., low. alt., chlorite*
Carb.		Ibbenbüren(IB)	Sub-litharenite	80/2/18	Qtz, clayferritic	subangular/well	concave-convex	mod. mat.,few. alt., (fsp.),kaol. & montmorillonite**

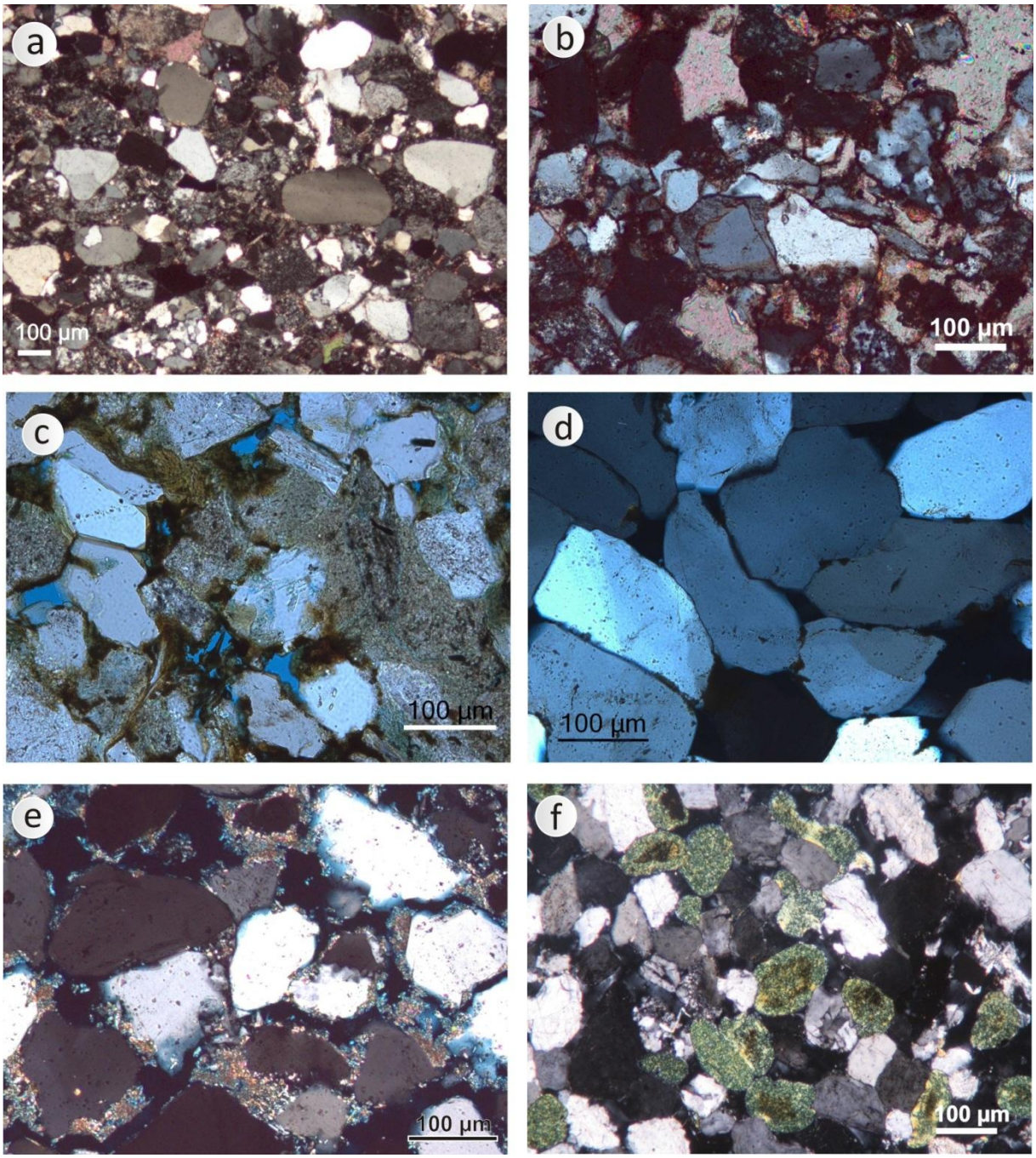

Fig. 4.4: Representative sandstone types: a Aeolian sandstone (dune deposit; Rotliegend, Bebertal sandstone) revealing a bimodal grain size distribution (x-pol.). b Sublitharenite with quartzitic and calcareous cementation as well as a haematitic overprinting, which is characteristic for fluviatile sandstones belonging to the Lower Triassic (Karlshafen sandstone; x-pol.). c Highly immature sublitharenite– litharenite with altered lithoclasts, feldspars as well as pseudomatrix (Hindfelden sandstone; II-pol.). d Quartz arenite (Upper Triassic/Rät, Seebergen) showing clean grain contacts, which allows pressure solution leading to concave– convex to sutured grain contacts (x-pol.). e Quartz arenite with early infiltration of illite forming clay boundaries between grains (Röhnberg sandstone; x-pol.). f Marine sandstone with glauconite grains (Cretaceous, Rüthen; x-pol.).

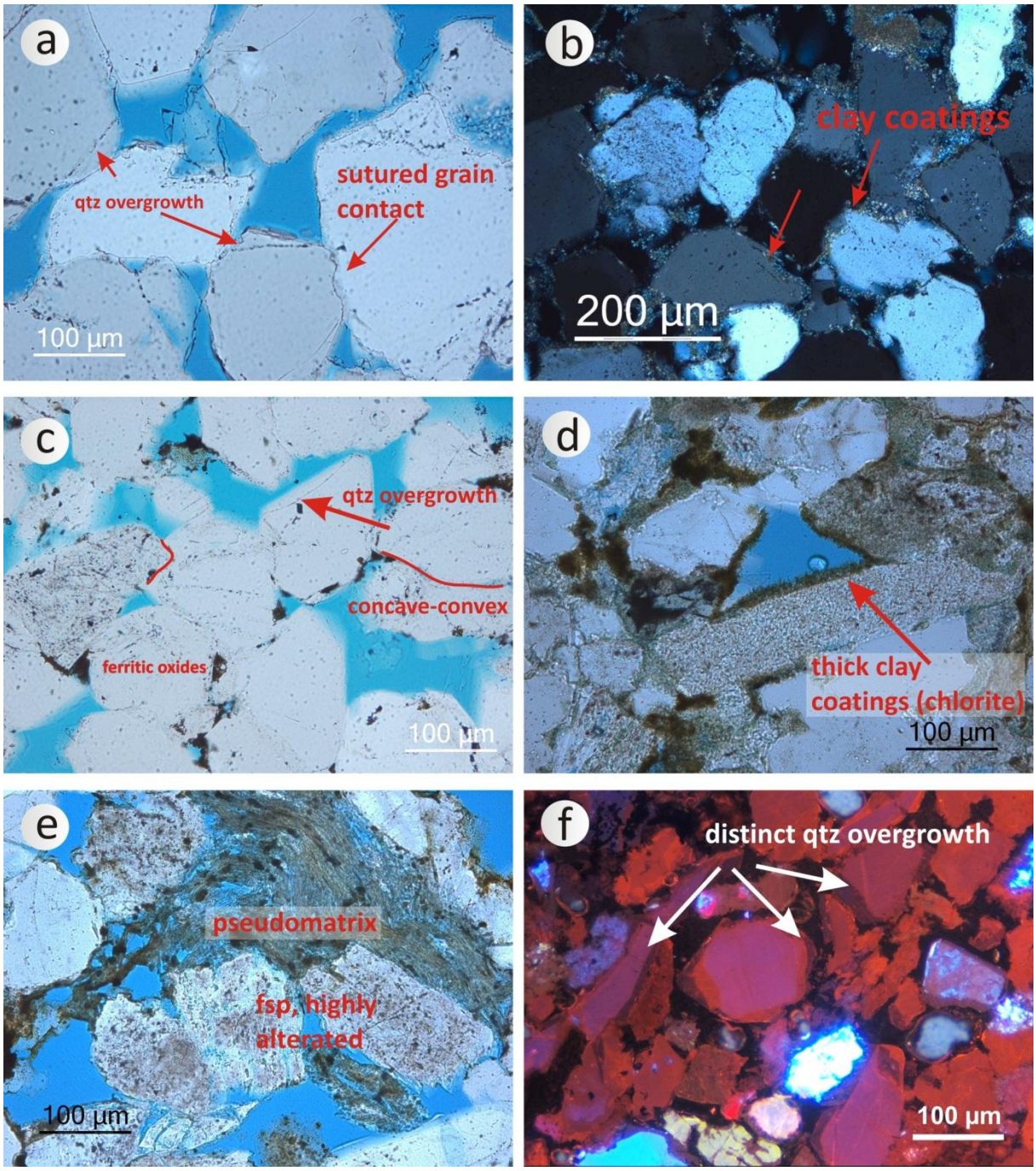

Fig. 4.5: Characteristic features for grain contacts and cementation. a Syntaxial quartz overgrowth as well as sutured point contact between quartz grains (II-pol.). b Clay coatings of needle-shaped illite lining the pores (x-pol.). c Quartz overgrowth, concave–convex grain contact as well as dark brown ferrous oxides present as rims and interparticle fillings (II-pol.). d Distinct clay coatings of chlorite at altered grain surfaces (II-pol.). e Squeezed pseudomatrix between altered detrital grains (II-pol.) and f distinct quartz overgrowths under cathodoluminescence.

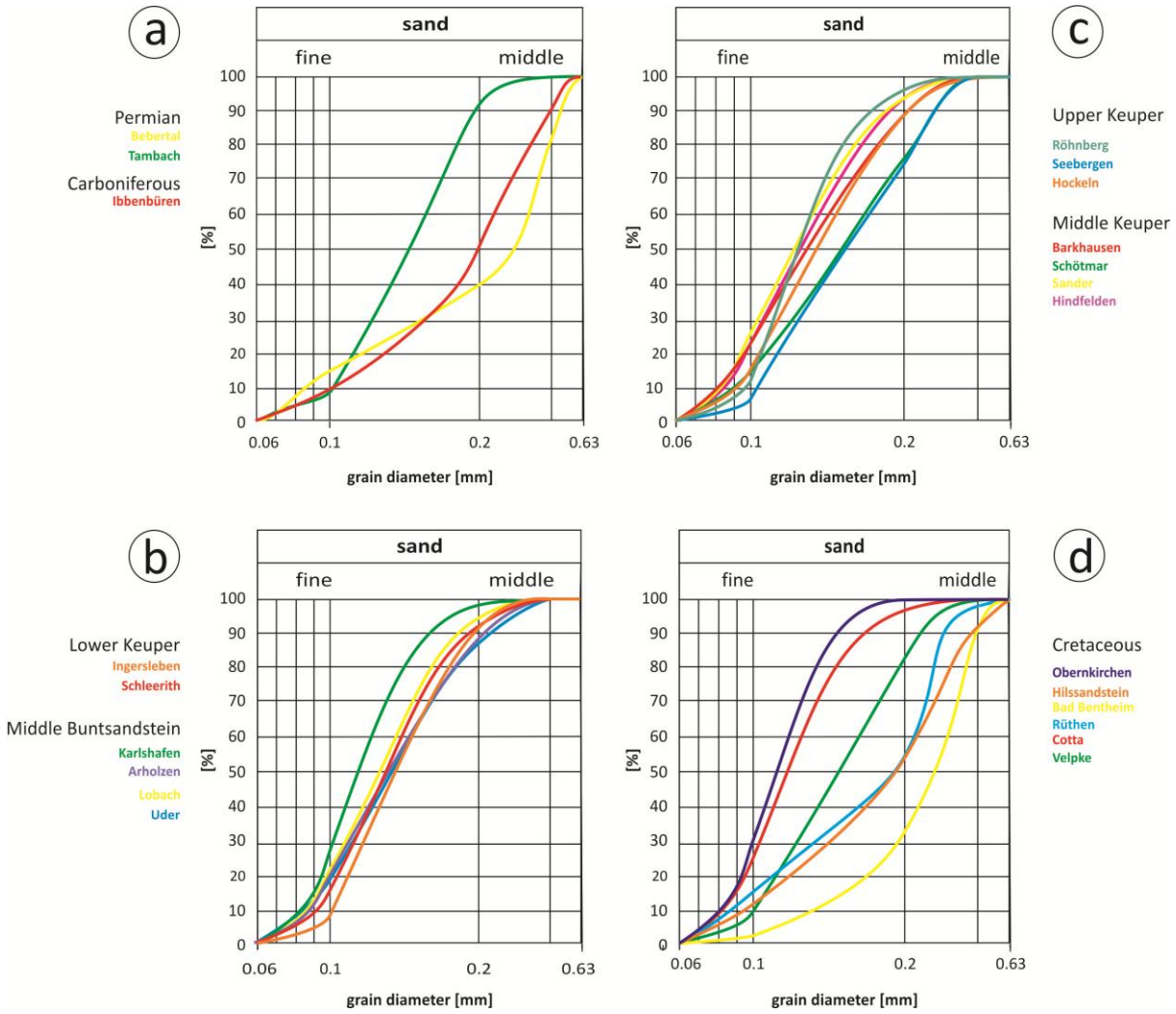

Fig. 4.6: Sorting of sandstones investigated: a Permian and Carboniferous sandstones, b Buntsandstein and Lower Keuper, c Upper Keuper and d Cretaceous. For sample abbreviations, see Table 4.1.

The average grain size of the Seebergen ranges from 150 to 200 µm, the Röhnberg about 100 µm and of sandstone Velpke and Hockeln around 125 µm. Results of XRD analyses for the Seebergen indicates traces of kaolinite, but no other clay minerals (Fig. 4.7) and with a very low CEC of 0.2 meq/100 g. In contrast, the Röhnberg sandstone shows high kaolinite contents and also swellable clay minerals (Fig. 4.7), where the CEC equals 1.5 meq/100 g.

Cretaceous sandstones investigated in this study (Table 4.1) are the Cotta, Rüthen, Bad Bentheim, Hilssandstein and Obernkirchen marine and mature sandstones, which all show a quartz arenitic composition. Polycrystalline quartz grains often occur and in the case of the Rüthen, Cotta and Hilssandstein sandstones glauconite grains are present (Fig. 4.4f). After Tucker (2001), sandstone Rüthen has been defined as hybrid sandstone, since here the glauconite occurs to a significant proportion. The few feldspars that occur are only slightly altered by sericitization. With the exception of the Obernkirchen sandstone, whose grains are subangular, the sandstones are subrounded to round. Sandstone Obernkirchen also shows very high amount of quartz cementation, whereas at the other sandstones syntaxial quartz cementation is much lower. In addition, the Cotta sandstone

contains a clayey matrix and distinct altered feldspars and therefore is more immature. Rüthen, Bad Bentheim and Obernkirchen sandstones exhibit pore-lining illite and pore-filling kaolinite (Fig. 4.5b). The grain contact of the Bad Bentheim sandstone is generally pointed, but also concave–convex contact occurs (Fig. 4.5a). In contrast, the Rüthen and Obernkirchen sandstones mainly show concave–convex grain contacts, and the Cotta and Hilssandstein sandstones predominantly reveal elongated to concave–convex grain contacts. Lowest grain sizes are found in the Obernkirchen sandstone with an average of around 80 lm, whereas the largest occur in the Bad Bentheim sandstone with an average of around 250 µm. The sorting of these sandstones is well pronounced. Results from the XRD analyses confirm the presence of high kaolinite contents and swellable clay minerals in the Bad Bentheim sandstone, but the CEC only shows a very low value of 0.1 meq/100 g. Furthermore, the sqrt illustration overemphasises the very low intensities of illite (Fig. 4.7b). In the Bad Bentheim sandstone, illite occurs as mixed phase along with swellable clay minerals.

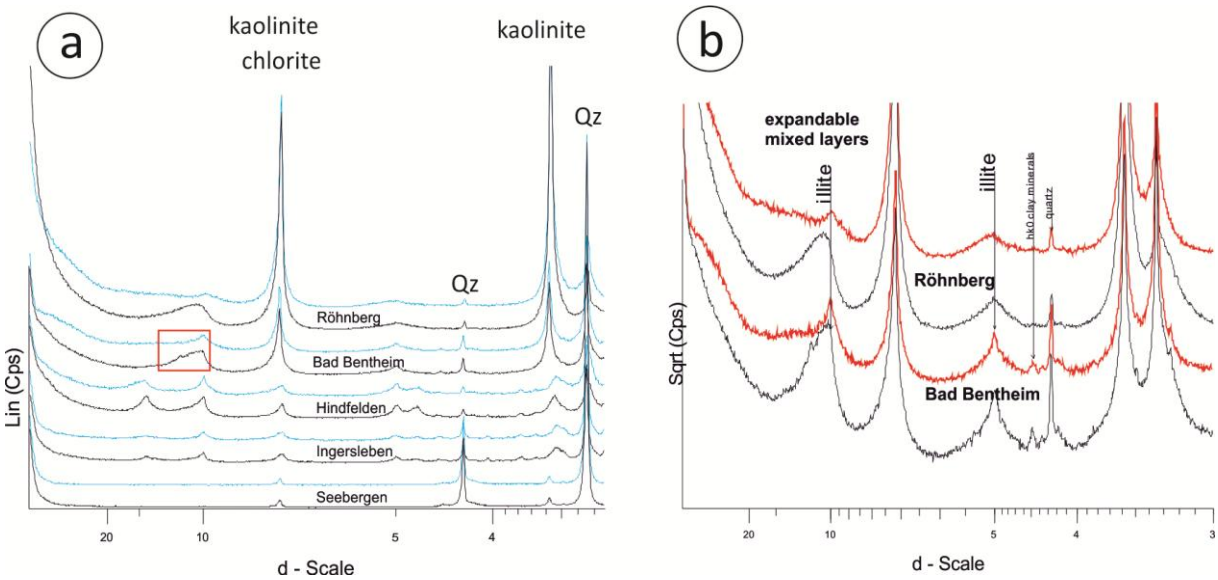

Fig. 4.7: Mineral content of clay fractions (textural preparates) from the Seebergen, Ingersleben, Hindfelden, Bad Bentheim and Röhnberg sandstones measured at textural specimen. Blue line/red: ethylene glycolate; black line: air dried. Red rectangle marks the area with the presence of swellable clay minerals e.g. in sandstone Bad Bentheim.

4.11 Petrophysical Parameters and Weathering Behaviour

4.11.1 Univariate and Bivariate Distribution

Whisker plots document the distribution of all samples of one rock property (Fig. 4.8). Most of the data exhibit a symmetrical distribution, with the exception of the coefficient of water absorption and the compressive strength. The mean and the median of the matrix density is 2.66 g/cm^3 (third quartile 2.64 g/cm^3 respectively 2.68 g/ cm^3), a value that corresponds to the high amount of quartz and feldspar. Deviations from these data are caused by the presence of non-quartzitic rock fragments and by the occurrence of authigenetic minerals such as chlorite, calcite, haematite or glauconite that usually occur in marine sandstones. According to this, outliers observable probably can be explained

by data of immature sandstones. The bulk density is characterized by a wide scattering (1.78–2.45 g/cm3) reflecting the highly variable porosity of sandstones (1–33 %; mean 16.8 %; first quartile 12 %, third quartile 22 %), with an average value of 2.14 g/cm3. Both the matrix and bulk density show a very low variance (Table 4.2).

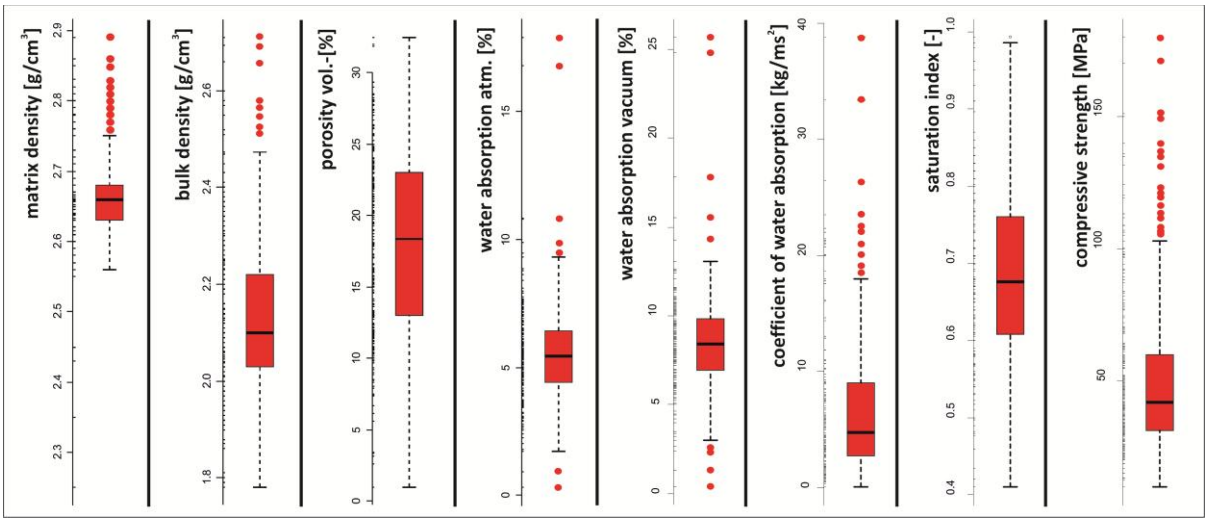

Fig. 4.8: Whisker plots of petrophysical properties from: matrix density, bulk density and effective porosity [n = 305; Chitsazian (1985), David (2006), Grimm (1990), Holzwarth (1996), Kirsten (2009), Massallam (1973), Mosch and Siegesmund (2007) and own samples], water uptake under atmospheric and vacuum conditions, capillary water uptake [n = 214; David (2006), Grimm (1990), Kirsten (2009) and own samples], s value of 286 as well as compressive strength [n = 246; David (2006), Kirsten (2009), Mosch and Siegesmund (2007), Holzwarth (1996) and own samples]. The red box indicates the range at which 50 % of the mean data are found and the black bar within the box the median. The red dots represent outliers, which are outside the interquartile ranges.

Porosity data are characterized by a normal distribution with a median and mean of 17.45 %. Fifty percent of the data range between 12 and 22 % porosity and outliers do not occur. The water absorption is characterized by a smaller range of quartiles and whiskers, but also shows extreme outliers. The median water absorption under atmospheric conditions (5.4 wt%) is markedly lower than the water absorption under vacuum (8.5 wt%). Furthermore, some outliers in both directions are observable. The coefficient of water absorption (w value) is characterized by a mean of 6.25 kg/ms^{-2} and a median of 4.3 kg/ ms^{-2}, by 2.2 kg/ms^{-2} for the first quartile and 7.5 kg/ms^{-2} for the third quartile. Many outliers are also observable here, but only upwards. The position of the median defines a skewed distribution. The Bad Bentheim sandstone shows the highest coefficient of water absorption with a value of about 40 kg/ms^{-2}. The saturation index varies from 0.4 to 0.99 (mean 0.67, median 0.68) and only shows one outlier. The compressive strength of all sandstones shows a median of 43 MPa and a mean of 51.68 MPa (first quartile 34 MPa, third quartile 63 MPa). The lowest compressive strength is 12 MPa and the highest one 107 MPa. However, some sandstones reach values of up to 160–180 MPa, such as the Permian and Middle Keuper sandstones of Tambach and Barkhausen.

Porosity and compressive strength show marked differences and interrelations between each other, taking into account different lithotypes and their stratigraphic position as documented in Fig. 4.9 for four selected characteristic sandstones. Poorly altered and strongly compacted sublitharenites such as the Karlshafen and Arholzen Weser sandstones (Fig. 4.9b; Tables 4.1, 4.3) show the lowest porosity. Pure quartz arenites (mean and median porosity: 15 %) include sandstones with distinct quartz overgrowths and no early infiltration by clay. Sandstones of the Upper Keuper (SE) and of Cretaceous age (OB) commonly fall into this group. Weakly compacted and weakly cemented quartz arenites (median 24 %) and strongly altered sublitharenites– litharenites (median porosity 25 %) show the highest porosity data. The latter group displays the most distinct scattering and is predominantly represented by sandstones of Lower and Middle Keuper (HS and IS; Tables 4.1, 4.3).

Considering the stratigraphic position of the sandstones analysed, the following relationships can be delineated. With increasing stratigraphic age, the porosity generally decreases, indicating that porosity is a function of time and burial depth (e.g. Wilson 1994, Koch and Sobott 2008). Sandstones of the Buntsandstein show a median porosity of 17 %. Those of the Lower and Middle Keuper exhibit the highest porosities (a mean of 24 %). Similar porosities exist in the sandstones of the Upper Keuper and the Cretaceous, with a mean porosity of 17.5 %. Therefore, sandstones of the Upper Keuper and the Cretaceous do not follow the time/burial trend as shown by elder sandstones. This is probably due to the fact that at low burial, the primary parameters of depositional environment and of eogenetic cementation as well as early formed secondary porosity always have a major effect. Moreover, they are not completely overprinted and hidden by deeper burial alteration and homogenization.

Also, the distribution of compressive strength was grouped according to the lithotypes and stratigraphic position (Fig. 9b). The median for strong compacted and/or cemented quartz arenites amounts to 87 MPa, whereas weak compacted quartz arenites exhibit with 56 MPa a distinct lower compressive strength. Sublitharenites, which contain 5–25 % unstable lithic rock fragments, are strongly compacted and cemented and have a median compressive strength of 103 MPa. Weakly compacted and cemented, altered sublitharenites–litharenites exhibit the lowest compressive strength with 37 MPa as median. The compressive strength dependent on stratigraphy shows for Permian and Lower Triassic (Buntsandstein) sandstones the highest values, whereas in sandstones belonging to Middle and Lower Keuper (Upper Triassic) the lowest compressive strength is observable (median: 37 MPa).

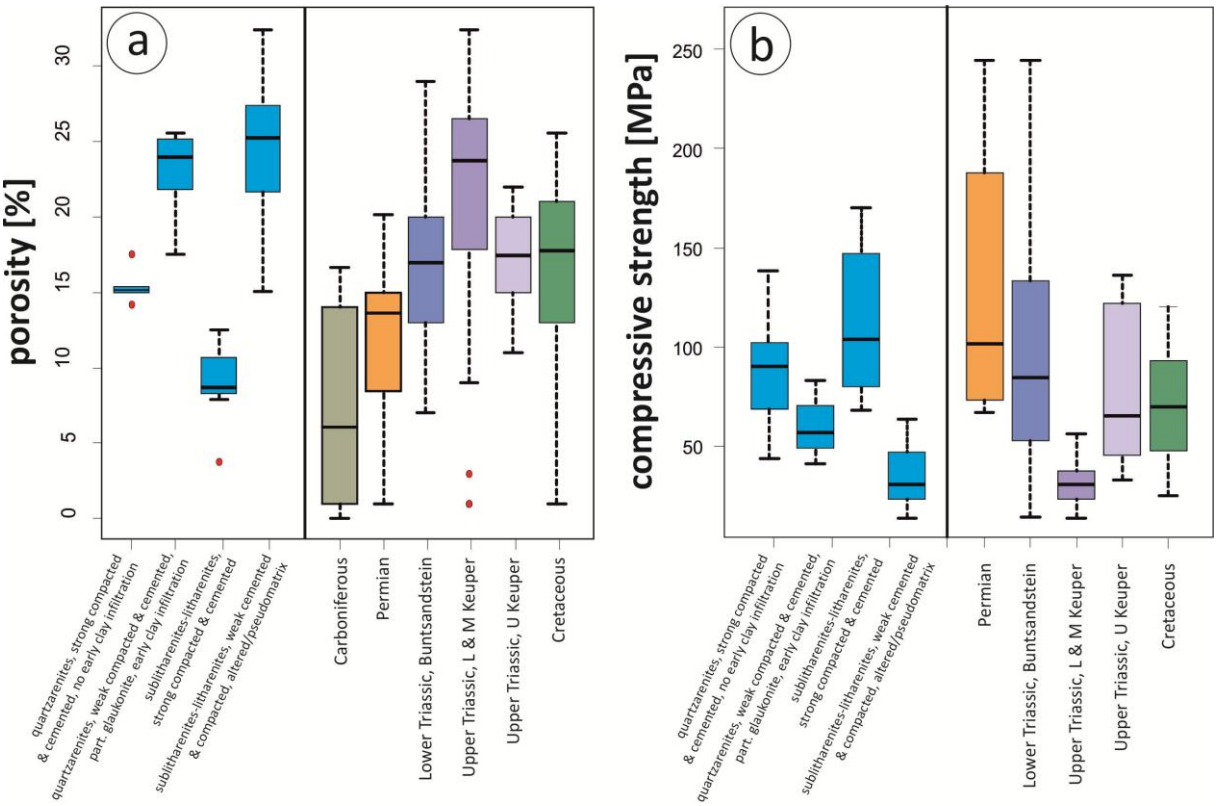

Fig. 4.9: Whisker plots of a porosity ordered according to lithotype and to stratigraphic age [n = 258; David (2006), Fitzner (1970), Kirsten (2009), Holzwarth (1996) and this study] and b compressive strength ordered according to lithotype and stratigraphic age. [n = 258; Chitsazian (1985), David (2006), Fitzner (1970), Kirsten (2009), Holzwarth (1996) and this study].

Three different types of sandstones can be recognized based on the pore radii distribution (I—bimodal, II—unimodal unequal and III—unimodal equal). Predominantly, litharenites of Upper Triassic age (Lower and Middle Keuper, HS, SA, SL; Tables 4.1, 4.3) with very low maturity show a bimodal pore radii distribution (Fig. 4.10I). Microsized pores are caused by the alteration of less stable components and/or the presence of a pseudomatrix. The second maximum of capillary pores reflects relics of primary intergranular porosity, which was closed by different degrees due to cementation and compaction. Unimodal unequal (Fig. 4.10II) distributions of pore radii can be predominantly observed in sublitharenites, but they can also occur in quartz arenites. In sublitharenites, this pore radii distribution can be attributed to moderate to well sorting, weak alteration of unstable grains and a moderate degree of cementation and compaction as documented by the Weser sandstones of Lower Triassic age (Buntsandstein, KA, AH, UD). Quartz arenites, which show such a distribution of pore radii, are generally well sorted and exhibit a more immature character due to the infiltration of clay minerals (Cretaceous and Upper Triassic sandstones; Upper Keuper, SE). Unimodal equal distributions of pore radii (Fig. 4.10III) are mainly found in well-sorted highly mature quartz arenites, in which no infiltration of clay minerals occurred as documented by the Cretaceous sandstones (VE, RÜ, HI, OBI). In general, an increase of maturity is correlated with the pore radii distribution from bimodal to unimodal unequal to unimodal equal.

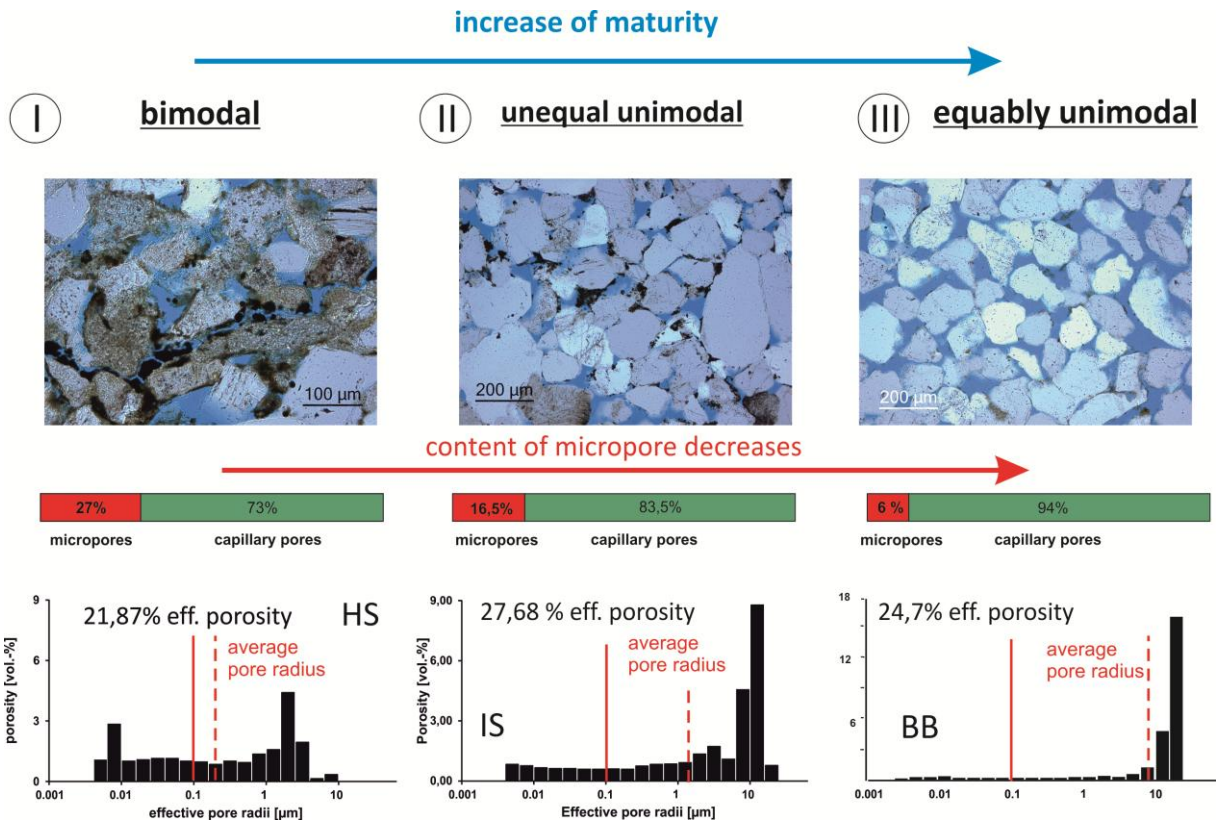

Fig. 4.10: Schematic documentation of pore radii distribution, development of maturity and amount of micropores: (I) bimodal with two maxima, (II) unimodal unequal and (III) unimodal equable. The bars indicate the ratio of micropores to capillary pores. The vertical red lines in the diagrams indicate the boundary between micro- and capillary pores and the dashed line the average pore radius.

No correlation seems to exist between grain size and compressive strength or between grain size and porosity (Fig. 4.11). According to Schießl and Alfes (1990), sandstones with smaller grain size should exhibit higher strength, since the amount of grain contacts per volume should be higher in finer grained sandstones. Indeed, Schießl and Alfes (1990) take into account the number of grain contacts. However, the kind of grain contact stays unconsidered. Thereby, a quartz– quartz grain contact should behave different from a quartz– lithoclast, or quartz–feldspar grain contact. In consequence, independent of grain size, the lithology (content of mechanical stable/unstable grains) should have higher impact on strength than grain size. Müller et al. (2002) observed a linear relationship between porosity and grain size, whereby with increasing grain size a decrease of porosity should be observable. Based on the large data set in this study, this cannot be confirmed. This investigation assumes that modification of pore space during diagenesis and initial sorting mainly rules the final porosity, whereby the grain size has little effect.

The bivariate analysis of correlations between petrophysical properties commonly reflects a linear or exponential relationship (Fig. 4.12). In sandstones with similar matrix density as the siliciclastic detrital grains, porosity correlates to bulk density (correlation coefficient = 0.4114). High porosity is related to low bulk density and vice versa (Fig. 4.12a). Newly formed mineral phases and/or detrital minerals with different density (e.g. glauconite, calcite, dolomite etc.) will result in a negative

correlation. The average value for all sandstones amounts to 15 % porosity at a bulk density of 2.25 g/cm3. Compressive strength decreases exponentially with an increasing coefficient of water absorption (Fig. 4.12b; correlation coefficient = 0.3497). Here, the average value of the probability ellipsoid for all the sandstones investigated amounts to 70 MPa at 5 kg/ms-2. The water absorption, dependent on porosity, increases linearly with a correlation coefficient of R = 0.46 under vacuum and R = 0.37 under atmospheric pressure (Fig. 4.12c). The ultrasonic velocity shows a linear correlation (R = 0.4712) to porosity (Fig. 4.12d).High velocity correlates with low porosity. The average value of 80 % probability ellipsoid amounts to 2,700 m/s and a porosity of 13.5 %. Also, a linear relationship between ultrasonic velocity and compressive strength is observable. Here, the velocity increases with increasing compressive strength (Fig. 4.10e; R = 0.6581). The average value of the ellipsoid equals 2,700 m/s and 50 MPa. The relationship between compressive strength, flexural strength (R = 0.6074) and porosity is illustrated in Fig. 4.12f: in general, both strengths decreasewith increasing porosity. Therefore, the gradient between porosity and compressive strength is higher than the flexural strength. Furthermore, a positive linear relationship between compressive strength and flexural strength (Fig. 4.12g; R = 0.6074) and between compressive strength and bulk density (R = 0.3993) is obvious (Fig. 4.12h).

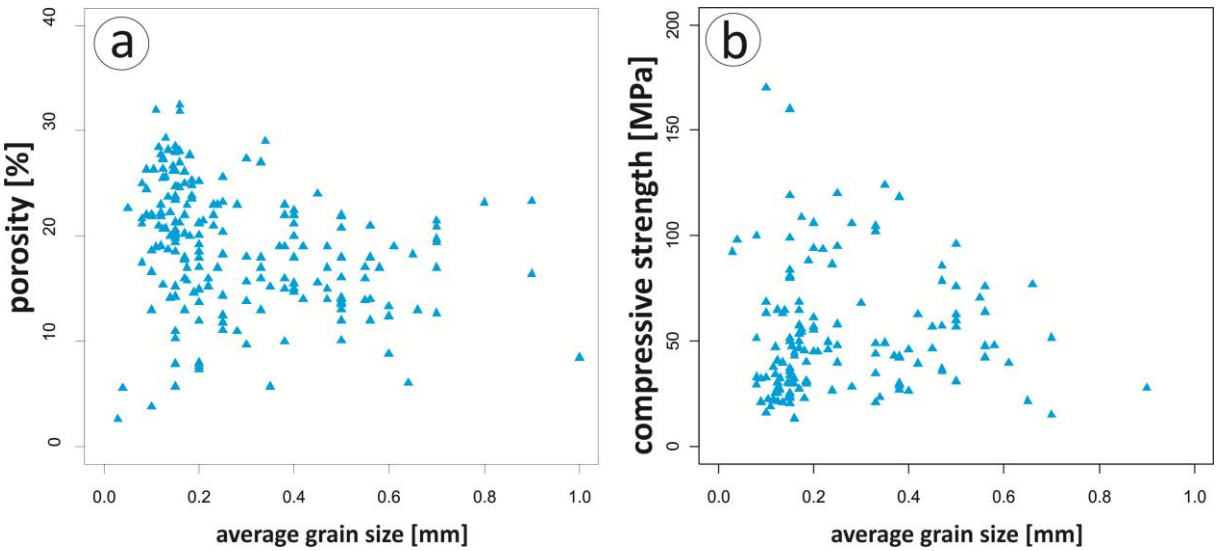

Fig. 4.11: Diagrams, showing the relationship between porosity and grain size, and between compressive strength and grain size dependent on sandstone type. (Fitzner 1970, n = 22; David 2006, n = 56; Kirsten 2009, n = 45; Grimm 1990, n = 72, this study = 22).

Table 4.2: Mean and variances of data distributions of matrix- and bulk density, porosity, water absorption under atmospheric and vacuum conditions, coefficient of water absorption, saturation index and compressive strength. Data origin of David (2006), Fitzner (1990), Grimm (1990), Kirsten (2009), Holzwarth (1996), Mosch & Siegesmund (2007), and own sandstones.

	matrix density [g/cm3]	bulk density [g/cm3]	Porosity vol.-[%]	water abs. (atm.) vol.-[%]	water abs. (vac.) [%]	coefficient of water absorption	saturation index [-]	compressive strength [MPa]
mean	2.66	2.14	17.45	7.41	8.47	6.25	0.68	51.68
variance	0.01	0.02	34.67	4.25	8.29	39.02	0.01	767.96

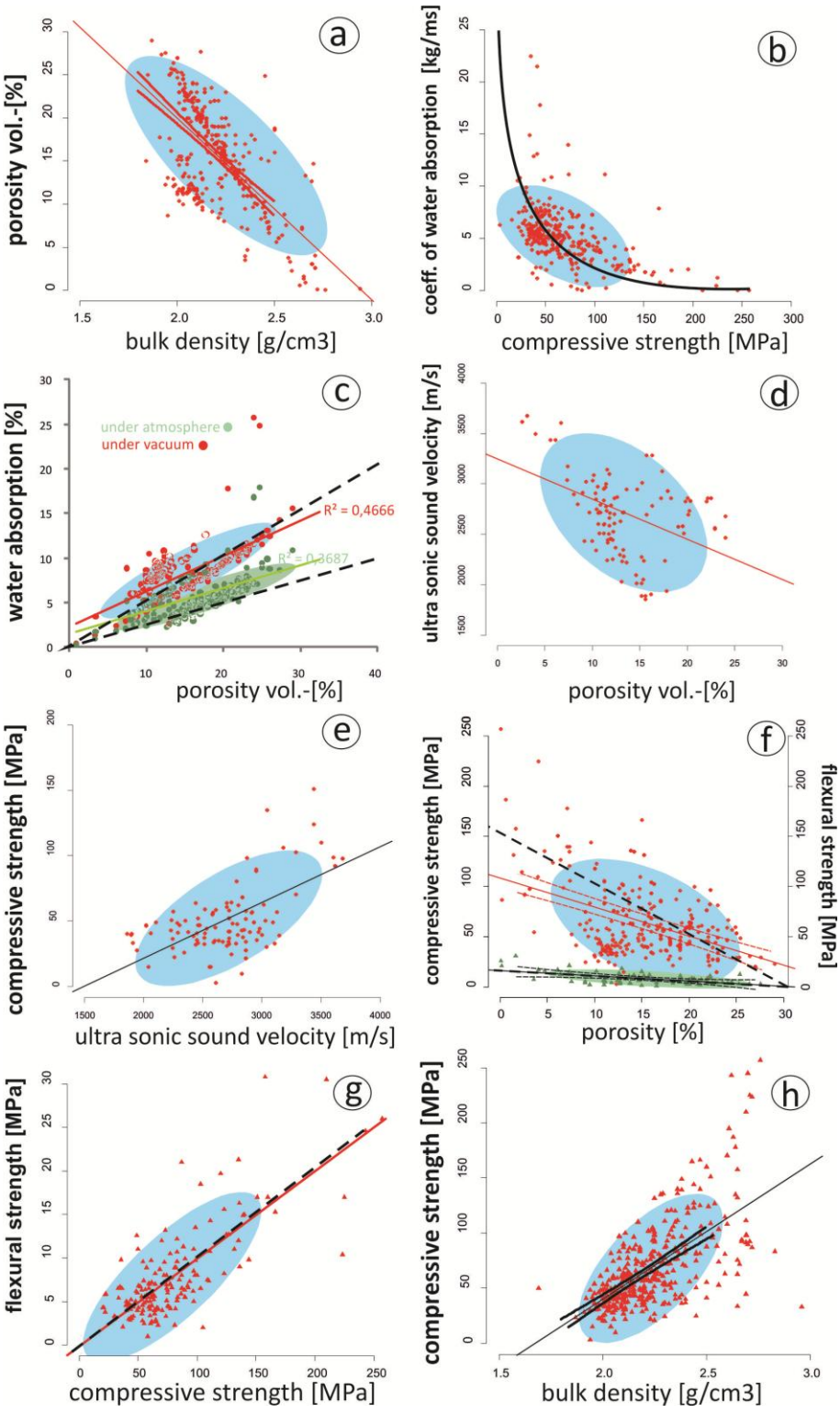

Fig. 4.12: Regression diagrams between different petrophysical properties. The blue ellipsoid predicts an 80 % probability of the data. The black dashed line next to the regression line represents the ratio between two properties in some cases. a Porosity versus bulk density [n = 305; Grimm (1990), Kirsten (2009), David (2006), Holzwarth (1996), Mosch and Siegesmund (2007), Wenzel and Häfner (2003), and this study], b capillary water uptake versus compressive strength [n = 305; David (2006), Holzwarth (1996), Kirsten (2009), Mosch and Siegesmund (2007), and this study], c water uptake under atmospheric pressure and under vacuum versus porosity [n = 214; Kirsten (2009), David (2006), Grimm (1990), and this study], d ultrasonic velocity versus porosity [n = 89; Fitzner (1970), Kirsten (2009), and this study], e compressive strength versus ultrasonic velocity [n = 89; Fitzner (1970), Kirsten (2009), and this study], f compressive and flexural strength versus porosity, g flexural strength versus compressive strength and h compressive strength versus bulk density.

The regression analysis of basic parameters shows besides the approximate linear relationships, a partially distinct scattering. This distribution and interrelationship of parameters can be explained in greater detail, when also considering characteristics of petrographic composition and fabric. These interrelationships between strength and porosity to parameters such as pore radii distribution, grain contact, degree of alteration (i.e. maturity) and content of unstable lithic fragments is determined with confidence regions of 80 % probability (Fig. 4.13). Sandstones with a unimodal equal pore radii distribution in direction show a higher compressive strength than sandstones with unimodal unequal pore radii distributions (Fig. 4.13a). In contrast, sandstones with a bimodal pore radii distribution show a larger scattering of data as indicated by the ellipsoid with 80 % probability covering a wider range.

The interrelationships between compressive strength, porosity and type of grain contacts are well documented (Fig. 4.13b). Sandstones with low compressive strength and high porosity mainly exhibit pointed and elongated grain contacts. In contrast, sandstones with sutured and concave– convex contacts exhibit higher compressive strengths. Although the average data of the compressive strength for concave–convex grain contacts in the sandstones is lower than the data for sutured grain contacts, outliers of sandstones with concave–convex grain contacts show strengths with up to 170 MPa. Therefore, these two types of grain contacts (concave–convex and sutured) can probably be both considered equivalent and stabilizing. The interrelationship between compressive strength and degree of alteration to maturity is documented in Fig. 4.13c. Sublitharenites and litharenites with highly altered feldspars and unstable lithic fragments and high amounts of chlorite in pseudomatrix exhibit a very low compressive strength and a high porosity. Quartz arenites, which show a low degree of compaction and cementation, also display low compressive strengths and high porosities. Besides the pore radii distribution, type of grain contacts and the degree of alteration, the compressive strength is also related to the content of unstable lithic fragments. Generally, a decrease of the compressive strength with increasing amounts of unstable lithic fragments is observable as shown by sandstones with up to 5, 15 and 30 % unstable lithic fragments. Furthermore, the interrelationship of these three groups to porosity is indicated by the inclination of the three correlation lines (Fig. 4.13d). The main reason for this interrelationship is the content of unstable lithic fragments such as volcanic and clayey clasts, which commonly occur in sandstones of Upper Triassic (Lower- and Middle-Keuper) age.

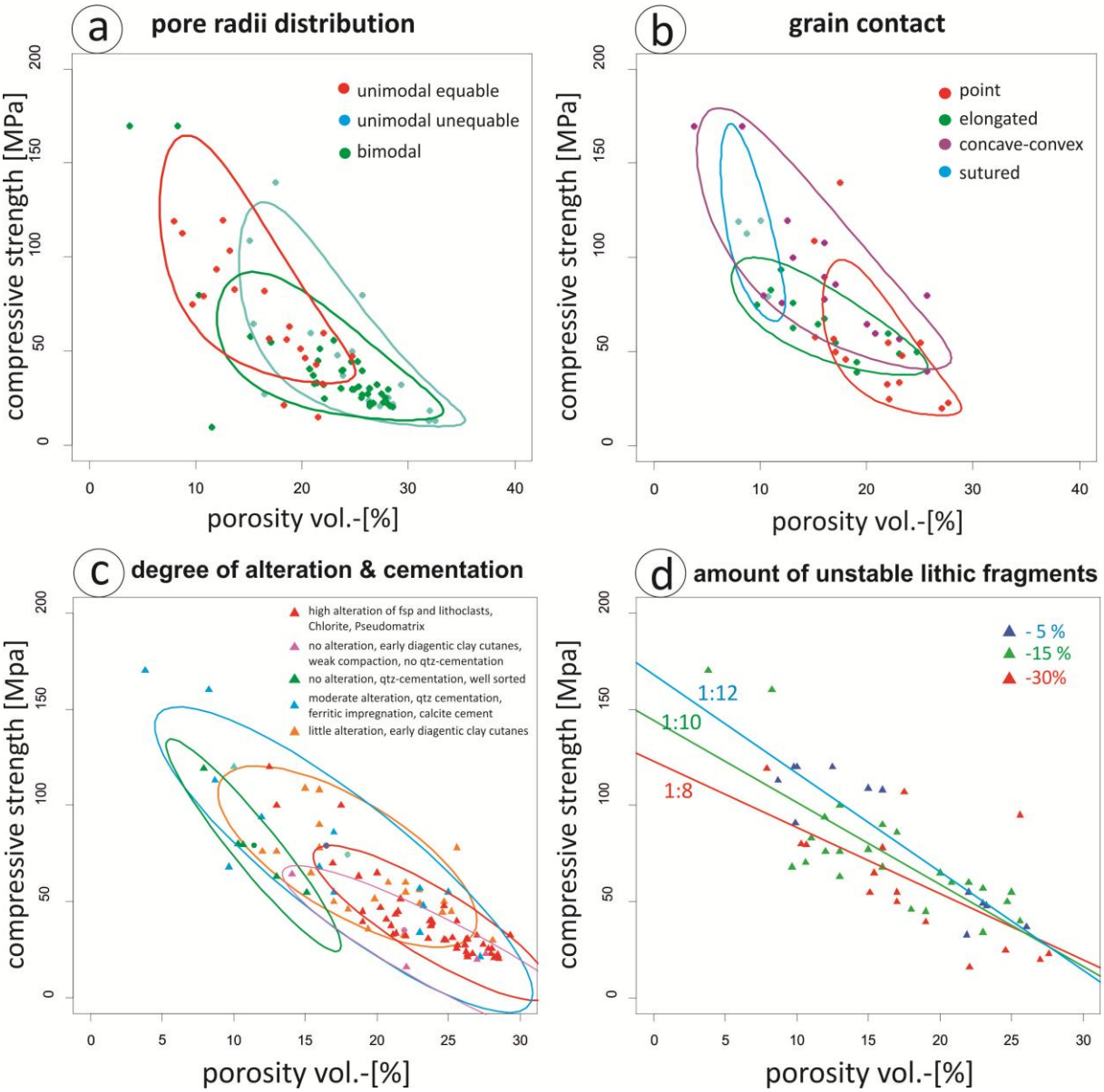

Fig. 4.13: Diagrams showing the interrelationship between strength and porosity to a pore radii distribution (n = 76), b type of grain contacts (n = 120), c degree of alteration and cementation (n = 120) and d amount of unstable lithic fragments (n = 120). Data origin from this study, Bartelsen (2008), David (2006), Fitzner (1970), Kirsten (2009) and Seidel (2004).

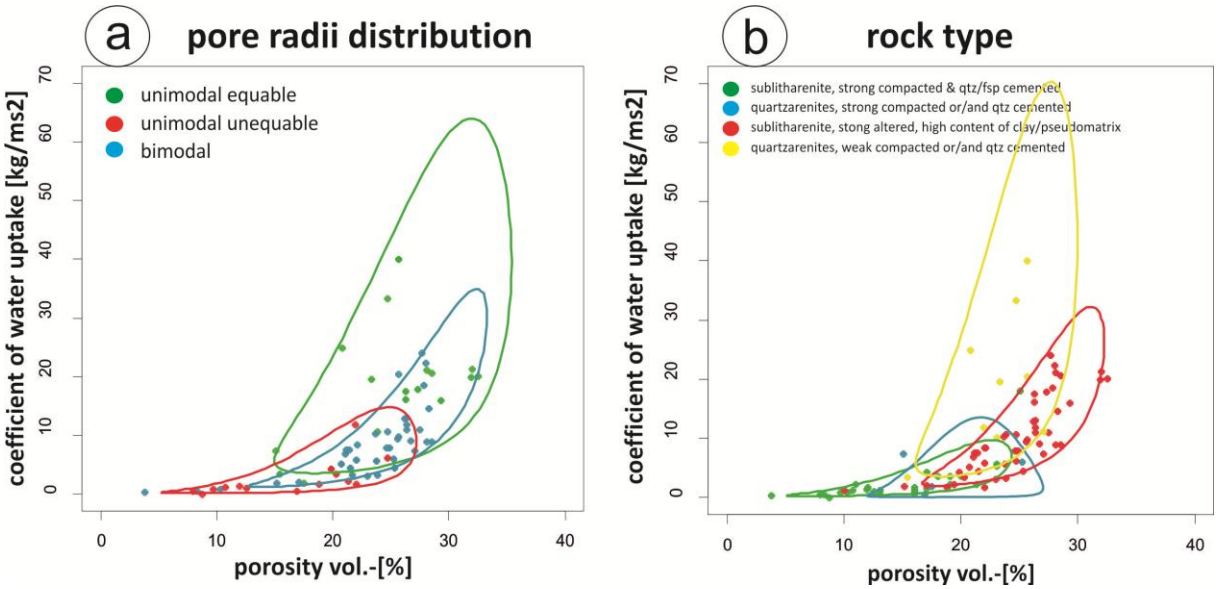

Fig. 4.14: Coefficient of water absorption dependent on porosity. Ellipsoids mark confidence regions of 80 % probability of a pore radii distribution (n = 92, Kirsten 2009; David 2006 and data of this study) and b rock types and degree of alteration, sorting and compaction [n = 87, Fitzner 1970; Kirsten 2009 and data of this study]

Also within the water absorption, further details are recognizable: The coefficient of water absorption and the porosity also show interrelationships to the pore radii distribution (Fig. 4.14a) and the different rock types with varying degrees of alteration (Fig. 4.14b). Ellipsoids confirm that sandstones with unimodal equal pore radii distribution exhibit higher w values in dependence to porosity, whereas sandstones with unimodal unequal pore radii distribution show much lower w values. Medium ranges show sandstones with bimodal pore radii distribution. This probably can be attributed to the high content of capillary pores, which promote the absorption of water in the pore space. Furthermore, the coefficient of water absorption is highest for weakly cemented and less compacted quartz arenites. In contrast, quartz arenites that are more compacted and cemented show less absorption of capillary water. Sublitharenites, which are strongly compacted and cemented, show low to medium water absorption and low porosity. The 80 % confidence region of strongly altered sublitharenites covers a wide range and overlap with the confidence region of strongly compacted quartz arenites and sublitharenites. Well-sorted sublitharenites show the highest porosity and also a high degree of water absorption.

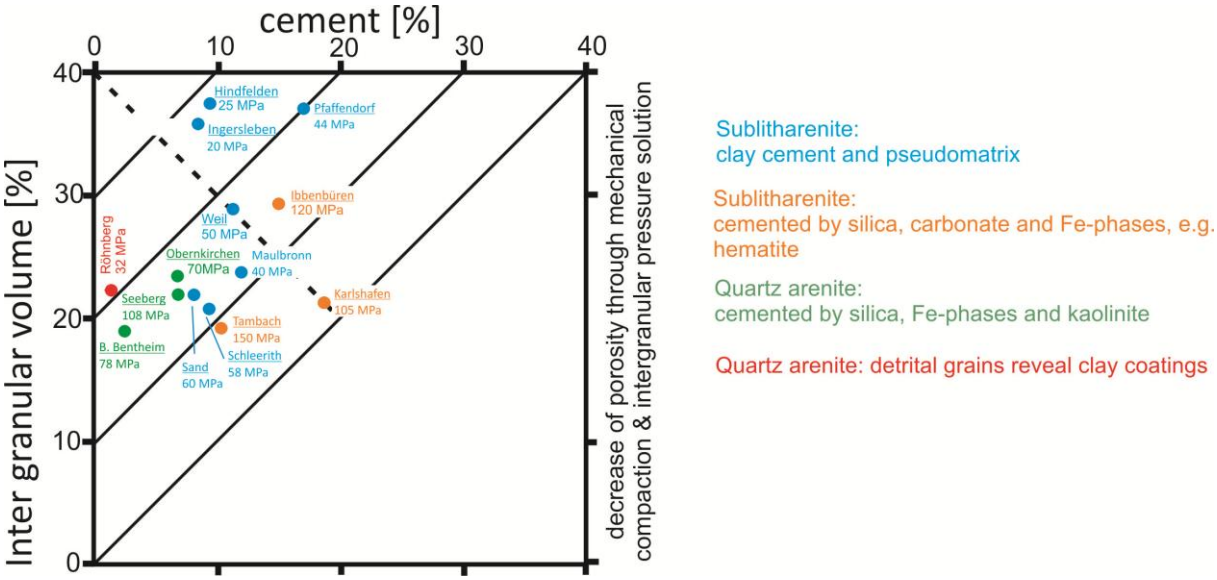

Fig. 4.15: Houseknecht diagram with selected sandstones and data of compressive strength

The ‘‘Houseknecht diagram’’ is used to evaluate which diagenetic processes reduced the intergranular volume in order to determine the reservoir quality of a sandstone (Fig. 4.15; Houseknecht 1987). In the present paper, the Houseknecht diagram is used to illustrate the interrelationship between amount and type of cement as well as intergranular pore volume (minus cement porosity) and compressive strength. Generally, the compressive strength increases with decreasing amount of inter granular volume in dependence on the type of mineral cement (Fig. 4.15). Sublitharenites containing a clay cement or pseudomatrix show a decrease of compressive strength with increasing intergranular pore volume and a decreasing amount of cement. Sublitharenites, which are cemented by silica, carbonate and Fe phases, exhibit the highest strength (105–150 MPa), an intergranular volume between 20 and 28 % and content of 10–20 % cement. These sandstones are Carboniferous, Permian and Lower Triassic in age. Quartz arenites with an intergranular volume of about 20–25 % and a low amount of cement (~5–8 %) show a compressive strength ranging between 70 and 100 MPa.

Table 4.3: Petrophysical characteristics of all 22 sandstones analyzed. These data together with numerous data from the literature is the database for the interrelationships of selected petrophysical parameters and weathering resistance (see Fig. 4.18/4.19). * = Bartelsen (2009)/Ruedrich et al (2011), **Seidel (2004)/Ruedrich et al (2005).

stratigraphy		sample	porosity [%]	w-value [kg/m*s 2]	compr. strength [MPa]	pore radii distribution	hygric dilatation [mm/m]	group of salt resistance
Cretaceous	Upper	Cotta	25.20	6.10	45.00**	bimodal	0.01	C**
		Rüthen	25.60	20.40	40.00**	bimodal	0.18	C**
	Lower	Obernkirchen	17.50	2.00	100.00	unimodal equable	0.11	A
		Hilssandstein	20.80	24.90	60.00**	unimodal equable	0.02	C**
		Bentheim	25.60	40.70	95.00	unimodal equable	0.02	A
Upper Triassic	Rhät	Velpke	24.70	33.40	50.00**	unimodal equable	0.03	B**
		Seebergen	15.80	1.80	108.91	unimodal unequal	0.01	A
		Röhnberg	21.87	11.85	32.83	unimodal equal	0.15	C
		Hockeln	15.40	3.40	65.00**	bimodal	0.19	C**
	Schilfsand-stein	Barkhausen	3.80	0.40	170.00*	bimodal	0.93	A
		Schötmar	10.30	0.90	80.00*	bimodal	1.11	B**
		Hindleben	22.07	18.05	16.10	bimodal	5.21	C
		Sander	17.00	20.05	54.71	bimodal	1.25	C
	Letten-kohlen-keuper	Ingersleben	27.71	31.03	23.10	unimodal equable	2.80	C
		Schleerith	15.26	2.01	55.00	bimodal	0.98	C
Lower Triassic	Middle Buntsand-stein	Karlshafen	7.90	0.50	119.14	unimodal unequal	1.35	A
		Arholzen	10.68	1.20	79.43	unimodal unequal	1.39	A
		Lobach	11.94	1.35	94.00*	unimodal unequable	0.60	B
		Uder	23.26	19.59	48.00*	unimodal equable	0.58	B
Permian		Bebertal	9.68	0.93	68.00	unimodal unequal	0.54	B
		Tambach	8.28	0.58	160.00*	bimodal	0.57	A
Carb.		Ibbenbüren	12.50	1.00	120.00**	unimodal unequal	0.53	A**

4.12 Weathering Properties

Two of the most important weathering mechanisms in sandstones are hygric dilatation and salt splitting. In the literature, the data regarding the weathering properties of sandstones are commonly based on hygric dilatation under water saturation and on salt splitting tests with different types of salt (e.g. sodium chloride, sodium sulphate, magnesium sulphate). The data used for the diagram in Fig. 4.17 are predominantly based on salt splitting tests using $Na_2(SO^4)$.

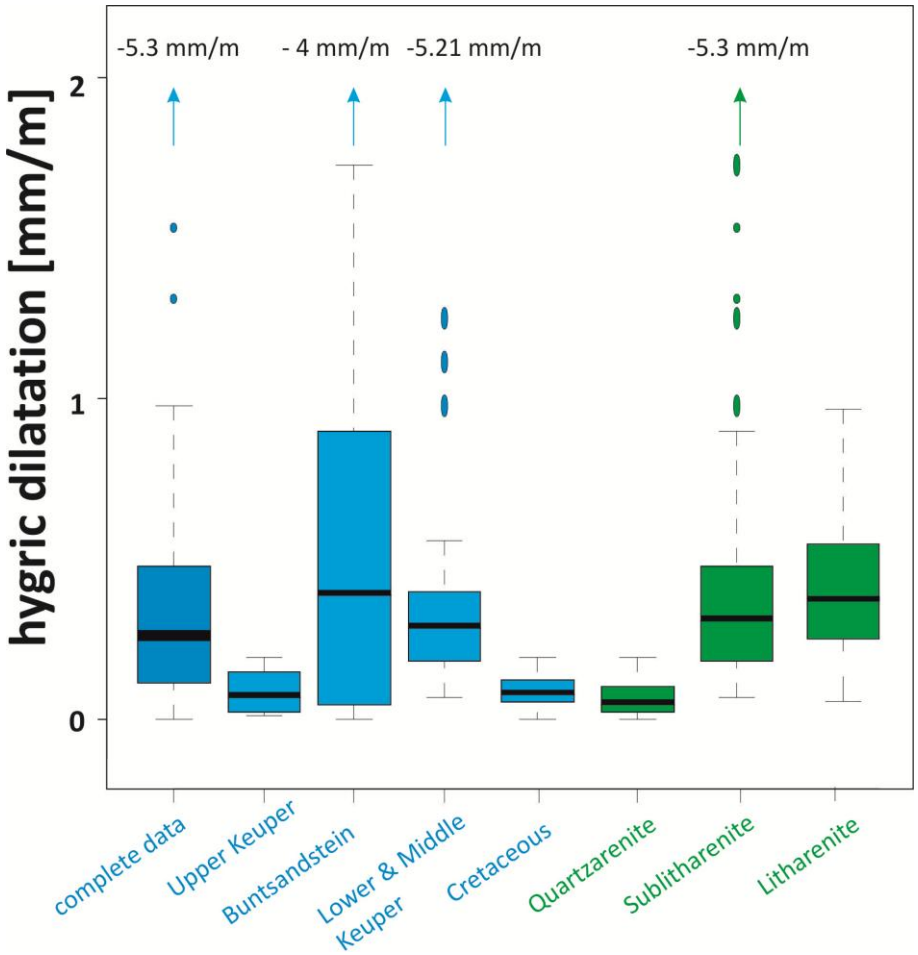

Fig. 4.16: Hygric dilatation of all sandstones analysed and from literature of Kirsten (2009), David (2006), Holzwarth (1996) (Upper Keuper, Lower and Middle Buntsandstein, Lower and Middle Keuper; quartz arenites, lithic arenites and sublitharenites).

The mean hygric dilatation of all sandstones analysed is 0.49 mm/m (highest values range from 1.2 to 5.21 mm/m; Fig. 4.16). Quartz arenites show a very low hygric dilatation (mean = 0.05 mm/m). Sublitharenites and litharenites show a dilatation with a mean of 0.59 mm/m. Sorting the hygric dilatation according to stratigraphic age, sandstones of the Upper Keuper (Rät) and Cretaceous (Wealden) show very low dilatation, although these quartz arenites can contain low amounts of swelling clay minerals (e.g. the Bad Bentheim and Röhnberg sandstones, Tables 4.1, 4.3). This may be due to the position of clay minerals within the pore space and also the type of pore radii distribution, which is almost unimodal equal and does not promote hygric dilatation. Distinctly higher values belong to the sandstones of the Lower Triassic Buntsandstein, which exhibit a mean hygric dilatation of 0.56 mm/m and a wider scattering of the first and third quartile. Lower and Middle Keuper sandstones show a narrow range of hygric dilatation, but also some very high values of up to 5.21 mm/m, which reflect litharenites of the Upper Triassic (Lettenkohlenkeuper and Schilfsandstein). This extraordinary high value belongs to the Middle Keuper Hindfelden sandstone (Table 4.3), which occurs in the Thuringia Basin. Sandstones of Cretaceous show with 0.12 mm/m the lowest hygric dilatation in average.

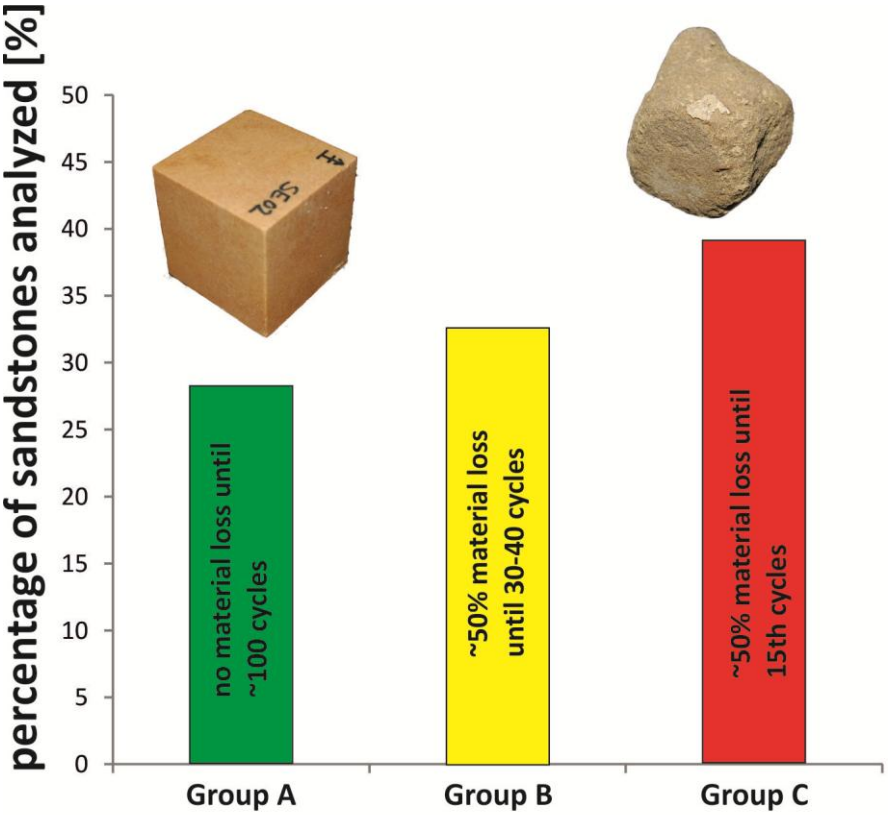

Fig. 4.17: Sandstones of different sandstones [n = 48; David (2006), this study] with salt resistances classified into Group A (no material up to 100 cycles), Group B (50 % material loss up 30–40 cycles) and Group C (50 % material loss until the 15th cycle).

In salt splitting tests (Fig. 4.17), 28.3 % of all sandstones (Group A) analysed show no loss of material up to 100 cycles. 32.6 % of the sandstones (Group B) lose 50 % of their material in the range of 30–40 cycles. 39.1 % of the sandstones (Group C) show 50 % material loss already during the first 15 cycles. Sandstones with the best salt resistance (Group A; Upper Keuper and Cretaceous, Table 4.3) are predominantly composed of quartz arenites. They seldom fall into Group B or C, such as the Röhnberg or Cotta sandstone, which is very weakly compacted and cemented and exhibits high amount of clay cutanes on detrital quartz grains, respectively, a clayey matrix like sandtone Cotta. Litharenites are primarily positioned in Group C, and subordinate in Group B. In contrast, sublitharenites show no clear preference to group since every group is represented. The strongly compacted Weser sandstones mostly belong to Group A or B. In contrast, the sandstones of the Lower and Middle Keuper (Schilfsandstein, Lettenkohlenkeuper, e.g. SA, SL, HS, IS; Table 4.3) mainly fall into Group C and subordinate in Group B.

The interrelationship between the coefficient of water absorption and porosity in the three groups of salt resistance is documented in Fig. 4.18a. Sandstones with a high porosity and a high coefficient of capillary water absorption show the lowest resistance against salt splitting. In contrast, sandstones with low porosity and low capillary water uptake show a very high resistance against salt splitting. Similar interrelationships are obvious when considering the compressive strength versus porosity (Fig. 4.18b). Sandstones with high compressive strength and low porosity are most stable against salt splitting, in contrast to sandstones with low compressive strength and high porosity, which show the lowest salt resistance. In Fig. 4.18c, four classes of hygric dilatation are defined that show a distinct

overlapping of the confidence ellipsoids. Sandstones with low compressive strength and high porosity primarily belong to the classes of higher hygric dilatation. Four groups of hygric dilatation can be identified when the sorption and the amount of micropores are regarded (Fig. 4.18d). Samples with different amounts of micropores and sorption plot in markedly different ellipsoids of 80 % confidence. Sandstones which show a hygric dilatation of less than 0.1 mm/m have the lowest amount of micropores. Nevertheless, they can show a sorption ranging between 0.2 and 1.5 wt%. Sandstones with a hygric dilatation of 0.1–0.5 mm/m have a higher amount of micropores and water absorption up to 4.5 wt%. Sandstones with a hygric dilatation of 0.4–5.0 mm/m show the best normal linear correlation between sorption and the amount of micropores.

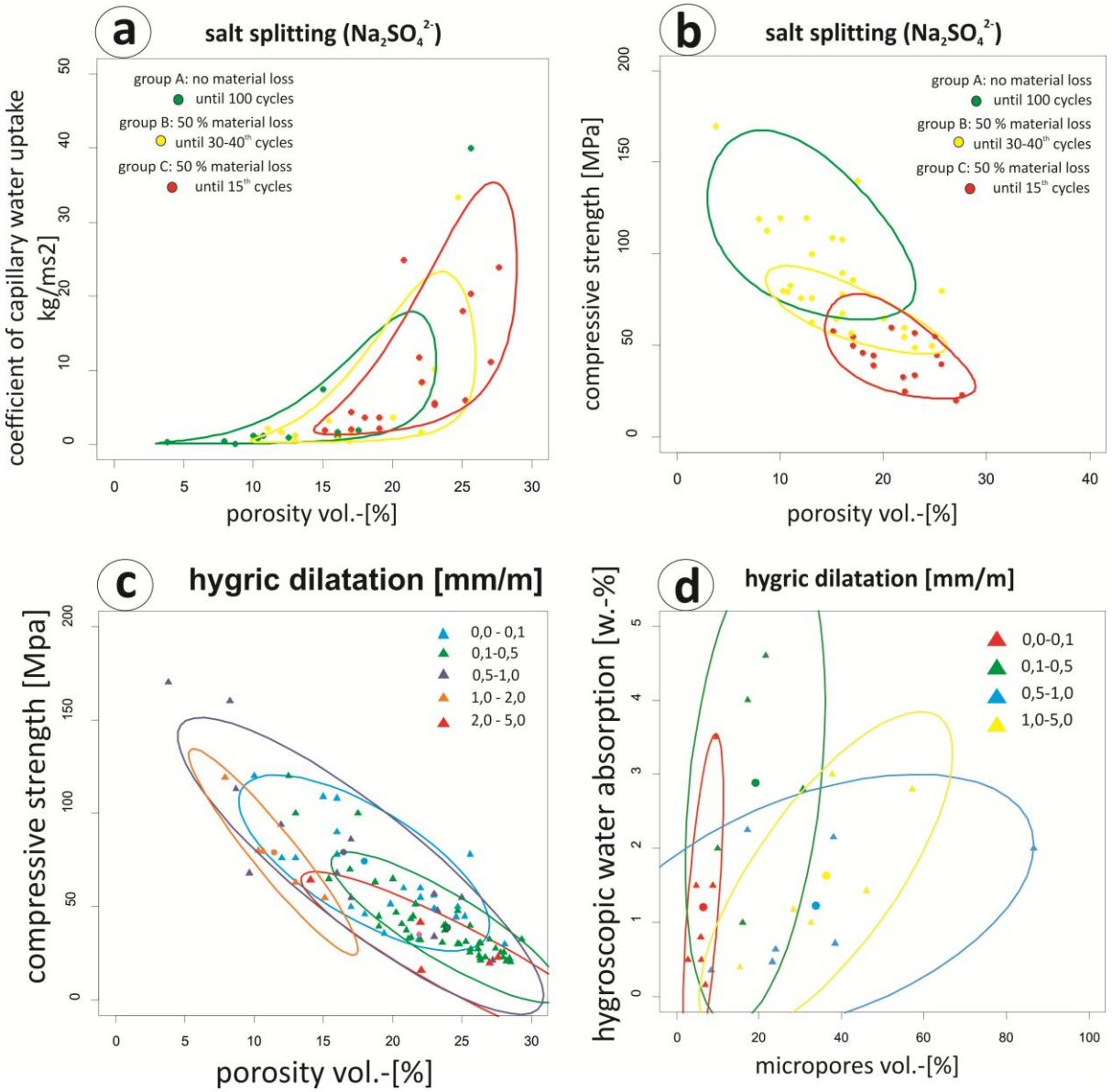

Fig. 4.18: Diagrams showing the interrelationships between selected petrophysical parameters and salt resistance: a coefficient of water absorption, porosity and groups of salt resistance (n = 48; David 2006 and own), b compressive strength, porosity and salt resistance (n = 48; David 2006 and own samples), c compressive strength, porosity and hygric dilatation (David 2006; Kirsten 2009; Holzwarth 1996 and own samples) and d sorption (weight increase at 100 % rel. air humidity), content of micropores and hygric dilatation. Ellipsoids illustrate the 80 % confidence regions.

4.13 Multicorrelation of Sandstone Properties using Principal Component and Cluster Analysis

The principal component analyses consider the porosity, capillary water absorption, compressive strength, salt resistance as well as hygric dilatation data (data from present study, Bartelsen 2008; David 2006; Seidel 2004, Fig. 4.19). An orientation of variables within the diagram confirms a positive linear correlation between compressive strength and the number of cycles in salt splitting tests as well as between capillary water uptake and porosity. Between compressive strength, salt resistance and capillary water uptake as well as porosity, a negative correlation is well expressed. Hygric dilatation and porosity show no correlation to each other, whereas a positive correlation of compressive strength to salt resistance is obvious (Table 4.4). The three groups of different pore radii distribution (Fig. 4.19a) form clear clusters in the principal component analysis. The variance of sandstones with unimodal equal pore radii distribution is characterized by a high capillary water uptake and porosity. In contrast, the variance of samples with unimodal unequal pore radii distribution is concentrated in the field of salt resistance and compressive strength. The sandstone data exhibiting a bimodal pore radii distribution show more scattering and are characterized by a high hygric dilatation and lower compressive strength.

Adding lithotypes to the principal component analysis (Fig. 4.19b), it is obvious that quartz arenites show a unimodal equal pore radii distribution. Strongly compacted and cemented sublitharenites–litharenites are characterized by variable data with regard to salt weathering, compressive strength and hygric dilatation. Most of these sandstones show high compressive strength and are resistant against salt splitting, but the hygric dilatation can vary significantly. These sandstones predominantly show a unimodal unequal pore radii distribution. In contrast, sublitharenites– litharenites with a high content of unstable lithic fragments and/or pseudomatrix show a higher hygric dilatation and high porosity with a well-developed tendency for capillary water absorption. These sandstones primarily show a bimodal pore radii distribution.

By including micropores, the primary intergranular pore volume (minus cement porosity), unstable lithic fragments and the sorption into the principal component analysis (Fig. 4.19c) further interrelationships can be recognized. The hygric dilatation shows a positive correlation to the amount of unstable lithic fragments and sorption. Subordinately, an interrelationship between the amount of micropores and degree hygric dilatation can also be observed. The present porosity always shows a positive linear correlation to the primary intergranular pore volume (minus cement porosity) in the sandstones analysed.

Weakly compacted quartz arenites with minor amounts of cement are characterized by high coefficients of water absorption, a high amount of primary intergranular pores and high porosity as

well as a small hygric dilatation, low sorption and minor amounts of micropores. These sandstones commonly show moderate to low salt resistance and compressive strength. The extraordinary Bad Bentheim sandstone exhibits a high capillary water absorption and high porosity and is characterized by medium compressive strength and high salt resistance.

Strongly compacted and cemented quartz arenites are characterized by high compressive strength and salt resistance and low amounts of intergranular pore volume as well as a low coefficient of water absorption, small amounts of micropores and a very low sorption. Strongly compacted and cemented sublitharenites–litharenites are characterized by small amounts of intergranular pores, minor water absorption and a low degree of hygric dilatation combined with a low amount of micropores. Strongly altered sublitharenites–litharenites show a high degree of water absorption and many micropores as well as a low amount of intergranular pores. The Hindfelden sandstone exhibits an extraordinarily high degree of hygric dilatation, many micropores and unstable lithic fragments, and low salt resistance and compressive strength.

In the cluster analysis shown in Fig. 4.19d, the different lithotypes based on similar material and weathering properties show a very good grouping (I, II, III, IV, and V) and indicate a well-expressed weathering resistance. Sandstones showing low salt resistance and/or distinct hygric swelling are found in the pink ellipsoid (I). They consist of strongly altered sublitharenites–litharenites (e.g. the Ingersleben and Hindfelden/Middle and Lower Keuper sandstones), but also weakly compacted quartz arenites (of Cretaceous and Lower and Triassic/Buntsandstein, e.g. sandstone Rüthen, Hilssandstein, Uder and Velpke). Sandstones that are found in the orange ellipsoid are mostly quartz arenites and sublitharenites–litharenites, which are weakly compacted and cemented, medium to low strength, show a porosity >20 % and a high coefficient of water absorption. Furthermore, they are characterized by a medium to low weathering resistance, since they only show weak salt resistance. Sandstones belonging to this group are e.g. Röhnberg and Cotta. In Group III, altered sublitharenites– litharenites and weakly compacted quartz arenites can be found. They are characterized by porosity between 10 and 20 %, medium strength as well as medium weathering resistance, which is confirmed by their affiliation in salt Group B and low hygric dilatation. Sandstones belonging to this group are Schleerieth, Sander (Upper Triassic/Lower and Middle Keuper) and Hockeln (Upper Triassic, Rhät). Sandstones of Group IV include the sublitharenites–litharenites, which are strongly compacted and cemented such as the Weser sandstones and also the Permian Tambach and Bebertal sandstones. They are characterized by a well-pronounced salt resistance and also a distinct hygric swelling. Within Group V, strongly compacted quartz arenites and sublitharenites are found, which are characterized by low porosity, high strength, low water absorption and, therefore, a very well-developed weathering resistance, since they only show little hygric dilatation and high salt resistance. Sandstones belonging to this group are, e.g. Seebergen,

Arholzen, Obernkirchen and Ibbenbüren. Only sample Bad Bentheim does not fit in any group and is separated from the remaining sandstones.

To summarize, the sandstones which belong to Group IV and V can be defined as weathering resistant, whereas sandstones of Group I and II only show weak weathering resistance. Group III includes samples that can be defined as medium resistant.

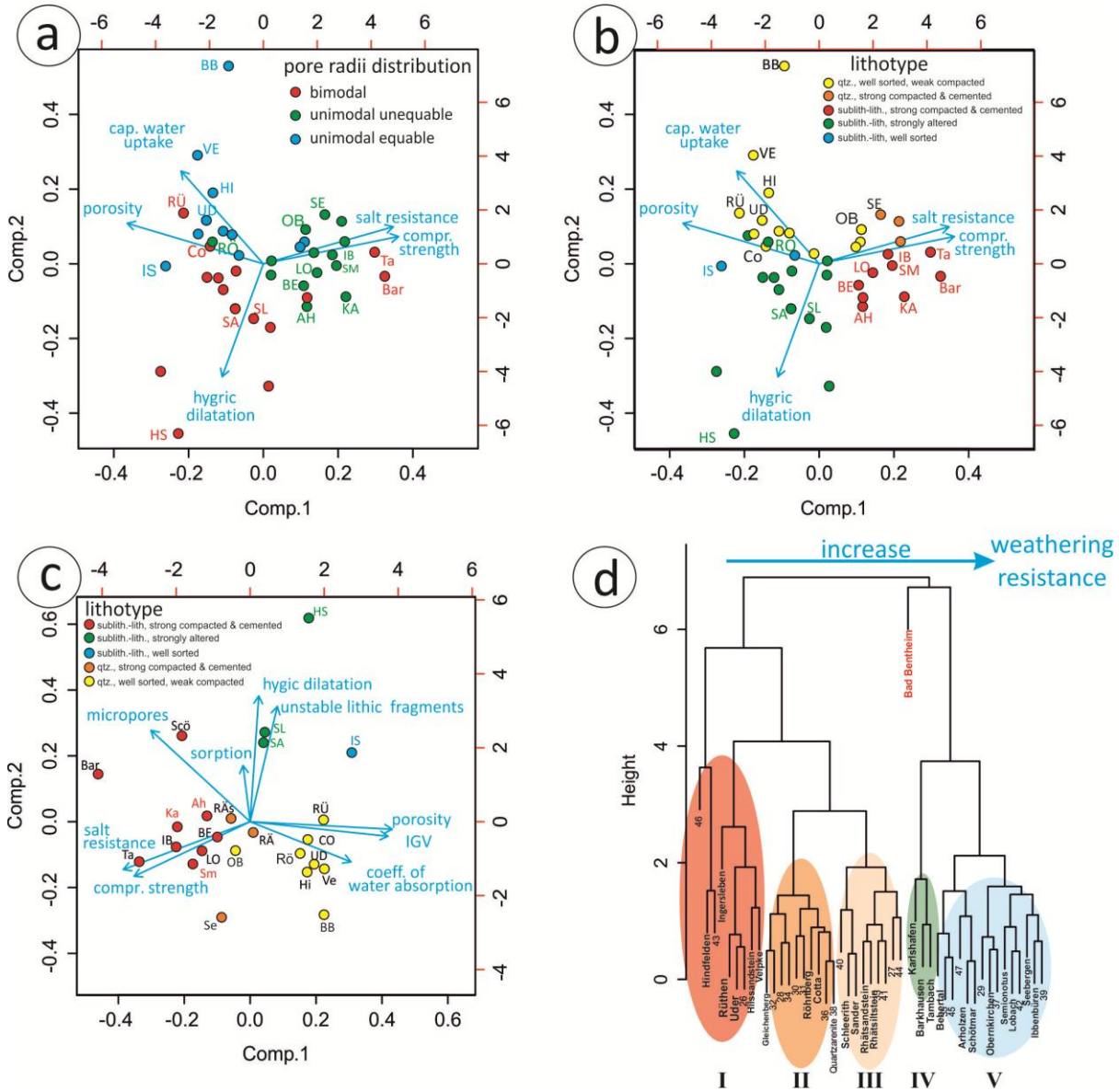

Fig. 4.19: Diagrams showing principal component analyses in dependency on a pore radii distribution, b lithotype (abbreviations: qtz quartz arenite, sublith. sublitharenites, lith. litharenites) and c additional properties like sorption, micropores, unstable lithic fragments and intergranular volume in interrelationship to different lithotypes. d Cluster analyses with clusters based on petrophysical properties of different sandstones. From the left to the right, the weathering resistance increases (for explanation see text; analyses include own data as well as data of Bartelsen (2008), David (2006), Kirsten (2009), Seidel (2004)).

Table 4.4: Components and loadings of principle component analysis of Fig. 4.18 a) and b).

	Comp. 1	Comp. 2	Comp. 3	Comp. 4	Comp. 5
Parameter	0.57	0.23	0.14	0.03	0.02
Loadings					
Porosity	-0.55	0.255			0.796
Hygric dilatation	-0.17	0.71	-0.64		0.111
Compressive strength	0.542	0.172	-0.25	-0.69	0.366
Cap. water absorption	-0.33	0.586	-0.61	-0.11	-0.41
Salt resistance	0.521	0.234	-0.34	0.710	0.228

The loadings are documented for each rock property

4.14 Discussion and Conclusions

The statistical analyses from the combined petrographical, petrophysical and fabric data of the sandstones with differing geological age and composition show that multiple interlocking parameters control their material properties. In the sandstones analysed, the univariate data distribution highlights the interrelationships between compressive strength and amount of porosity with lithology and stratigraphic position. Furthermore, a general decrease of porosity in dependency to burial time and depth can be observed, which confirms the study of Koch and Sobott (2008) and the modelling of Scherer (1987) and Waples (2002). The sorting as textural parameter of the sandstones simultaneously affects the porosity. In contrast, no linear correlation is reflected by the average grain size to porosity, which was also found out by studies of unconsolidated sands (Beard and Weyl 1973).

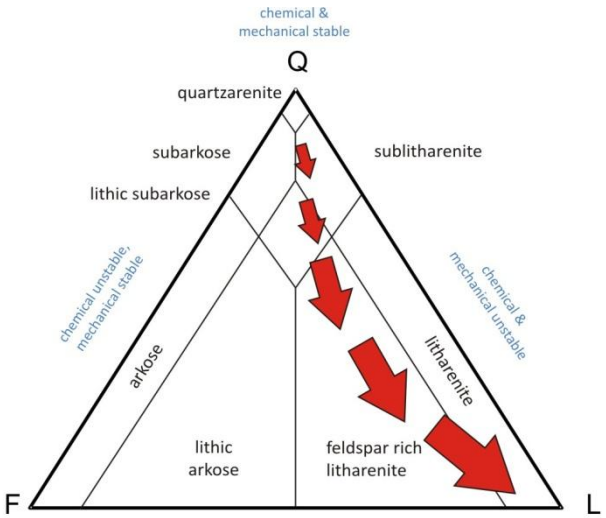

Fig. 4.20: Simplified illustration of relationship between lithology (Q quartz, F feldspar, L lithoclast), mechanical properties during compaction and pore space development. Arrows show trend of porosity decrease through compaction and decrease of chemical and mechanical stability with increasing amount of unstable lithic fragments and resulting weathering resistance (Modified after McBride 1963).

The compressive strength shows interrelationships to the pore radii distribution, the type of grain contacts, the primary intergranular volume (minus cement porosity) as well as to the degree of alteration, amount of cementation and content of unstable lithic fragments. Furthermore, a wellexpressed interrelationship between the amount of mechanical stable grains and the

compressive strength can be confirmed. Moreover, a high compressive strength is associated with a longer time and increasing depth of burial, which also correlates with a lower amount of porosity. After Füchtbauer (1967) and Houseknecht (1984), a negative relationship between grain size and volume of quartz cement exists. Regarding a stabilizing effect by quartz cementation on sandstones, also a positive correlation between grain size and strength should be observable. However, a relationship between average grain size and strength was not detected.

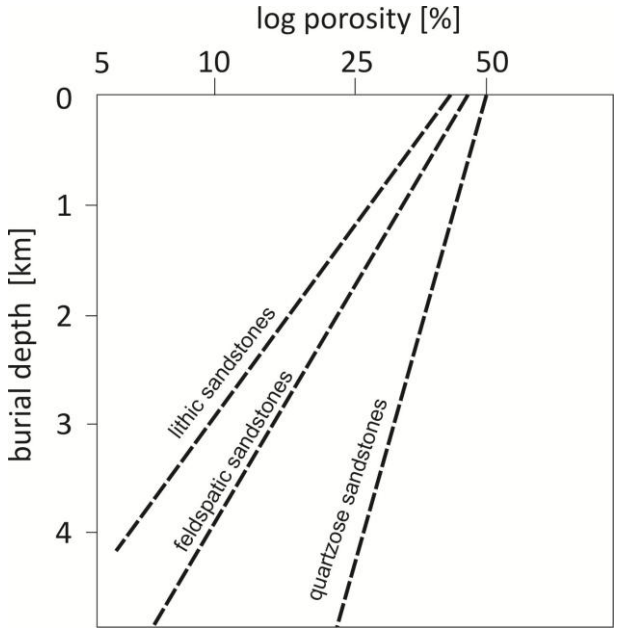

Fig. 4.21: Porosity relationship for sandstones of different composition. Modified after Dickinson (1985).

The amount, size, and geometry of the pores significantly affect the weathering resistance of a natural building stone, since they trigger the water balance (Fitzner and Snethlage 1982; Putnis et al. 1995; Putnis and Mauthe 2000; Ruedrich et al. 2011). As documented in this study, the properties such as capillary water absorption, water absorption under normal conditions and under vacuum, as well as the resulting saturation degree are closely related to the porosity characteristics of a given sandstone. The sorption depends significantly on the amount of micropores (Peschel 1983; Klopfer 1985; Siegesmund and Dürrast 2011). Moreover, the pore radii distribution defines the kind of water transport (Ruedrich and Siegesmund 2006; Siegesmund and Dürrast 2011) and, therefore, significantly influences weathering resistance of sandstones (Fitzner and Snethlage 1982).

Compressive strength, porosity and pore radii distribution can be defined as general key parameters for the prediction of salt resistance and hygric dilatation. However, these parameters are the result of the primary mineral composition (compositional maturity) and the diagenetic development (lithification; type and intensity of cementation; formation of secondary porosity) Stück et al. (2011). Based on these parameters, a model for the interpretation of the diagenetic development of the different sandstone types and their material properties will be discussed below. The goal of this

model is to characterize the development of pore space geometry and to predict/estimate their possible weathering behaviour.

4.15 Diagenetic Sequences in different Sandstone Types and the Development of Pore-Space Geometry and Compressive Strength

Transport mechanisms and the physicochemical eogenetic conditions in the depositional milieu (water chemistry; intrastratal solution) of detrital grains are the basic parameters for the following diagenetic pathways during eogenetic alterations and finally trigger the material properties markedly. The initial porosity is fixed with deposition of the unconsolidated sediment, as expressed by the textural and compositional maturity. Houseknecht (1988) postulates an initial porosity for subarkosic wackes deposited in meandering river systems of 60 %, and for subarkoses from braided rivers with 40 %. Analyses of artificial grain mixtures of natural sands show that poorly sorted sands have a porosity of 27.9 %, weakly sorted sands 30.7 %, moderately sorted 34 %, well-sorted 39 % and for very well-sorted sands 40.8 % (Beard and Weyl 1973). These data are consistent with the data of sandstones analysed in the present study. Well-sorted quartz arenites show the highest intergranular pore volume of 25–30 %, whereas moderately sorted sandstones show a lower intergranular pore volume (15–20 %). However, where unstable lithic fragments are altered to pseudomatrix in sandstones, the intergranular volume and secondary porosity can increase greatly. After Schmidt and McDonald (2012), secondary porosity is also caused by mesogenetic leaching of carbonate minerals such as calcite, dolomite and siderite. Besides the primary composition, clay infiltration or Fe-oxide rims formed during eodiagenesis have a marked influence on the later grain overgrowth by silica (Cecil and Heald 1971) and the formation of special clay mineral cements. When clay rims observed are thick (2–5 µm), quartz overgrowth is hindered. If Fe–organic complexes are present during the mesodiagenetic burial stage, authigenic chlorite cement rims can be formed around grains. If Fe–organic complexes or other Fe phases are missing, illite cement rims are commonly formed (Surdam et al. 1989). Besides the influence of clay minerals on the later cementation, the content of clay minerals in general affects the acoustic velocities and also the compressive strength of sandstones (Kowallis et al. 1984; De Martine et al. 1976; Han et al. 1986). In general, increasing clay contents result in decreasing ultrasonic velocities independent of the degree of consolidation.

Grains can be differentiated into mechanical and chemically stable/unstable components (McBride 1963, Fig. 4.20). Therefore, during compaction under burial conditions, the content of ductile grains plays an important role for the further development of the pore space. Large differences in the porosity during burial diagenesis are generated by mechanical and chemical compaction (Surdam et al. 1989; Hartmann et al. 2000). In comparison to feldspathic and lithic sandstones, quartz arenites require deeper burial conditions for compaction (porosity decrease) to the same degree (Fig. 4.21,

Dickinson 1985). Regression analysis between compressive strength and amount of porosity shows that the content of unstable lithic fragments markedly influences the data documented in the strength–porosity plot. This confirms that the higher the content of unstable lithic fragments, the lower is the grain contact between stable grains probable. Moreover, the type of grain contacts has an influence on compressive strength. Sandstones with predominantly concave–convex and sutured grain contacts exhibit a higher compressive strength than sandstones with pointed and elongated grain contacts. Compressive strength also varies within the groups of grain contact due to the different kinds and intensity of cementation. In addition, the kind of unstable lithic fragments is also important for later cementation. If volcanic detritus is present, hydration reactions are favoured and the formation of authigenic feldspar is common. In contrast, abundant chert fragments can inhibit quartz cementation and thus preserve porosity (Surdam et al. 1989).

Furthermore, our results also show that porosity and compressive strength are dependent on the burial time. As Scherer (1987), Waples (2002) and Koch and Sobott (2008) documented, sandstones of the same sorting and the same quartz content which were buried into the same depth can show different amounts of porosity that is related to the different time of burial.

These interrelationships are also reflected by all the data of sandstones recently analysed as schematically summarized in Fig. 4.22. Pure quartz arenites are commonly well sorted (high maturity), have a primary porosity of 39–40 %, a unimodal pore radii distribution and reveal capillary pores of 0.1–10 lm radius. During the closer packing of grains, pressure solution starts at the point contacts (chemical compaction) and porosity further decreases. Depending on a possible infiltration of clay during eogenesis or not, a quartz dissolution/cementation reaction takes place. If there is no clay infiltration, the sandstone may be more intensively compacted and a high contact thickness (Füchtbauer 1988) occurs, which is defined by the grain contact length in the entire sandstone and depends on the type of grain contact. The potential for quartz pressure solution is given in clay-bearing sandstones since K2O increases the pH value. This promotes the solution of quartz (Füchtbauer 1974) and therefore also influences the porosity modification. The pore radii distribution commonly reveals the same unimodal equal distribution as in the beginning diagenetic stages. Nevertheless, the average pore size becomes smaller because of the reduction of larger gusset pores by quartz cementation. The pore radii distribution of sandstones, which are much more strongly compacted, can shift to unimodal unequal and smaller capillary pores. In the same way, the water absorption increases due to the presence of more capillary pores.

These interrelationships are observable in Upper Triassic (Rhät; e.g. RÖ, SE, Tables 4.1, 4.3) and Cretaceous (e.g. BB, RÜ, OB, VE, Tables 4.1, 4.3) quartz arenites investigated in this study. Dependent on burial time and sorting, the porosity is between ~15 and 30 %. Sandstones belonging to the Upper

Triassic exhibit a porosity of around 15–20 % (e.g. SE, Tables 4.1, 4.3), whereas younger sandstones belonging to the Cretaceous show a porosity ranging from 25 to 30 %. According to Blöcher et al. (2007), a homogeneous pore size distribution results in a higher compressive strength. This can be transferred to the quartz arenites that show a unimodal equable pore radii distribution. Because no unstable lithic fragments are present, these two sandstone types of Upper Triassic and Cretaceous show a medium to high compressive strength (70–150 MPa). Within the glauconite-bearing Cretaceous sandstones, furthermore a weak negative relationship to compressive strength is observable (e.g. HI, CO, RÜ). Further impact on strength can have a clayey matrix, which distinctly decreases the rock strength like in case of sandstone Cotta. Simultaneously, if early clay infiltration took place and clay rims are formed around detrital grains, quartz overgrowths are inhibited and micropores occur in increasing amounts, which both clearly decreases the compressive strength (e.g. RÖ, Tables 4.1, 4.3). Here, the kind of infiltrated clay minerals are also important: While porefilling kaolinite reduces porosity and has little effect on permeability, lining the pores with illite has little effect on porosity, but permeability becomes considerably reduced by blocking pore throats (Stalder 1973; Tucker 2001). According to Stonecipher et al. (1984), low permeability promotes cementation. In contrast, in sandstones with high permeability, solutions do not remain in pore spaces long enough to build local concentration that promotes precipitation of cement. However, in both cases the pore size distribution through clay minerals is modified from unimodal equal to unimodal unequal. This results in a lower strength (50–80 Pa), since the heterogeneity of pore size distribution increases and the porosity (~25 %) is preserved by prohibited cementation of silica or calcite by the presence of clay minerals. Because of the effect of clay mineral cements, which can be compared to clay matrix and/or pseudomatrix, the grain contacts of detrital grains are predominantly point contacts.

When the content of unstable lithic fragments and/or feldspar increases, such as in subarkoses, sublitharenites and litharenites, the development of pore space and compressive strength is independent of each other (Fig. 4.22). In these sandstones, the compositional and textural maturity is much lower than in quartz arenites. Furthermore, the ratio between textural to compositional maturities also significantly influences the quality of the latter natural building stone. The so-called Weser sandstones (Lower Triassic; Tables 4.1, 4.3: samples KA, LO, AH) are examples of this sandstone type. The primary porosity of the moderate- to well-sorted sandstone is 34–39 %. The pore radii distribution is unimodal unequal. During eogenesis, haematite impregnation occurs. With advancing burial compaction, feldspar alteration and quartz dissolution commonly takes place. Subsequent to quartz cementation, authigenic clay minerals are formed due to the alteration of feldspars or unstable lithic fragments and also carbonate cementation occurs. The intergranular pore space decreases markedly due to compaction and cementation. The alteration of feldspar and

unstable lithic fragments create a small amount of micropores. The final pore radii distribution is unimodal unequal and the compressive strength is dependent on the degree of alteration and cementation that is medium to high (70–150 MPa). The coefficient of capillary water absorption is low (~0–5 kg/ms^{2-}), because only a very small amount of capillary pores is developed and porosity is mostly low. Sandstones of similar composition but longer burial history such as the Carboniferous and Permian sandstones (Tables 4.1, 4.3; samples IB, TA, BE) show a similar pore size distribution, but markedly lower porosity (up to 10 %) and a higher compressive strength (70–160 MPa). Due to the lower porosity, also the water absorption is weakly pronounced.

Sublitharenites and litharenites of the Upper Triassic Schilfsandstein and Lettenkohlenkeuper show very low textural and compositional maturity (e.g. HS, IS, SA, SL; Tables 4.1, 4.3). The grains are angular to subangular and unstable components are moderately altered. The primary porosity also ranges from 34 to 39 %, because the rock is moderately well sorted. However, the textural maturity is characterized by contents of squeezed altered unstable lithic fragments to pseudomatrix, which distinctly decreases the textural maturity of these sandstones. After deposition, porosity decreases through compaction and silica cementation. Partially, organic fragments parallel to bedding destabilize the fabric (e.g. HS, IS). The alteration of (volcanic) clasts to clay minerals and clayey matrix tends to be squeezed between more rigid grains (pseudomatrix), even during the initial stages of diagenesis at shallow burial. This also prohibits a free circulation of fluids and leads to restricted cementation. Porosity decreases through further compaction and the content of micropores increases greatly because of the altered unstable lithic fragments. This finally leads to sandstone with a low compressive strength, because in this rock with heterogenous pore radii distribution a stable grain framework does not exist anymore. The bimodal pore radii distribution supports high water absorption. The maximum in capillary pores promotes the capillary water absorption and the maximum in micropores the sorption. Statistical data of the different lithologies, fabric properties and type of grain contact, compressive strength, porosity and pore radii distribution are documented and summarized schematically in Fig. 4.22.

Considering the lateral change of sorting, an increase of textural maturity and decrease of grain size with increasing transport distance from the source area should be developed for each sandstone. Accordingly, a lateral change of primary composition due to the content of unstable grains, sorting and primary porosity should be developed. However, the increase of maturity has to be regarded under very local conditions with alternating directions and cannot be transferred by only considering the original source area of the sediment. For example, the Keuper sandstones of the Burgsandstein (Vindelizian Keuper) should show an increase of compositional and textural maturity from SE to the NW direction. However, these sandstones were predominantly deposited in channels of alluvial fans,

and therefore they show a highly variable maturity. Thus, general statements on lateral development of material properties are not possible in the present study.

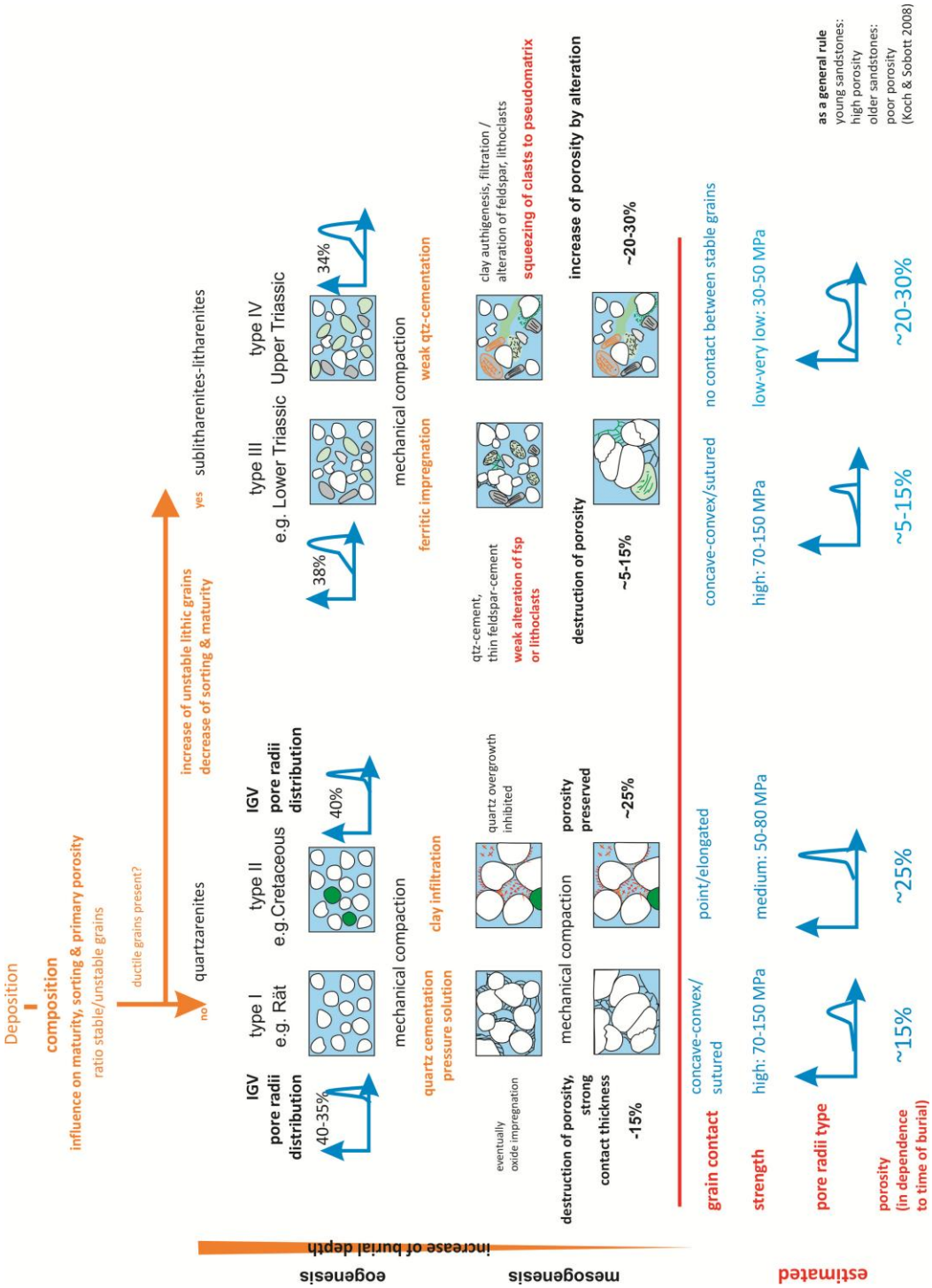

Fig. 4.22: Development of pore space and compressive strength of different sandstone types. After deposition, the primary composition and sorting rule the (primary) porosity (intergranular volume = IGV) and the pore radii distribution. Therefore, mature quartz arenites show higher porosity than more immature sublitharenites–litharenites. This porosity is modified through clay infiltration, alteration, cementation and compaction. During eogenesis, clay infiltration can occur that creates micropores and prohibits quartz overgrowths during later mesogenesis, which is why the porosity is preserved. Compaction and cementation decrease the porosity during further diagenesis, and thus contact thickness can increase, which finally leads to higher strength. Estimated for each lithotype are grain contact, strength, pore radii type and porosity. Since the controlling parameters during diagenesis can vary, the material properties also have to be interpreted as flowing transitions.

4.16 Weathering Behaviour in Dependence to Composition

Regression analysis and principal component analyses allow the prediction of pore space, compressive strength and water absorption for sandstones of differing lithology. Weathering behaviour can therefore be estimated because these parameters show linear correlations to the petrophysical properties. Although porosity is a key for characterizing the weathering behaviour of the sandstones, the same amounts of porosity can lead to different resistances against salt splitting or hygric dilatation. The results of the salt splitting tests agree with other studies on German sandstones (Snethlage and Wendler 1997; Fitzner and Snethlage 1982; Zehnder and Arnold 1989; Ruedrich et al. 2006), where it was documented that sandstones with a high amount of very small capillary pores and micropores are highly sensitive to salt splitting. According to Snethlage and Wendler (1997), the pore space characteristics control the solution transport and in consequence also the distribution and amount of salt in the rock. Thus, a correlation between the stability against salt splitting, pore size distributions and lithotype is well expressed. Furthermore, the compressive strength is also important for the interpretation of stability against salt splitting, because the rock has to withstand increasing crystallization pressures of the salt (Goudie and Vlies 1997; Scherer 1999), which should not surmount the degree of internal stability indicated by the compressive strength. Accordingly, highly mature quartz arenites, which are weakly compacted (high porosity), exhibiting a high amount of micropores due to the infiltration of clay minerals, have a low-medium compressive strength (e.g. Rö, Tables 4.1, 4.3) and show only a moderate resistance to salt splitting (Group B–C). The Bad Bentheim sandstone surprisingly is a rock with a very high resistance to salt splitting and hygric dilatation, although the rock shows high porosity, medium compressive strength, high capillary water absorption and swellable clay minerals (Tables 4.1, 4.3). This confirms the special position of sandstone Bad Bentheim, illustrated also by cluster analyses (Fig. 4.18d). The pore radii distribution with only clear maxima in large capillary pores probably does not induce any stress during salt crystallization, since crystal growth can take place within the free pore space without any resistance. The homogeneous pore space could be responsible for the medium strength as mentioned above (Blöcher et al. 2007).

Highly compacted and cemented quartz arenites without the infiltration of clay predominantly exhibit a very high resistance against salt splitting, because the distribution of pore radii indicates just a very low amount of micropores and also only low porosity (e.g. SE, Tables 4.1, 4.3). Sandstones enriched in unstable feldspars and lithic fragments, which are highly compacted and cemented, commonly show a high compressive strength, low porosity and favourable pore radii distribution (e.g. unimodal unequal), and therefore are also resistant against salt splitting. Sublitharenites and litharenites with common altered rock fragments and pseudomatrix show the lowest resistance against salt splitting. The pore radii distribution is characterized by a large amount of micropores

caused by the alteration of unstable lithic fragments (partially squeezed to pseudomatrix) and a compressive strength which is too low to withstand the increasing internal pressure by salt crystallization. The lowest salt resistance of the sandstones analysed are found, e.g. in the Ingersleben and Hindfelden sandstones of the Upper Triassic (Schilfsandstein, Lettenkohlenkeuper) (Tables 4.1, 4.3).

Different reasons are discussed for the process of hygric dilatation. After De La Calle and Suquet (1988), Weiss et al. (2004), Dixon and Weed (1989) and Moore and Reynolds (1997), the dilatation is mainly caused by the presence of expending clay (intracrystalline swelling). Also discussed is the model of disjoining pressure, comparable to the intercrystalline swelling caused by interaction withinthe electrical double layer at the mineral surfaces (Morales Demarco et al. 2007; Ruedrich et al. 2011). This process is limited on very small pore channels. The analyses of hygric dilatation in the present study confirm that the amount of micropores triggers the weathering processes markedly, which confirms a relationship to the presence of clay minerals, since they create these micropores. Experiments on clay mixtures prove that swelling clay minerals begin to expand at a relative air humidity of 45 % (Xiang and Czurda 1995). However, many sandstones show a volume increase already at 15 % air humidity (Morales Demarco et al. 2007; Ruedrich et al. 2011). Because swelling clay minerals (montmorillonite; mixed layers) only occur in very minor amounts in the sandstones analysed, other parameters might also be responsible for the hygric dilatation measured. This is underlined in the test with the quartz arenites (e.g. Cretaceous; Bad Bentheim sandstone). Both strongly compacted as well as poorly compacted quartz arenites rarely show hygric dilatation (mean: 0.05 mm/m), although they exhibit swellable clay minerals (e.g. BB, Tables 4.1, 4.3). Probably also the position of the clay minerals and micropores within the sandstone is important for hygric dilatation. In contrast, sandstones exhibiting bimodal pore radii distribution and high alteration of unstable lithic fragments/feldspars or pseudomatrix show the greatest hygric dilatation. Maybe the position of clay in the shape of huge altered lithic fragments promotes water retention behaviour. Eventually also permeability affects the hygric dilatation, since sandstones with high values of hygric expansion exhibit low permeability caused by the content of altered unstable lithic fragments. Sandstones of this type belong to sublitharenites–litharenites of Schilfsandstein and Lettenkohlenkeuper (Upper Triassic). The highest value of hygric dilatation was measured in the Hindfelden sandstone (Upper Triassic, Schilfsandstein). This extraordinary value probably can be traced back to the combined effects of swellable clay minerals and the bimodal pore radii distribution with the high amount of micropores, caused by the presence of altered lithic fragments. Also, heavily compacted and cemented Lower Triassic sublitharenites with unimodal unequal pore radii distribution exhibit distinct hygric dilatation (e.g. KA, AH, Tables 4.1, 4.3). Therefore, we assume that hygric expansion can be connected with the interaction of the presence of micropores, the type and spatial

arrangement of clay minerals on surfaces of detrital grains and on the content of altered unstable lithic fragments (see also discussion in Ruedrich et al. 2011).

4.17 Summary—Quality Catalogue for Sandstones

The results of the present study indicate that statistical analyses of a very large number of sandstones can be used to predict the material and weathering behaviour of these natural stones. Multiple parameters affect the material properties of these heterogeneous rocks. The possible problems of compiling a data set from many different sources also have to be kept in mind. Furthermore, petrographical and petrophysical parameters can change locally within each individual rock and, therefore, the material properties can also vary considerably.

Linear interrelationships between the basic parameters of porosity, pore radii distribution and compressive strength can be established for each sandstone lithotype defined. Because these parameters correlate with the weathering properties, a prediction for salt resistance and hygric dilatation can be made for each sandstone type. Material properties are dependent on different magnitudes of influences. Thus, the transition between the different lithotypes is fluent and, therefore, the weathering behavior is common. Figure 4.23 schematically summarizes the petrographical and petrophysical properties as well as their resistance against salt splitting and hygric dilatation. In general, the construction suitability is determined by different classes from the combination of the salt resistance and hygric dilatation results, in which all other parameters are incorporated with a very large confidence.

In the present study, two types of quartz arenites and two types of sublitharenites–litharenites as natural building stone could be distinguished:

High mature quartz arenites, which are strongly compacted and cemented with little early infiltrated clay minerals and mainly sutured concave–convex grain contact. They exhibit a compressive strength between 70 and 150 MPa, a porosity up to 15 % and a unimodal unequal pore radii distribution. Due to the low hygric dilatation and high salt resistance (Group A), they can be defined as weathering resistant.

- Quartz arenites, which are weakly compacted and cemented, with point-elongated grain contact, partially containing glauconite grains and high content of early infiltrated clay minerals. The compressive strength is between 50 and 80 MPa, the porosity amounts to ~25 % and the pore radii distribution is unimodal equal. Due to the low hygric dilatation but medium-low salt resistance, the rock can be defined as moderate– well weathering resistant.
- Sublitharenites (-litharenites) with a low-medium content of altered unstable lithic rock fragments and feldspars, high-medium content of quartz cement as well as illite and/or

kaolinite at grain surfaces. The compressive strength is 70–150 MPa and medium to high, the porosity is between 5 and 15 % and the pore radii distribution unimodal unequal. The salt resistance belongs to group A–B and hygric swelling amounts to 0.5–1.0 mm/m.

- Sublitharenites (–litharenites) with high content of altered unstable lithic fragments and/or feldspars, little quartz cement and weak grain contact between the few stable detrital grains. The lithic fragments are mostly squeezed to pseudomatrix. The compressive strength is 30–50 MPa and very low and the porosity is 20–30 % and very high. Due to the high values of hygric dilatation and the low salt resistance, this sandstone type can be defined as not weathering resistant.

Despite the material properties of dimension sandstones discussed in this paper, the evaluation of a suitable replacement stone must additionally take into account the compatibility of a replacement stone to the adjacent rocks. For example, moisture properties such as capillary and sorptive water absorption and water saturation of the original and replacement rock should be of the same magnitude. A case study considering this interaction of original and replaced dimension stones is presented by Graue et al. (2011) for the Cologne cathedral.

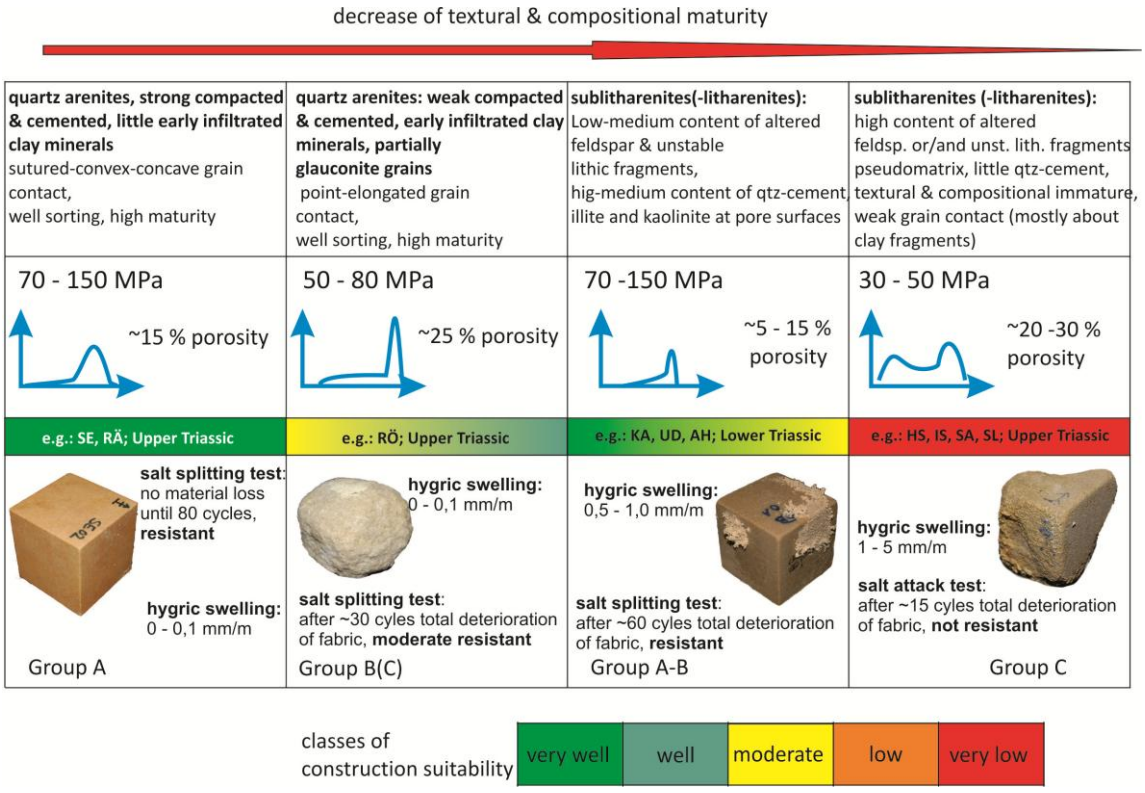

Fig. 4.23: Illustration summarizing a quality catalogue for sandstones. From left to right, the textural and compositional maturity increases. Coloured bars indicate the classes of construction suitability. In general, four different sandstone types with characteristic fabric types were classified material parameter such as porosity and compressive strength, as well as the weathering properties characterized by salt resistance and hygric swelling, are also determined. Salt resistance is divided into three groups: Group A (no material loss up to 100 cycles), Group B (50 % material loss up 30–40 cycles), and Group C (50 % material loss up to 15 cycles). The transition between each lithotype is interpreted as being fluent.

Acknowledgments

We would like to thank the Deutsche Bundesstiftung Umwelt for supporting the long-term PhD fellowship for H. Stück (AZ 20008/997). Furthermore, gratitude also goes to Dr. O. Nenadic and Dr. J. Schuhmacher for the constructively support of statistics, Dr. R. Dohrmann und Dr. S. Kaufhold for analysing the clay mineral compositions (BGR), and Christian Gross for editing the English. Special thanks go to Dr. J. Ruedrich† for his help and unreserved discussions on all experimental results.

References

Aigner T, Bachmann G (1992) Sequence stratigraphic framework of the German Triassic. Sedimentary Geology 80:115–135

Bartelsen T (2008) Gefügeabhängiges Verwitterungsverhalten tonmineralführender Sandsteine durch hygrothermisch induzierte Dehnungsprozesse, unpublished diploma thesis, Göttingen

Beard DC, Weyl PK (1973) Influence of texture on porosity and permeability of unconsolidated sand. AAPG Bull 57:349–369

Beutler G, Schubert J (1987) Fazielle Entwicklung des Mittleren Lettenkeuper im Thüringer Becken. Z Geol Wiss 15:475–484

Blöcher G, Bruhn D, Zimmermann G, McDermott C, Huenges E (2007) Investigation of the undrained poroelastic response of sandstones to confining pressure via laboratory experiment, numerical simulation and analytical calculation. Geological Society Special Publications, London

Burley SD, Kantorowicz JD, Waugh B (1985) Clastic diagenesis. In: Brenchley PJ, Williams BJP (eds) Sedimentology: recent developments and applied aspects. Special publication 18. Geological Society of London, Bath, pp 89–226

Cecil CB, Heald MT (1971) Experimental investigation of the effects of grain coatings on quartz overgrowth. J Sediment Petrol 41:582–584

Chitsazian AH (1985) Beziehungen zwischen dem Mineralbestand, Gefüge und technologischen Eigenschaften der Niedersächsischen ,,Wealden‘‘-Sandsteine (Unterkreide)-Mitteilungen aus dem Geologischen Institut Hannover, Diss

Choquette PW, Pray LC (1970) Geological nomenclature and classification of porosity in sedimentary carbonates. Am Assoc Petrol Geol Bull 54:207–250

David C (2006) Buntsandstein-Bausandstein, Marburger Bausandstein unter der Lupe. Zeitschrift der Marburger Geowissenschaftlichen Vereinigung e.V., 3, Marburg

De La Calle C, Suquet H (1988) Vermiculite. In: Bailey SW (ed.) Hydrous phyllosilicates. Reviews in Mineralogy. Mineralogical Society of America 19:455–496

De Martine DC, Beard D, Danburg JS, Robinson JH (1976) Variation of seismic velocities in sandstones and limestones with lithology and pore fluid at simulated in situ conditions: Proceedings of the EGPC exploration seminar, Cairo

Dickinson WR (1985) Interpreting provenance relations from detrital modes of sandstones. In: Zuffa GG (ed) Provenance of arenites. Reidel, Dordrecht, pp 333–361

Dixon JB, Weed SB (1989) Minerals in soil environments. 2nd edition Soil Science Society of America

Dohrmann CF, Kühn I (2009) Angewandte Statistik für die biologischen Wissenschaften. Helmholtz Zentrum für Umweltforschung-UFZ

Fitzner B (1970) Die Prüfung der Frostbeständigkeit von Naturbausteinen. Aachen, Diss

Fitzner B (1988) Untersuchung der Zusammenhänge zwischen dem Hohlraumgefüge von Natursteinen und physikalischen Verwitterungsvorgängen. Mitt. Ing.-u.Hydrogeologie, 29, Aachen

Fitzner B, Snethlage R (1982) Einfluß der Porenradienverteilung auf das Verwitterungs-verhalten ausgewählter Sandsteine. Bautenschutz und Bausanierung 3:97–103

Füchtbauer H (1967) Der Einfluss des Ablagerungsmilieus auf die Sandsteindiagenese im Mittleren Buntsandstein. Sediment Geol 1:159–179

Füchtbauer H (1974) Zur Diagenese fluviatiler Sandsteine. Geol Rundsch 63(3):904–925

Füchtbauer H (1988) Sedimente und Sedimentgesteine. 4. Auflage, 1141 S., Stuttgart (Schweizerbart)

Gilbert CM (1954) Sedimentary rocks, p.251–384 in Williams, H., Turner, F.J. and Gilbert, C.M. Petrography: San Francisco, W.H. Freeman & Co., 406 p.

Goudie A, Vlies H (1997) Salt weathering hazards. Wiley, Hoboken

Graue B, Siegesmund S, Middendorf B (2011) Quality assessment of replacement stones for the Cologne Cathedral: mineralogical and petrophysical requirements. Environ Earth Sci 63(7–8):1799–1822

Grimm WD (1990) Bildatlas wichtiger Denkmalgesteine der Bundesrepublik Deutschland. Bayrisches Landesamt für Denkmalpflege, 50, München

Han D, Nur A, Morgan D (1986) Effect of porosity and clay content of wave velocities in sandstones. Geophysics 51(11):2093–2107

Hartmann DJ., Beaumont EA, Coalson E (2000) Predicting sandstone reservoir system quality and example of petrophysical evaluation. Predicting reservoir system quality and performance. In: Hartmann DJ, Beaumont EA (eds) Exploring for oil and gas traps, Beaumont EA, Foster NH (eds) Treatise of petroleum geology, handbook of petroleum geology, 1999

Hayes JB (1984) Sandstone porosity evolution. Short course notes, AAPG, Sandstone diagenesis School

Holzwarth D (1996) Werksandsteine der Region Vorderpfalz (westlicher Grabenrand des Obberheingrabens) und ihre petrographischen sowie geotechnischen Eigenschaften. Diss, Mainz

Houseknecht DW (1984) Influence of grain size and temperature in intergranular pressure solution, quartz cementation, and porosity in a quartzose sandstone. J sediment petrol 54(2):348–361

Houseknecht DW (1987) Assessing the relative importance of compaction processes and cementation to reduction of porosity in sandstones. Am Assoc Petroleum Geol Bull 71(6):642–663

Houseknecht DW (1988) Intergranular pressure solution in four quartzose sandstones. J Sed Petrology 58:228–246

Houseknecht DW, Pittman ED (eds) (1992) Origin, diagenesis & Petrophysics of Clay Minerals in Sandstones. Special Publication 47. Society of Sedimentary Geologists, Tulsa

Katzung G (1975) Tektonik, Klima und Sedimentation in der Mitteleuropäischen Saxon-Senke und in angrenzenden Gebieten. Z Geol Wiss 3(11):1453–1472

Kirsten H (2009) Herkunft, Eigenschaften und Konservierungsmöglichkeiten von Lettenkeuper-und Schilfsandsteinen an Baudenkmalen in Thüringen. Diss, Weimar

Klopfer H (1985) Feuchte. In: Lutz et al.: Lehrbuch der Bauphysik. Teubner Verlag, Stuttgart, pp 265–434

Koch R, Sobott R (2008) Sandsteine: Entstehung, Eigenschaften, Verwitterung, Konservierung, Restaurierung. In: Siegesmund, Snethlage (eds) Schriftenreihe der Deutschen Gesellschaft für Geowissenschaften, vol 59, pp 145–174

Koch R, Baier A, Lorenz H, Fritsch A (2003) Sandsteine des Keupers als Naturwerksteine in und um Nürnberg (Exkursion B am 22. April 2003). Jber Mitt oberrhein geol Ver NF 85:45–64

Kowallis B, Jones LEA, Wang HF (1984) Velocity–porosity–clay content: systematics of poorly consolidated sandstones. J Geophys Res 89:10355–10364

Massallam K (1973) Sedimentologie, Petrographie und Diagenese der Valendis Sandsteine Erdölfeld Leiferde-Gifhorner Trog (Unterkreide – NW-Deutschland). Diss, Univ. Hamburg

McBride EF (1963) A classification of common sandstones. J Sediment Petrol 33(3):664–669

Moore DM, Reynolds RC Jr (1997) X-ray diffraction and the identification and analysis of clay minerals. Oxford University Press, Oxford

Morad S, Ketzer JM, De Ros LF (2000) Spatial and temporal distribution of diagenetic alterations in siliclastic rocks: implications for mass transfer in sedimentary basins. Sedimentology Suppl 1:95–120

Morales Demarco M, Jahns E, Ruedrich J, Oyhantacabal P, Siegesmund S (2007) The impact on partial water saturation in rock strength: an experimental study on sandstones. Zeitschrift der Deutschen Gesellschaft für Geowissenschaften 158:869–882

Mosch S, Siegesmund S (2007) Statistisches Verhalten petrophysikalischer und technischer Eigenschaften von Naturwerksteinen. Z Dtsch Geol Ges 158/4:821–868

Müller H, Luckert J, Röper D (2002) Sandsteinverwitterung durch bauschädliche Salze—Ergebnisse der Säulensanierung des Belvedere auf dem Pfingstberg/Potsdam—Brandenburgische Geowissenschaftliche Beiträge 9:1–15; Kleinmachnow

Paul J (1982) Der Untere Buntsandstein des Germanischen Beckens. Geol Rundsch 71:795–811

Paul J, Wemmer K, Ahrend H (2008) Provenance of Triassic siliciclastic sediments in Central Europe. Z dt geol Ges 159:641–650

Peschel A (1983) Natursteine. VEB Deutscher Verlag für Grundstoffindustrie, Leipzig

Pettijohn FJ (1975) Sedimentary rocks. Harpers u. Brothers, New York

Pettijohn FJ, Potter PE, Siever R (1987) Sand and sandstone. Springer, New York

Plein E (1993) Bemerkungen zum Ablauf der paläogeographischen Entwicklung im Stephan und Rotliegend des Norddeutschen Beckens. Geol Jb A131:99–116

Putnis A, Mauthe G (2000) The effect of pore size on cementation in porous rocks. Geofluids 1:37–41

Putnis A, Prieto M, Fernandez-Diaz L (1995) Supersaturation and crystallisation in porous media. Geol Mag 132:1–13

Rac MV, Chernyshev SN (1970) Klüftigkeit und Eigenschaften geklüfteter Gesteine (russ.), Moskau (Nedra)

Ruedrich J, Seidel M, Kirchner, Siegesmund S (2005) Salzverwitterung, hygrische und thermische Dehnung als auslösende Schadensquantitäten. In: Siegesmund S, Auras M, Ruedrich J, Snethlage R (eds) Geowissenschaften und Denkmalplfege ZDGG, vol 156/1, pp 59–74

Ruedrich J, Siegesmund S (2006) Fabric dependence of length change behaviour induced by ice crystallization in the pore space of natural building stones. In: Fort R, Alvarez de Buergo M, Gomez-Heras M et al (eds) Heritage, weathering and conservation. Taylor & Francis Group, London

Ruedrich J, Bartelsen T, Dohrmann R, Siegesmund S (2010) Building sandstone integrity affected by the process of hygric expansion. Environ Earth Sci. doi:10.1007/s12665-010-0767-0

Ruedrich J, Bartelsen T, Dohrmann R, Siegesmund S (2011) Moisture expansion as a deterioration factor for sandstone used in buildings. Monument under threat. Environ Earth Sci 63:7–8

Scherer M (1987) Parameters influencing porosity in sandstones: a model for sandstone porosity prediction. Am Assoc Petroleum Geologists Bull 71(5):485–491

Scherer GW (1999) Crystallization in pores. Cem Conr Res 29:1347–1358

Schießl P, Alfes C (1990) Festigkeit und Verformung von Sandstein—Bedeutung für die Verwitterungsresistenz und Meßmethoden. Denkmalpflege und Naturwissenschaften im Gespräch, Sonderheft aus der Publikationsreihe des Verbundsforschungsprojekts Steinzerfall und Steinkonservierung:10–17, Berlin

Schmidt V, McDonald DA (2012) The role of secondary porosity in the course of sandstone diagenesis. In: Scholle PA, Schluger PR (eds) SEPM Society for Sedimentary Geology. Aspects of Diagenesis, vol 26, pp 175–207

Seidel G (2003) Geologie von Thüringen, Schweizerbart'sche Verlagsbuchhandlung, Stuttgart, 2. Aufl.

Seidel M (2004) Gefügeabhängige Verwitterung von Sandsteinen durch Kristallisation von Eis und Salzen im Porenraum un published diploma thesis, 159 pp, Göttingen

Siegesmund S, Dürrast H (2011) Physical and mechanical properties of rocks. In: Siegesmund S, Snethlage R (eds) Stone and architecture. Springer, Berlin, pp 97–225

Snethlage R, Wendler E (1997) Moisture cycles and sandstone degradation. In: Baer NS, Snethlage R (eds) Saving our architectural heritage, the conservation of historic stone structures. Elsevier, Hoboken, pp 7–24

Sobott R, Koch R (2009) Die Qualität von Naturwerksteinen aus dem Steinbruch Worzeldorf bei Nürnberg—Petrographische, diagenetische und gesteinsphysikalische Kenndaten (Mittlerer Keuper, Oberer Burgsandstein). Geol. Bl. NO-Bayern, 59, pp 419–444, Erlangen

Stück H, Siegesmund Siegfried, Ruedrich J (2011) Weathering behaviour and construction suitability of dimension stones from the Drei Gleichen area (Thuringia, Germany). Environ Earth Sci 63:1763–1786. doi:10.1007/s12665-011-1043-7

Stonecipher SA, Winn RD Jr., Bishop MG (1984) Diagenesis of the Frontier Formation, Moxa Arch: a function of sandstone geometry, texture and composition, and fluid flux. In: McDonald DA, Surdam RC (eds) Clastic Diagenesis: AAPG Memoir 37, pp 289–316

Stalder PJ (1973) Influence of crystalline habit and aggregate structure of authigenic clay minerals on sandstone permeability. Geol Mijnbouw 52:217–219

Strack D, Stapf RG (1980) Ist der Kreuznacher Sandstein des Rotliegenden äolisch oder fluviatil entstanden? Geol Rundsch 69(3):892–921

Surdam RC, Dunn TL, MacGowan DB, Heasler HP (1989) Conceptual models for the prediction of porosity evolution with an example from the Frontier Sandstone, Big-Horn Basin, Wyoming. In: Coalson EB, Kaplan SS, Keighin CW, Oglesby LA, Robinson JW (eds) Sandstone Reservoirs: Rocky Mountain Association of Geologists, pp 7–21

Tukey J (1977) Exploratory data analysis. Addison-Wesley. ISBN 18750-201-07616-0

van Brakel J, Modry S, Svata M (1981) Mercury porosimetry: State of the art. Powder Technol 29:1–12

van der Plas L, Tobi AC (1965) A chart of judging the reliability of point counting results. Am J Sci 263:87–90

Waples DW (2002) Evolution of sandstone porosity through time. The modified Scherer Model: a calculation method applicable to 1-D maturity modeling and perhaps to reservoir prediction. Nat Resour Res 11:257–272

Wenzel A, Häfner F (2003) Die roten Werksandsteine der Westpfalz.IFS Bericht Nr. 15-2003, p 27

Weiss T, Siegesmund S, Kirchner D, Sippel J (2004) Insolation weathering and hygric dilatation as a control in building stone degradation. Environ Geol 46(3-4):402-413

Wilson MD (1994) Non-compositional controls on diagenetic processes. In: Wilson MD (ed) Reservoir Quality Assessment and Prediction in Clastic Rocks: SEPM Short Course 30, pp 183–208

Worden R, Morad S (2000) Quartz cementation in sandstones. Special publication 29, International Association of Sedimentologists. Blackwell Science, Oxford

Wurster P (1964) Geologie des Schilfsandsteins. Mitt Geol Staatsinstituts Hamburg 33:1–140

Xiang W, Czurda K (1995) Einfluss des Kationenaustausches auf die Hydratation und Dehydratation von Tonmineralen. Festschrift zum 60. Geburtstag von Helfried Möller. Geol. Paläontologische Mitteilungen Innsbruck, Bd. 20:107–119

Tucker M (2001) Sedimentary petrology—revised. Blackwell Science Inc, Oxford

Zehnder K, Arnold A (1989) Crystal growth in salt efflorescence. J Crystal Growth 97:513–521

Chapter 5

Numerical Modeling of Moisture Transport

This chapter is largely identical to the manuscript entitled "Numerical Modeling of Moisture Transport in Sandstone: The Influence of Pore Space, Fabric and Clay Content" that is published in Environmental Earth Sciences DOI: 10.1007/s12665-013-2405-0.

Authored by: Heidrun Stück • Rudolf Plagge •Siegfried Siegesmund

5 Numerical Modeling of Moisture Transport

5.1 Abstract

In the present study a numerical modeling of moisture distribution under real climate conditions within sandstone monoliths is accomplished, based on detailed material specific transport- and storage functions. The impact of lithology and pore radii distributions is modeled with consideration of i) the single sandstone monolith, ii) the sandstone monolith with clay layers and iii) the sandstone monolith with clay layers and hydrophobic treatment. The results reveal that the unimodal equal pore radii distribution of the quartz arenite promotes quickly a (capillary) water uptake during driving rain (liquid stage), but due to its missing smaller capillaries a high drying velocity leads to an almost dry pore space, since moisture can only absorbed via gaseous stage (e.g. summer). On the contrary, the sublitharenite with a unimodal unequable pore radii distribution is characterized by a distinctly higher water content, since in addition smaller pores also allow the absorption of moisture via sorption. Moreover, the high clay content promotes a retarded interaction with the environment, which is also reflected by the high vapor diffusion resistance. The highest water content shows the sandstone with highest clay content and bimodal pore size distribution. Here over nine magnitudes of water transporting pores is involved at water transport and storage. Results reveal also that moisture accumulations during droughts trace the deterioration shape of rounding. For all sandstones highest annual fluctuations are observable within the rim zone of the monolith, while the center is characterized by more stable moisture content, which mainly depends on rising water content of the bedrock. The presence of clay layers has for each sandstone specific consequences. However, within the whole sandstone the stress index is increased and stress location is displaced to the boundaries of clay layers. Results of modeling the hydrophobic treatment reveal that this conservation strategy is only useful for sandstones where all moisture is absorbed in liquid stage, why then all water absorption is hindered. In case of sandstones with bimodal and unimodal unequal pore size distributions moisture uptake is possible also via sorption. Accordingly, moisture accumulates behind the zone of hydrophobic treatment. This finally will lead to stress transfer to the outer rim during salt- or ice crystallization and will be responsible for flaking.

5.2 Introduction

Many studies dealing with the weathering resistance of sandstone show that deterioration processes are mostly governed by the presence of water since water is involved in nearly all weathering processes (Snethlage 1984, Weiss 1992, Künzel 1994, Krus 1995, Künzel & Krus 1995, Mirwald 1997). Water transport and storage mechanisms are strongly associated with sandstone's pore space and pore sizes (Klopfer 1985, Fitzner & Snethlage 1982, Fitzner 1988, Ruedrich & Siegesmund 2006, Ruedrich et al. 2011).

Commonly, the suitability of a sandstone as a building stone is evaluated with standard values by measuring petrophysical properties. These single values are mostly used in the natural stone industry without consideration of lithology or pore-radius distribution. Coevally, these single-standard values do not reveal the location of moisture accumulation, but cooperate/correspond exactly with many kinds of deterioration. To what extent heterogeneities such as clay layers have influence on moisture accumulation and distribution cannot be evaluated in detail either. With respect to the conservation methods of natural stones, hydrophobic treatment is often applied. This treatment has been recently connected to a negative impact on surface ranges and has been held responsible for the development of flaking because, moisture accumulation is assumed to be directly behind the treated rock area. Finally, a temporal consideration of these dynamic processes within the context of boundary conditions (climatic fluctuations) cannot be made with these values.

With regard to these questions, the numerical modeling of moisture transport and storage under various climatic conditions is essential for the analysis and identification of moisture accumulation. Therefore, the present study focuses on modeling these processes within sandstone monoliths. Moreover, realistic results require a detailed determination of all parameters involved that are able to describe the coupled heat and moisture transport and storage processes.

Therefore three characteristic sandstone types, differing in composition and material properties, have been analyzed. Each type represents different diagenetic developments and depositional environments (Stück et. al 2012). The results of this study should be able to translate to a wide spectrum of sandstones in general. Particularly, pore-space properties will be taken into account. Furthermore, in order to investigate the influence of heterogeneities within sandstones, clay layers have been inserted within the models. The effect of hydrophobic treatment on sandstone surfaces has been modeled in addition.

5.3 Transport and Storage Mechanisms within Porous Media

In general, the pore space of sandstone is characterized by a wide spectrum of pore sizes. Furthermore, for each pore size, a specific transport mechanism for water and moisture transport takes place.

Moisture transport in porous media can be generally divided into a liquid and a vapor phase (Kießl & Gertis 1980, Stockhausen 1981, Klopfer 1985, Künzel 1994, Krus 1995), through which transport processes follow a relationship between flux density (current density) and its respective potential-gradient. The water vapor is moved by diffusion, which represents a balance as a result of differences in concentrations and can essentially be traced back to differences in vapor pressure. The vapor pressure, again, depends on relative air humidity, temperature, and, consequently, on saturated vapor pressure. The liquid phase of water depends on transport gradients. However, here, the driving force is the capillary pressure.

Moisture accumulation within the pores can be divided into a hygroscopic range and an over-hygroscopic range (Fig. 5.1; e.g. Kießl 1983). When the main transport mechanism is water vapor diffusion and the storage mechanism is adsorption, the pore acts hygroscopically. This is the case in which a dry pore is present: Here, no water transport can take place since the pore walls absorb all the water that arises. With the increasing thickness of the water molecule layer, the bottlenecks of the pores also start to fill with water. In this case, the water vapor diffusion is almost totally inhibited, while the liquid water transport increases. The hygroscopic phase is mainly dependent on relative air humidity.

In the over-hygroscopic phase, the transport mainly takes place in the liquid stage, and the storage mechanism is capillary condensation. Moreover, the amount of water transported in the liquid stage is much higher than in the vapor stage. With the increasing thickness of sorbate layer, the air is analogous to a swimming/floating bubble within the pores until it is completely displaced. The super-saturated phase is primarily present when higher amounts of liquid water are available; it is dependent on the pore radii.

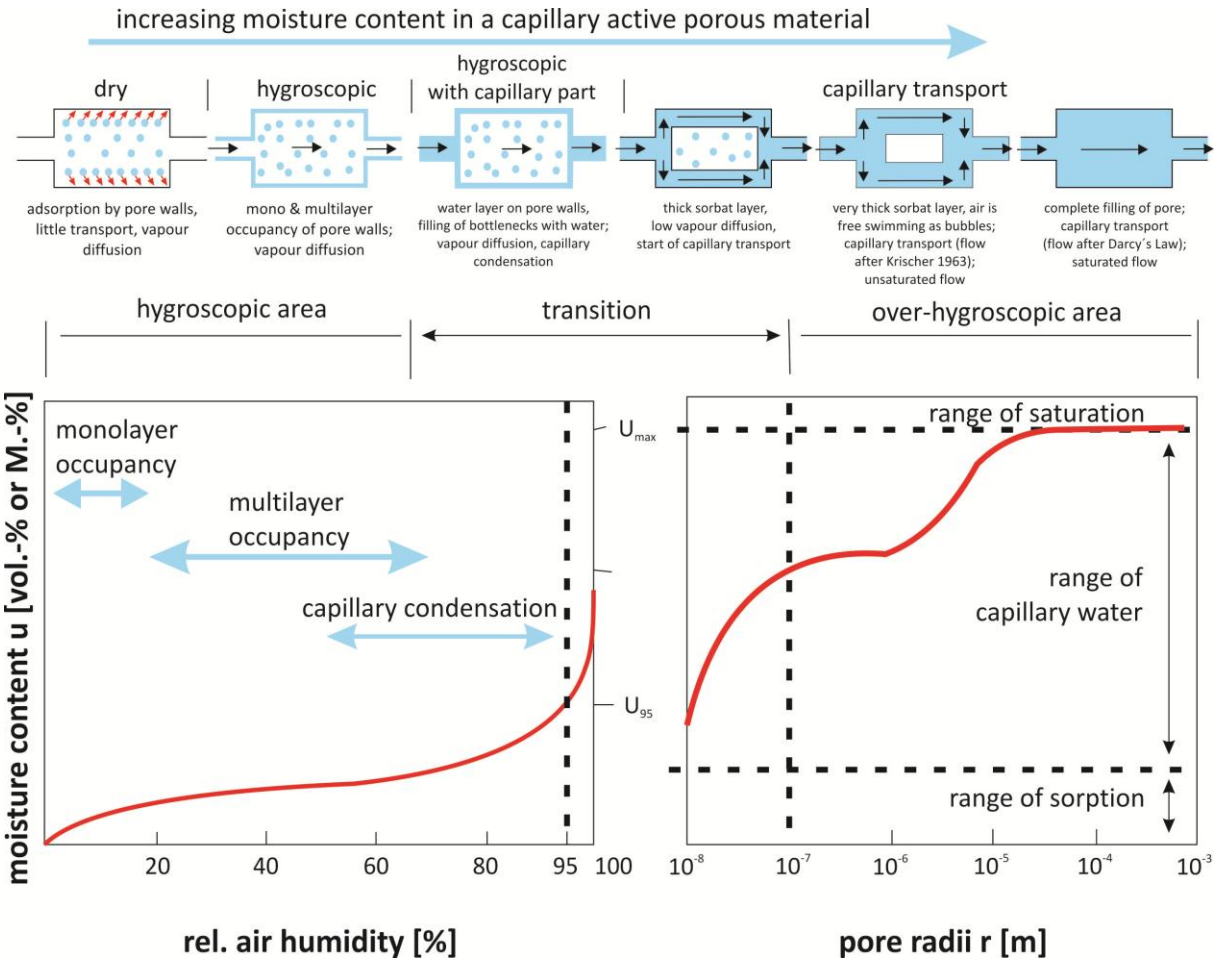

Fig. 5.1: Schematic illustration of water transport mechanisms and moisture content with dependence on relative air humidity and pore radii (modified after Kießl 1983).

5.4 Material Properties

5.4.1 Material: Characteristic Sandstone Types

The selection of samples within this study is based on statistical analyses of the petrophysical and petrological properties of more than 300 sandstone specimens, allowing identification of three characteristic types of sandstone and their associated material behavior and especially pore radii distribution (Stück et. al. 2012). Therefore, the results of the modeling of these three sandstone types in the present study will be representative of and transferable to other sandstones. Aside from the composition, they differ in depositional environment and diagenetic history. The type “quartz arenite” belongs to the Cretaceous age, was deposited in a shallow marine environment and is represented by the sandstone Bad Bentheim (Germany, west of Osnabrück). On the contrary, the immature sublitharenite was deposited during the Middle Buntsandstein (Lower Triassic) in a fluvial environment and originates from Karlshafen (Germany, northwest of Göttingen), and belongs to the so-called *Wesersandstones*. The highly immature feldspathic litharenite was deposited during the Upper Triassic (Schilfsandstein) and is result of a lagoon-type fluvial system, which is documented by

the content of organic plant particles. This type is represented by the sandstone type “Sander”, which belongs to the famous Main River deposits (Germany, near to Schweinfurt).

The quartz arenite Bad Bentheim is weakly compacted and cemented, with point-elongated grain contact, partially containing glauconite grains and characterized by a high content of early-infiltrated clay minerals (Fig. 5.2 a). The compression strength amounts to 95 MPa and the porosity ~25%. Due to the low hygric swelling but medium-to-low salt resistance (Table 5.1), the rock can be defined as high weathering resistant. According to the high porosity, combined with high coefficient of water absorption and medium strength, but high weathering resistance this sandstone was defined as outlier within the group of quartz arenites (Stück et. al 2012).

The sublitharenite Karlshafen exhibits a low-to-medium content of altered, unstable lithic rock fragments and feldspars (Fig. 5.2b) and a high-to-medium content of quartz cement, as well as illite and/or kaolinite at the grain surfaces. The compressive strength is very high at ~119 MPa, and the porosity of 7.90% is rather low. The salt resistance is very well-developed, and the hygric dilatation is with 1.35 mm/m (Table 5.1) very high. Therefore the rock can be defined as moderate to well weathering resistant.

The feldspathic litharenite Sander demonstrates a sandstone with high content of altered, unstable lithic fragments and/or feldspars, a low content of quartz cement and weak grain contact in between the few stable detrital grains (Fig. 5.2c). The lithic fragments are mostly squeezed to a pseudomatrix. The compressive strength is very low at 54 MPa, and the porosity of 17% is very high (Table 5.2). Due to the high values of hygric dilatation and the low salt-resistance (Table 5.1), this sandstone type can be defined as not weathering resistant.

Table 5.1: Petrophysical and weathering properties of sandstones investigated. WS = water saturated.

sample	porosity [%]	w-value [kg/m*s2]	compr. strength [MPa]	hygric dilatation [mm/m]; WS	salt resistance: number of salt attack cycles (DIN 52111)
Bentheim	25.60	40.70	95.00	0.02	85
Karlshafen	7.90	0.50	119.14	1.35	100
Sander	17.00	20.05	54.71	1.25	35

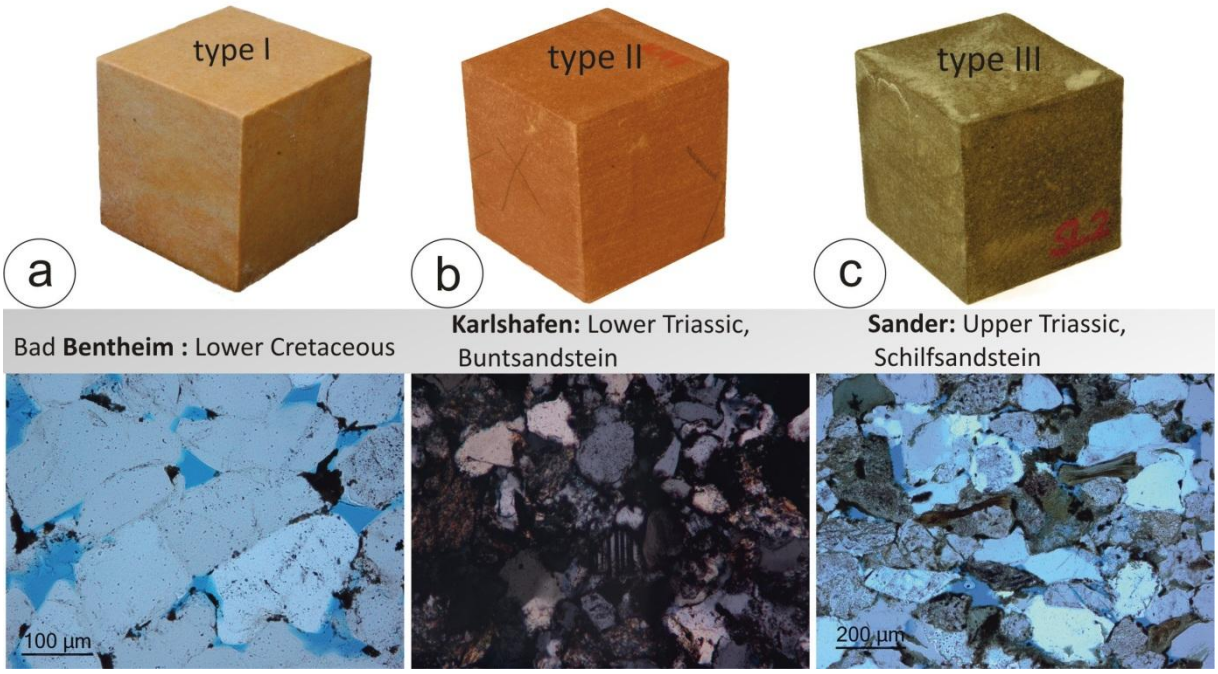

Fig. 5.2: Characteristic sandstone types: (a) weakly compacted quartzarenite with poor quartz cementation and mostly point-elongated grain contact; sandstone Bad Bentheim, (b) strongly compacted sublitharenite, which is cemented by quartz and calcite and impregnated with iron oxides; sandstone Karlshafen and (c) feldpathic litarenite, which is weakly compacted and cemented and strongly altered, expressed by a high content of pseudomatrix; sandstone Sander.

5.5 Measurement & Results of Material Parameters

5.5.1 Measurements

Behind the processes described above (Chapter 5.3), challenging petrophysical parameters interlock each other. When modeling sandstone hygrothermal properties, detailed knowledge of storage and transport coefficients is required. For this purpose, standard parameters, such as bulk density, matrix density and total and effective porosity, were determined following DIN standards. Concerning the thermal properties of the rocks, specific heat-conductivity and heat-capacity were determined; both are important to heat and moisture transfer within the rock.

Parameters of moisture and water transport and storage include the measurement of water retention (ISO 11 274), sorption isotherms (DIN EN ISO 12571), the capillary water uptake coefficient (EN ISO 15148) and water vapor diffusion (EN ISO 12572). For the measurable parameters, standard, symbol and unit of each method, see Table 5.2.

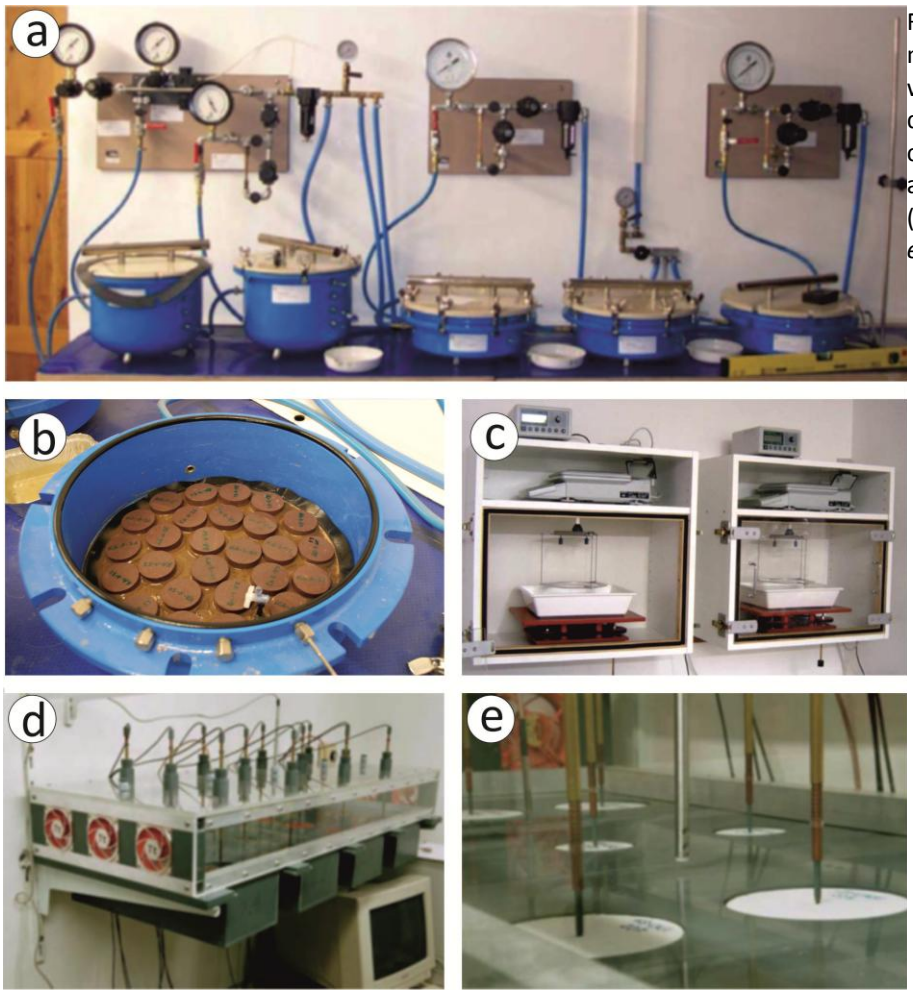

Fig. 5.3: Facilities for the measurement of: *a* and *b* water retention to detect sorption, *c* capillary water absorption coefficient (one-dimensional), *d* and *e* drying experiment.

Water retention is divided into a hygroscopic and an over-hygroscopic part. For measurement of over-hygroscopic moisture storage, capillary saturated samples are placed on ceramic plates and are dehydrated little by little using capillary pressure (Fig. 5.3a, b). When capillary balance is reached at a pressure stage, the moisture content is gravimetrically determined. The hygroscopic moisture storage is determined via hygric *sorption isotherms*. After two months of conditioning at 100% relative air humidity, the samples are stored in a desiccator with K_2SO_4 at a relative air humidity of 96.7%. After reaching a balance, the water content is gravimetrically determined, and the samples are conditioned for the next step of relative air humidity. Via this step by step conditioning at a decreasing relative air humidity, the samples are gradually dehydrated. Along with the results of water retention, the entire moisture storage function is determined. Based on this, the pore volume distribution is calculated (see Chapter 5.8.1).

The *capillary water uptake coefficient* characterizes the properties of a mostly dried material, the absorption of water from the surface and its transport within the pore space. During the measurement, different moisture stages are reached, and accordingly also the transport gradient changes, which results in a continuously decreasing flux (Fig. 5.3c). At the end of measurement, conditions of equilibrium are achieved, which is called the capillary moisture content θ_{cap}. At low

relative humidity, the moisture transport takes place in the vapor stage via water vapor diffusion. Therefore, the *water vapor diffusion resistance* was determined by describing the amount of water vapor which is transported at a vapor pressure gradient through the pore space. Hence, the dry-cup method was used for lower humidities (0-35%), and the wet-cup-method for higher relative air humidities can be executed at different humidity stages (84.6% with KCl, 95% with $KHCO_3$). These measurements were accomplished in isotherm conditions. The sample is vapor-proofed and fixed on a vessel, which is filled with a saturated saltwater solution or a desiccant in order to reach defined relative humidity conditions. For measurements, the vessels are stored in a climatic chamber at a constant temperature and relative air humidity. Under the influence of a partial-pressure water gradient between the air spaces of the sample surface, the water vapor migrates through the sample. After reaching a stationary balance, a constant weight change (vessel) per time unit arises, which corresponds to a diffusion current at the applied air-moisture gradient.

The drying experiment was accomplished at cylindrical samples of 50 mm length and 50 mm in diameter. During the drying of the sample in an evaporation facility (Fig. 5.3 d, e), simultaneously the boundary conditions are detected. This allows a better interpretability of determined data.

Table 5.2: Experiments accomplished that are necessary for the generation of material functions.

experiment	Measurable parameters	DIN	symbol	unit
Heat flow	Heat conductivity of dry Sample		λ_{dry}	[W/mk]
Calorimeter	Specific heat capacity of dry sample		c_p	[J/kgK]
Density measurement, helium pycnometry	Bulk density		ρ_b	[kg/m^3]
	Matrix density		ρ_m	[kg/m^3]
	Porosity		Φ	[m^3/m^3]
Moisture retention	Moisture content over capillary pressure	ISO 11 274	$\theta_i(pc)$	[m^3/m^3]
Sorption	Moisture content over relative air humidity	DIN EN ISO 12571	$\theta_i(\varphi)$	[m^3/m^3]
Drying	Moisture content in dependence to time		$\theta_i(t)$	[m^3/m^3]
Water vapor diffusion	Dry-cup/wet-cup vapor diffusion resistance	EN ISO 12572	μ_{dry}	[-]
			μ_{wet}	[-]
Flow measurement at saturated samples	Liquid water conductivity at saturation		$K_i(\theta_{eff})$	[s]

5.6 Results

5.6.1 Sandstone Bad Bentheim

The sandstone Bad Bentheim is characterized by a very low vapour diffusion resistance, medium heat-conductivity, and the highest heat capacity (Table 5.3). Capillary pressure allows the highest water absorption at a limited pore spectrum (Fig. 5.4 a, b), and the pore radii distribution is characterized by limited peak within the larger capillary pores. This “shape” of pore volume

distribution determined with water retention is comparable to the pore radii distribution determined with mercury porosimety after Brakel et. al (1981) and therefore corresponds to the classification of unimodal equable pore radii distribution after, e.g., Ruedrich & Siegesmund (2006) and Stück et. al. (2012), (Fig. 5.5a, b).

The liquid and vapour conductivity (Fig. 5.4e) as well as capillary moisture saturation is the highest of all the sandstones analysed here. In contrast, the sandstone cannot assimilate moisture via sorption, as proved by the sorption isotherm (Fig. 5.4c). Moreover, the sandstone is characterized by the highest drying velocity (Fig. 5.4f).

5.6.2 Sandstone Karlshafen

The sandstone Karlshafen is characterized by the highest water vapor diffusion resistance and lowest vapour conductivity (Fig. 5.4d), highest heat conductivity and medium heat capacity (Table 5.3). The capillary pressure promotes very low amounts of water absorption within smaller capillaries (Fig. 5.4a, b). The pore volume distribution is characterized by low volumes within smaller capillaries and micropores (Fig.4 5.b). Here the “shape” of pore volume distribution corresponds to the unimodal unequable pore radii distribution after Ruedrich & Siegesmund 2006 and Stück et. al. (2012), (Fig. 5. 5 c, d). The liquid conductivity (Fig. 5.4e) and capillary moisture saturation is the lowest of all sandstones analysed. Furthermore, the sandstone is characterized by a low drying velocity (Fig. 5.4f).

5.6.3 Sandstone Sander

The water vapor diffusion resistance amounts to 25.85 [-] and is, therefore, medium-to-high. Coevally, this rock is characterized by the lowest heat conductivity and capacity. The capillary pressure allows high amount of water absorption over a wide spectrum of different pore sizes. The shape of the pore volume distribution corresponds to the bimodal pore radii distribution measured by mercury porosimetry (Ruedrich & Siegesmund (2006), Stück et. al (2012)). The liquid conductivity and capillary moisture uptake exhibit medium values. The drying velocity is the lowest of all sandstones analyzed (Fig. 5.5d).

5.6.4 Clay Layers

The material properties of the clay layer are characterized by a high porosity of ~35% with an unimodal pore volume distribution (Fig.5.6), a very low heat conductivity and high heat capacity. The liquid conductivity is similar to that of the sandstone Sander, and the capillary moisture saturation, at 0.25 [m^3 /m^3], is the highest of all the materials (Table 5.3).

Table 5.3: Petrophyiscal properties determined for compilation of the material data base.

sample	μ-value: wet cup/dry-dup [-]	Heat conductivity [W/mK]	Heat capacity [J/kgK]	Liquid conductivity [s]	Capillary Moisture saturation [m^3/m^3]
Karlshafen	178.52	3.28	795.98	$1.1*10^{-11}$	0.06
Bad Bentheim	11.93	2.57	909.78	$1.01*10^{-7}$	0.147
Sander	25.85	1.41	717.09	$5.6*10^{-9}$	0.134
Clay layer	14.2	0.87	868.00	$2.34*10^{-9}$	0.25

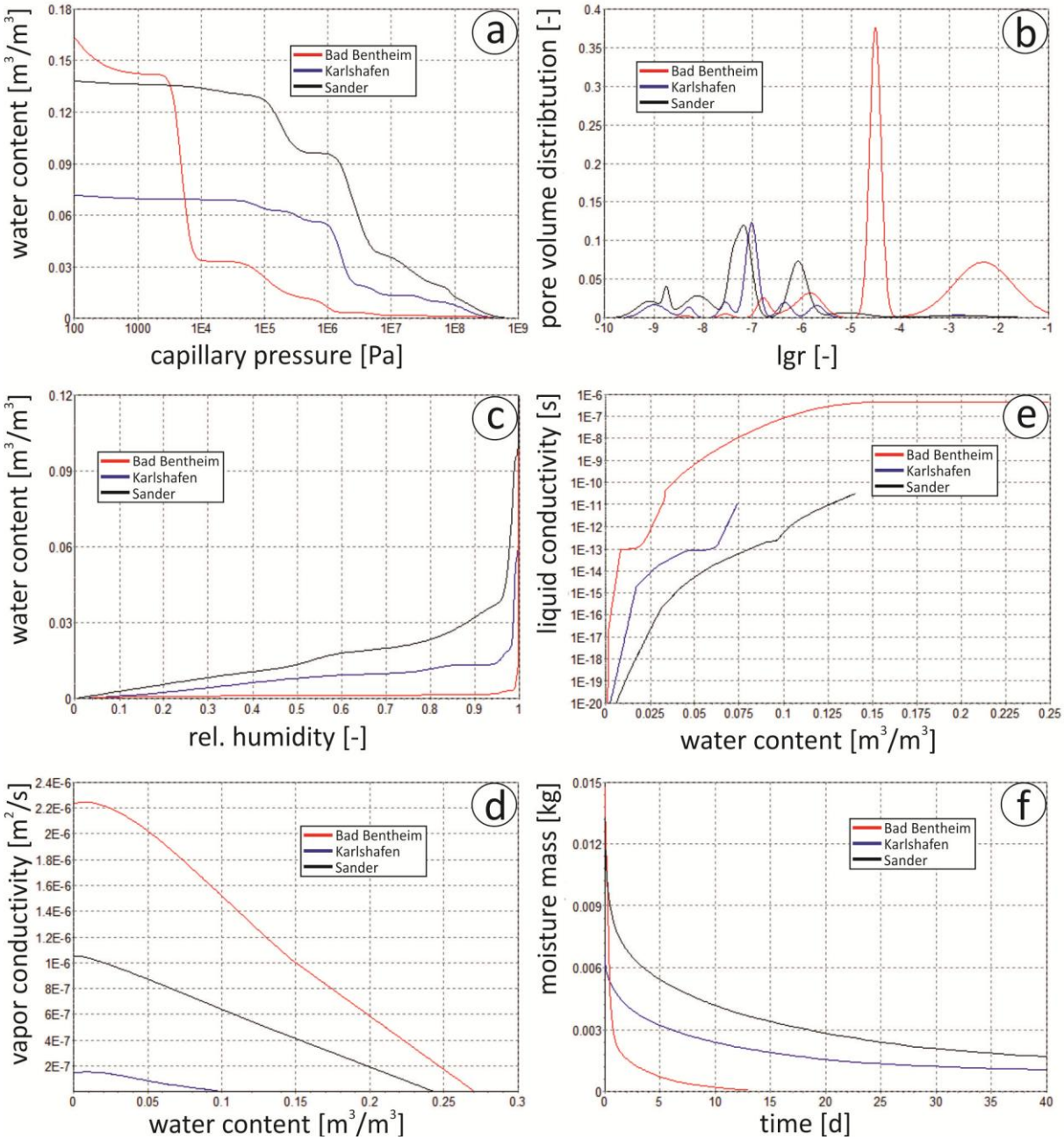

Fig. 5.4: Measured material properties for each sandstone; a) capillary pressure, b) pore volume distribution, c) sorption isotherm, d) vapor conductivity, e) liquid conductivity, f) drying behavior.

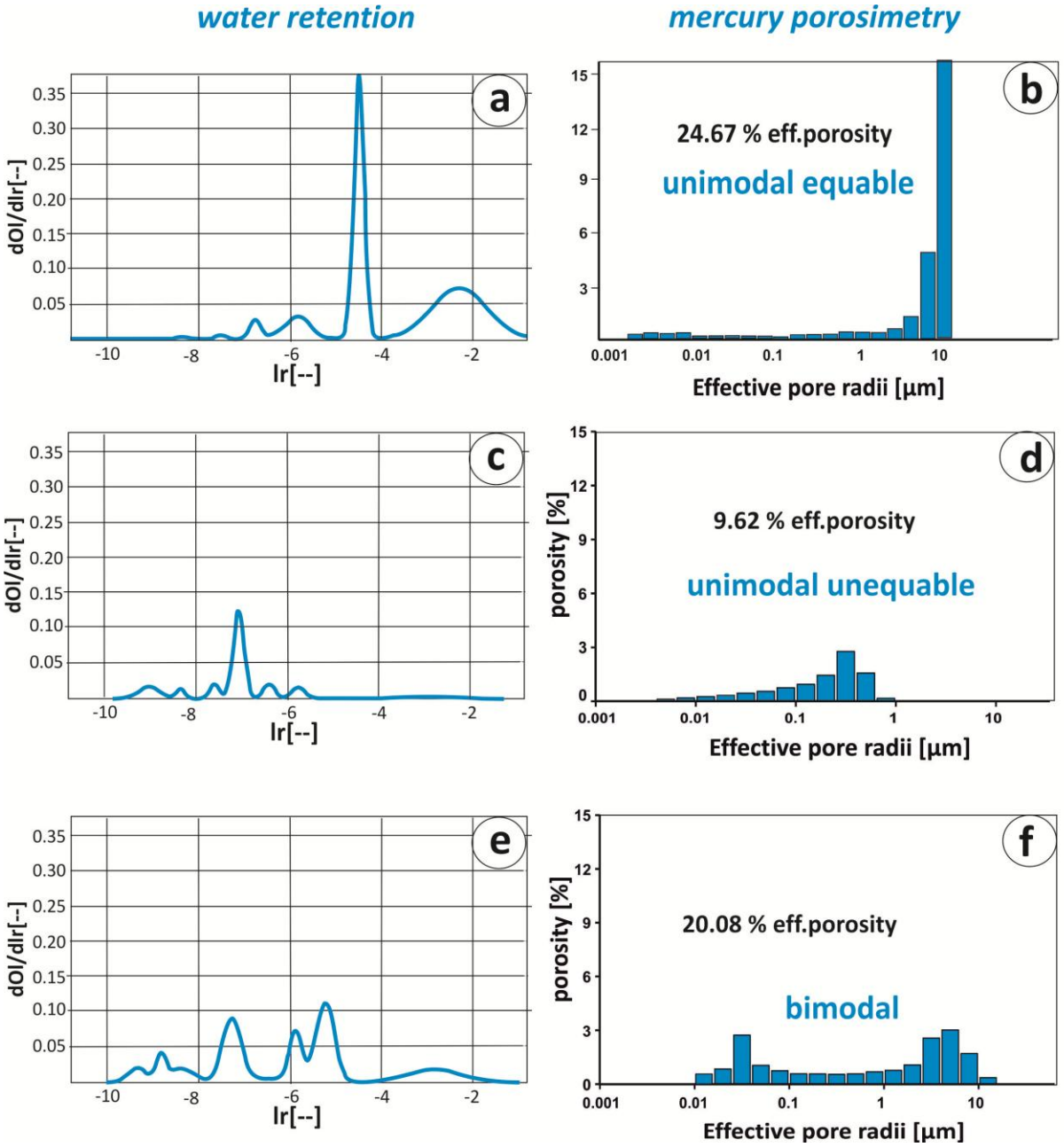

Fig. 5.5: Pore radii/volume distributions of the three sandstone types analyzed, each determined via water retention experiments and mercury porosimetry: a), b) sandstone Bad Bentheim with unimodal equable pore radii distribution, c), d) sandstone Karlshafen with unimodal unequable distribution and e), f) sandstone Sander with bimodal distribution.

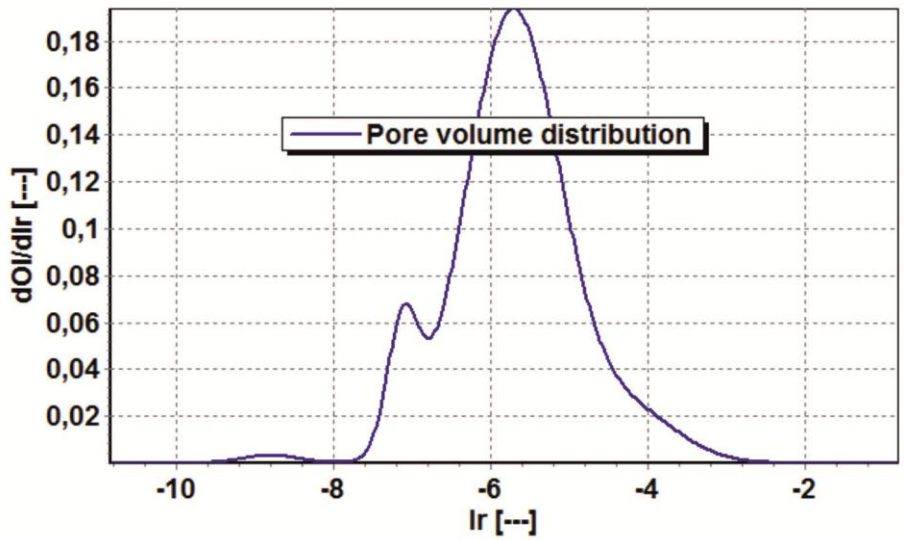

Fig. 5.6: Pore-volume distribution of clay used in numerical modeling.

5.7 Calculated Models and Climate Data

In order to analyze the temporal course of water distribution dependent on sandstone type, climatic environment and the influence of heterogeneities such as clay layers, a simplified construction was chosen. Furthermore, a simplified construction is necessary for reducing the calculation time.

Therefore, a sandstone monolith 150 cm in height and 50 cm in width was created (Fig. 5.7). Since, in natural environmental conditions, contact to bedrock is present, a 1.5 m-deep rock of the same material was calculated. Each of the three sandstones (Bad Bentheim, Karlshafen and Sander) was modeled for three different situations: the single sandstone, the sandstone with clay layers and the sandstone with clay layers and hydrophobic treatment at its surface. The model with clay layers includes three clay layers in horizontal orientations of 1, 10 and 1 cm in height. The hydrophobic treatment was defined with a factor of 100 of smaller capillary water uptake.

The construction was compiled as a two-dimensional planar, bidirectional transport model. Boundary conditions include vapor diffusion, heat conduction and short-wave and long-wave radiation, as well as rain. Since the monolith also has contact with the bottom, heat conduction and water contact was also added as boundary condition.

The time of numerical modeling totals 3 years under real climatic conditions, as situated in Essen (Germany; e.g. Fig. 5.8). Therefore, so-called test reference years (TRY) were chosen, which were determined by real climatic data from the Deutsche Wetterdienst (DWD). The orientation of the monolith is north to south. Output files include next to water mass density (liquid and vapor stage [kg/m^3]) and temperature distribution within the complete sandstone also measuring points, arranged as a top-down vertical profile. The points are positioned at boundary contacts between different materials and depending on expositions (Fig. 5.7, Tab. 5.4). Since the main focus of the

present study is predominantly aimed at moisture distribution, the water mass density is presented and discussed in detail.

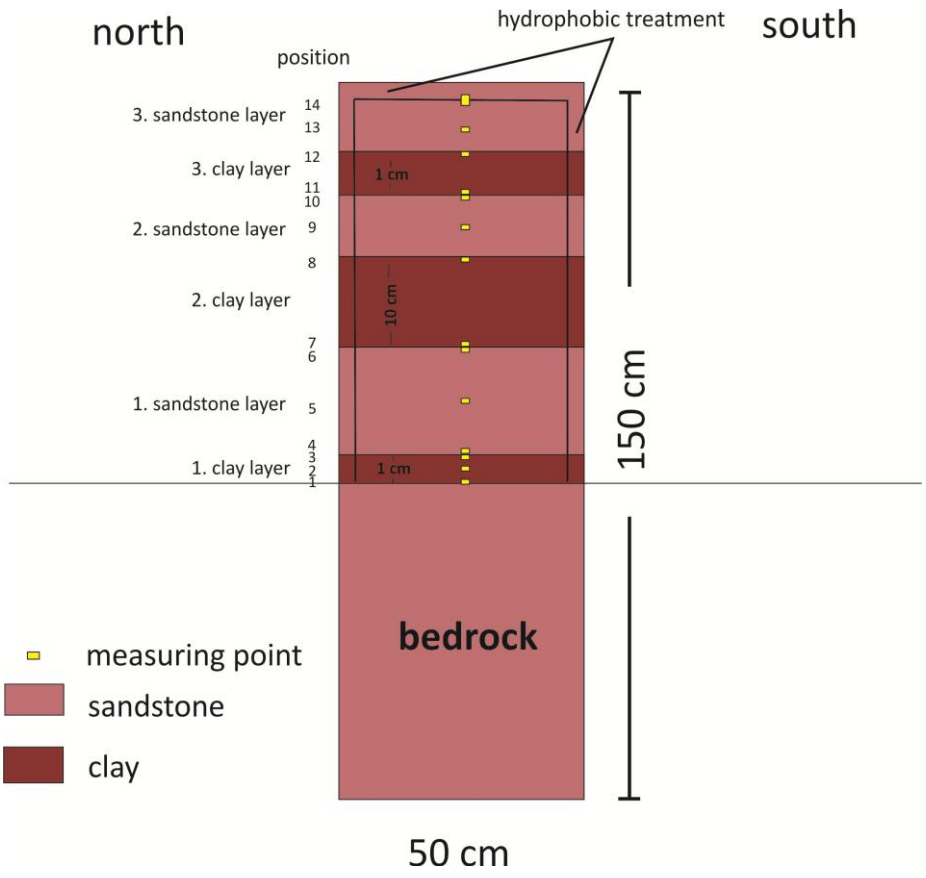

Fig. 5.7: Sketch of model: Sandstone monolith of 150cm in height and 50 cm in width. The model was calculated for three different situations: the single sandstone, the sandstone with three clay layers and the sandstone with clay layers and hydrophobic treatment at its outer surface.

Table 5.4: Position and material of measure points. Abbreviation MP = measure point.

Measure point	Sandstone with clay layers	MP	Sandstone with clay layers	MP	Sandstone with clay layers & hydrophobic treatment	MP	
1	Lowest clay layer	9	Middle of second sandstone layer	1	Lowest clay layer	8	Middle of second sandstone layer
2	Middle of lowest clay layer	10	Top of second sandstone layer	2	Middle of lowest clay layer	9	Top of second sandstone layer
3	Lowest clay layer, boundary with sandstone	11	Third clay layer, deepest part	3	Lowest clay layer, boundary with sandstone	10	Third clay layer, deepest part
4	First sandstone layer	12	Top of third clay layer	4	Lowest sandstone layer	11	Top of third clay layer
5	Middle of first sandstone layer	13	Middle of third sandstone layer	5	Middle of first sandstone layer	12	Middle of third sandstone layer
6	Top of first sandstone layer	14	Top of third sandstone layer	6	Top of first sandstone layer	13	Upper part of third clay layer
7	Second clay layer, deepest part			7	Second clay layer, deepest part	14	Top of third sandstone layer
8	Top of second clay layer				Top of second clay layer		H

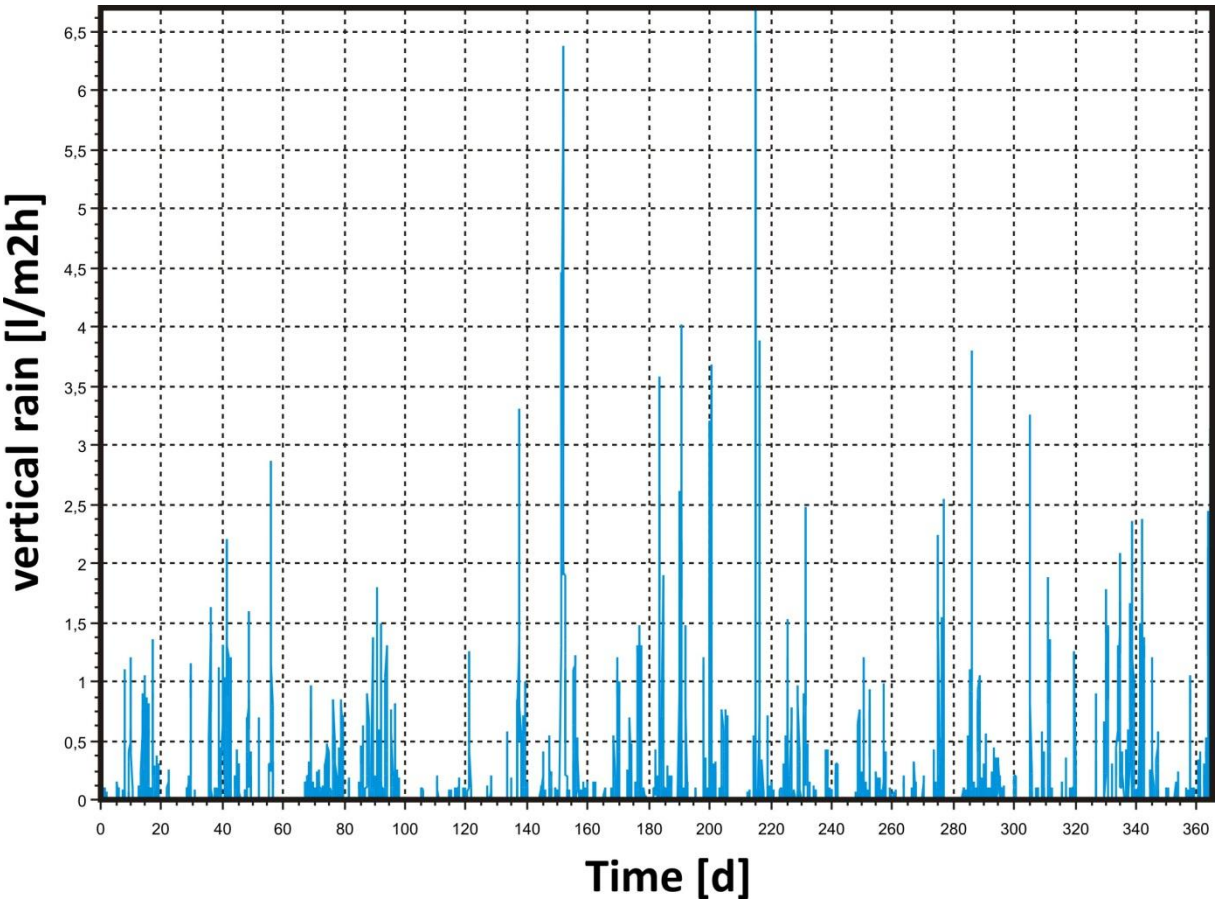

Fig. 5.8: Example of one climatic magnitude: Amount of vertical rain with dependence on time; test reference year for Essen (Germany).

5.8 The Basis of Numerical Modeling: Model Generation and Material Functions

The software used in the present study is based on thermodynamic foundations and was developed for modeling coupled heat and moisture transfer within capillary-porous media (e.g. Grunewald 1997). Mainly, the model integrates all of the aforementioned principles of transport and storage. Moisture transport is described via vapor diffusion and capillary flux. The driving force for vapor diffusion is the vapor pressure gradient and for capillary flux is the gradient of capillary pressure. Moisture storage is described via the material functions of moisture storage and sorption isotherm. Capillary transport is described by the capillary pressure model and is based on the Darcy and Hagen-Poisseulle Law. In the following, the material parameters and material functions are presented in further detail. For more details about the background of numerical modeling within the present study the reader is also referred to Grunewald (1997), Scheffler (2008), Scheffler & Plagge (2009) and Nicolai et al. (2008).

5.8.1 Generation of Material Functions

As already mentioned above, the hygrothermal simulation of, respectively, moisture and water transport calculations are based on coupled differential equations for transport and storage

coefficients. However, these coefficients need to be proved based on laboratory experiments and interpreted before being applied. Modeling a specific material requires a set of material functions, including material and model parameters, which describe real running processes in the most accurate way. The creation of material models takes place in three stages: Modeling, calibration and validation. In the present study, a material model was used, which was developed at the Institute for Engineering Physics of Dresden (TU Dresden, Germany). This model presents in a whole moisture range calibrated, thermodynamically based transport model for coupled liquid water, water vapor- and heat transport.

The moisture storage function consists of a hygroscopic moisture range, which is determined by sorption isotherm and the over-hygroscopic moisture range, which is determined with suction power. Both sorption and suction power can be presented as continuous functions. Based on this, the transport functions of liquid water and water vapor can be derived and calibrated with the help of further experiments (e.g. drying experiment, Chapter 5.9).

Fitting of Moisture Storage Function

The moisture storage function is based on a multimodal functional approach and is linked with a logarithmic normal pore-radii distribution. The fitting is made over measured values of a hygroscopic (e.g. sorption/retention) and super-hygroscopic (e.g. capillary water uptake) moisture range. Whereby, the parameter *pC represents* the logarithm of capillary pressure, θ_l the volume content of liquid phase, and *N* the modality (number of peaks within the pore-volume distribution). S_i represents the standard deviation of logarithms of capillary pressures (pC_i) at the particular peak positions with (θi) characteristically measured volumetric water content. "e*rf*" presents the parameter of Gauss distribution.

$$\frac{\partial}{\partial pC}\theta_1(pC) = \sum_{i=1}^{N}\left[\frac{\theta_i}{\sqrt{2\prod S_i}}\cdot\exp\left(\frac{(pC-pC_i)^2}{2\cdot S_i^2}\right)\right] \qquad \text{Pore-volume distribution}$$

$$\theta_1(pC) = \sum_{i=1}^{N}\left[\frac{\theta_1}{2}\cdot\left(1+erf\left(\frac{(pC_i-pC)}{\sqrt{2\cdot S_i}}\right)\right)\right] \qquad \text{Moisture storage function}$$

The moisture storage function is determined by the integral of pore-volume distribution over all pore classes.

Modeling of Liquid Conductivity

For the derivation of the transport function of liquid water and water vapor from the pore structure, two models are combined with each other. Whereby, the liquid conductivity is derived from the pore

structure according to the model of Hagen Poiseuille and the moisture conductivity according to the model of Burdine (1953). The model of Burdine assumes parallel, circular capillaries, and the liquid water flow depends on the gradient of capillary pressure and surface tension, as well as on the interaction between water and pore surface. The possible flow volume of individual capillaries follows the Hagen-Poiseuille Law and can be transferred via connection with the pore-radii distribution to all capillaries (depending on pore radius).

The summation of all pores reveals the flow density of liquid water, depending on the largest water-filled capillary radius.

The volume-flow density of a single capillary is as follows:

$$V_k(r) = \frac{\pi \cdot r^4}{8\eta_1} \cdot \left[\rho_1 \cdot g_k + \frac{\partial p_c}{\partial x_k} \right]$$

And the liquid conductivity is as follows:

$$j_k^{ml} = -\left[\frac{\rho_l}{8\eta_l} \cdot \tau \cdot \int_{Rmin}^{K} \pi \cdot r^4 \cdot \frac{dn}{dr} \cdot dr \right] \cdot \left[\rho_l \cdot g_k + \frac{\delta \rho_c}{\delta X_k} \right]$$

Whereby j_m^{kl}=liquid conductivity, r = capillary radius, ρ_l = water density, η_1= kinematic viscosity, τ = tortuosity, ρ_c= capillary pressure and x_k= spatial coordinate.

The function of conductivity connects in the super-hygroscopic range at the measurements of water vapor diffusion (wet-cup) and is added in the area of capillary saturation by further values of moisture conductivity (Darcy).

The pore model used here describes, in a very simplified way, liquid transport within the pore system. A completely networked liquid phase is assumed, which allows consistent capillary flow within the rock. Coevally, this includes a *parallel* running liquid and vaporous transport within the upper capillary, respective to the saturated moisture range. However, below the capillary range, the liquid phase is present in the shape of “liquid islands”. These islands are capillaries not linked together and can only communicate about vapor phase. This case involves *serial* liquid water and vapor transport. In contrast to parallel transport, the serial transport is more efficient in the vaporous phase, while, in the liquid phase, the transport is much less efficient. Accordingly, the volume proportion increases with the water content within ranges of parallel transport. Contrastingly, the volume proportion decreases with serial transport.

Since liquid and vapor transport should be considered together, a model which combines serial and parallel liquid and vapor transport is applied. This describes the influences of liquid islands communicating via the vapor phase and surface film. It simultaneously allows modeling of the

moisture dependence of vapor transport and provides the scaling of liquid conductivity in the hygroscopic and adjacent super-hygroscopic range.

Model Approach for Water-Vapor Diffusion

A model for the description of serial and parallel liquid and vapor water transport is referred to as the *SP-model* and is defined as follows. The model assumes a porous material in which parallel and serial liquid water and water vapor transport take place. Both serial and parallel ranges exhibit pores according to the pore volume distribution function.

Where serial transport takes place, vapor molecules diffuse through air-filled pore space on both sides of the "liquid islands" from higher to lower vapor pressure. Capillary condensation proceeds at the capillary meniscus, which faces higher capillary pressure. At the opposite capillary meniscus, equivalent amounts of water molecules evaporate at the same time. Between both capillary meniscuses, the water is transported via the liquid phase. Within the water-filled pores of serial areas, the vapor resistance is much smaller than within the air-filled pores. Therefore, the vapor pressure gradient is assumed to be zero.

The number of parallel structured areas (p) in the rock is not consistent, but is defined relative to water content. When less water is present in the pore space, less connection between the liquid islands is possible, and a parallel transport is unlikely. However, with increasing water content, the pores become filled and areas arise progressively where parallel transport then takes place. For a description of the moisture-dependence of parameters, an adjustment parameter h is inserted here, which is connected to the relative water content. The parameter is materially dependent and determined via inverse modeling in the drying experiment.

5.9 Verification Experiments for Material Functions: Continuous Water Uptake and Drying

The applied material function based on Hagen-Poiseullie and Burdine (1957) assumes circular pores with an idealized length. Since this does not correspond with the real pore shape, tortuosity is integrated and the results are fitted with the results of drying (Fig. 5.9b) and water uptake (Fig. 5.9b) experiments. Accordingly, a calibration of the functions with water uptake and drying experiments is required. Therefore, comprehensive data, including initial, boundary and transition conditions are required with high temporal resolution.

Drying behavior strongly depends on geometric and climatic conditions because measurement data are influenced by these parameters. Hence, additional detection of these boundary conditions during the measurement allows a distinct improvement in interpretability and allows verification of material functions. The parameters are varied within the numerical simulation until sufficient accordance

between simulation and experimental results is given. The adjustment parameters serve to scale the transport parameters of the capillary and hygric moisture range, whereby liquid conductivity and the vapor diffusion coefficient are scaled with the drying experiment. To control the super-saturated moisture range, a numerical simulation of capillary water uptake is accomplished, and a sample with the same dimensions as the experimental test specimen is modeled.

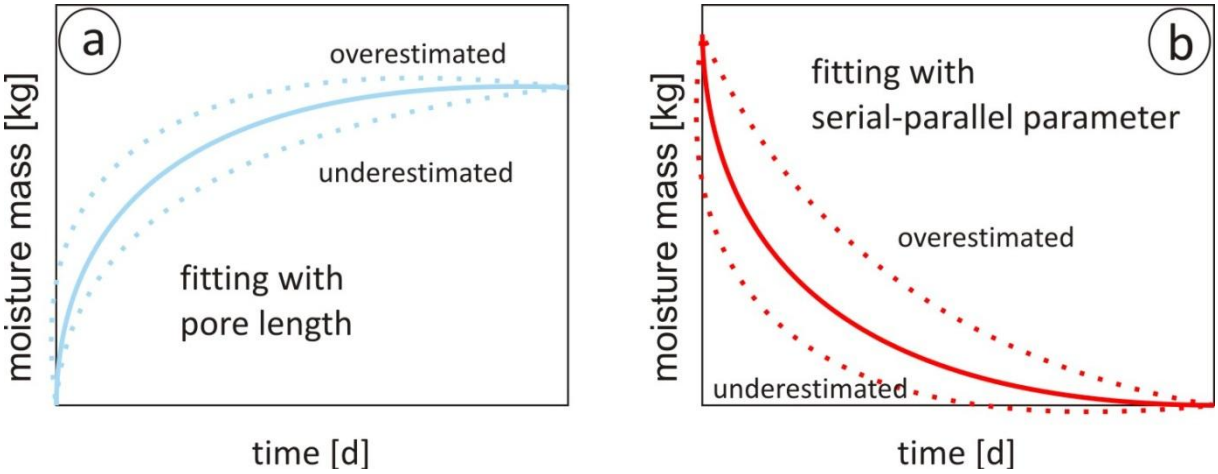

Fig. 5.9: a) Verification experiments with the water uptake coefficient are fitted with pore lengths; b) drying experiment with fitting parameter of serial-parallel transport.

5.10 Calibration of the Material Model & Material Functions: Example of wetting & drying

The physical model approach mentioned above results in moisture-dependent transport functions. The vapor diffusivity is expressed by vapor diffusion through the air, is reduced by the vapor diffusion resistance of the particular material (μ_{dry}) and is multiplied by the corresponding proportion of the parallel serial model.

$$D_v(\theta_r, T) = \frac{D(T)}{\mu_{dry}} \cdot \frac{1-\theta_r}{[\theta_r^h + (1-\theta_r)(1-\theta_r)^2 \cdot (1-\theta_r^h)]} \qquad \text{Vapor transport}$$

Through multiplication of the relative liquid water conductivity ($K_r(\theta_l)$) of the pore model with the measured conductivity at saturation (K_s) and the connection with the serial parallel model of the liquid water, conductivity can be determined.

$$K_l(\theta_l) = K_r(\theta_l) \cdot K_s \cdot K_{l-corr} \cdot \frac{1}{\left[1 + \frac{(1-\theta_r)^2 \cdot (1-\theta_r^h)}{\theta_r^h}\right]} \qquad \text{Liquid transport}$$

In this way, the parameters *h* and $K_{l\text{-corr}}$ had to be adjusted in different experiments. The parameter $K_{l\text{-corr}}$ serves the correction of liquid water conductivity in the high moisture range, which is based on the water-uptake experiment near capillary saturation. With the help of parameter *h*, the low moisture range is adjusted and is based on the drying experiment.

5.11 Results

5.11.1 Water & Moisture Distribution in Sandstone Monoliths

The results of modeling the water and moisture distribution confirms that each sandstone type is characterized by a different water and moisture balance.

The temporal process of moisture and water content changes within the sandstones (here, for example, the sandstone Karlshafen) clearly exhibits fluctuations, which reflect the annual interaction of the sandstone with the environment. The highest amount of water content is observable during winter (October-February), whereas the lowest is observable each summer. At the same time, distinct differences occur when considering the position within the rock. Additionally, the establishment of equilibrium first occurs in the beginning of the third year. In the first and second years, the maximum of water uptake for this rock has not been compiled (Fig. 5.10). Hence, in the following presentation of results, only the third year will be considered.

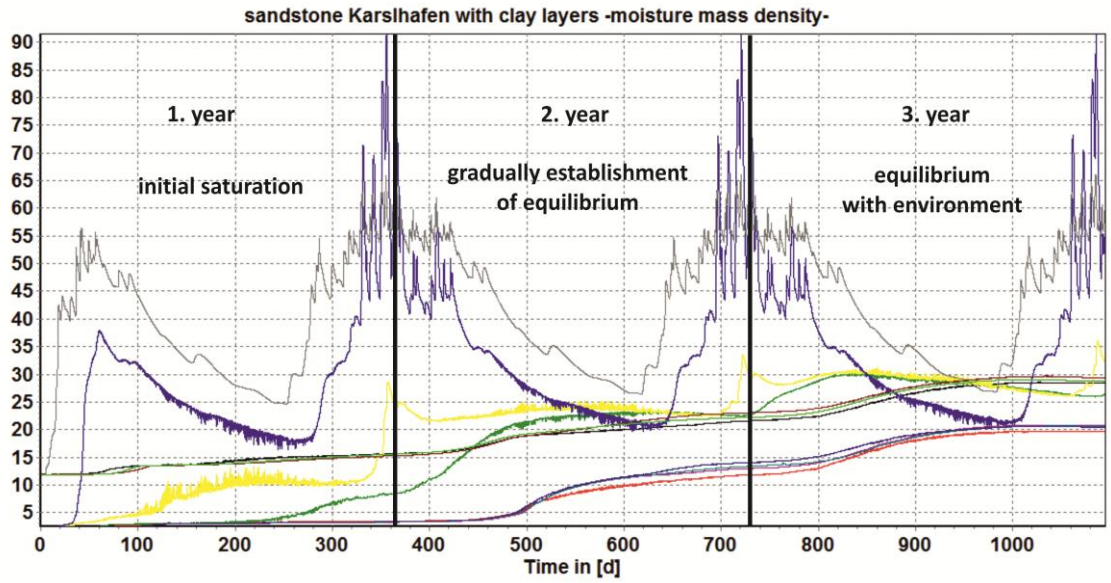

Fig. 5.10: Example illustrating the establishment of equilibrium between rock and its natural environment within three years. In the first year, the moisture mass density within the rock was still low, whereas in the second year a distinct increase is observable. Equilibrium arrives in beginning of the third year.

5.11.2 Differences in Moisture Distribution Dependent on Sandstone Types

For all sandstones analyzed, the water mass density and the relative air humidity strongly vary within the rock, dependent on position (Fig. 5.11, 5.12). In the deepest part of the monolith (point 1; Fig. 5.11), consistent water content is observable. With increasing position closer to the surface, the water mass density first decreases (point 2, 4, 8; Fig. 5.11) and coevally stronger variations within the temporal sequence arise. These are for all sandstones well developed from September to March and then exceed the amounts of water mass densities of underlying rock areas.

These general trends are also observable for the relative air humidity: In the lower part of the sandstones, a temporally- and locally- consistent amount of humidity is observable, while, with increasing height, the air humidity is subject to strong fluctuations. Directly at the sandstone surface (point 15, Fig. 5.12c), the sandstone Bad Bentheim is characterized by strong fluctuations, whereas those in the sandstone Karlshafen are very poorly and in the sandstone Sander medium developed (Fig. 5.12d).

Additionally, the levels of water mass density vary considerably between the rocks. The sandstone Bad Bentheim (Fig. 5.11a) shows the lowest values of water mass density on average. In summer time the top area is almost dried and also towards the core the water mass density is with ~10 - 15 kg/m^3 very low. The sandstone Karlshafen (Fig. 5.11b) is characterized in the lower rock area with ~20-60 kg/m^3 in average by a distinct higher water mass density than sandstone Bad Bentheim. The peaks of temporal fluctuations at the surface (point 10, 12) from September to March are, in contrast to sandstone Bad Bentheim, smaller but occur more frequent. The sandstone Sander (Fig. 5.11c) exhibits the highest value of water mass density with ~75-160 kg/m^3 in the lowest rock part (point 1 - 3) and ~60 kg/m^3 in the higher rock areas (Fig. 5.11c, Fig. 5.12). The peaks of temporal fluctuations from September to March arise more infrequently than at sandstone Karlshafen, but are more intensive. Both sandstone Karlshafen and Sander are in the top area of the monolith also during summer time characterized by fluctuations of water mass density, and never reach the almost constant dried condition as sandstone Bad Bentheim.

Moreover, the sandstones are characterized by staggered water uptake over time: At point 4, the sandstones Bad Bentheim (Fig. 5.11a) and Sander (Fig. 5.11c) demonstrate a distinct peak (e.g. May / June), while in the sandstone Karlshafen (Fig. 5.11b), this water input is characterized by a flattened and elongated peak. This trend continues until point 6. Afterwards, small-sized peaks are also observable here.

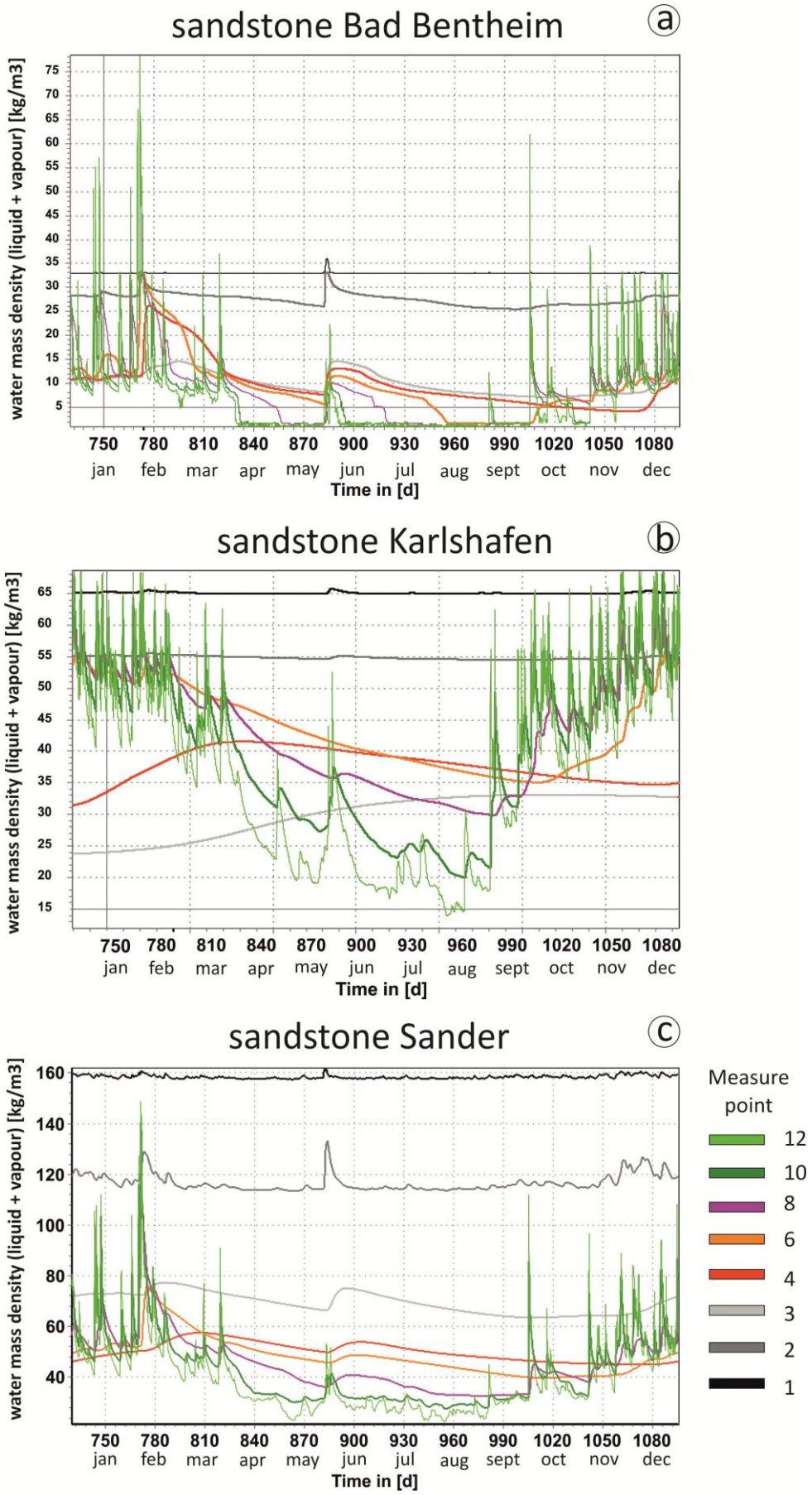

Fig. 5.11: Diagrams showing the water mass density in a) sandstone Bad Bentheim, b) sandstone Karlshafen and c) sandstone Sander monolith at selected measure points within the center of the monoliths (3rd Test Reference Year of Essen, Germany).

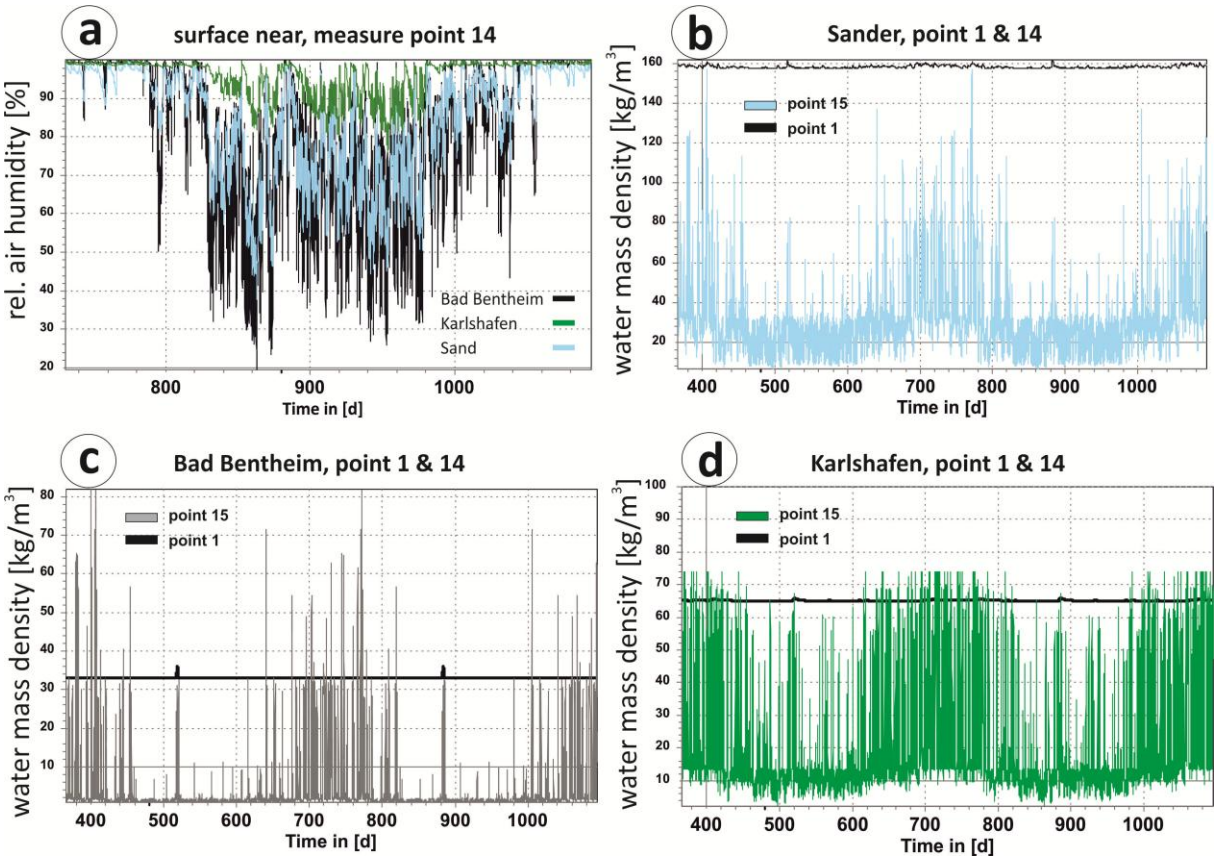

Fig. 5.12: a) Diagram of relative air humidity vs. time. It is clear to see that near surface the air humidity is underlain strong fluctuations. The sandstone Karlshafen shows few fluctuations, while the sandstone Bad Bentheim is characterized by intense and numerous fluctuations; in b), c) and d), the water mass density of the undermost and top rock areas (point 1 and 14) of all three sandstones is presented.

5.11.3 Changes in Moisture Distribution in the Context of Heterogenities (Clay Layers)

The results of water mass density and air humidity clearly show that the presence of clay layers changes the water distribution within the sandstones. In general, in all sandstones investigated from bottom to top, a similar influence is observable. Moreover, the highest values of water mass density are still recognizable for winter times, while the summer is characterized by the lower values in average. Coevally, the temporal course and the fluctuations differ with each individual rock.

In the deepest clay layer, the water content is highest for the sandstone Bad Bentheim (Fig. 5.13 a), whereas in the sandstones Karlshafen and Sander, the amount is very low (Fig. 5.13 b, c). In the case of the sandstone Karlshafen, the curves show few fluctuations with relation to time; the water content changes only a little with regard to position, and the three curves (points 1, 2 and 4, Fig. 5.13 b) run almost parallel to each other. The sandstone Sander shows a distinct variation between points 1 and 2, whereas the clay layer of Bad Bentheim exhibits a water mass density consistent with position.

While, in the overlying sandstone layer of Bad Bentheim (points 4, 5 6, Fig, 5.13 a), a distinct decrease in water mass is observable, in the sandstones Sander and Karlshafen, an increase in contrast to the underlying clay layer is recognizable. Furthermore, in the lowest part of the

sandstone layer, the sandstone Bad Bentheim shows few but intensive fluctuations, whereas, in the middle and upper areas, the water content remains consistently lower than for the underlying clay layer. Both the sandstones Sander and Karlshafen display consistent water mass density within the first sandstone layer. From the second to the third clay layer, the water mass density increases for each rock, whereby the increase is most evident in the sandstone Bad Bentheim.

As the height within the rock increases, first fluctuations are also observable in the clay layers. The highest levels of water content can be detected for the top clay and sandstone layers (Fig.5. 13). However, although the water content of the top sandstone layer, on annual average, is higher than that of the underlying clay layer, the highest amounts within the complete rock can be detected for the clay layer from January to March. Furthermore, in contrast to the single sandstone, the amount of water content increases in the presence of clay minerals.

In the uppermost sandstone layer (e.g. point 14; Fig. 5.13), again, the sandstone Karlshafen reacts most slowly and is the most temporally staggered in water input, whereas the other sandstones react similarly over time. Furthermore, the amplitude of the curves in the sandstone Karlshafen are generally not that intensive, unlike Bad Bentheim and Sander.

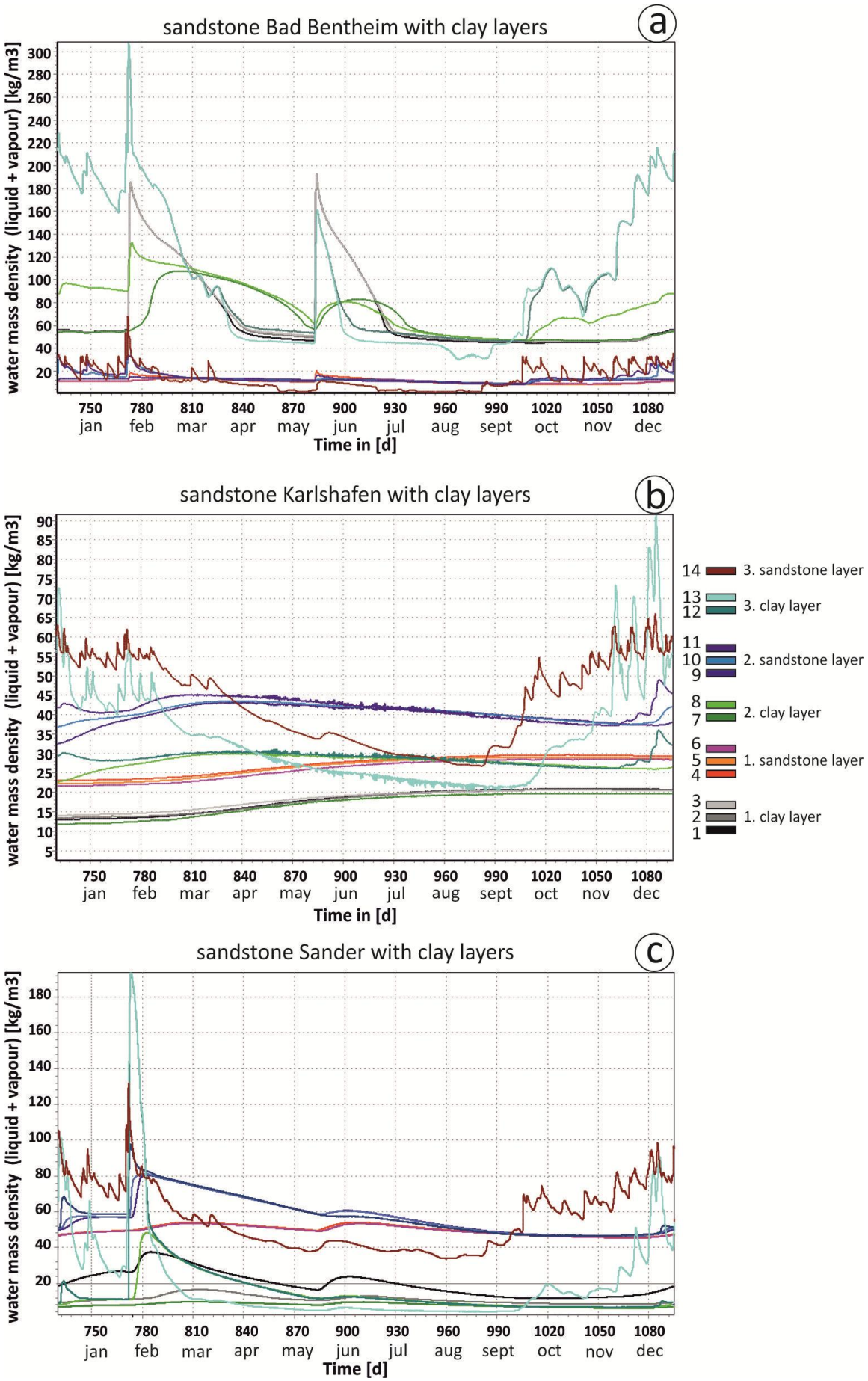

Fig. 5.13: Water mass densities for all measuring points of the sandstone monoliths a) Bad Bentheim, b) Karlshafen and c) Sander with clay layers (3rd Test Reference Year of Essen, Germany).

5.12 Hydrophobic Treatment and Moisture

The hydrophobic treatment on the outer surface of the sandstone clearly influences the water content within all rock types. In general, the water content decreases considerably in contrast to the untreated samples. Thereby a converse observation can be made concerning the annual course of water content: Now during the wintertime the lowest water content is observable, while the highest are present during summer. Coevally, the results of the different rock types and their clay layers are well pronounced.

For all points measured on the sandstone Karlshafen (Fig. 5.14b), a distinct decrease in water content (~5-20 kg/m^3) is observable. Closer inspection reveals that the curves of the clay layers are separated from one of the sandstone areas since the content of water mass density within the clay layers noticeably decreases. Furthermore, the first small-scale fluctuations are visible at the second sandstone layer and occur most intensely within the third clay layer.

The sandstones Bad Bentheim (Fig. 5.14a) and Sander (Fig. 5.14c) still indicate the presence of clay layers. This effect is very clearly visible in the sandstone Bad Bentheim, wherein only the water content of the top layer decreases. Both the lowest clay layer and the sandstone layer clearly show annual fluctuations in water content. However, in contrast to the untreated sandstone, the peaks are not that insensitive. The water content of the treated hydropobe area (point 14) is, in the case of the sandstones Karlshafen and Sander, only slightly decreased when compared with the first and second sandstone layers. Dissimilarly, the sandstone Bad Bentheim demonstrates a clear decrease throughout the lower sandstone layers.

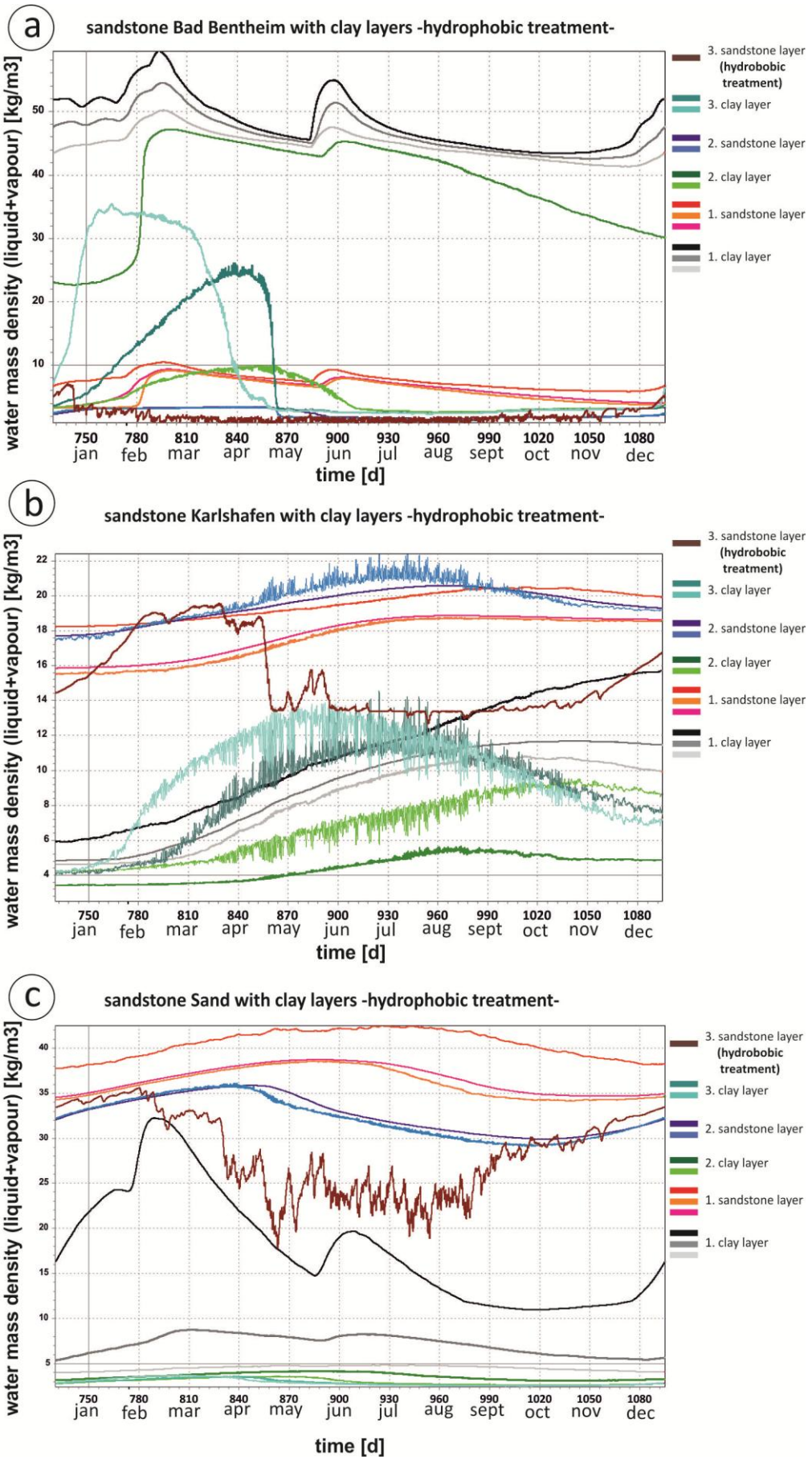

Fig. 5.14: Water mass density for all measuring points of the a) sandstone Bad Bentheim, b) sandstone Karlshafen and c) sandstone Sander with hydrophobic treatment.

5.13 Discussion

5.13.1 General Transport Mechanisms and Processes in the Sandstone Monoliths

Generally, the water mass densities observed prove that they are the result of the interaction between material-specific parameters (e.g. porosity, pore-volume distribution, sorption, capillary water uptake coefficient, water vapor diffusion coefficient, liquid conductivity and drying behavior) and the environmental conditions (e.g. rain, sunshine, temperature, relative air humidity, wind and sky radiation). Pursuing, these parameter follow the processes of thermodynamics, on which the material functions of the numerical modeling are based. Accordingly, the driving forces of moisture transport are the gradients, e.g. in vapor and capillary pressure. Thus, the unfolding of common processes can be observed in the monolith (Fig. 5.15a):

In the lowest parts of the sandstone monolith, the water mass density mainly depends on the vertically rising groundwater (-2m depth in bedrock), which has also been proven by many studies of real objects. This process depends on the current hygroscopic and capillary transport properties of the bedrock. In general, the transport mechanism here is dominated by capillary transport. The influence is distinctly recognizable until measure point 3. During wintertime, the capillary transport is hindered at low temperatures since water changes the density/aggregate state and, as a consequence, its surface tension. Accordingly, during this time, amount of rising water is very low. Additionally, after a long, dry period during summertime, a decrease in rising water is very notable. This decrease is accompanied by a simultaneous increase in vapor transport. When, after this drying period, a driving rain event occurs, the bedrock is predestined to absorb water via capillary absorption, inducing a capillary rise in water. Averaged over the course of the year, the uprising component of the lower rock part presents a very stable parameter and results in an almost consistently soaked, “slowly reacting” rock part since this part is fed by groundwater.

Parallel to the vertical transport, a horizontal input/output of water occurs that is caused by an exchange with the environment. Depending on external conditions of vapor pressure (relative air humidity and temperature) and capillary pressure, vapor diffusion and capillary water transport takes place. When outside conditions are characterized by a high temperature and low relative air humidity (e.g. drought in summer), the rim area of the sandstone starts to dry. Moreover, vapor diffusion and capillary transport take place in the direction of lower vapor pressure and capillary pressure. Depending on the drying properties of the rock, a driving rain that commences afterwards inevitably induces capillary water uptake since capillary pressure is low in the unsaturated pores. Since the content of super-saturated water increases towards the center of the rock, the capillary pressure also increases, and, as a consequence, the capillary transport decreases. According to this, an overlap of rising and the horizontal component is responsible for the degree of water mass

density. A high relative air humidity attunes after the long dry period, and water is absorbed easily since the gradient between outside and inside conditions is high. In this situation, a driving rain event can also induce high capillary water uptake within the rock. However, the degree of water uptake depends on the degree of saturation. Since stable and permanent moisturization is present towards the center, the capillary transport decreases from the outside to the center (capillary pressure gradient).

With increasing height up to the top (points 6-11), a significant influence of climatic effect is noticeable, which is documented by annual fluctuations within the curves of the water mass density. Therefore, as height increases, the rock is characterized by increased wetting and drying cycles, which is proven by a more strongly alternating curve shape. Rapid alternation of drying and humidification, which is caused by variable outside conditions, induces stress within the fabric of the rim area and is still recognizable in the ~50 cm depth of the rock. The influence of rising water from the bedrock is overlapped with increasing height.

Driving-rain effects are easiest to recognize in the part of rock surface (point 10-14). Simultaneously, it can be assumed that areas of laterally-oriented surfaces are influenced much earlier by climatic fluctuations (evaporation, humidification, etc.). Moreover, behavior in the context of warm and dry external conditions strongly depends on the drying properties of each rock.

Furthermore, a difference in water mass density with regard to the orientation of the monolith is recognizable: The northwardly-oriented side is less affected by sunshine than the southwardly-oriented one, which, naturally, has an impact on the distribution of water mass density within the rock due to the slowed drying. The southwardly-oriented plane is much more exposed to solar radiation and rain events because this side is characterized by a more intensive but potentially quickly changing moisturization.

To summarize, the results clearly confirm and reflect observations in the laboratory and under natural environmental conditions, wherein the rim zone is characterized by strong annual fluctuations of water/moisture content, while the part close to the bedrock is characterized by uprising capillary transport from underground. Accordingly, the core of the sandstone monolith is distinguished by an almost stable but high water content, while outwardly temporary fluctuating water content increases. Subsequently, damaging processes such as hygric dilatation and salt- and freeze-thaw weathering are concentrated on the rim zone. In the context of salt weathering, already minor fluctuations of relative humidity are assumed to result in repeated changes of salt dissolution and crystallization, since threshold for deliquescence may be multiple exceeded (e.g. Price 1993; Warke et al. 2011). To what extent the lithology and its associated pore-volume distribution has an impact on the water mass density will be discussed in the following section.

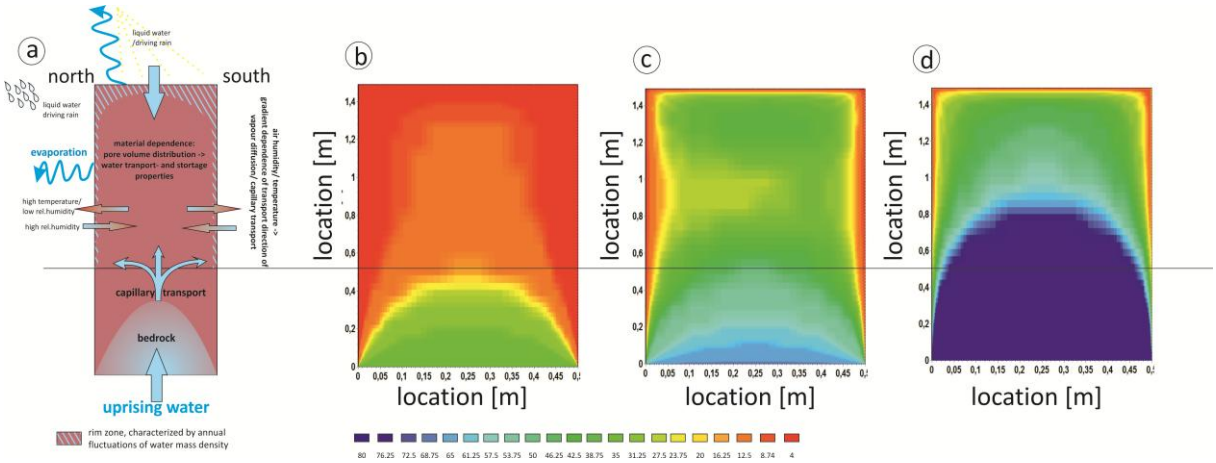

Fig. 5.15: Schematic illustration of main processes within the monoliths: a) moisture distribution (water mass density [kg/m^3]) in the middle of April during a dry period for the b) sandstone Bad Bentheim, c) sandstone Karlshafen and d) sandstone Sander.

5.13.2 The Sandstone Bad Bentheim

Due to its water transport and storage properties the sandstone Bad Bentheim is characterized by the lowest water mass density of all sandstones investigated (Table 5.3, Fig.5.4). In the deepest part of the sandstone, the uprising water of the bedrock is limited since hygroscopic transport does not take place due to the low absorption capacity; only super-hygroscopic capillary transport takes place due to the high capillary water uptake. This uptake is hindered because all capillary active pores are filled with air and, therefore, do not influence the conductivity of water. However, when pores are filled in certain conditions, the high-drying velocity and liquid conductivity cause fast removal on the outside of the rock (dependent on outer conditions).

These properties result in insensitivity to changes in relative air humidity (little sorption). Moreover, since the sandstone mainly assimilate water via capillary water uptake, the content of water only depends on available moisture in the liquid phase. Therefore, the sandstone Bad Bentheim absorbs water only during driving rain events, which explains the large intensive peaks during September to March. During summer time the high temperature and low air humidity, in conjunction with a high drying velocity at this time, leads to a very low water mass density within the whole monolith, and the remaining water content within the center dwindles (Fig. 5.15 b).

The results prove that the outlier of quartzarenites (Chapter 2.1) with high porosity and a high capillary water uptake coefficient can exhibit much less water within its pore space than sandstones with very low porosity and a very low capillary water uptake coefficient (e.g. sandstone Karlshafen). Porosity and the capillary water uptake coefficient have been described by many authors as a positive linear function (Mosch & Siegesmund 2010, Stück et al. 2012). However, the pore-volume distribution in interaction with the combined consideration of water transport and storage properties (capillary and vapor uptake and transport) seems to be necessary to explain the deviating from the average behavior. In particular, the high drying velocity and very low vapor-diffusion

resistance promotes the rapid dehydration of the rock. Alongside the pore volume distribution, the associated clay minerals and their arrangement between the pores and on the grains seem to play a crucial role in the water and vapor conductivity. Since only few clay minerals (pore filling kaolinite) in the sandstone Bad Bentheim are located within the gusset between the large quartz grains, they will not promote much water absorption via capillary condensation or sorption.

Additionally, in the context of hygric swelling, the limited number and the location of clay minerals are of paramount importance since this weathering process is mostly associated with micropores built up by the network of (swellable) clay minerals. Since Anderson et al. (2010), also non-swellable clay minerals like kaolinite in the investigated sandstone have also resulted in crystalline swelling at varying relative humidities. However, we assume that the crystalline swelling of kaolinite in Bad Bentheim cannot lead to swelling since the swelling takes place in the free space of large capillary pores. This support studies of Ruedrich et. al (2010), who postulates a relationship between the position of clay minerals and stress transfer leading to hygric dilatation.

The results of very low water content confirm the studies of additional weathering processes of the sandstone Bad Bentheim: The sandstone is resistant against salt attacks (Ruedrich et al. 2005, Ruedrich & Siegesmund 2006, Stück et al. 2012). Following the model of capillary pressure in the context of salt weathering, the missing micropores may also be responsible for the high resistance against salt attacks (Putnis et al. 1995, Putnis & Mauthe 2000).

Accordingly, the sandstone Bad Bentheim, representing highly-mature quartzarenites, can be characterized as a highly-qualitative construction material in humid climate conditions by numerical modeling.

5.13.3 The Sandstone Karlshafen

Crucial to the higher quantity of water mass density in the lower rock parts (in comparison to Bad Bentheim) is the result of the combination of high sorption capacity, capillary water uptake and slow liquid conductivity (Table 3, Figs. 4, 11). The low liquid conductivity and high vapor diffusion resistance causes a slow streaming out of the rock, which is also documented via the medium drying behavior. The continuous decrease of uprising amount of water can be traced back to the decreasing gradient of water content between overlaying rock areas. These areas are due to the high sorption capacity almost saturated as a result of low capillary pressure.

The alternation of the annual water mass density clearly increases with increasing height, which also originates from the medium drying velocity and high sorption capacity. Coevally, the vapor conductivity (high vapor resistance) promote a long-term retention of water (Fig. 5.11 b, e.g. points 3-8) in the deeper part and center part of the monolith. As a consequence, the sandstone reacts by

becoming staggered over time. The rim zone (Fig. 5.11 b, points 10 & 12) is much more sensitive to the climate variability of relative air humidity and temperature than the sandstone Bad Bentheim.

This is also comprehensible in the strong alternation of moisture during early spring to summer at the rim zone (point 15, Fig 5.12 d): While the sandstone Bad Bentheim, during this time, displays a more or less consistent low moisturization (point 15; Fig. 5.12 c), the sandstone Karlshafen is characterized by a generally weakened moisturization, but by peaks with the same intensity as during winter and autumn. In addition, after a long drying period in summer time, only the rim zone is characterized by a decrease in water content, whereas, behind this zone, the moisture content increases dramatically (Fig. 5.15c). This can again be explained by protracted moisture loss as the result of high vapor-diffusion resistance. At the same time, the distribution of the uprising component with the overlap of the present moisture within the upper rock areas result in a concave moisture front since the liquid phase (higher liquid conductivity, Table 5.3) can be more easily transported outwards. When salts are present, this zone will be the location of precipitation and will lead to deterioration. This concave shape aligns with observations made in the natural environment, where rounding is often observed at the lower parts of monoliths (Fig. 5.18a).

Again, our results show that the porosity and the capillary water uptake coefficient of a sandstone are not the only indicators for evaluating possible moisture distribution or the amount of water within the pore space. In particular, the pore sizes and the “pore building” material are the controlling/defining parameters. The pore space of the sandstone Karlshafen is next to intergranular pores formed by clay minerals. These clay minerals represent the highly specific surface for adsorption and desorption capacity, which is also revealed by the high cation exchange capacity of 2.1 meq/100 mg and by the high vapour diffusion resistance. Furthermore, the presence of micropores created by altered lithoclasts, micas and pseudomatrix lead to a capillary condensation and can lead to characteristic delamination (Rodriguez-Navcarro et al. (1997), Sebastián et al. (2008)) via hygric dilatation, as in case of the sandstone Karlshafen. Here, the arrangement of clay minerals present by altered lithoclasts can induce stresses to the rock fabric during moisturization (Ruedrich et al. 2010). Accordingly, the main contributor to the deterioration process of the sandstone Karlshafen is the high quantity of hygric dilatation (~1 mm/m). Regarding medium salt weathering resistance and the medium water content combined with “clay-micropores”, the sandstone can be classified medium weathering resistant. However, with respect to the high strength as a result of the high content of quartz cementation, the sandstone will withstand stress development during salt crystallization to a certain degree.

To summarize, the numerical modeling proves that sublitharenites´ moisture distribution, such as in the sandstone Karlshafen, result from the kind of and distribution of clay minerals characterized by

high water vapor diffusion resistance, as well as high sorption capacity and medium capillary water uptake, which finally results in medium, permanent moisturization. Furthermore, the stress index is much higher than for quartz arenites like the sandstone Bad Bentheim, especially in the outer rim zone. Regarding the high amounts of hygric dilatation, the distinctive fluctuations in the rim zone will lead to deterioration of the fabric.

5.13.4 The Sandstone Sander

Due to the "unfavorable" water transport properties of the sandstone Sander, the water mass density is the highest on average. Here, the water uptake via sorption in the hygroscopic state allows water vapor diffusion (small vapor diffusion coefficient) and high capillary water uptake via the capillary transport. In contrast to the other sandstones already at point 2, low annual fluctuations are observable, and, coevally, the rising water from the bedrock decreases dramatically with increasing height (Fig. 5.11 c). This can be traced back to the low drying velocity and liquid conductivity: The saturated pores filled by high sorption values create only a small potential/gradient for further capillary transport. Hence, the water mass density decreases as it moves upwards. The rock, due to the sorption, is characterized by permanently high saturation, and the capillary water uptake is hindered with respect to the high capillary pressure. The annual fluctuation occurring down to the deepest part of the rock (point 2, Fig. 5.11c) can be attributed to the lack of uprising-water input in the bedrock. As a consequence, no consistent value of water mass density can attune, and the rock is characterized by permanently alternating moisture content. Similarly to the sandstone Karlshafen, a long dry period does not result in low water content. Again, only the rim zone is distinguished by evaporation. Simultaneously, the uprising component of the water content increases and, therefore, ensures a permanently high-moisture core (Fig. 5.15d). The intensity of amplitude is larger than in the sandstone Karlshafen since, in general, the water content is higher. In contrast to the other sandstones, during early spring and summer, the rim of the rock (point 15; Fig. 5.12 b) levels off at a low moisturization value (~20 kg/m^3), but shows strong alternation over time.

Herein, the results confirm that a bimodal (Fig. 5.5 e, f) pore volume/radii distribution, promotes water uptake in any way possible since nearly nine orders of magnitude are involved in the water transport. In particular, the micropore building clay minerals are, hence, important to the sorption capacity and, as a consequence, sensitive to changes in climatic conditions. In combination with its capillary pressure/water content, this leads to high moisturization over the entire time. The sandstone Sander continues in the same way as the sandstone Karlshafen, concerning its lithology resulting from water transport properties: bimodal pore-volume distribution as a consequence of a higher number of clay minerals by higher alteration of lithoclasts, as well as higher porosity. Regarding the weathering properties of the sandstone Sander´s permanent but strongly alternating

moisturization, this leaves potential for any kind of weathering mechanism. The rock is characterized by a high hygric dilatation, which occurs with respect to the strong alternation many times per year. The high CEC of the sandstone Sander represents a high potential for the absorption of H_2O molecules, in addition to cations on and within the small clay mineral pores. Furthermore, the bedding caused by micas/clay minerals that are oriented in parallel to the bedding will lead, again, to capillary condensation and to a characteristic delamination (Rodriguez-Navcarro et al. (1997), Sebastián et al. (2008)).

Coevally, the alternating curves of water mass density reveal that the stress index with respect to the ongoing weathering processes is very high. Associated with low-to-medium strength, this rock is predestinated for deterioration caused by low salt-resistance and high hygric dilatation. Therefore, the results of numerical modeling clearly reflect the real weathering properties of the rock and verify laboratory and field analyses of this sandstone.

5.13.5 Influence of Heterogeneities (Clay Layers)

Due to the presence of clay layers, the water mass density and water flow described above for each sandstone monolith changes. This can be attributed to the insertion of a new gradient for capillary and vapor transport, resulting from the new material properties of the clay layer. However, the presence of these heterogeneities in each sandstone monolith has completely different consequences since the properties of the clay and sandstone layer produce different gradients and promote the water transport through the rock to different degrees.

In contrast to the single sandstone monolith of Bad Bentheim, the content of water mass density within the sandstone layers are slightly decreased. Meanwhile, the clay layers contain 3 to 9 times as much water (annual fluctuations) than the sandstone parts. Since the clay layers are characterized by much higher capillary moisture saturation, liquid conductivity, water vapor diffusion and sorption capacity, they also absorb water in the liquid and vapor phase. Consequently, within the monolith, only they are subject to changes in relative air humidity (vapor diffusion/transport) and predominantly absorb water during driving rain events (capillary water transport/ Fig. 5.16a).

Within the sandstone parts, the processes change little in contrast to the single sandstone monolith: the sandstone Bad Bentheim is not able to insert or store water via sorption and, therefore, is not subject to changes in relative air humidity. Indeed, the highly-moist clay layers provide water in the liquid phase for the overlying sandstone sections. However, the absorbed water is quickly propelled outwards due to the drying velocity and liquid conductivity. Only during driving rain events do the capillary properties allow absorption of the liquid phase (Fig. 5.16a). However, the high drying velocity and liquid conductivity, again, lead to only a temporary increase in water mass density. Therefore, water mass density within the sandstone remains almost completely unchanged.

Coevally, the clay layers divide the sandstone into three sections. Due to their reduced volumes, they also have a larger reaction surface. This promotes even faster drying of the sandstone parts and results in a reduction of annual alternations. Further influences of clay layers are comprehensible during a driving rain event (23th May/3rd year; Fig. 5.16a): The thickness seems to be important to the water content since the 10 cm-thick layer absorbs much less water than the thinner layers. The smaller thickness most likely lead to a more rapid drying and, hence, the overall gradient is higher for the absorption of water that is suddenly available. After a longer drying period (Fig. 5.17 a), the thickest clay layer also exhibits an unchanged high water mass density, whereas the smaller ones are almost entirely dried out. In this context, an increase in stress and concentration at the boundaries which is caused by the differences in water content is likely (e.g. during ice/salt crystallization/hygric dilatation). Capillary condensation arises both within the clay layer and at the interface of the sandstone layer, which leads to stress within the fabric of the sandstone.

To summarize, the presence of clay layers in the monolith only causes a negligible decrease in water content in the sandstone parts, whereas the clay layers act as a water absorber. As a consequence, the stress induced by annual alternations (stress index) also decreases. However, considering the sandstone monolith as a whole, the stress index should be increased by the presence of clay layers.

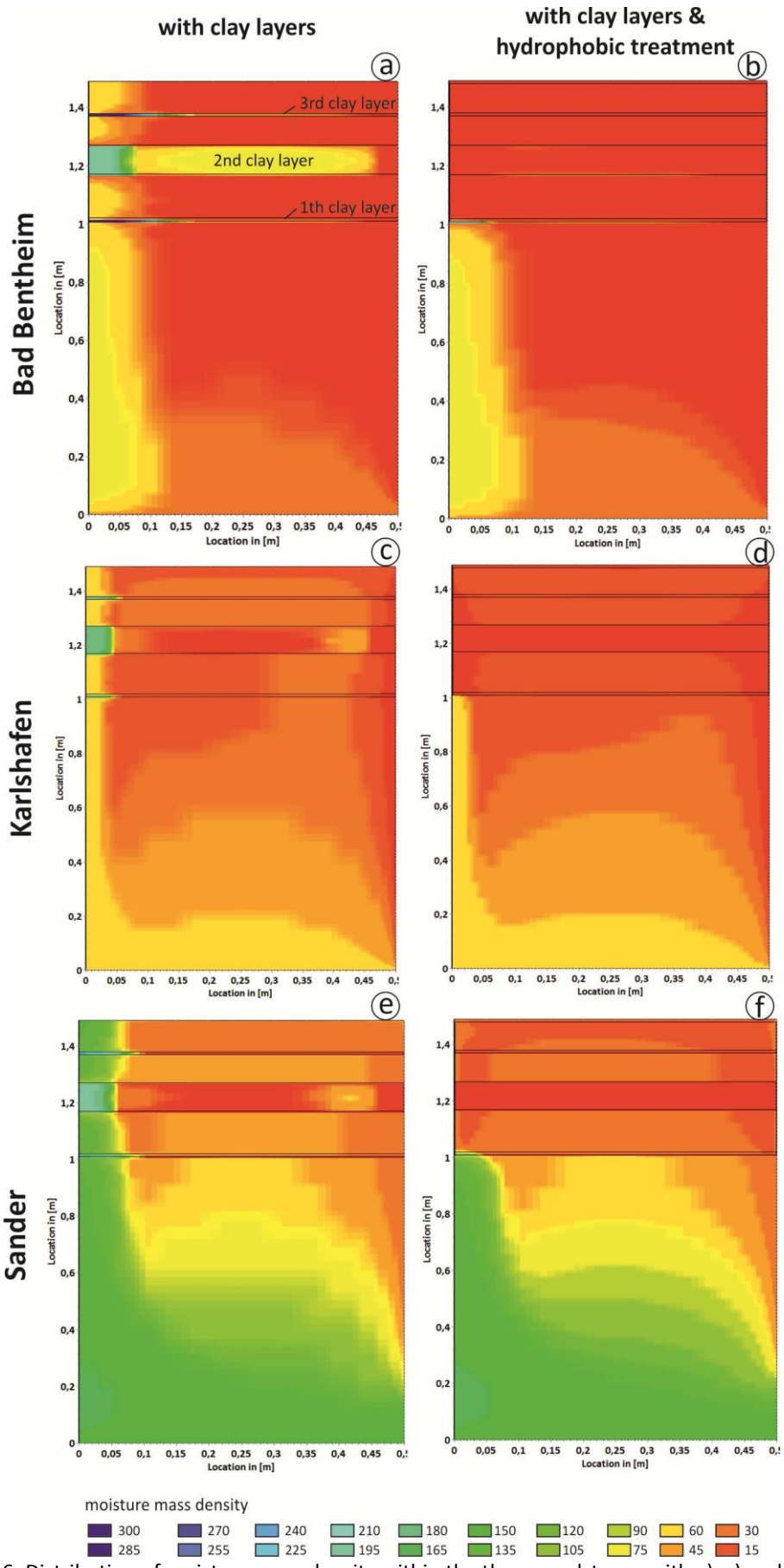

Fig. 5.16: Distribution of moisture mass density within the three sandstones with a), c) and e) clay layers and with b), d) and f) clay layers and hydrophobic treatment. The illustrations represent the moisture content during a driving rain event (23th May / 3rd year).

At the sandstone Karlshafen, the presence of clay layers expresses something different: On one hand, a more distinct decrease in water mass density within the sandstone layer in contrast to the single sandstone monolith is observable, and, on the other hand, the clay layers contain much less water than the sandstone parts. The decrease in water mass density can be traced back to the function of clay layers as a barrier to uprising water and water coming from above. The higher water mass density of the sandstone parts can be attributed to the conspicuous differences in material properties, creating a stronger gradient for water transport and storage. For example, the vapor diffusion resistance of the sandstone Karlshafen is twelve 12 larger than that of the clay layer. Indeed, the sandstone Karlshafen absorbs gaseous water from underlying clay layers and from outside via sorption, but only slowly pushes out the absorbed water. Accordingly, the average water mass density is higher than that of the clay layer. This also results in a slow reaction to outer conditions. Converse behavior is observable when liquid water is available since the lower absorption of capillary water in contrast to the clay layer leads to decreased absorption within the sandstone parts. This is especially reflected during driving rain events: The sandstone only absorbs one-third of the clay layer, but the exchange with the clay layers also results in a higher water mass density at the boundaries.

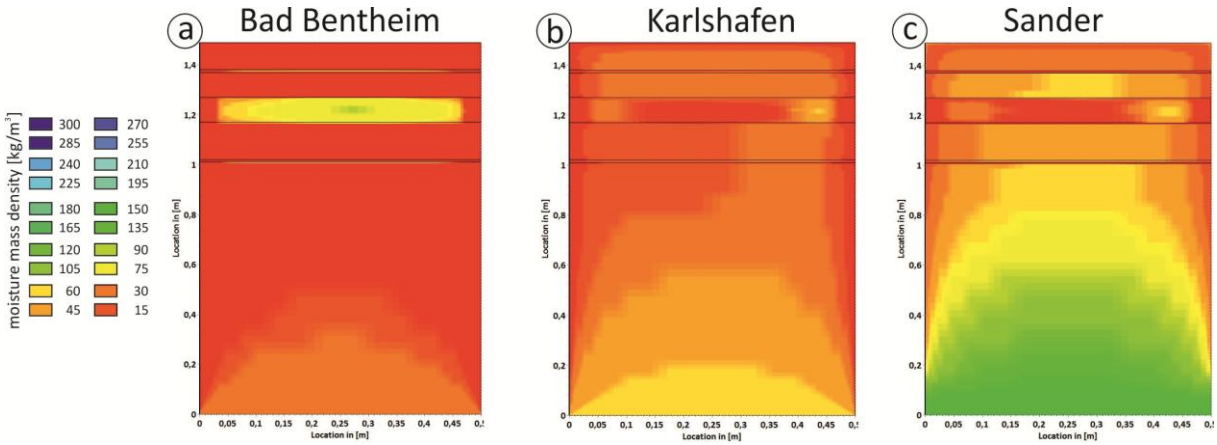

Fig. 5.17: Distribution of water mass density after a long drying period at sandstone monoliths with clay layers.

Similarly to the sandstone Bad Bentheim, the clay layers divide the sandstone monolith into three smaller volumes, promoting a faster drying rate in these three sandstone bodies. Subsequently, the annual fluctuations within the surface are reduced. Coevally, the different drying velocities of sandstone and clay layers should lead to a stress with respect to different amounts of hygric dilatation. The moisture distribution during the drying period (Fig. 5.17 c) shows a round shape at the edges of the monolith. This probably leads to long-term loading, to a rounding of the edges. Furthermore, driving rain events are only visible within the second, 10cm-thick clay layer (Fig. 5.16c). This is most likely connected with the high capillary moisture saturation of the clay layer.

In summary, the presence of clay layers result in a distinct decrease in water mass density, as well as of annual fluctuations. This is especially comprehensible in the uppermost sandstone layer, wherein the annual fluctuations are almost no longer present. However, the short-term peak values at the boundary surfaces in between the sandstone and clay layers (e.g. driving rain event) represent a new source and displacement of stress in the fabric. With respect to the high values of hygric dilatation of the sandstone Karlshafen, these peak values should also lead to the reaching of maximum values of dilatation. Therefore, the stress index, in general, should increase in comparison to the single sandstone monolith.

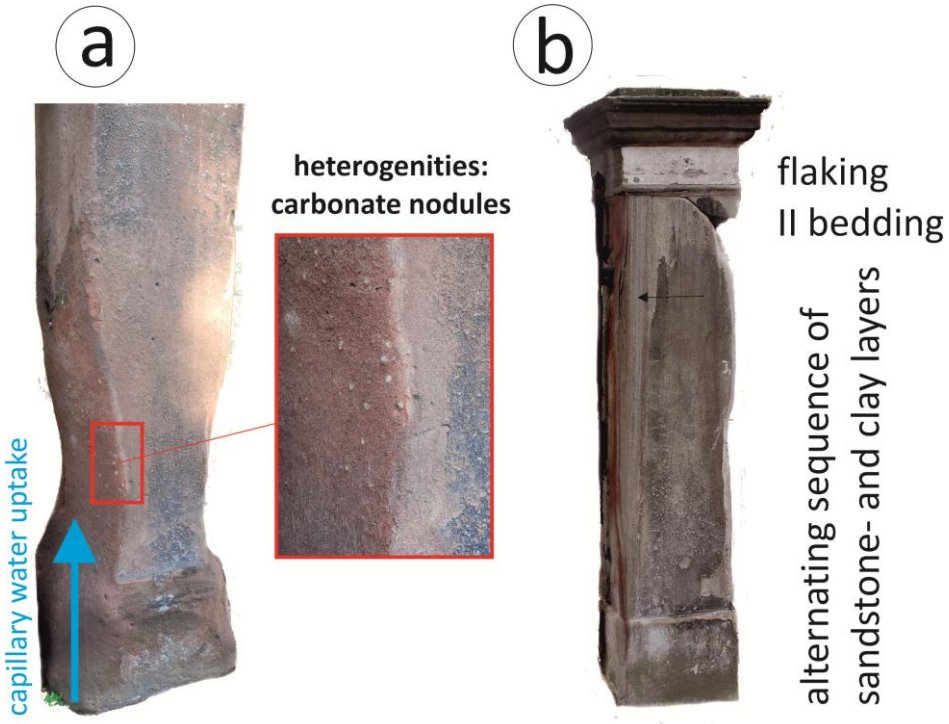

Fig. 5.18: a) Sandstone pillar with strongly deteriorated area close to the bottom, b) sandstone pillar with vertical bedding. The alternating sequence of sandstone and clay layers lead to flaking and fabric-caused weathering.

In addition, within the Sander monolith, the sandstone parts exhibit, on average, a higher water mass density than the clay layers. However, here, the differences are much more pronounced since sorption and capillary water uptake are considerably higher than in the sandstone Karlshafen. Furthermore, the distinct low water vapor diffusion resistance easily allows the migration of vapor throughout the entire monolith. Nevertheless, the different drying velocity promotes the faster drying of the clay layers.

Here likewise, the clay layers divide the monolith into different sections and function as a barrier since they absorb all uprising water and advance it quickly. Therefore, annual fluctuations within the overlaying sandstone layer is weakened and the water quantity stays consistent since the two overlaying clay layer also act as protecting and absorbing areas for water coming from above. During a driving rain event (Fig. 5.16 e), the difference between the clay layer and sandstone layer suddenly

all but disappears as a result of the capillary water uptake being mutually similar. At the same time, the penetration depth within the thin clay layers, in contrast to sandstone Karlshafen, increases. It can be anticipated that these differences, in the long run, induce the stress of ice/salt crystallization and most likely lead to the flaking of clay/sandstone layers (e.g. Fig. 5.18 b).

To recap, at the sandstone Sander, the annual fluctuations also decrease, but the internal stress is increased by the differences in moisture distribution.

5.13.6 Influence of Hydrophobic Treatment

When the sandstones become treated with water repellence, the interaction with the environment, naturally, has to change as well. Water repellence essentially reduces capillary water uptake from the outside within the outer rim of the sandstone. However, the uprising water from the bedrock is not hindered – rather, the exchange with the environment via capillary transport is likely prevented.

Again, results show that the presence of the treated material can be considered a separate material that changes the potential of the transport mechanism. A negative impact has often been discussed since, for example, scaling is associated with this treatment (e.g. Snethlage 1984, Nimmrichter & Linke 2008). Our results confirm that, directly behind the hydrophobically treated part, accumulations of moisture are observable, while the hydrophobic part is almost completely dry (e.g. Fig. 5.19 a, b). This accumulation can grant the potential of inducing stress development at ~1 cm depth in the rock. However, since the transport of water within a rock is not ruled by capillary processes alone, the effect strongly depends on the remaining content of water. Therefore, the impact of hydrophobic treatment is different for each sandstone.

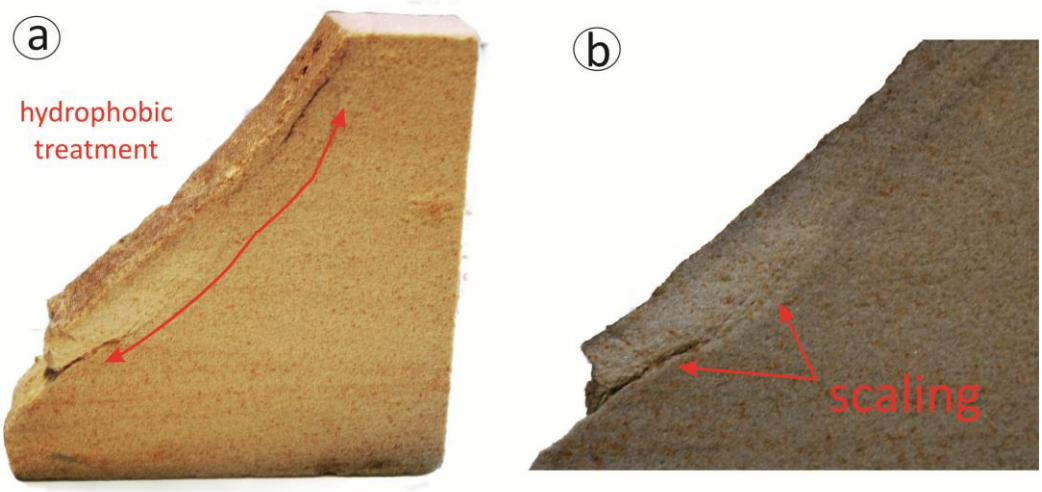

Fig. 5.19: Wetted sample with rim of hydrophobic treatment: The lighter parts represent the dry area with hydrophobic treatment; the dark ones are untreated and wetted. At the boundary between these parts, parallel surface cracks are observable, which will lead to a short-term loss of this rock part.

Since the sandstone Bad Bentheim assimilates water only through capillary transport and uptake, here, the conspicuously reductive effect on water mass density is apparent. Therefore, the amount of water continuously increases from the top down. In addition, the annual fluctuations are no longer that intensive and coevally stagger over time (Fig. 5.15a). This, finally, results in a moisture content that only is dependent on the amount of rising water from the bedrock. Consequently, the complete fluctuations and, accordingly, the stress induced are decreased by the presence of the hydrophobic treatment. The water content of the clay layers is also indistinguishable from the sandstone parts. Only during a driving rain event do small peak values arise within the clay layers. This can be attributed to the large pore spectrum and to the fact that the clay is also able to insert water via sorption. As a result, the clay layers still exhibit a higher water mass density than the sandstone layer. In conclusion, when the moisture transport in a sandstone mainly takes place via capillary transport and the amount of uprising from bedrock is barely present, a hydrophobic treatment can be useful. Additionally, in the sandstone Karlshafen, the treatment results in a decrease in water mass density in both the sandstone and the clay layer. This can be explained by the decreased entrance of capillary absorbed water in the outer rim of the sandstone. Simultaneously, the large differences between the water mass density of the second and third years plead for a protraction of equilibrium within the sandstone (Fig. 5.14 b). This can be attributed the fact that the high sorption capacity allows high absorption, depending on relative air humidity, but the high vapor resistance does not easily allow for an attuning of equilibrium. Remaining sources of water absorption are still the uprising component from the bedrock and the exchange with the environment at lower relative air humidity. Indeed, accumulations behind the rim of hydrophobic treatment are not observable, the differences between clay layer and sandstone layer saturation are negligible and the uprising component is also distinctly decreased. However, the higher alternating curves within the clay and partially sandstone layers, in general, should induce higher stresses within the entire monolith. Therefore, a treatment with water repellence is, in case of the sandstone Karlshafen, not advisable.

Through the treatment of the sandstone Sander, especially within the clay layer, the water mass density decreases while, in the sandstone layers, only the uppermost shows a decrease in water mass density. This can be traced back to the circumstances of the focus of water uptake in the sandstone Sander presenting the sorption; it is not that influenced by the lack of the capillary uptake of water. Contrary to the sandstone Karlshafen, the fluctuations here decrease considerably, which finally causes a reduction in stress index. Furthermore, for example, after a driving rain event (Fig. 5.16 f), accumulations of water behind the treatment are clearly apparent. The concentration of water within the ~1cm depth will lead to stress during freeze-thaw weathering or salt weathering, located at the boundary between the hydrophobic treatment and the untreated rock section.

Accordingly, a hydrophobic treatment, in the case of the sandstone, Sander also is not recommended.

The change of annual course at all samples can be explained by the fact, that during a rainy winter where predominantly liquid water is available the treatment reduces all water absorption from outside, while in the summer the water absorption mainly takes place via vapour stage by high humidity. Therefore a vice versa behavior concerning the amount of water absorption is observable.

5.14 Conclusions

The material functions applied here for the modeling of the moisture distribution within sandstones under different climatic conditions provide a unique way of asserting a very detailed evaluation and information about moisture accumulations which are critical to weathering behavior. The model outputs, based on detailed detection of material parameters and the material function used, reflect very well the specific material behavior of each sandstone observed in natural environment and by laboratory data. In summary, the following conclusions can be drawn:

- In general, within the monoliths, a capillary uprising from the bedrock is observable, which, with increasing height, is overlain by the horizontal and vertical exchange with the environment. Annual fluctuations increase with reaching the rock surface. Zones of strong alternating moisture content are the rim area and especially the edge towards the bottom since that is where upcoming water from the bedrock as well as driving rain events rule the content. For all sandstones the water content is highest in winter times.
- The results confirm that the lithology and its associated pore space of sandstones regulate moisture content and its accumulation. The quartz arenite (Bad Bentheim) characterized by very high porosity and mainly capillary pores, exhibits the lowest water content within the pore space, which is contrary to the generally positive correlation between porosity and water uptake. However, this aligns with its well-constructed suitability. According to its low sorption capacity, moisture storage and also water uptake via capillary transport is highly unlikely. The large capillary pores only become active when liquid water, as in case of driving rain events, is available. However, the high drying velocity leads to a quick forwarding out of the pore space and results in permanently low water content of the sandstone Bad Bentheim. Accordingly, sandstones which are not able to store the absorbed moisture, such as Bad Bentheim, should be resistant against salt- and/or ice crystallization .
- In contrast, the clay-bearing sublitharenite Karlshafen is characterized by medium water uptake and high sorption capacity, but high water vapor resistance. Accordingly, this sandstone shows high protraction concerning external changes within e.g. relative air

humidity. During a drying period, the uprising capillary water from the bedrock results in a concave-shaped moisture front. Probably this can explain the often observed deterioration phenomena of rounding within a lower monolith part. The rim zone is characterized by strong fluctuations and will be the location of salt- and/ or ice crystallization and hygric dilatation. Moreover, in combination with high vapour diffusion resistance and low drying velocity, moisture is almost present for hygric swelling. However, the high compressive strength will prevent rapid weathering in the context of salt or ice crystallization.

- The sandstone Sander is characterized by permanent high water content since, due to its lithology, it is characterized by the participation of pore sizes over nine orders of magnitude. The feldspatic litharenite with clayey matrix is generally characterized by the highest water mass density, as well as by very high annual fluctuations, which leads to, for example, a constant expansion and following contraction caused by hygric dilatation. Here also during a dry period a concave shape of moisture front is observable and will lead to rounding regarding ice- or salt crystallization. Paired with low strength properties, the rock is also not able to withstand the stress induced by ice or salt crystallization as long as the sandstone Karlshafen.

- The pore volume distribution and the content and the kind of clay minerals, their arrangement and their pore-building framework can be connected with transport and storage properties. Accordingly, the quartzarenite Bad Bentheim, with only a little pore-filling kaolinite, is predetermined for little sorption capacity, whereas the sublitharenite Karlshafen and feldspathic litharenite Sander are characterized by high sorption capacity due to their high content of clay minerals. The very high vapor diffusion resistance of the sandstone Karlshafen can be attributed to the high amount of smectite, which absorbs water molecules with high binding energy.

- In each sandstone type, clay layers have a specific impact. However, in all samples, the clay layers react as a barrier, presenting obstructions to water migration and dividing the monolith into three sections. At the interface, capillary condensation arises, which then leads to an increase in stress throughout the entire monolith. For all sandstones, the annual fluctuations of the uppermost sandstone layer decrease, but, coevally, small peaks at the interfaces occur where previously no such peaks were present. The clay layers lead, therefore, to a stress displacement from the top rim zone to the interfaces. Meanwhile, the annual fluctuations within the sandstone parts decrease since the clay layers protect the underlying parts.

- The hydrophobic treatment strongly decreases the water mass density, which is absorbed via capillary routes. The importance for the entire water balance of the monolith depends on the remaining transport mechanisms and their associated pore-volume distribution. When the main water absorption takes place via capillary paths, the treatment can be useful since no water can accumulate within the rock. This is the case of the sandstone Bad Bentheim, showing a unimodal pore-radii distribution. In contrast, when the sandstone absorbs water via sorption (hygroscopic) alongside capillary transport (super-hygroscopic), a negative impact from the treatment is observable. Moreover, directly behind the rim of treatment, an accumulation of water is observable, which finally induces stress during freeze-thaw and salt attack cycles. Consequently, cracks arise between the boundaries of the treated and untreated areas, which can lead to scaling of the outer rock surface. This occurs in samples with bimodal pore-volume distribution.
- Further effect of the treatment is the reversion of annual water absorption: Since during winter times more liquid water is available, here also the effect of treatment in particular is observable. In consequence, during summer times the water content is increased compared to that of untreated monoliths.

Acknowledgement

We would like to thank the Deutsche Bundesstiftung Umwelt for supporting the long-term PhD fellowship of H. Stück (AZ 20008/997). Further gratitude goes to Dr. Akós Török for his thorough and helpful review.

References

Anderson R.F, Ratcliffe I, Greenwell H-C, Williams P-A, Cliffe S, Coveney PV (2010) Clay swelling – a challenge in the oilfield. Earth Science Reviews 90: 201-216.

Brakel J, Modry S, Svata M (1981) Mercury Porosimetry: State of the art. Powder Tech 29: 1-12.

Burdine NT (1953) Relative permeability calculations from pore-size distribution data. Trans AIME 198:71–78

Fitzner B (1988) Untersuchung der Zusammenhänge zwischen dem Hohlraumgefüge von Natursteinen und physikalischen Verwitterungsvorgängen. Mitt. Ing.-u.Hydrogeologie, 29, Aachen.

Fitzner B, Snethlage R (1982) Einfluß der Porenradienverteilung auf das Verwitterungsverhalten ausgewählter Sandsteine. Bautenschutz und Bausanierung, Nr. 3-1982: 97-103.

Grunewald J (1997) Diffusiver und konvektiver Stoff- und Energietransport in kapillarporösen Baustoffen, Dissertation, TU Dresden, Fakultät für Architektur, Institut für Bauklimatik.

Kießl K, Gertis K (1980) Feuchtetransport in porösen Baustoffen. Eine Literaturauswertung zur rechnerischen Erfassung hygrischer Transportphänomene. Forschungsberichte aus dem Fachbereich Bauwesen 13, Universität Essen Gesamthochschule.

Kießl K (1983) Kapillarer und Dampfförmiger Feuchtetransport in mehrschichtigen Bauteilen. Diss. Univ. Essen.

Klopfer H (1985) Feuchte. In: Lutz, P., Jenisch, R., Klopfer, H. et al. (eds) Lehrbuch der Bauphysik.

Krischer O (1963) Die wissenschaftlichen Grundlagen der Trocknungstechnik. Springer-Verlag, Berlin-Göttingen-Heidelberg.

Krus M (1995) Feuchtetransport- und Feuchtespeicherkoeffizienten poröser mineralische Baustoffe. Theoretische Grundlagen und neue Messtechniken. Diss. Univ. Stuttgart.

Künzel H (1994) Verfahren zur ein- und zwei dimensionalen Berechnung des gekoppelten Wärme- und Feuchtetransports in porösen Bauteilen mit einfachen Kennwerten. Diss. Univ. Stuttgart.

Künzel H.M., Krus M (1995) Beurteilung des Feuchteverhaltens von Natursteinfassaden durch die Kombination von rechnerischen und experimentellen Untersuchungsmethoden. Intern Z Bauindstansetzen1: 5-20.

Mirwald P (1997) Physikalische Eigenschaftender Gesteine. In: Berufsbildungswerk des Steinmetz- und Bildhauerhandwerks e.V. (ed) Ebner Verlag, Ulm.

Mosch S, Siegesmund S (2007) Statistische Bewertung gesteinstechnischer Kenndaten von Natursteinen. Z dtsch Ges Geowiss 158/4: 821-868.

Nicolai A, Grunewald J, Plagge R, Scheffler G (2008) Development of a Combined Heat, Moisture, and Salt Transport Model for Unsaturated Porous Building Materials, in Simulation of Time-Dependent Degradation of Porous Materials, Research Report on Priority Program DFG SPP 1122, eds. L. Franke, G Deckelmann & R. Espinosa-Marzal, Cuilliver Verlag, ISBN 978-3 86727-902-4, S. 67-84.

Nimmrichter J, Linke R (2008) Evaluation of hydrobization on Compact Limestone and Calcareous Tuff with Negative Result – Case Studies of the Facades of the Cathedral of Salzburg and Gothic Churches in Upper Austria. 11th International Congress on Deterioration and Conservation of Stone. 15-20 September 2008, II, 1019-1025, Torun, Poland.

Price CA (1993) Preventive conservation of salt-contaminated masonry in Wakefield Tower, HM Tower of London. Inst Archaeol Bull 30: 121 – 133.

Putnis A, Mauthe G. (2000) The Effect of Pore Size on Cementation in Porous Rocks. Geofluids, 1: 37-41.

Putnis A, Prieto M & Fernandez-Diaz L (1995) Supersaturation and Crystallization in Porous Media. Geol. Mag. 132: 1-13.

Rodriguez-Navarro C, Hansen E, Sebastián E, Ginell W (1997) The Role of Clays in the Decay of Ancient Egyptian Limestone Sculptures. J Am Inst. Cons 36: 151-163.

Ruedrich J, Kirchner D, Seidel M, Siegesmund S (2005) Deterioration of natural building stones induced by salt and ice crystallisation in the pore space as well as hygric expansion processes. In: Siegesmund S, Auras M, Ruedrich J, Snethlage R (eds) Geowissenschaften und Denkmalpfleg. Zeitschrift Deutsche Geologische Gesellschaft 156(1):59-73

Ruedrich J, Siegesmund S. (2006) Fabric Dependence of Length Change Behavior Induced by Ice Crystallization in the Pore Space of Natural Building Stones. In: Fort R, Alvarez de Buergo, M. Gomez-Heras, M. et al. (eds.) Heritage, Weathering and Conservation. Taylor & Francis Group, London.

Ruedrich J, Bartelsen T, Dohrmann R, Siegesmund S (2010) Building sandstone integrity affected by the process of hygric expansion. Environ Earth Sci. doi: 10.1007/s12665-010-0767-0

Ruedrich J, Bartelsen T, Dohrmann R, Siegesmund S (2011) Moisture expansion as a deterioration factor for sandstone used in buildings. In: Monument under threat-environmental Earth sciences, vol. 63, Springer, Berlin, pp 7–8

Scheffler A (2008) Validation of Hygrothermal Material Modeling under Consideration of the Hysteresis of Moisture Storage.

Scheffler G, Plagge R (2009) A whole range hygric material model: modeling liquid and vapour transport properties in porous media. Int. J Heat Mass Transf. doi: 10.1016/j.ijheatmasstransfer.2009.09.030.

Sebastián E, Cultrone G, Benavente D, Linares Fernández L, Elert K, Rodriguez-Navarro C (2008) Swelling Damage in Clay-Rich Sandstones Used in the Church of San Mateo Tarifa (Spain). J Cult Heritage 9: 66-76.

Snethlage R (1984) Steinkonservierung 1979-1983. Arbeitsheft 22. Bayrisches Landesamt für Denkmalpflege, Munich.

Stockhausen N (1981) Die Dilatation hochporöser Festkörper bei Wasseraufnahme und Eisbildung, Diss TU Munich.

Stück H, Koch R & Siegesmund S (2012) Petrographical and Petrophysical Properties of Sandstones: Statistical Analysis as an Approach to Predict Material Behavior and Construction Suitability. Environmental Earth Sciences DOI 10.1007/s12665-012-2008-1

Warke PA, Smith PJ, Lehane E (2011) Micro-environmental change as a trigger for granite decay in offshore Irish lighthouses: implications for the long-therm preservation of operational historic buildings. Environ Earth Sci 63: 1415-1423. Doi 10.1007/s12665-010-0662-8.

Weiss G (1992) Die Eis- und Salzkristallisation im Porenraum von Sandsteinen und ihre Auswirkungen auf das Gefüge unter besonderer Berücksichtigung gesteinsspezifischer Parameter. Münchner Geowiss Abh B 9, Verlag Dr. Friedrich Pfeil, Munich.

6 Summarizing Discussion

The results of this work, i.e. from the onsite-studies of dimension stones (Chapter 3), the statistical analyses of petrography, petrophysical and weathering properties (Chapter 4) as well as from the modeling of moisture distribution (Chapter 5) reveal that the evaluation of the durability and construction suitability of sandstones is only possible under consideration of detailed composition and fabric analyses since they have significant influence on the material properties.

Moreover, the here presented study can show that the consideration of sedimentary and diagenetic parameters may give important hints for the basic parameter commonly measured to describe the quality of a natural stone (e.g. porosity, strength).

In the following, the main relationships, found by the studies presented in the afore mentioned chapters will be summarized and integrative discussed. Where appropriate, a link to the respective chapters is given, were those relationships are discussed in greater detail.

6.1 On-Site Study of Natural Stones

The connections between lithology, diagenesis and depositional milieu are well-reflected within the local study of six sandstones used as dimension-stones in the Drei Gleichen area (Chapter 3). Results reveal that sandstones exhibit significant differences in material- and weathering behavior under the same surrounding environmental conditions (e.g. exposition, rainfall, temperature), when differing in lithology and depositional milieu. This is expressed by different intensities of macroscopical weathering phenomena such as crusts, efflorescences, scaling, flaking or alveolars (Chapter 3.5.1., Fig. 3.7; Fig.6.1).

For example, on-site, the sandstone *Hindfelden* (Upper Triassic, Schilfsandstein; Chapter 3.5.1) shows distinctive relief controlled by bedding as the main deterioration shape and could be defined as the most susceptible to weathering (Fig.6.1 a). In contrast, the sandstone Wachsenberg (Upper Triassic, Semionotus-fm., Chapter 3) is characterized by minor scaling and can be (with respect to the other five sandstones) defined as the most suitable for construction. This also aligns with the results of numerical modeling, wherein moisture distribution in the same climate condition strongly varies with lithotype (Chapter 5, Chapter 6.1.3 and Chapter 6.2).

However, sandstones belonging to the same stratigraphic age and composition can also exhibit major differences in their material- and weathering behavior. For example, of the three analyzed Rhät sandstones *Röhnberg*, *Gleichenberg* and *Seebergen,* which were deposited close to each other, only the latter one could be considered an appropriate dimension or replacement stone since only this rock shows little disintegration. Contrary, the sandstone Röhnberg is characterized by well

pronounced sanding as predominant deterioration shape, whereas the sandstone Gleichenberg often shows alveolar weathering (Fig.6.1 b). Those differences in compositional and stratigraphic identical sandstones can be attributed to differential diagenetic pathways (see below and Chapter 4).

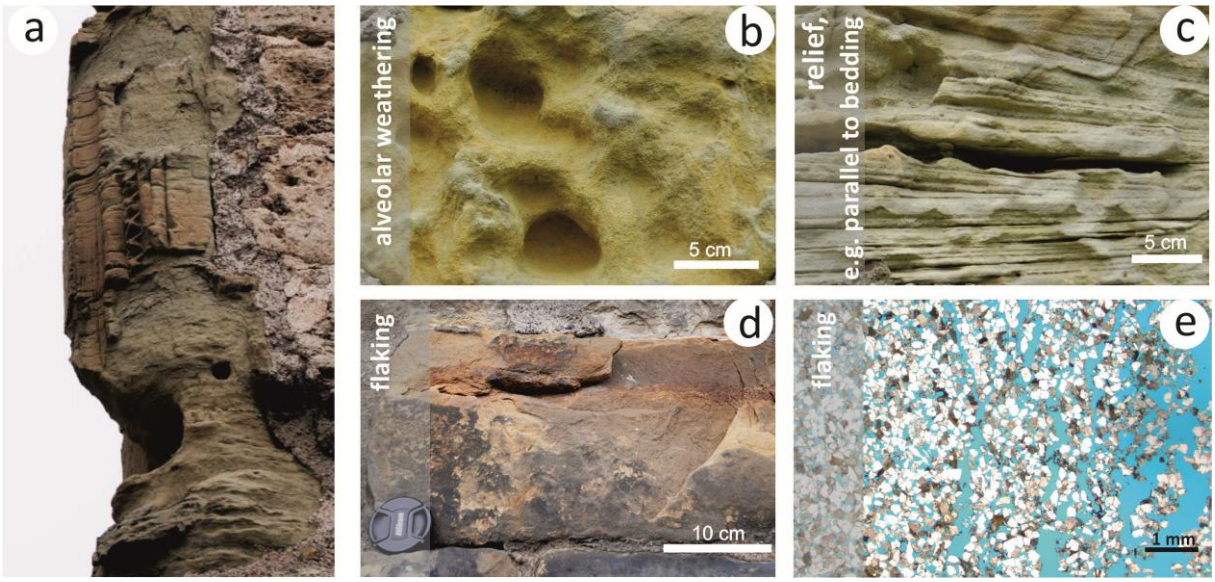

Fig. 6.1: Deterioation phenomena, observed at dimension sandstones at Castle Drei Gleichen. a) weathering resistance of iron-rich parts within sandstone Hindfelden, b) alveolar weathering, d) relief, material loss along clay layers/parallel bedding, d) flaking and e) flaking illustrated in thin section (II-pol.): the left part presents the still consolidated sandstone surface, towards the right side, the cohesion of grains decrease.

Next to the lithology, the appearance of decay phenomena depends on the position of the stone within the wall. Most of the decay phenomena are found close to the bottom of the wall (~1 m above the ground), which is e.g. expressed by scaling, crusts, efflorescences and reliefs. The cumulative crusts and efflorescences observable here are probably due to the permanent moisture penetration via capillary percolation of water from the bottom.

As proven by the detailed petrographical and petrophysical analyses of these sandstones (Chapter 3.10, 3.11), the different construction suitability and respectively weathering behavior is not only the result of their depositional environment, but, in particular, their diagenetic histories, which lead to strong variations in the fabric and their petrophysical properties.

6.2 Interrelationship between Material Properties and Weathering Behavior

These general observations discussed in chapter 6.1, which are based on the small selection of sandstones at the Gleichen Castle (Chapter 3) can be confirmed and extended with the statistical analyses of an extensive data set, which is based on sandstones of varying composition, sedimentary origin and diagenetic development (Chapter 4). Additionally, the larger data set allowed identification of a further relationship between a single parameter (e.g. porosity, pore radii distribution, strength, water transport and storage properties) and is also essential for evaluation and prediction of the construction suitability of heterogeneous rock such as sandstone. In the following, the meaning and relationships of the key parameters of porosity, pore radii distribution and strength,

water transport-and storage mechanism (Chapter 5) and weathering properties are represented individually, for a subsequent final derivation of the construction suitability of different lithotypes. For this purpose, in the following, an integrative discussion of the results and finding of the chapters 3, 4, and 5 is accomplished.

6.2.1 Porosity and Strength as Results of Lithology and Diagenesis

Porosity has been proven by this study to be one of the key parameters for construction suitability since it has a direct and indirect effect on most of the petrophysical properties of the rocks. Additionally high porosity has a disadvantageous impact on weathering behavior (e.g. Hirschwald 1912, Fitzner 1970, Poschlod 1990, Ruedrich et. al 2005, Ruedrich et al. 2010).

The statistical analyses of petrographical and petrophysical properties (Chapter 4) confirm a strong interconnection of porosity and strength with the lithology and diagenetic path (Chapter 4, Fig.4.22). Porosity development is controlled by transport mechanisms and the physicochemical eogenetic conditions in the depositional milieu of detrital grains (e.g. water chemistry, intrastratal solution). These are the basic parameters for the following diagenetic pathways during eogenetic alterations and finally trigger material properties such as porosity and strength, markedly.

Initial porosity is fixed with the deposition of the unconsolidated sediment and depends on the sorting which, in turn, is the result of the primary composition of detrital grains. A very well sorting was determined for marine deposits (coastal rim) of the Upper Cretaceous and marine to lacustrine-terrestrial of the Upper Triassic (Rhät), whereas the fluviatile deposits, e.g. of the Lower Triassic (Buntsandstein) and the brackish-marine delta deposits of the Upper Triassic (e.g. Lettenkohlenkeuper) are characterized by a well-to-moderate sorting (Chapter 4, Table 4.1). Dependent on diagenetic processes of, for example, compaction, cementation and/or alteration, this primary porosity becomes modified.

According to the differentiation in the mechanically and chemically stable/unstable components of grains during compaction under burial conditions (McBride 1963, Chapter 4; Fig. 4.20), the content of ductile grains plays an important role in the development of the pore space. In comparison to feldspathic and lithic sandstones, quartz arenites require deeper burial conditions for compaction (decrease in porosity) to the same degree (Chapter 4; Fig. 4.21, Dickinson 1985).

These relationships are reflected by the results of univariate statistical analyses, (whisker-plots, Chapter 4.11.; Fig. 4.8, Fig. 4.9) wherein, in respect to stratigraphy, different characteristic porosities and strength values are observable. Thereby, a general decrease in porosity, depending on burial time and depth, can be observed. These findings confirm the study of Koch and Sobott (2008) and the modeling of Scherer (1987) and Waples (2002). The same trend is also observable for the

strength of sandstones. However, sandstones belonging to the same stratigraphic age can also exhibit major differences in strength and porosity. For example, as proven by the on-site study of Drei Gleichen (Chapter 3, Table 3.4), of the three Rhät sandstones *Röhnberg*, *Gleichenberg* and *Seebergen,* deposited close to each other, the latter is characterized by very high strength and low porosity, whereas the other two behave inversely. This is attributed to the fact that they have the same composition but different diagenetic development, resulting in differing porosities and strengths. Statistical multivariate analyses show that weakly compacted and cemented quartz arenites, for example the sandstone Röhnberg and strongly altered sublitharenites-litharenites (e.g. the sandstones Hindfelden and Ingersleben; Tables 3.4 and 4.3), show the highest porosity and coevally the lowest compressive strength. In contrast, quartz arenites and sublitharenites which are strongly compacted and cemented are characterized by lower porosity and high strength (to this group also belongs sandstone Wachsenburg, Chapter 3, Table 3.4).

These dependencies are also reflected within the results of bivariate statistical analyses of porosity and compressive strength (Chapter 4.11, Fig. 4.13). The results show next to a linear relationship, a connection to the type of pore-radii distribution, the type of grain contacts, the primary intergranular volume (minus cement porosity), as well as to the degree of alteration, the amount of cementation and content of unstable lithic fragments.

Sandstones with predominantly concave–convex and sutured grain contacts exhibit a higher compressive strength than sandstones with pointed and elongated grain contacts. Compressive strength also varies within the respective group of grain contacts, e.g. due to the different kinds and intensity of cementation. Cementation itself is influenced by the kind and amount of unstable lithic fragments in the rock. If volcanic detritus is present, hydration reactions are favored, and the formation of authigenic feldspar is common. In contrast, abundant chert fragments can inhibit quartz cementation and, thus, preserve porosity (see also Surdam et al. 1989). With respect to the connection of unstable lithic fragments the following relationship is assumed: the higher the content of unstable lithic fragments, the lower the probability of grain contact is between stable grains.

Strongly linked with the development of porosity the pore radii distribution has also been proven (Chapters 3.7.1 & 4.11). Within the small data set presented in chapter 3, four types of pore radii distribution were differentiated (Chapter 3.7.1) based on the “shape” of pore radii classes. Within the larger data set presented in Chapter 4, the differentiations were reduced to three pore radii distribution types (bimodal, unimodal unequal, unimodal equable), because the large dataset suggest classifying the type I and IV (see Chapter 3.7.1, Fig. 3.16) as subtypes of the unimodal equable type and not as own types (see Chapter 4.11, Fig. 4.10).

The statistical analyses also show that the origin of each pore radii type can be linked with diagenetic and lithological parameters of the rock sample. For example, litharenites of Upper Triassic age (Lower and Middle Keuper, HS, SA, SL; Chapter 4, Tables 4.1, 4.3) show a bimodal pore-radii distribution with a maximum in microsized and capillary pores (Chapter 4.11 Fig. 4.10 I). The bimodal distribution can be attributed to their very low maturity. More specifically, the maximum in microsized pores can be attributed to the alteration of less stable components and/or the presence of a pseudomatrix, whereas the maximum of capillary pores reflect relics of primary intergranular porosity, which has been closed to different degrees due to cementation and compaction.

Unimodal unequal (Chapter 4.11; Fig. 4.10 II) distributions of pore radii can be predominantly observed in sublitharenites, but they can also occur in quartz arenites. In sublitharenites, this pore-radii distribution type can be attributed to moderate-to well sorting, weak alteration of unstable grains and a moderate degree of cementation and compaction as documented by the Weser sandstones of the Lower Triassic age (Buntsandstein, KA, AH, UD; Chapter 4, Tables 4.1, 4.3). Quartz arenites, with this type of pore radii distribution are generally well-sorted and exhibit a more immature character due to the infiltration of clay minerals (Cretaceous and Upper Triassic sandstones, e.g. RÖ; Upper Keuper, SE).

Unimodal equable distributions of pore radii (Chapter 4.11; Fig. 4.10 III) are mainly found in well-sorted, highly mature quartz arenites, in which no infiltration of clay minerals has occurred as documented by the Cretaceous sandstones (VE, RÜ, HI, OBI, Chapter 4.11, Tables 4. 1, 4.3). In general, an increase in maturity is correlated with the pore-radii distribution from bimodal to unimodal-unequal to unimodal-equal.

6.2.2 Water Transport and Storage Properties with Respect to Pore Space Properties

As seen within the statistical analyses and the results of the numerical modeling of sandstones (Chapters 4 & 5), the water transport and storage properties of sandstones are closely related to its porosity and the pore-radii distribution (Chapter 4.11, 5.14). First of all, we could confirm that the coefficient of capillary water absorption, water vapor diffusion (μ-value), water absorption under normal conditions and under a vacuum, as well as the resulting degree of saturation are characterized by a positive linear relationship to porosity. Moreover, we could show that the pore-radii distribution defines the kind of dominant water transport. The results of our statistical analyses therefore support previous findings of Fitzner (1970), Ruedrich and Siegesmund 2006, Heinrichs and Fitzner (2007), Mosch & Siegesmund (2007) and Siegesmund and Dürrast (2011). Sandstones with unimodal equable pore-radii distribution show, in general, a higher coefficient of capillary water absorption than those with bimodal distribution. The lowest absorption coefficient has been proven for sandstones with unimodal unequal pore-radii distribution. Moreover, the bivariate analyses

reveal a distinct relationship between the coefficient of water uptake and the type of lithology, which, in turn, proves that generally each lithology has a characteristic pore-radii distribution (Chapter 4.11). Additionally, the principle component analyses (Chapter 4.13) shows that the sorption behaviour of a sandstone depends on its amount of micropores. This supports previous postulates by Peschel (1983), Klopfer (1985) and Siegesmund and Dürrast (2011).

These observations can also be confirmed and extended by the analyses of the numerical modeling of the distribution, transport and storage of moisture within the pore space (Chapter 5). In this modeling approach, one model was developed for each of the three different pore radii distribution types, whereby each parameter participating in the behavior of moisture transport and storage is considered in analyzing the moisture content and migration under different climates.

As the model considers a simplified sandstone monolith, the following general processes can be observed: A capillary uprising from the bedrock takes place, which, with increasing height, is overlain by the horizontal and vertical exchange with the environment. Annual fluctuations increase with reaching the rock surface. Zones of strong alternating moisture content are the rim area and especially the transition towards the bottom zone of the monolith, since that is where water rises from the bedrock and driving rain events rule the water content. This confirms observations made in the natural environment, where zones near the bottom are in connection with salt object to strong deterioration. Moreover, in a humid climate such as in Germany high contents of water mass density are present during winter times (September to March), while during summer times the rocks are almost dried.

Driving forces for these main processes in general are gradients within capillary and vapour pressure, which in turn depend on multiple interlocking parameter (see Chapter 5.3, Fig.5.1), ruled also by the material behavior of the porous media.

Therefore, large differences in moisture distribution and content arise with respect to the different sandstones (Bad Bentheim, Karlshafen and Sander, Chapter 5.13.2 – 4; Fig. 5.11) and their associated pore radii distribution, since this parameter can be shown to control these processes. The lowest moisture content was observable for the quartz arenite Bad Bentheim (Chapter 5.13.2), which was weakly compacted and cemented with a high porosity and unimodal-equable pore-radii distribution. Statistical analyses reveal that this sandstone can be defined as an outlier, since he is characterized by high porosity, medium strength and high coefficient of capillary water absorption. The results of numerical modeling reveal that its few micropores prevent the sandstone from assimilating moisture via sorption. Furthermore, along with the pore-radii distribution characterized by only large capillary pores and missing micropores, a fast absorption of liquid water (driving rain) and coevally a high drying velocity is also connected. This leads to an almost dried pore space during summer times,

while during winter times the sandstone is characterized by frequently, large peaks due rain events and assimilation of liquid water.

The feldspathic litharenite Karlshafen (unimodal unequal pore radii type) is characterized by medium water uptake and high-sorption capacity but high vapor-diffusion resistance due to its small amount of small capillary pores and content of micropores. Accordingly, this sandstone shows high protraction concerning external changes within relative air humidity (Chapter 5.13.3). This leads in combination with a high liquid conductivity (Table 5.3) after a long drying period in summer time, to a decrease of water within the rim zone, whereas, behind this zone, the moisture content increases dramatically (Fig. 5.15c). This can again be explained by protracted moisture loss as the result of high vapor-diffusion resistance. At the same time, the distribution of the uprising component from the bedrock with the overlap of the present moisture from the upper part result in a concave moisture front, since the liquid phase (higher liquid conductivity, Table 5.3) can be more easily transported outwards.

For a sublitharenite with bimodal pore-radii distribution and high porosity (sandstone Sander; Chapter 5.13.4) the highest moisture content can be observed. In case of the sandstone Sander pore sizes over nine orders of magnitude are involved in water transport and storage, and promote high absorption of liquid water and, vapour via sorption dependent on relative humidity both during winter and during summer times.

The aforementioned processes show the complexity of moisture movement and enrichment within their pore space (see also Chapter 5). By comparison of the above mentioned modeling results, and the results from the onsite studies at Drei Gleichen Castle (Chapter 3) we could show that the same main mechanisms in moisture transport can be observed within the modeled sandstone monolith and the brickwork of the Drei Gleichen Castle, although the latter consists of different rock types with different water transport and storage properties. For example, capillary water uptake from the bottom transports the liquid water upwards and leads to a stronger deterioration than in upper parts of the wall. In contrary, the upper part of the wall is characterized by the exchange of vaporous moisture via sorption/diffusion and uptake of liquid water under rain conditions. Therefore, it can also be assumed that the water has to migrate through different materials with different water transport and storage properties on its way up, which, as a consequence, lead to specific moisture enrichments, e.g. after or during a driving rain event. When a replacement stone with other moisture transport and -storage “values” is inserted within this existing system, a redistribution of moisture enrichment will attune. This supports studies by Graue et al. (2011) which can show that the choice of a replacement stones has to be made in respect to the water transport and storage properties of the remaining ashlars.

Results reveal also that the relationship between the content of micropores, sorption and vapor-diffusion resistance also may also depend on the occurring clay minerals. For example, the sandstone Karlshafen exhibiting 32% micropores, has a vapor-diffusion resistance of ~180 [-], whereas the sandstone Sander´s pore space is built up of 46% micropores and only exhibits a μ-value of 25 [-]. Indeed, an increasing proportion of micropores correlates with increasing pore surface and promotes the sorption of relative humidity (e.g. Ruedrich und Siegesmund 2006, Heinrichs and Fitzner 2007). However, the content of micropores does not absolutely result in the same influence during moisture transport and storage. Deviations from general tendency may be explained by an influence of the arrangement and position of clay minerals, e.g. the different morphology of illite in dependence to illite polytypism (see e.g. Moore and Reynolds 1997 and references therin). For example, Deuttrich (1993) has already found nine types of illite, which differ in their arrangement within the pore space. In addition, Wilson and Pitman (1979) have already differentiated between pore-filling (Fig. 6.2 b), pore-lining (Fig.6.2 d), pseudomorphous replacement/pseudomatrix (Fig.6.2 d) and fracture-filling authigenic clay minerals in sandstones and assume a strong interconnection between those and the reservoir quality of a sandstone. The results of numerical modeling confirm that the clay minerals within the sandstone Karlshafen lead to a high retardation effect during moisture transport. In contrast, in the sandstone Sander, the much higher content of micropores does not have that effect. The network-building clay minerals within the sandstone Karlshafen are present as replacement minerals for lithoclasts and feldspar, whereas, in the sandstone Sander, clay minerals are also present next to this as a pseudomatrix (Fig.6.2 d), pore-lining and pore-filling clay minerals. The sandstone with the highest liquid- and vapor velocity and lowest sorption is the sandstone Bad Bentheim, with a unimodal equable pore-radii distribution and “clean” grain surfaces, as well as few pore-filling kaolinite (Fig. 6.2 a, b).

Thus, it can be assumed that the position and arrangement has a significant impact on the processes of water and vapor migration within the pore space. Probably, with respect to the varying adsorptive properties for each type of clay mineral, water will pass the micropores of clay minerals with different stages of resistance.

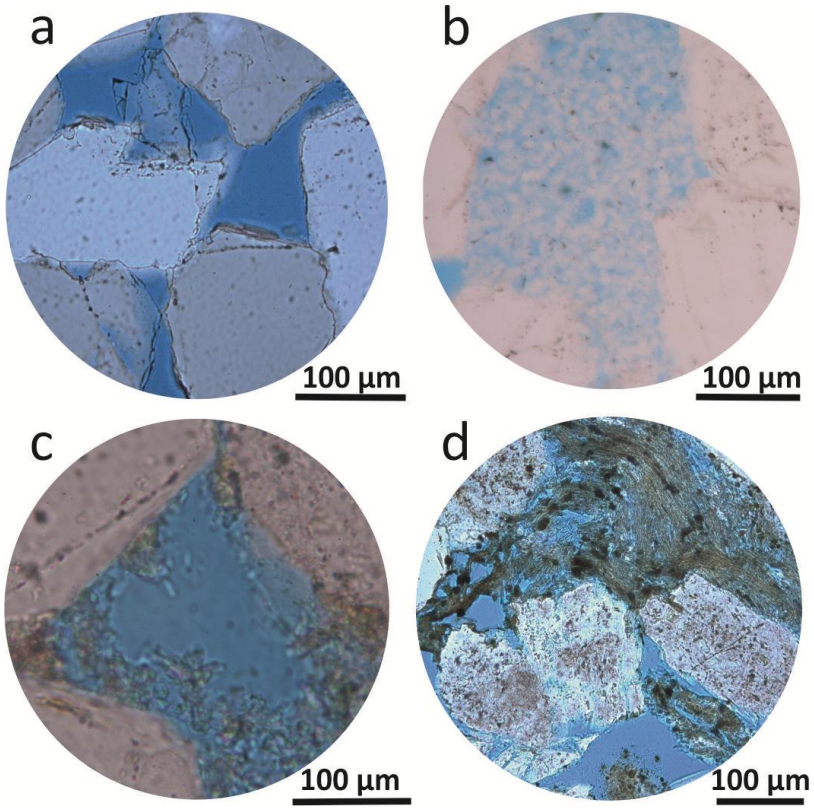

Fig. 6.2: Clay minerals and their spatial arrangement in pore space of different sandstones: a) clean surface of detrital quartz grains at the quartz arenite Bad Bentheim, b) pore-filling kaolinite between detrital quartz grains of sandstone Bad Bentheim, c) pore-lining illite at detrital quartz grains at e.g.the sandstone Röhnberg and d) pore network present as a pseudomatrix within the sandstone Ingersleben.

6.2.3 Weathering Properties

A large number of studies dealing with the weathering behavior of sandstones show that hygric dilatation and salt weathering are the most important weathering mechanisms. In combination, they are leading to manifold deterioration shapes of sandstones and a strong deterioration in general. Based on our findings especially from the numerical modeling, the mechanisms of hygric dilatation and salt weathering behavior can be further constrained with respect to lithology and pore radii types.

Hygric dilatation

Different reasons are discussed for the process of hygric dilatation, whereby a common is the reason in the presence of expending clay minerals (intracrystalline swelling; De La Calle and Suquet 1988, Weiss et al. 2004, Dixon and Weed 1989 and Moore and Reynolds 1989). More recent studies postulate the model of disjoining pressure, comparable to the intercrystalline swelling caused by interaction with the electrical double layer at the mineral surfaces and limited to very small pore channels (Morales Demarco et al. 2007, Ruedrich et al. 2011). Moreover, Ruedrich et al. (2011) found that the distribution of clays within the sandstones affects the hygric dilatation. Thereby, it is assumed that clay minerals that are present as replacements of lithoclasts can induce stress in the rock fabric, while clay present as coating is assumed to be not that critical for the accommodation of this stress increase.

Our studies form the large data set from shows that the hygric dilatation correlates positively to the content of unstable lithic fragments and the sorption, as well as to micropores (Chapter 4.16, Fig. 4.19). Therefore the results confirm the study of Ruedrich et al. (2011), wherein the position of clay was especially responsible for the stress transfer. Coevally, this also confirms the observations concerning the affect of the arrangement of clay minerals within the pore space on water transport and storage and underlines the meaning of micropores (see Chapter 6.2.2). This, in turn, can be used to estimate the hygric swelling behavior in relation to the different lithotypes (Chapter 4.16).

Moreover, the solely reason of hygric dilatation in expanding clay minerals could be excluded based on the following: Experiments on clay mixtures have proven that swelling clay minerals begin to expand at a relative air humidity of 45 % (Xiang and Czurda 1995) since the interlayer space is also hydrated then. Salles et al. (2009) found that water enters the interlayers at >10% humidity. However, many sandstones already show a volume increase at 15% air humidity (Morales Demarco et al. 2007; Ruedrich et al. 2011). Because swelling clay minerals (montmorillonite, mixed layers) only occur in very minor amounts in the analyzed sandstones, it seems reasonable that also other parameters might be responsible for the measured hygric dilatation. This is underscored in the present study in the test of the quartz arenites (e.g. Cretaceous, the Bad Bentheim sandstone, Upper Triassic (Rät), the Röhnberg sandstone; Chapter 4, Table 4.3). Both, strongly-compacted and poorly-compacted quartz arenites rarely show hygric dilatation (mean: 0.05 mm/m), although they do exhibit swellable clay minerals (e.g. BB, RÖ; Tables 4.1, 4.3). Here, the position of the clay minerals and micropores within the sandstone may also play an important role in the hygric dilatation.

Contrary, show sublitharenites-litharenites with bimodal and also unimodal unequal pore radii distribution well developed hygric dilatation, when alteration of unstable lithic fragments or feldspar lead to content of micropores or to low permeability (Chapter 4.16). Therefore, we assume that hygric dilatation is caused by an interlocking of several parameters such as the presence of micropores, the type and spatial arrangement of clay minerals within the pore space and on the content of altered unstable lithic fragments.

Another important factor of possible deterioration of the rock by hygric dilatation is the fact that an equilibrium at a given relative air humidity will rarely be achieved under the natural climate (e.g. Franzen and Mirwald 2004, Chkirda et al. 1990). The results of our numerical modeling constrain these findings, since the quickly sequence of annual fluctuations confirm that equilibrium of hygric dilatation will barely reached (Figure 5.13). Moreover, it can be assumed that from the analyzed sandstones, only the Sandstone Karlshafen with high retention capacity will achieve equilibrium within the core, whereas equilibrium will not be achieved at the outer rim due to the stronger

alternations. Indeed, the amounts of dilatation will be smaller within the rim but will attune more often and there will lead to deterioration of the fabric.

Salt Weathering

Salt weathering is considered as being the most damaging weathering process in sandstones. Therefore, the mechanisms of salt damage, the origin of salts, the interaction of salts with the environment and the mobility and solubility of different salts are investigated and discussed by many authors (e.g. Zehnder and Schoch 2009, Steiger 2005, Ruedrich et al.2007). The deteriorating effect of salts in general can be manifested in manifold shapes such as granular disintegration, scaling, delamination and blistering (e.g. Snethlage and Wendler 1997) or alveolization (e.g. Seidel 2010).

Many of them have also been proven in the here presented on-site study (Chapter 3.5.3) as well as with the salt-attack test with sodium sulphate in laboratory experiments (Chapter 3.9.3, Fig.3.19). Our experiments show, that each sandstone sample is characterized by a specific deterioration pattern. For example, while the sandstone Röhnberg shows predominantly granular disintegration (sanding; Chapter 3.9.3), the sandstones Hindfelden and Ingersleben are characterized by several deterioration shapes, named as rounding, scaling and flaking, as well as back-weathering of iron-rich areas (Fig.6.1 a). Both sandstone Hindfelden and Ingersleben represent litharenites-sublitharenites, are strongly altered and contain a pseudomatrix. The deterioration shape of rounding could be further constrained by the numerical modeling of moisture distribution at the sandstone Karlshafen (strongly compacted and moderate altered sublitharenite, Table 4.1, 4.3). It is assumed, that the aforementioned concave shape of moisture distribution within the lower part of the rock (Chapter 6.6.2), will be the location of precipitation of salts and will lead to deterioration phenomena of rounding. This aligns with observations made in the natural environment, where rounding is often observed at the lower parts of monoliths (Fig. 5.18a).

Sandstones which are not affected by salt loading with sodium sulphate belong to the strongly compacted quartz arenites, e.g. the sandstone Seebergen or, statistically proven as an outlier, the quartz arenite Bad Bentheim which is only weakly-compacted and cemented.

The statistical analyses reveal that highly compacted and cemented quartz arenites without the infiltration of clay exhibit a predominantly very high resistance against salt splitting because the distribution of pore-radii indicates a very low quantity of micropores and only low porosity (e.g. SE, Tables 4.1, 4.3). According to Snethlage and Wendler (1997), the pore-space characteristics control the solution transport and, consequentially, the distribution and amount of salt within the rock. Thus, based on our results, a correlation between stability against salt splitting, pore-size distributions and lithotype is observable.

Moreover, the number of cycles a sample withstand salt loading is strongly linear to its strength and also depends on the type of pore-radii distribution (Chapter 4.16; Fig. 4.19). This dependency on strength can be attributed to the stress induced by crystal growth, which the rock has to withstand (e.g. Goudie and Vlies 1997, Scherer 1999). Along with the pore-radii distribution, the water transport and storage is also connected and, therefore, controls the enrichment of the salt solution. Moreover, sandstones with an unimodal unequable pore-radii distribution are especially characterized with high salt resistance. Additionally, a relationship to the coefficient of capillary water uptake reveals that the higher the w-value, the lower the salt resistance. This stands in accordance to other studies, focused on sandstones (Snethlage and Wendler 1997; Fitzner and Snethlage 1982; Zehnder and Arnold 1989; Ruedrich et al. 2006), wherein it is documented that sandstones with a high amount of very small capillary pores and micropores are highly sensitive to salt splitting. Interestingly, little linear relationship was observed to the solely content of micropores.

Accompanying salt resistance and pore-space characteristics is the drying behavior of sandstones. It is commonly assumed that the faster the pore space of a natural stone dries, the lower the probability the stone will suffer salt damage (Steiger et al. 2011). This can be also observed at the sandstone Bad Bentheim, who is characterized by a very high drying velocity (Chapter 5.13.2). Again, a dependence on the arrangement of clay can be assumed, which has an impact on water transport and storage. According to Steiger et al. (2011), the moisture retention of clays will lead to an accumulation of salts in these layers and can ultimately lead to the deterioration of delamination. This is confirmed by our studies, where clay bearing sandstones (with bimodal and unimodal unequable pore radii distribution) are higher sensible to salt weathering than sandstone without them (Chapter 4.16, Fig.4.19).

6.2.4 Anisotropy, Heterogeneities and Influence of Clay Layers

Due to their genesis and different sedimentary structures, sandstone is a very heterogenous material which is, among other things, reflected by a well-developed anisotropy of some material properties. Commonly, anisotropy is caused by compositional differences as well as by structural parameters (e.g. Siegesmund and Török 2011), including parameters of, for example, varying grain size or grain shape. The sandstone investigated during the on-site study shows a differently pronounced anisotropy for compressive and tensile strength, as well as for the coefficient of capillary water absorption.

The (tensile and compressive) strength is usually perpendicular to bedding higher than parallel to it, as observed in our and previous studies (e.g. Koch and Siegesmund (2005), Ruedrich and Siegesmund (2007) Morales et al. 2007, Mosch and Siegesmund 2007, Bartelsen 2008, Kirsten 2009). According to the samples investigated (Chapter 3, Table 3.4), the anisoptropy is well-pronounced in sandstones

which are strongly compacted with high contact-thickness, such as the sandstone Seebergen, or in those which are characterized by a distinct bedding, such as the sandstone Hindfelden and Ingersleben. The degree of grain interlocking and its influence on strength was also found and investigated by Siegesmund and Dahms (1994), Siegesmund (1996) and Brosch et al. (2000).

Within the coefficient of water uptake, an inverse behavior was discovered since perpendicular to the bedding, the smaller value is observable than when parallel to it. Therefore, the anisotropy for sandstones with a well-pronounced bedding is higher than for sandstones without it. This is comprehensible for the sandstone Ingersleben (Chapter 3.10.2, Table 3.4). The grain shape and orientation probably also lead to a better connection of pores parallel to the bedding since the pores are stretched or elongated along, for example, micas or other layer-silicates. A contrary behavior of anisotropy, e.g. at the sandstone Gleichenberg (Table 3.4), can only be explained by a heterogeneity.

In the context of heterogeneities and weathering phenomena, for example carbonate- or silica nodules, liesegang´sche rings (e.g. the sandstone Seebergen, Chapter 3.5.3) are important since a different material behavior is accompanied by these structures. However, the most common and important heterogeneity in sandstones is the presence of clay layers, resulting from a sedimentary origin. From the viewpoint of the natural stone industry, clay layers can facilitate extraction from the massive rock and lead to easy splitting along the bedding planes (Hoffmann and Siegesmund 2007). However, when these heterogeneities are present within a natural building stone, a negative impact can be observed since they cause local differences in pore-space properties and strength, and, among other things, this changes the moisture circulation within the whole rock. These heterogeneities represent latent zones of weakness and working surface for weathering and, therefore, often result in material loss leading to various deterioration shapes, e.g. delamination/relief controlled by bedding as in case of sandstone Hindfelden (Chapter 3.5.3, Fig.3.7).

As numerical modeling demonstrates (Chapter 5.13.5, Fig.5.13), the presence of clay layers creates a change in stress location, in contrast to a sandstone without clay layers. Coevally and independently from rock type, the clay layers react as a barrier because they present obstructions to water migration and divide the modeled monolith into three sections. At the interface, capillary condensation arises, which then leads to an increase in stress throughout the entire monolith. This confirms the study of Steiger et al. (2011), who postulates that moisture retention of clay minerals will also lead to an accumulation of salts, finally causing delamination of the rock. Simultaneously for all sandstones, the annual fluctuations of the uppermost sandstone layer decrease, while small peaks at the interfaces occur where previously no such peaks were present. The clay layers lead, therefore, to a stress displacement from the top rim zone to the interfaces. Meanwhile, the annual fluctuations within the sandstone parts decrease since the clay layers protect the underlying parts.

6.2.5 *Influence of Hydrophobic Treatment*

Hydrophobic treatment is used to prevent water assimilation via capillary water uptake and, therefore, aims to make the rock surface impermeable to liquid water. A negative impact is often connected with this conservation strategy since it is assumed that the treatment seals the surface and also influences the vapor diffusion of the rock (Snethlage & Sterflinger 2011).

The results of numerical modeling reveal that an application of the water repellent should only be made on the premise that detailed knowledge of the water transport and storage properties of a particular rock exist (Chapter 5). Indeed, in each sandstone modeled (Chapter 5.13.6, Fig. 5.14), a distinct decrease in the water mass density is generally achieved and also the annual fluctuation decrease. However, the changes are much more comprehensive. The annual moisture content changes because, in the wintertime, more liquid water is available than in summer (Central Europe). Therefore, a changed sequence in the weathering mechanism can also be assumed.

Moreover, directly behind the hydrophobically treated part, accumulations of moisture are observable, while the hydrophobic part is almost completely dry (Chapter 5.13.6, e.g. Fig. 5. 19 a, b). This accumulation can grant the potential of inducing stress development at ~1 cm depth in the rock. However, since the transport of water within a rock is not ruled by capillary processes alone, the effect strongly depends on the remaining content of water. Therefore, the impact of hydrophobic treatment is different for each sandstone.

When the moisture transport in a sandstone mainly takes place via capillary transport, assimilation via sorption is low and the amount of uprising from bedrock is barely present, a hydrophobic treatment can be useful (sandstone Bad Bentheim; Chapter 5.13.6, Fig. 14 a). Contrary, once the uprising component from the bedrock lead to a high amount of liquid water, and also a high assimilation by sorption occurs, the hydrophobic treatment will prevent a drying of the monolith and will result in a moisture accumulation behind the treatment. This was observable for sandstone Sander with a bimodal pore radii distribution. In case of sandstone Karlshafen with a unimodal unequal pore radii distribution, accumulations behind the rim of hydrophobic treatment are not observable, the differences between clay layer and sandstone layer saturation are negligible and the uprising component is also distinctly decreased. However, the higher alternating curves within the clay and partially sandstone layers, in general, should induce higher stresses within the entire monolith. Therefore, a treatment with water repellence is, in case of the sandstones Sander and Karlshafen, not advisable.

6.3 Derivation of Construction Suitability for Different Lithotypes

In the following chapter the analytical results presented in the Chapters 3-5 will be summarized into a classification of the construction suitability of sandstones. In order to do so, results from the aforementioned individual chapters will be repetitively summarized and, as addition, integratively discussed. Special attention will be paid on the material behaviors associated to the defined sandstone types. The latter will be discussed with regards to compositional and digenetic aspects (e.g. Chapter 4.15) as well as in context to relationships between those parameters, which could be established by the results of our results from numerical modeling and statistical analyses.

The description of the different suitability types below is ordered by a decrease in textural and compositional maturity. However, the borders between those types and their anticipated material behavior have to be regarded as flowing transitions.

Quartz Arenites with Very Good Construction Suitability

Quartz arenites belonging to this category of construction suitability are strongly compacted and cemented, are characterized by few early-infiltrated clay minerals, are resistant against salt attack, exhibit no or little hygric dilatation and, therefore, can be evaluated with a high construction suitability. This type of sandstone has often been observed in natural stones belonging deposits of Upper Triassic (Rhät) (e.g. the sandstone Seebergen, Chapter 3.11, 4.17). Material and weathering behavior can be derived from the following relationships and processes:

Since pure quartz arenites are highly mature and are, as a consequence, well-to-very-well sorted, a primary porosity of 39 - 41% can be assumed after deposition (Beard & Weyl 1973). The sorting and degree of porosity result in a unimodal pore-radii distribution with capillary pores of 0.1–10 µm radius. With the tighter packing of grains, the pressure solution starts at the points contact (chemical compaction), and porosity decreases further. With increasing degree of compaction, also the contact thickness increase between the grains of similar hardness. Through the compaction, the pore-radii distribution commonly remains the same – unimodal equal – as in the beginning diagenetic stages. Coevally and accompanied by the compaction, the formerly large pores become smaller because of the reduction of larger gusset pores by quartz cementation. When quartz arenites are much more strongly compacted and cemented, the pore-radii distribution may shift to unimodal-unequal and smaller capillary pores (Fig.6.3). The finally porosity is about ~15% and the strength of these sandstones is, at around 70-150 MPa, considered medium to high since no unstable lithic fragments are present, and a high contact-thickness occurs due to being accompanied by the high degree of compaction, which contributes to a strong grain cohesion.

Since, in these sandstones, smaller capillary pores characterize the pore-radii distribution, and few clay minerals are present, the resulting water transport and storage properties lead to low moisture

content within their pore space. The coefficient of water absorption as well as sorption will be very low, as in the case of, for example, the sandstone Seebergen (Table 4.3). With regard to the observations made of water transport and storage within the chapter of numerical modeling (Chapter 5.13), neither long-term retention of water can be assumed as comparable to the sandstone Karlshafen due to the missing clay minerals, nor can a high drying-velocity and forwarding of liquid water, as in the case of the sandstone Bad Bentheim since, here, much smaller capillary pores are present. The weathering properties of this type of sandstone arise due to its low porosity, unimodal-unequable pore-radii distribution and high strength, characterized by a high salt-weathering resistance. Moreover, due to its composition and pore radii distribution little hygric dilatation can be observed (Chapter 4, Chapter 6.1.3).

Quartz Arenites with Moderate –Well Construction Suitability

Highly mature quartz arenites, which are weakly compacted and cemented and exhibit a high quantity of micropores due to the infiltration of clay minerals, and show only moderate resistance to salt splitting and little hygric dilatation. This group of sandstones often correlates to sandstones of the Upper Triassic and Cretaceous (e.g. the sandstone Röhnberg, Tables 4.1, 4.3; Chapter 4.17).

Due to the composition after deposition, a primary porosity between 39 to 40.8 % can again be assumed. One more time, the sorting and degree of porosity result in a unimodal pore-radii distribution with capillary pores of 0.1–10 µm radius. However, the further development of pore space and strength runs differently and results in distinctly different material behavior in contrast to the other type of quartz arenite. If, during eodiagenesis, clay infiltration takes place, and clay rims are formed around detrital grains, quartz overgrowths are inhibited and micropores occur in increasing amounts, both of which clearly decrease the compressive strength (e.g. RÖ, Tables 4.1, 4.3; Chapter 4.15) due to the lower cementation and heterogeneity of pore space (Blöcher et al. 2007).

Porosity is coevally preserved by the absence of cementation. The pore-size distribution through clay minerals then is modified from unimodal equal to a certain degree unimodal unequal and the porosity (~25%) is preserved by the prohibited cementation of silica or calcite in the presence of clay minerals. The grain contacts of detrital grains are predominantly present as point contacts. When the clay minerals are in between the grain contacts, they might also be able to reduce the strength since cohesion is not possible via the grains. Moreover, within the glauconite-bearing Cretaceous sandstones, a weak negative relationship to compressive strength is observable (e.g. HI, CO, RÜ, Chapter 4, Table 4.1, 4.3).

Connected with the high porosity and unimodal-unequable pore-radii distribution with (large) capillary pores and micropores, the rock will be able to absorb moisture via a capillary path as well as very well by sorption (Fig.6.3). However, when clay infiltration is as small as in case of Bad Bentheim,

and the pore radii distribution therefore unimodal equable, very small amounts of water are found within the pore space over the whole year (see Chapter 5.13.2; Fig.6.3). The few micropores built up by kaolinite within the sandstone Bad Bentheim promote rarely assimilation via sorption, nor do they retain water within their pore network. However, it can be assumed that, with the increasing number of micropores and clay minerals positioned at pore throats and smaller capillary pores, as in case of the sandstone Röhnberg (Fig.6.2c), the sorption will also increase and the drying behavior decrease. Also accompanying the content of the sorption of moisture by clay minerals is the fact that the rock can assimilate next to water during driving rain events also by exchange via rel. humidity. This may result in a higher stress index since the susceptibility to changes in moisture also leads to a higher stress index over the course of the year, e.g. during salt weathering.

Consequently, also the salt resistance decreases with increasing clay content by shifting from unimodal equable to unimodal unequable pore radii distribution. Contrary, a pore space built up with only clear maxima in large capillary pores probably does not induce any stress during salt crystallization, since crystal growth can take place within the free pore space without any resistance.

Sublitharenites-Litharenites with Well Construction Suitability

The construction suitability changes when unstable lithic fragments and/or feldspar are present (Chapter 4.15). Sublitharenites and litharenites, which are strongly compacted and cemented and are characterized by a medium degree of alteration, show hygric dilatation of ~0.5-1.0 mm/m and are well salt resistant (Group A-B; Chapter 4.7). Accordingly, they exhibit a medium-to-well construction suitability. These sandstones predominantly belong to the Lower Triassic of the Buntsandstein, the Permian and the Carboniferous.

The development of construction-suitable sandstone with this primary composition runs differently from that of quartz arenites, since the compositional and textural maturity is much lower. Due to the moderate-to well sorting, the primary porosity amounts to 34–39%, and the pore-radii distribution is unimodal-unequal. During eogenesis, haematite impregnation often occurs and, with advancing burial compaction, feldspar alteration and quartz dissolution commonly take place. Followed by quartz cementation, authigenic clay minerals are formed by the alteration of feldspars or unstable lithic fragments, and carbonate cementation also occurs. The alteration of feldspar and unstable lithic fragments create a small amount of micropores.

The final pore radii distribution is unimodal-unequal, the porosity about ~5-15% and the compressive strength is dependent on the degree of alteration and cementation, medium-to-high (70–150 MPa). Sandstones of similar composition but longer burial history as sandstone of Lower Triassic, such as the Carboniferous and Permian sandstones (Chapter 4, Tables 4.1, 4.3; samples IB, TA, BE), show a similar pore radii distribution but markedly lower porosity and a higher compressive strength.

With respect to the pore-radii distribution, this rock type will be able to assimilate water in liquid and vapor stages. As proven by the statistical analyses the coefficient of capillary water absorption will be low due to the smaller capillary pores, and the sorption with dependence on the clay mineral content will be high (Chapter 4.15, Fig. 4.19, Fig.6.3). Deviations from this trend can be arise contingent upon the amount of cementation and compaction, where then also larger capillary pores can occur and will result in a higher w-value (Fig. 6.3). Moreover, as revealed by the numerical modeling of a sandstone monolith of this group (sandstone Karlshafen, Chapter 5.13.3), the vapor diffusion resistance can be strongly increased by the presence and arrangement of clay minerals, which then will lead to a "slowly reacting" inner part and a strong fluctuating outer rim of a dimension stone (Chapter 6.2.3).

However, in combination with the high strength, the strong fluctuations in connection with the high amounts of hygric swelling and their accompanied stress development, can be compensated to a certain degree. Due to the high strength, low porosity and pore radii distribution, the salt resistance is well developed.

Sublitharenites-Litharenites with Very-Low-to–Low Construction Suitability

Sublitharenites-Litharenites belonging to this category are characterized by the lowest construction suitability since they exhibit high values of hygric dilatation and low resistance against salt loading. They show very low textural and compositional maturity (e.g. HS, IS, SA, SL; Chapter 4.17, Tables 4.1, 4.3), exhibit high porosity, a bimodal pore-radii distribution and low strength and belong to the Upper Triassic of Schilfsandstein and Lettenkohlenkeuper.

The primary porosity also ranges from 34 to 39% because the rock is moderately well-sorted. After deposition, porosity decreases through compaction and silica cementation. Organic fragments parallel to bedding partially destabilize the fabric (e.g. HS, IS; Chapter 3 & 4). The alteration of (volcanic) clasts into clay minerals and a clayey matrix tends to be squeezed between more rigid grains (pseudomatrix) during even the initial stages of diagenesis at shallow burial. This also prohibits the free circulation of fluids and leads to restricted cementation. Porosity decreases through further compaction, and the content of micropores increases greatly because of the alteration of unstable lithic fragments. In consequence, the textural maturity distinctly decreases. This finally leads to a sandstone with a low compressive strength because, in this rock with a heterogenous pore-radii distribution, a stable grain framework no longer exists. The porosity is in between 30 – 50 MPa.

The lithology and associated bimodal pore-radii distribution results in a permanently high water content since, due to its lithology, it is characterized by the participation of pore sizes over nine orders of magnitude. Therefore, the rock will be able to absorb water in vapour and liquid stage, dependent on the position of the maxima in capillary and micropores. Moreover, the degree of

sorption may vary in dependence to the degree of alteration and the pore building clay minerals (Fig.6.3). The numerical modeling of moisture within this sandstone type (the sandstone Sander) generally reveals a very high water mass density as well as very high annual fluctuations over the whole year, which will lead to stress inducement within the fabric.

Paired with low strength properties, the rock is also not able to withstand the stress induced by salt crystallization and hygric dilatation for as long as the sandstone Karlshafen is.

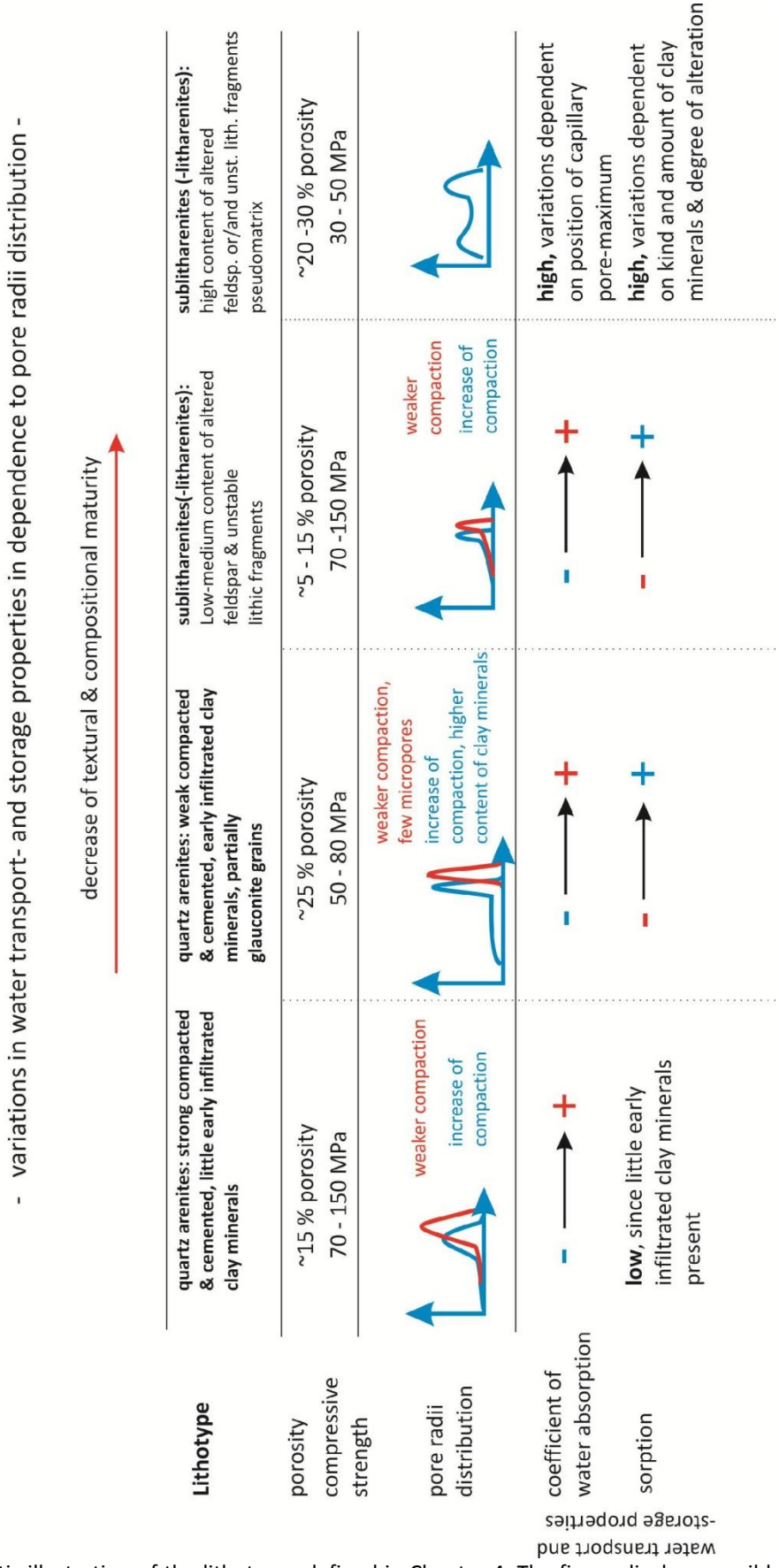

Fig. 6.3: Schematic illustration of the lithotypes defined in Chapter 4. The figure displays possible variations in the water transport and storage properties in dependce to the pore radii distributions. The illustration presents a supplementary extension of the quality catalogue established in Chapter 4, Fig. 4.23.

7 General Conclusions

In relation to the aims of this thesis (see Chapter 1), the following chapter briefly summarizes the main conclusions, which can be drawn from our results presented in Chapters 3 through 6. Special attention has been paid to the increased knowledge of the relationship between material properties and weathering behavior of sandstones as well as the evaluation and prediction of their construction suitability.

1. The on-site study and laboratory analyses of dimension-stones reveal a strong interconnection between lithology and construction suitability. Our studies show that even sandstones of the same stratigraphy and with a close proximity of their depositional areas may demonstrate major differences in their petrophysical properties. Those differences are attributed to diagenetic processes, leading to particular modifications of the primary sandstone composition. Therefore, we conclude that the standard classification of sandstones (McBride 1963) has to be substantiated with analyses of fabric in order to characterize sandstone types and associated materials in terms of their deterioration behavior.

2. Results of our statistical analyses confirm a distinct correlation between the material properties of sandstones and their composition, depositional environment, stratigraphic association and diagenetic path. Our data also confirm that the development of porosity, pore-radii distribution and strength are strongly connected to one another. Additionally, we can show that the latter can be characterized as the key parameter for the evaluation of construction suitability.

3. Our analyses show that, within the linear relationship between strength and porosity (see above), there is also a relationship between those parameters and the content of unstable lithic fragments, the type of grain contact, the degree of alteration and the type of pore-radii distribution. For example, with an increasing amount of unstable rock fragments, direct contact between mechanically and chemically unstable grains becomes more likely, while the strength of the rock becomes higher with increasing contact thickness.

4. Our statistical analyses prove a clear relationship of the final porosity and the pore-radii distribution of a sandstone with its primary composition and grain-sorting after deposition, and, subsequently, with its modification during diagenetic processes. Based on our statistical analyses, three different types of sandstones are distinguishable according to their pore-radii distribution and differ in these aforementioned parameters: unimodal-equal, unimodal-unequal and bimodal.

   Unimodal-equal distributions of pore radii are mainly found in well-sorted, highly mature quartz arenites, in which no infiltration of clay minerals have occurred (e.g. during early diagenesis). The Cretaceous sandstones analyzed are of this type.

Unimodal-unequal distributions of pore radii were found in sublitharenites, but they may also occur in quartz arenites. In sublitharenites, this distribution is attributed to moderate-to-good-sorting, weak alteration of unstable grains and a moderate degree of cementation and compaction as documented e.g. by the Lower Triassic Weser sandstones. Quartz arenites belonging to this pore-radii distribution are generally well-sorted and exhibit a more immature character than those belonging to the unimodal type, due to the infiltration of clay minerals.

Bimodal pore-radii distribution can be predominantly observed for litharenites with very low maturity and of Upper Triassic age. The pore-radii maxima are located within the microsized pores and capillary pores. We conclude that the maximum within microsized pores is caused by the alteration of less stable components and/or the presence of a pseudomatrix. In contrast, we attribute the second maximum in capillary pore sizes to reflect relics of primary intergranular porosity, which were closed to different degrees due to cementation and compaction.

Generally, our data show that a increase in maturity correlates with a change in pore-radii distribution from the bimodal type (most immature) to unimodal-unequal and, finally, to unimodal-equal (most mature).

5. Based on our detailed statistical analyses of the material, petrophysical and petrographical properties, stratigraphy and the diagenetic paths of different sandstones, we can define four sandstone types which differ in their composition and diagenetic history. These types represent groups of identical or very similar weathering behavior, strength, porosity and pore-radii distribution and, thus, can be used to predict the construction suitability of any sandstone according to its classification in one of these four groups. The groups are defined as follows:

   Group 1: Highly mature quartz arenites, which are strongly compacted and cemented with only small amounts of early-infiltrated clay minerals and predominantly sutured concave-convex grain contact. They exhibit a compressive strength between 70-150 MPa, a porosity of up to 15 % and a unimodal-unequal pore-radii distribution. Due to the low hygric dilatation and high salt resistance (Group A, see Chapter 4), they can be defined as resistant to weathering.

   Group 2: Quartz arenites, which are weakly compacted and cemented, have point-elongated grain contact, partially contain glauconite grains and have a high content of early-infiltrated clay minerals. The compressive strength is between 50 and 80 MPa, the porosity amounts to up to ~25 % and the pore-radii distribution is unimodal-equal. Due to the low hygric dilatation but medium-low salt resistance, the rock can be defined as moderately-to-highly-resistant to weathering.

Group 3: (Sub)litharenites with low-to-medium content of altered, unstable lithic rock fragments and feldspars and medium-to-high content of quartz cement, as well as illite and/or kaolinite at grain surfaces. The compressive strength is 70–150 MPa and medium-to-high, the porosity is between 5 and 15 % and the pore-radii distribution is unimodal-unequal. The salt resistance belongs to group A–B (see Chapter 4), and hygric swelling typically amounts 0.5–1.0 mm/m. In addition, the compressive strength is high. The governing parameter for the weathering resistance is the amount of hygric swelling. Generally, this type has to be considered to represent moderate weathering resistance.

Group 4: (Sub)litharenites with high content of altered, unstable lithic fragments and/or feldspars, little quartz cement and only weak grain contact between the few stable detrital grains. Former lithic fragments are mostly squeezed to a pseudomatrix. The compressive strength is low at 30–50 MPa, and the porosity is high at 20–30 %. The resistance to salt weathering is low (group C, see Chapter 4), while the hygric dilatation is generally high. Due to the high values of hygric dilatation and the low salt resistance, this sandstone type can be defined as not resistant to weathering.

6. Our numerical modeling of moisture distribution under different climatic conditions provides a unique way of asserting a very detailed evaluation of moisture accumulation and its critical influence on the weathering behavior of sandstones. Our results confirm that the lithology and its associated pore space regulate both moisture content and moisture accumulation. Our models also allow us to evaluate the influence of clay-mineral layers within sandstones, as well as the effects of hydrophobic treatment on those processes. In general, the results from our modeling approach correspond to the observations made in on-site studies of sandstones, which are exposed to natural environmental conditions. Thus, numerical modeling allows us to predict those weathering and deterioration phenomena for a given sandstone.

   Additionally, our models confirm that the water transport and water storage behavior of sandstones strongly depends on the material itself, especially when it comes to the pore-radii distribution. The differentiation of sandstones based on their pore-radii distribution into three different classification types (see above and Chapter 4) could be constrained by the numerical modeling, which proves that those types show crucial differences in their water transport and storage properties.

   Based on our modeling results, we can also conclude that the presence of clay layers markedly influences the moisture distribution within a rock. In all analyzed samples, the clay layers react as barriers, presenting obstructions to water migration and dividing the modeled sandstone monolith into different sections. At the interface, capillary condensation arises, which then leads to an increase in stress through salt and/or hygric dilatation throughout the entire monolith.

Additionally, for all modeled sandstones, the annual moisture fluctuations of the layer above this clay barrier decrease, but, coevally, small moisture peaks occur along these interfaces. Thus, clay layers lead to stress displacement from the rims (where the highest stress normally occurs, caused by high fluctuations of, for example, moisture or salt content) to the center of the monolith. This confirms the observations made in the natural environment. In contrast, the annual fluctuations within the parts of the sandstone below the clay layer decrease since the clay layers protect those underlying parts.

The numerical modeling of the effects of hydrophobic treatment as a conservation strategy for sandstones implies that such treatment needs to be used with caution. Although our data show that the treatment may strongly decrease the water content within a sandstone, our results also reveal that, behind the zone of the treatment (i.e. several cm below the surface), an accumulation of moisture arises. The significance of this effect for the entire water balance of the sandstone monolith depends on the remaining transport mechanisms and their associated pore-volume distribution. When the main water absorption takes place via capillary paths, the treatment can be useful for 'dehydrating' a sandstone since no water can accumulate within the rock. However, if water is taken up by capillary suction from the bedrock below the monolith, moisture accumulation will again arise because moisture compensation through capillary vapor diffusion to the rock surface is prohibited by the sealing of the hydrophobic treatment.

Thus, the effectiveness of any hydrophobic treatments must be evaluated in the context of the pore-radii distribution (especially the number of capillary pores) and the building technique (i.e. moisture barrier).

8 References

Please note: References cited in Chapter 3-5 are displayed at the end if the respective chapters.

Bartelsen T (2008) Gefügeabhängiges Verwitterungsverhalten ton¬mineralführender Sandsteine durch hygrothermisch induzierte Dehnungsprozesse, unpublished diploma thesis, Göttingen

Brakel J, Modry S, Svata M (1981) Mercury Porosimetry: State of the art. Powder Tech 29: 1-12.

Brosch S, Schachner K, Bluemel M (2000) Prelimnary investigation results on fabrics and related mechanical properties of an anisotropic gneiss. J Struc Geo 22: 1773-1787.

Chkirda S, Kintrup H, Müller-Rochholz J (1999) Sorptionsmessungen von Baumberger Kalksandsteinen mit kapazitiven Feuchtefühlern. Berichsband 69, 10. Feuchtetagung. Berlin, p. 18

De La Calle C, Suquet H (1988) Vermiculite. In: Bailey SW (ed.) Hydrous phyllosilicates. Reviews in Mineralogy. Mineralogical Society of America 19:455–496

Deuttrich T (1993) Tonmineral-Diagenese in Rotliegend-Sandsteinen des Norddeutschen Beckens. Dissertation Universität Mainz.

Dickinson WR (1985) Interpreting provenance relations from detrital modes of sandstones. In: Zuffa GG (ed) Provenance of arenites. Reidel, Dordrecht, pp 333–361

Dixon JB, Weed SB (1989) Minerals in soil environments. 2nd edition Soil Science Society of America

Dohrmann CF, Kühn I (2009) Angewandte Statistik für die biologischen Wissenschaften. Helmholtz Zentrum für Umweltforschung- UFZ

Fitzner B (1970) Die Prüfung der Frostbeständigkeit von Naturbausteinen. Aachen, Diss

Fitzner B, Snethlage R (1982) Einfluß der Porenradienverteilung auf das Verwitterungsverhalten ausgewählter Sandsteine. Bautenschutz und Bausanierung. Nr 3:97–103

Franzen C, Mirwald PW (2004) Moisture content of natural stones: static and dynamic equilibrium with atmospheric humidity. Environ Geol 46:391–401.

Goudie A, Vlies H (1997) Salt weathering hazards. Wiley, Hoboken

Heinrichs, K., Fitzner, B. (2007): Stone Monuments of the Nemrud Dag Sanctuary/Turkey – Petrographical Investigation and Diagnosis of Weathering Damage. Z.dt. Ges. Geowiss., 158/3, p. 519-548, Stuttgart.

Hiltmann W, Stribrny B (1998) Handbuch zur Erkundung des Untergrundes von Deponien und Altlasten: Band 5: Tonmineralogie und Bodenphysik. Springer 297p

Hirschwald J (1912) Die Prüfung der natürlichen Bausteine auf ihre Verwitterungsbeständigkeit. Verlag W Ernst & Sohn, Berlin.

Hoffmann, A., Siegesmund, S. (2007): Investigation of Dimension Stones in Thailand: an Approach to a Methodology for the Assessment of the Stone Deposits. Z. dt. Ges. Geowiss., 158/3, p. 375 - 416, Stuttgart.

Kirsten H (2009) Herkunft, Eigenschaften und Konservierungs¬möglichkeiten von Lettenkeuper-und Schilfsandsteinen an Baudenkmalen in Thüringen. Diss, Weimar

Klopfer H (1985) Feuchte. In: LUTZ et al (eds) Lehrbuch der Bauphysik. Teubner Verlag, Stuttgart, pp 265–434

Koch A, Siegesmund S (2005) Gesteinstechnische Eigenschaften von Sandsteinen. Naturstein 5:84–91.

Koch R, Sobott R (2008) Sandsteine: Entstehung, Eigenschaften, Verwitterung, Konservierung, Restaurierung. In: Siegesmund, Snethlage (eds) Schriftenreihe der Deutschen Gesellschaft für Geowissenschaften, vol 59, pp 145–174

Moore DM, Reynolds RC Jr (1997) X-ray diffraction and the identification and analysis of clay minerals. Oxford University Press, Oxford

Morales M, Jahns E, Ruedrich J, Oyhantc¸abal P, Siegesmund S (2007) The impact of partial water saturation in rock strength: an experimental study on sandstones. Z. dt. Ges Geowiss 158(4): 869–882

Mosch S, Siegesmund S (2007) Statistisches Verhalten petrophysikalischer und technischer Eigenschaften von Naturwerksteinen. Z Dtsch Geol Ges 158/4:821–868

Nicolai A, Grunewald J, Plagge R, Scheffler G (2008) Development of a Combined Heat, Moisture, and Salt Transport Model for Unsaturated Porous Building Materials, in Simulation of Time-Dependent Degradation of Porous Materials, Research Report on Priority Program DFG SPP 1122, eds. L. Franke, G Deckelmann & R. Espinosa-Marzal, Cuilliver Verlag, ISBN 978-3 86727-902-4, S. 67-84.

Peschel A (1983) Natursteine. VEB Deutscher Verlag für Grundstof¬findustrie, Leipzig

Poschlod K (1990) Das Wasser im Porenraum kristalliner Naturwerksteine. Münchener Geowiss Abh B 7, Verlag Dr. Friedrich Pfeil, Munich.

Ruedrich J, Kirchner D, Seidel M, Siegesmund S (2005) Deterioration of natural building stones induced by salt and ice crystallisation in the pore space as well as hygric expansion processes. In: Siegesmund S, Auras M, Ruedrich J, Snethlage R (eds) Geowissenschaften und Denkmalpfleg. Zeitschrift Deutsche Geologische Gesellschaft, 156/1, 59–73

Ruedrich J, Bartelsen T, Dohrmann R, Siegesmund S (2010) Building sandstone integrity affected by the process of hygric expansion. Environ Earth Sci. doi: 10.1007/s12665-010-0767-0

Ruedrich J, Bartelsen T, Dohrmann R, Siegesmund S (2011) Moisture expansion as a deterioration factor for sandstone used in buildings. Monument under threat. Environ Earth Sci 63:7–8

Ruedrich J, Siegesmund S (2006) Salt and ice crystallisation in porous sandstones. Environ Geol 52(2):225–249

Ruedrich J, Siegesmund S (2007) Salt induced weathering: an experimental approach. Environ Geol 52:225–249

Salles F, Douillard JM, Denoyel R, Bildstein O, Julien M, Beurroies I, Van Damme H (2009) Hydration sequence of swelling clays: Evolution of specific surface area and hydration energy. J Colloid Interface Sci 333:510–522

Scheffler G, Plagge R (2009) A whole range hygric material model: modeling liquid and vapour transport properties in porous media. Int. J Heat Mass Transf. doi: 10.1016/j.ijheatmasstransfer.2009.09.030.

Scherer GW (1999) Crystallization in pores. Cem Conr Res 29:1347–1358

Scherer M (1987) Parameters influencing porosity in sandstones: a model for sandstone porosity prediction. Am Assoc Petroleum Geologists Bull 71(5):485–491

Siedel H (2010) Historic building stones and flooding: changes of physical properties due to water saturation. J Perform Constr Facil 24(5). doi:10.1061/(ASCE)CF.1943-5509.0000066

Siegesmund and Török (2011) Building Stones. In: Stone in Architecture, Siegesmund & Snethlage (eds), Springer, Berlin-Heidelberg.

Siegesmund S (1996) The significance of rock fabrics for geophysical interpretation of geophysical anisotropies. Geotekt Forsch 85: 1-123.

Siegesmund S, Dahms M (1994) Fabric-controlled anisotropy of elastic, magnetic and thermal properties. In: Bunge HJ, Siegesmund S, Skrotzki W, et al. (eds) Textures of Geological Materials. DGM Informationsgesellschaft, Oberursel.

Siegesmund S, Dürrast H (2011) Physical and mechanical properties of rocks. In: Siegesmund S, Snethlage R (eds) Stone and architecture. Springer, Berlin, pp 97–225

Snethlage R, Sterflinger K (2011) Stone conservation In: Stone in Architecture, Siegesmund & Snethlage (eds), Springer, Berlin-Heidelberg.

Snethlage R, Wendler E (1997) Moisture cycles and sandstone degradation. In: Baer NS, Snethlage R (eds) Saving our architectural heritage, the conservation of historic stone struc¬tures. Elsevier, Hoboken, pp 7–24

Steiger M (2005a) Crystal Growth in porous materials − I: the crystallization pressure of large crystals. J Cryst Growth 282:455–469

Steiger M, Charola AM, Sterflinger K (2011) Weathering and Deterioration. In: Stone in Architecture, Siegesmund & Snethlage (eds), Springer, Berlin-Heidelberg.

Surdam RC, Dunn TL, MacGowan DB, Heasler HP (1989) Concep¬tual models for the prediction of porosity evolution with an example from the Frontier Sandstone, Big-Horn Basin, Wyo¬ming. In: Coalson EB, Kaplan SS, Keighin CW, Oglesby LA, Robinson JW (eds) Sandstone Reservoirs: Rocky Mountain Association of Geologists, pp 7–21

Tukey J (1977) Exploratory data analysis. Addison-Wesley. ISBN 18750-201-07616-0

Waples DW (2002) Evolution of sandstone porosity through time. The modified Scherer Model: a calculation method applicable to 1-D maturity modeling and perhaps to reservoir prediction. Nat Resour Res 11:257–272

Weimann, MB (2001) Hygrische Eigenschaften von Polymerbeton im Vergleich zu porösen mineralischen Werkstoffen im Bauwesen. Thesis, Technical University, Zurich, p. 149.

Weiss T, Siegesmund S, Kirchner D, Sippel J (2004) Insolation weathering and hygric dilatation: two competitive factors in stone degradation. Environ Geol, Special Issue: Stone Decay Hazards, 46/3-4, S. 402–413

Wilson MD, Pitman ED (1979) Authigenic Clays in Sandstones: Recognition and influence on Reservoir Properties and Paleoenvironmental Analysis. Journal of Sedimentary Petrology 47(1):3-31

Xiang W, Czurda K (1995) Einfluss des Kationenaustausches auf die Hydratation und Dehydratation von Tonmineralen. Festschrift zum 60. Geburtstag von Helfried Möller. Geol. Paläontologische Mitteilungen Innsbruck, Bd. 20:107–119

Zehnder K, Arnold A (1989) Crystal growth in salt efflorescence. J Crystal Growth 97:513–521

Zehnder K, Schoch O (2009) Efflorescence of mirabilite, epsomite and gypsum traced by automated monitoring on-site. J Cult Heritage 10:319–330

9 Acknowledgement

Die vorliegende Arbeit entstand unter Anregung und Betreuung von Herrn Prof. Dr. Siegfried Siegesmund. Für seine Unterstützung, sein reges Interesse am Fortgang der Arbeit sowie für seine Ratschläge möchte ich mich an dieser Stelle bedanken.

Für die Übernahme des Korreferates, die gute Zusammenarbeit sowie für seine konstruktiven Vorschläge möchte ich mich bei Herrn Prof. Dr. Roman Koch bedanken.

Des Weiteren gilt Herrn Dr. Jörg Rüdrich ein besonderer Dank, für sein Interesse und seine Ideen sowie für seine Bereitschaft und Freude fachliche Fragen zu diskutieren.

Dr. Rudolf Plagge danke ich für die Realisierung der Modellierung, seine Hilfe und Unterstützung sowie für die schöne Zeit in Dresden.

Weiterhin möchte ich mich bei Herrn Dr. Werner Nagel, Dr. Jens Schuhmacher und Herrn Dr. Oleg Nenadic bedanken, die mich durch die Materie der Statistik begleitet haben.

Ein weiterer großer Dank geht an die Deutsche Bundesstiftung für Umwelt durch deren finanzielle Unterstützung die vorliegende Arbeit ermöglicht wurde.

Viele Menschen haben im Laufe der fast vier Jahre meinen Weg gekreuzt, haben auf unterschiedlichste Art und Weise zur Weiterentwicklung und zum Fortgang dieser Arbeit beigetragen. Für ihre Hilfsbereitschaft möchte ich ihnen an dieser Stelle herzlich danken:

- Manu, Wanja, Christian, Vika, Birte, Karl-Jochen, Stephan, Günter, Frau Hesse
- Ákos, Balász und Ruben
- Prof. Dr. Michael Hoppert
- Frank, Phillip, Gabriele, Heike, Sören, Anita
- Reini, Katti, Elmo, Alex, Sebastian

…..und alle, die ich hier vergessen haben sollte!

Abschließend möchte ich mich bei meiner Familie bedanken, für ihr Interesse, ihr Verständnis und jedwede Art von Unterstützung, die sie mir während dieser Zeit zukommen ließen. Insbesondere Frithjof sei an dieser Stelle genannt, auf dessen Hilfe und Unterstützung ich immer zählen konnte.